



Memo version 1.1

BESIII Analysis Memo

BAM-544

November 25, 2021

1 Measurement of CP-even fraction and strong-phase difference in
2 $D^0/\bar{D}^0 \rightarrow \pi^+\pi^-\pi^+\pi^-$

3 Xiaodong Shi^{a,b}, Sneha Malde^c, and Guy Wilkinson^c, Xinyu Shan^{a,b}, Haiping
4 Peng^{a,b}, and Yingchun Zhu^{a,b}

5 ^aUniversity of Science and Technology of China

6 ^bState Key Laboratory of Particle Detection and Electronics

7 ^cUniversity of Oxford

Internal Referee Committee

9 Baician Ke(Chair)^c, Lei Li^d, and Yingrui Hou^e

10 ^cShanxi Normal University

11 ^dBeijing Institute of Petro-chemical Technology

12 ^eUniversity of Chinese Academy of Sciences

13 HN : <http://hnbes3.ihep.ac.cn/HyperNews/get/paper544.html>

Abstract

15 A measurement of CP-even fraction and strong-phase difference in $D^0/\bar{D}^0 \rightarrow$
16 $\pi^+\pi^-\pi^+\pi^-$ is performed using the 2.93 fb^{-1} data set taken at $\sqrt{s} = 3.773\text{ GeV}$ collected
17 with the BESIII detector at BEPCII storage ring. The CP-even fraction of $D \rightarrow$
18 $\pi^+\pi^-\pi^+\pi^-$ is measured as $0.732 \pm 0.015 \pm 0.007$, where the first uncertainty is statistical
19 and the second is systematic uncertainty. The strong-phase difference is measured
20 with five binning schemes from CLEO-c and four BESIII binning schemes, where
21 the BESIII binning schemes are determined in this analysis by using the amplitude
22 model from the partial wave analysis of $D \rightarrow \pi^+\pi^-\pi^+\pi^-$ (BAM-00439). Both CP-even
23 fraction and strong-phase difference results will play an important role as key inputs
24 in the measurement of CKM angle γ/ϕ_3 at LHCb and Belle II.

25

Version Log

- 26 V0.0: the first version. Released to Charm Group.
27 V0.1: updated according to Prof.Ke's comments on Aug. 27th.
28 V0.2: updated according to Prof.Libby's comments on Aug. 31th.
29 V0.3: updated according to Prof.Ke's comments on Sep. 07th.
30 V0.4: updated according to comments on P&S meeting on Sep. 24th.
31 V0.5: updated according to comments by Prof.Dong on Sep. 26th.
32 V1.0: The version enter referee committee, same as V0.5.
33 V1.1: updated according to comments by Dr.Hou on Nov. 08th.

1 Contents

2	1 Publication Strategy	3
3	2 Introduction	4
4	3 Formalism	6
5	3.1 GGSZ method	6
6	3.2 Quantum correlations of $D^0\bar{D}^0$	7
7	3.3 CP-even fraction measurement	8
8	3.3.1 Using pure CP tag channels	8
9	3.3.2 Using $K_{S,L}^0\pi^+\pi^-$ tag channels	9
10	3.3.3 Using other self-conjugate tag channels	9
11	3.4 Strong-phase difference measurement	10
12	4 The BEPCII and BESIII detector	11
13	5 Data sets, MC simulation and external information	12
14	5.1 Data sets and MC simulation	12
15	5.2 Binning schemes of $4\pi^\pm$	13
16	5.2.1 BESIII's Equal $\Delta\delta_p^{4\pi}$ binning scheme	14
17	5.2.2 BESIII's Alternative binning scheme	15
18	5.2.3 BESIII's Optimal binning and Optimal AlterBin binning	15
19	5.2.4 Prediction of BESIII's binning schemes	17
20	5.3 Inputs from $K_S^0/K_L^0\pi^+\pi^-$	17
21	5.4 Other external inputs	19
22	6 Event Selection	20
23	6.1 Tag modes	20
24	6.2 General event selection	20
25	6.3 Singly tagged \bar{D}^0 selection	21
26	6.4 Double tagged \bar{D}^0 selection of fully reconstructed channels	27
27	6.5 Double tagged \bar{D}^0 selection of partially reconstructed channels	31
28	7 CP Even Fraction Measurement	34
29	7.1 With pure CP tag channels	34

1	7.2 With $\pi^+\pi^-\pi^0$ tag channel	35
2	7.3 With $K_S^0/K_L^0\pi^+\pi^-$ tag channels	35
3	7.4 With all channels	39
4	7.5 Systematic uncertainty	39
5	7.5.1 ST yields	41
6	7.5.2 DT yields	42
7	7.5.3 Input from $K_S^0/K_L^0\pi^+\pi^-$	42
8	7.5.4 Migration matrix	43
9	7.5.5 Peak background estimation with $K_S^0/K_L^0\pi^+\pi^-$ tagged	43
10	7.5.6 External inputs	44
11	7.5.7 Broken phase space due to K_S^0 veto	45
12	7.5.8 Results with all systematic uncertainty	45
13	8 Strong phase difference measurement	47
14	8.1 K_i measurement	47
15	8.2 c_i & s_i measurement	59
16	8.3 Comparison between two models	66
17	8.4 Systematic uncertainty	67
18	8.5 Cross check on CP even fraction	67
19	8.6 Impact on γ measurement	68
20	9 Summary and Discussion	70
21	Appendices	73
22	A Details about the bin schemes of $D \rightarrow 4\pi^\pm$	74
23	B Self-check on signal MC generation	75
24	C Self-check on ST	77
25	D Additional plots and tables in strong-phase difference measurement	78
26	D.1 Additional plots and tables in K_i measurement	78
27	D.2 Additional plots and tables in c_i , s_i measurement	78

¹ 1 Publication Strategy

² This note describes two sets of measurements for the channel $D \rightarrow \pi^+ \pi^- \pi^+ \pi^-$. The first is a
³ determination of the CP-even fraction (F_+); the second is a determination of the strong-phase
⁴ parameters (c_i, s_i) for a selection of binning schemes, which are developed from amplitude-based
⁵ analyses from BESIII and CLEO-c. Whereas the F_+ analysis is complete, the strong-phase
⁶ analysis is not final because the BESIII amplitude analysis on which it depends (BAM-00439)
⁷ has itself not been finalised. Therefore we propose to publish first the F_+ result, and afterwards
⁸ complete and publish the strong-phase measurements following the finalisation of BAM-00439.
⁹ Although this Memo contains a discussion of both studies, we ask the review committee to
¹⁰ initially focus on the F_+ measurement, which concludes in Section [7](#).

1 2 Introduction

2 The Cabibbo-Kobayashi-Maskawa (CKM) matrix is used to describe the couplings between
 3 charged-current $W^{+/-}$ interactions and the quarks. The elements of the CKM matrix are funda-
 4 mental parameters of the Standard Model (SM). The unitarity of the CKM matrix imposes six
 5 equations: $\sum_i V_{ij}V_{ik}^* = \delta_{jk}$ and $\sum_j V_{ij}V_{kj}^* = \delta_{ik}$, which provide a window to test SM and search for
 6 New Physics. These six combinations could be represented as triangles in the complex plane.
 7 The most commonly used one is

$$V_{ud}V_{ub}^* + V_{cd}V_{cb}^* + V_{td}V_{tb}^* = 0. \quad (1)$$

8 As Fig. 1 shown, three angles of the unitarity triangle are defined as:

$$\begin{aligned} \beta &\equiv \phi_1 = \arg\left(-\frac{V_{cd}V_{cb}^*}{V_{td}V_{tb}^*}\right), \\ \alpha &\equiv \phi_2 = \arg\left(-\frac{V_{td}V_{tb}^*}{V_{ud}V_{ub}^*}\right), \\ \gamma &\equiv \phi_3 = \arg\left(-\frac{V_{ud}V_{ub}^*}{V_{cd}V_{cb}^*}\right). \end{aligned} \quad (2)$$

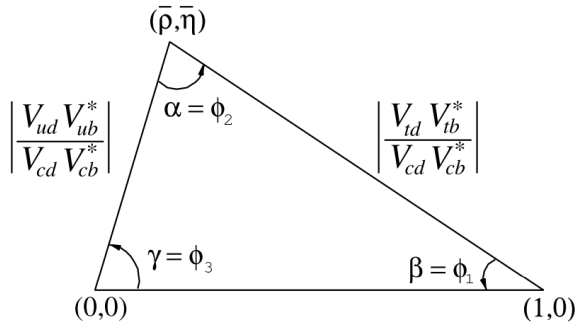


Figure 1: The unitarity triangle.

9 The γ angle doesn't depend on the CKM elements involving the top quark, so it can be
 10 measured in tree-level B decays, such as $B^{+/-} \rightarrow D^{(*)}K^{(*)+/-}$. In these B decays, the γ can be
 11 extracted through the interference of $b \rightarrow c\bar{s}$ and $b \rightarrow u\bar{s}$ processes. [1, 2, 3, 4] So the D meson
 12 could be both D^0 and \bar{D}^0 . And the decay final states could be chosen as self-conjugate states, such
 13 as $K_S^0/K_L^0\pi^+\pi^-$, $K_S^0/K_L^0K^+K^-$, $\pi^+\pi^-\pi^+\pi^-$, $K^+K^-\pi^+\pi^-$, $K_S^0\pi^+\pi^-\pi^0$... [4, 5] In these measurements,
 14 the D meson's decay information, such as CP-even fraction (F_+) or strong-phase difference
 15 ($\Delta\delta_D$) are needed. Although in principle these necessary information could be calculated from
 16 some amplitude models, [6, 7] this results from model calculation will cause model-dependent

1 uncertainty in the result of γ angle. An alternate way is measuring these information using
2 quantum-correlated $D^0\bar{D}^0$ data provided by a charm factory, which is model-independent.

3 The current experimental results of CP-even fraction and strong-phase difference are both
4 measured by CLEO-c with a $\psi(3770)$ data set corresponding to 818 pb^{-1} luminosity. [8, 9]

5 BESIII's 2.93 fb^{-1} of $\psi(3770)$ data set provides a chance to make a more precise measurement.

6 In this memo, we presented the measurement of the CP-even fraction and strong-phase difference
7 in $D \rightarrow \pi^+\pi^-\pi^+\pi^-$ using BESIII's data. For strong-phase difference, results of all bin schemes
8 (including 5 CLEO-c's binning schemes and 4 BESIII's binning schemes) are shown, but only

9 BESIII's binning schemes are valuable to be shown in the eventual paper.

10 This memo is organized as follows. The Section.3 shows the basic formulas in this analysis.

11 The Section.4 describes the BESIII detector. The Section.5 shows the data/MC sets and external
12 inputs used in this analysis. The Section.6 presents the event selections. The Section.7 shows the

13 CP-even fraction measurement. The Section.8 shows the strong-phase difference measurement.

1 3 Formalism

2 Let's discuss about γ measurement in decays $B^{+/-} \rightarrow DK^{+/-}$ first.¹ The amplitudes can be
 3 written as:

$$\mathcal{A}(B^- \rightarrow D^0 K^-) \equiv A_B, \quad \mathcal{A}(B^- \rightarrow \bar{D}^0 K^-) \equiv A_B r_B e^{i(\delta_B - \gamma)} \quad (3)$$

4 where the strong-phase of A_B is set to zero by convention, r_B is the ratio of these two decays and
 5 δ_B is the strong-phase difference between the these two amplitudes.

6 There are three methods depending on the final states of D:

- 7 • GLW method for (quasi-)CP final states, e.g. $K_S^0 \pi^0, \pi^+ \pi^- \pi^+ \pi^-$ etc; [1, 2]
- 8 • ADS method for Cabibbo favored (CF) and double Cabibbo suppressed (DCS) final states,
 9 e.g. $K^\pm \pi^\mp, K^\pm \pi^\mp \pi^\pm \pi^\mp$ etc; [3]
- 10 • GGSZ method for self-conjugate multibody final states, e.g. $K_S^0 / K_L^0 \pi^+ \pi^-, K_S^0 / K_L^0 K^+ K^-,$
 11 $\pi^+ \pi^- \pi^+ \pi^-$ etc; [4]

12 in both three methods, the decay information of D decays are needed (except the pure CP final
 13 stats). For $D \rightarrow \pi^+ \pi^- \pi^+ \pi^-$ case, both GLW and GGSZ methods can be used. For GLW method,
 14 the CP-even fraction of D decays is needed. [10] For GGSZ method, the strong-phase difference
 15 is needed.

16 3.1 GGSZ method

17 The GGSZ method is using self-conjugate multibody final states to extract γ . This method
 18 is well introduced in Ref.[4] and other similar analysis work in BESIII. [11, 12, 13] A brief
 19 introduction is shown in this section.

20 The amplitude of $D^0 \rightarrow 4\pi^\pm$ can be written as:

$$\mathcal{A}(D^0 \rightarrow 4\pi^\pm) \equiv A_f = a_f e^{i\delta_f}, \quad (4)$$

21 where the δ_f is the strong-phase at f phase space point, and A_f is normalized. Assuming no CP
 22 violation in $D \rightarrow 4\pi^\pm$ and neglecting second order effects due to charm mixing, the amplitude of
 23 $\bar{D}^0 \rightarrow 4\pi^\pm$ is:

$$\mathcal{A}(\bar{D}^0 \rightarrow 4\pi^\pm)_f = A_{-f} = a_{-f} e^{i\delta_{-f}}, \quad (5)$$

¹here only use $B^{+/-} \rightarrow DK^{+/-}$ as an example, other final states ($D^* K, DK^*$) should be similar.

¹ Then the amplitude of $B^- \rightarrow \bar{D}K^-, \bar{D} \rightarrow 4\pi^\pm$ is:

$$\begin{aligned}\mathcal{A}(B^- \rightarrow (4\pi^\pm)_D K^-)_f &= A_B(A_f + r_B e^{i(\delta_B - \gamma)} A_{-f}) \\ &= A_B(a_f e^{i\delta_f} + r_B e^{i(\delta_B - \gamma)} a_{-f} e^{i\delta_{-f}})\end{aligned}\quad (6)$$

² Then the reduced differential decay rate of such process is:

$$d\Gamma(B^- \rightarrow (4\pi^\pm)_D K^-)_f = |A_B|^2(a_f^2 + r_B^2 a_{-f}^2 + 2r_B a_f a_{-f} [\cos(\delta_B - \gamma) \cos(\Delta\delta_D) + \sin(\delta_B - \gamma) \sin(\Delta\delta_D)]), \quad (7)$$

³ where $\Delta\delta_D$ is $\delta_f - \delta_{-f}$, the strong-phase difference between $D^0 \rightarrow 4\pi^\pm$ and $\bar{D}^0 \rightarrow 4\pi^\pm$.

⁴ Experimentally, the phase space is always divided into several local phase space. Thus the
⁵ integration over one local phase space is:

$$\Gamma_i = \int_i d\Phi_f |A_B|^2(a_f^2 + r_B^2 a_{-f}^2 + 2r_B a_f a_{-f} [\cos(\delta_B - \gamma) \cos(\Delta\delta_D) + \sin(\delta_B - \gamma) \sin(\Delta\delta_D)]) \quad (8)$$

⁶ Using the following definitions:

$$\begin{aligned}K_i &\equiv \int_i a_f^2 d\Phi, \\ K_{-i} &\equiv \int_i a_{-f}^2 d\Phi, \\ c_i &\equiv \frac{1}{\sqrt{K_i \bar{K}_i}} \int_i a_f a_{-f} \cos(\Delta\delta_D) d\Phi, \\ s_i &\equiv \frac{1}{\sqrt{K_i \bar{K}_i}} \int_i a_f a_{-f} \sin(\Delta\delta_D) d\Phi,\end{aligned}\quad (9)$$

⁷ the Eq. 8 can be written as:

$$\Gamma_i = |A_B|^2(K_i + r_B^2 K_{-i} + 2r_B \sqrt{K_i K_{-i}} [\cos(\delta_B - \gamma) c_i + \sin(\delta_B - \gamma) s_i]), \quad (10)$$

⁸ Then this formula can be used to extract γ , if K_i , c_i , and s_i are well determined.

⁹ 3.2 Quantum correlations of $D^0 \bar{D}^0$

¹⁰ In the data set of 2.93 fb^{-1} taken at $\sqrt{s} = 3.773 \text{ GeV}$, the $D^0 \bar{D}^0$ pair is from $\psi(3770)$. So the
¹¹ $D^0 \bar{D}^0$ system should be anti-symmetric under charge conjugation. The wave function could be
¹² written as

$$|\psi(3770)\rangle = \frac{(|D^0\rangle |\bar{D}^0\rangle - |\bar{D}^0\rangle |D^0\rangle)}{\sqrt{2}} \quad (11)$$

¹³ Let's consider the decay of $\psi(3770) \rightarrow D^0 \bar{D}^0 \rightarrow fg$. (Through this memo, f represents the signal
¹⁴ channel $\pi^+ \pi^- \pi^+ \pi^-$ and g represents the tag channel.) The amplitude of such decay could be
¹⁵ written as

$$A(f, t_1; g, t_2) = \frac{(\langle f | H | D^0(t_1) \rangle \langle g | H | \bar{D}^0(t_2) \rangle - \langle f | H | \bar{D}^0(t_1) \rangle \langle g | H | D^0(t_2) \rangle)}{\sqrt{2}} \quad (12)$$

1 Using the definitions of $A_f = \langle f|H|D^0 \rangle$, $\bar{A}_f = \langle f|H|\bar{D}^0 \rangle$, $A_g = \langle g|H|D^0 \rangle$, $\bar{A}_g = \langle g|H|\bar{D}^0 \rangle$, $\Gamma = (\Gamma_1 +$
 2 $\Gamma_2)/2$, $x = (m_1 - m_2)/\Gamma$, $y = (\Gamma_1 - \Gamma_2)/\Gamma$, $A_{f\bar{g}} = A_f \bar{A}_g - \bar{A}_f A_g$, $A_{fg} = \frac{p}{q} A_f A_g - \frac{q}{p} \bar{A}_f \bar{A}_g$, by integrating
 3 the squared amplitude over $0 < t_1, t_2 < \infty$ and ignoring CP violation ($\frac{p}{q} = 1$), the decay rate is
 4 given by:

$$\frac{d\Gamma(f;g)}{d\Phi} \propto [(1 + \frac{y^2 - x^2}{2})|A_{f\bar{g}}|^2 + (\frac{y^2 + x^2}{2})|A_{fg}|^2] \quad (13)$$

5 Here only items larger than $O(x^2, y^2)$ are kept.

6 For the decay $\psi(3770) \rightarrow D^0 \bar{D}^0 \rightarrow f_i g_j$, i.e. the f final states is in i -th bin and g is in j -th bin,
 7 by integrating the decay rate over the phase space region i and j the Eq.13 could be written as

$$\begin{aligned} \Gamma[\psi(3770) \rightarrow D\bar{D} \rightarrow f_i g_j] \propto & (1 + \frac{y^2 - x^2}{2})[K_i^f \bar{K}_j^g + \bar{K}_i^f K_j^g - 2\sqrt{K_i^f \bar{K}_j^g \bar{K}_i^f K_j^g}(c_i^f c_j^g + s_i^f s_j^g)] \\ & + (\frac{y^2 + x^2}{2})[K_i^f K_j^g + \bar{K}_i^f \bar{K}_j^g - 2\sqrt{K_i^f \bar{K}_j^g \bar{K}_i^f K_j^g}(c_i^f c_j^g - s_i^f s_j^g)]. \end{aligned} \quad (14)$$

8 For the case only one D meson is tagged, which is known as single-tag, the g represents all
 9 possible final states and $K^g \equiv \bar{K}^g \equiv 1$, $s^g \equiv 0$ and $c^g \equiv y$. Then the Eq. 14 could be written as

$$\Gamma[\psi(3770) \rightarrow D\bar{D} \rightarrow f_i X] \propto (1 + y^2)[K_i^f + \bar{K}_i^f - 2\sqrt{K_i^f \bar{K}_i^f} c_i^f y] \quad (15)$$

10 3.3 CP-even fraction measurement

11 The CP-even fraction in total phase space is defined as:

$$F_+^f = \frac{\int |A_+|^2 d\Phi_f}{\int |A_+|^2 + |A_-|^2 d\Phi_f} = \frac{\int |A_f|^2 + |\bar{A}_f|^2 + 2|A_f||\bar{A}_f|\cos\delta_f d\Phi_f}{\int 2(|A_f|^2 + |\bar{A}_f|^2) d\Phi_f} \quad (16)$$

12 where $A_\pm = A_{D^0} \pm A_{\bar{D}^0}$ is the decay amplitude for a D meson in a CP -even or CP -odd state. In
 13 different tag channels, the F_+ can be present in the total decay rate and the number of selected
 14 events.

15 3.3.1 Using pure CP tag channels

16 For CP tag channels, by integrating the decay rate over the phase space, the expected double
 17 tag events and single tag events can be given by:²

$$N(4\pi^\pm, g) = 2N_{D^0\bar{D}^0}(1 + y^2)\mathcal{B}(4\pi^\pm)\mathcal{B}(g)[1 - \eta_{CP}^g(2F_+^{4\pi^\pm} - 1)], \quad (17)$$

$$N(g) = 2N_{D^0\bar{D}^0}(1 + y^2)\mathcal{B}(g)[1 - \eta_{CP}^g y], \quad (18)$$

18 where η_{CP} is the CP eigenvalue. Experimentally, a ratio of double tag events to single tag events
 19 could avoid from the uncertainties from $N_{D^0\bar{D}^0}$, $\mathcal{B}(4\pi^\pm)$, $\mathcal{B}(g)$, i.e. :

$$N^\pm \equiv N(4\pi^\pm, g)[1 - \eta_{CP}^g y]/N(g) = \mathcal{B}(4\pi^\pm)[1 - \eta_{CP}^g(2F_+^{4\pi^\pm} - 1)]. \quad (19)$$

²In this section, let's assume the efficiency is 100% and ignore possible peak background.

¹ With the N^\pm , the F_+ could be calculated by:

$$F_+ = \frac{N^+}{N^+ + N^-} \quad (20)$$

² 3.3.2 Using $K_{S,L}^0\pi^+\pi^-$ tag channels

³ For $K_{S,L}^0\pi^+\pi^-$ tag channels, the well-measured information in the local phase space could help
⁴ in $F_+^{4\pi^\pm}$ measurement. The binning scheme follows the “Equal $\Delta\delta_D$ BABAR 2008”. Since the
⁵ expected distribution of entries is symmetric, the events in the absolute bin number $|i|$ are
⁶ considered.

⁷ By integrating decay rate over total phase space of $4\pi^\pm$ and specific phase space, the expected
⁸ double tag events of bin $|i|$ tagged with $K_S^0\pi^+\pi^-$ is given by:

$$N(4\pi^\pm, |i|) = N_{D^0\bar{D}^0}(1 + y^2)\mathcal{B}(4\pi^\pm)[K_i + K_{-i} - 2\sqrt{K_i K_{-i}}c_i(2F_+^{4\pi^\pm} - 1)] \quad (21)$$

⁹ The first three terms should be same for all i case, then could be represented as a normal factor:

$$N(4\pi^\pm, |i|) = h[K_i + K_{-i} - 2\sqrt{K_i K_{-i}}c_i(2F_+^{4\pi^\pm} - 1)] \quad (22)$$

¹⁰ For the $K_L^0\pi^+\pi^-$ tag case, the formula is same except the reversed sign of the third term:

$$N'(4\pi^\pm, |i|) = h'[K'_i + K'_{-i} + 2\sqrt{K'_i K'_{-i}}c'_i(2F_+^{4\pi^\pm} - 1)] \quad (23)$$

¹¹ 3.3.3 Using other self-conjugate tag channels

¹² The other self-conjugate tag channels($\pi^+\pi^-\pi^0$, $4\pi^\pm$), also provide a chance to measure the $F_+^{4\pi^\pm}$.
¹³ In this section, only $\pi^+\pi^-\pi^0$ case is shown. Similar with Eq.19, the ratio of the expected
¹⁴ $\pi^+\pi^-\pi^0 v.s. 4\pi^\pm$ events to the expected $\pi^+\pi^-\pi^0$ single tag events can be given by:

$$\begin{aligned} N^{\pi^+\pi^-\pi^0} &\equiv N(4\pi^\pm, \pi^+\pi^-\pi^0)[1 - (2F_+^{\pi^+\pi^-\pi^0} - 1)y]/N(\pi^+\pi^-\pi^0) \\ &= \mathcal{B}(4\pi^\pm)[1 - (2F_+^{\pi^+\pi^-\pi^0} - 1)(2F_+^{4\pi^\pm} - 1)]. \end{aligned} \quad (24)$$

¹⁵ Combining with N^+ from Eq.19, the ratio $N^{\pi^+\pi^-\pi^0}/N^+$ can be given by:

$$\frac{N^{\pi^+\pi^-\pi^0}}{N^+} = \frac{[1 - (2F_+^{\pi^+\pi^-\pi^0} - 1)(2F_+^{4\pi^\pm} - 1)]}{2F_+^{4\pi^\pm}} \quad (25)$$

¹⁶ which can be rearranged as:

$$F_+ = \frac{N^+ F_+^{\pi^+\pi^-\pi^0}}{N^{\pi^+\pi^-\pi^0} - N^+ + 2N^+ F_+^{\pi^+\pi^-\pi^0}} \quad (26)$$

¹ 3.4 Strong-phase difference measurement

² The strong-phase difference $\Delta\delta_D$, expressed as c_i and s_i terms, are presented in quantum corre-
³ lated data $\psi(3770)$ decays, as shown in Sec. 3.2.

⁴ For CP tag channels, the double tag yield in $4\pi^\pm$'s i -th bin can be written as:

$$N(cp, i) = (N_{cp,ST})(K_i + K_{-i} - 2\sqrt{K_i K_{-i}} c_i \eta_{CP}) / (2N_{flavor,ST}) / (1 - \eta_{CP}^g y), \quad (27)$$

⁵ where the $N_{cp,ST}$ is the single CP tag yield, the η_{CP} is the CP eigenvalue, and $N_{flavor,ST}$ is the
⁶ single flavor tag yield. This equation is also symmetry for bin i and bin $-i$. Furthermore, this
⁷ equation can be extended to $\pi^+\pi^-\pi^0$ tag channel, with η_{CP} replaced by $(2F_+^{\pi^+\pi^-\pi^0} - 1)$.

⁸ For $K_S^0/K_L^0\pi^+\pi^-$ (or $K_L^0/K_L^0K^+K^-$) tag channels, the double tag yield in $4\pi^\pm$'s i -th bin and
⁹ $K_S^0/K_L^0\pi^+\pi^-$'s j -th bin can be written as:

$$N(i, j) = N_{D\bar{D}} * (K_i K_{-j} + K_{-i} K_j \mp 2\sqrt{K_i K_{-j} K_{-i} K_j} (c_i c_j + s_i s_j)) / (2N_{flavor,ST} N'_{flavor,ST}), \quad (28)$$

¹⁰ where the K_j , c_j , s_j , $N_{flavor,ST}$ are tag side's information, the \mp is associated with different CP
¹¹ eigenvalue of K_S^0 and K_L^0 . It's worth to mention that this equation is same for bin (i, j) and bin
¹² $(-i, -j)$.

1 4 The BEPCII and BESIII detector

2 The Beijing Electron Positron Collider II (BEPCII) [14] is a double-ring multi-bunch collider
3 with a reached design luminosity of $10^{33}\text{cm}^{-2}\text{s}^{-1}$ at 3.773 GeV, which is working at the center-of-
4 mass energy from 2 to 4.9 GeV.

5 The BESIII detector is a spectrometer located at the BEPCII, and its main parts are a
6 helium-gas-based drift chamber (MDC), a plastic scintillator time-of-flight (TOF), and a CsI(Tl)
7 electromagnetic calorimeter (EMC), which are all enclosed in a superconducting solenoid magnet
8 providing a 1.0T magnetic field. The solenoid is supported by an octagonal flux-return yoke
9 with modules of resistive plate muon counters (MUC) interleaved with steel. The acceptance
10 of charged particles and photons is 93% over 4π solid angle. The charged-particle momentum
11 resolution at 1 GeV/c is 0.5%, and the dE/dx resolution is 6% for the electrons from Bhabha
12 scattering. The EMC measures photon energies with a resolution of 2.5% (5%) at 1 GeV in the
13 barrel (end cap) region. The time resolution of the TOF barrel part is 68 ps, while that of the
14 end cap part is 110 ps. A detailed description of BESIII detector is provided in Ref. [15].

1 5 Data sets, MC simulation and external information

2 5.1 Data sets and MC simulation

3 The analysis is performed based on $(2931.8 \pm 0.2 \pm 13.8)$ pb $^{-1}$ $\psi(3770)$ data samples reconstructed
 4 with BOSS version V6.6.4.p02 collected with the BESIII detector at center-of-mass energy $\sqrt{s} =$
 5 3.773 GeV in years 2010 and 2011 [16]. The inclusive MC samples including $e^+e^- \rightarrow D^0\bar{D}^0$ (no
 6 quantum correlation), $e^+e^- \rightarrow D^+\bar{D}^-$, $e^+e^- \rightarrow$ non-DD, $e^+e^- \rightarrow q\bar{q}$, $e^+e^- \rightarrow \tau^+\tau^-$, $e^+e^- \rightarrow \mu^+\mu^-$,
 7 $e^+e^- \rightarrow \gamma J/\psi$, $e^+e^- \rightarrow \gamma\psi(3686)$, are generated with several times luminosity compared to data,
 8 shown as Tab 1. In the official $e^+e^- \rightarrow D^0\bar{D}^0$ inclusive MC sample, there are some possible peak
 9 background channels generated with wrong branching ratio. In this work, these processes are
 10 corrected according to PDG [17], shown as Tab 2.

Table 1: The summaries of inclusive MC information.

MC sample	Luminosity(\times data $\int \mathcal{L} dt$)	
	2010	2011
$D^0\bar{D}^0$	21.8	21.8
D^+D^-	10.9	10.8
non $D\bar{D}$	10.8	10.1
$q\bar{q}$	7.8	7.3
$\tau\tau$	10.8	10.1
$\mu\mu$	5	5
$\gamma J/\psi$	10.8	10.1
$\gamma\psi(3686)$	10.8	10.1

Table 2: The summaries of corrected branching ratios information.

channel	BR in inclusive MC (%)	PDG(2020) (%)
$D^0 \rightarrow \pi^+\pi^-\pi^+\pi^-$	0.673	0.756 ± 0.02
$D^0 \rightarrow \pi^+\pi^-\pi^0$	2.28	1.49 ± 0.06
$D^0 \rightarrow K_S^0 K^- \pi^+$	0.521	0.33 ± 0.05
$D^0 \rightarrow K_S^0 K^+ \pi^-$	0.323	0.217 ± 0.034
$D^0 \rightarrow K_S^0 \pi^+ \pi^- \pi^0$	6.17	4 ± 0.6
$D^0 \rightarrow \pi^+\pi^-\pi^0\pi^0$	2.085	1.02 ± 0.09

Table 3: The summaries of tag channels.

type	tag channel
Flavoured	$K^\pm\pi^\mp, K^\pm\pi^\mp\pi^0, K^\pm\pi^\mp\pi^\pm\pi^\mp, K^\pm e^\mp\nu$
CP even	$K^+K^-, \pi^+\pi^-, K_S^0\pi^0\pi^0, K_L^0\pi^0, K_L^0\omega, \pi^+\pi^-\pi^0$
CP odd	$K_S^0\pi^0, K_S^0\eta(\gamma\gamma, \pi^+\pi^-\pi^0), K_S^0\eta'(\rho\gamma, \pi^+\pi^-\eta(\gamma\gamma)), K_S^0\omega, K_L^0\pi^0\pi^0$
Self-conjugate	$K_S^0\pi^+\pi^-, K_L^0\pi^+\pi^-, K_S^0KK, \pi^+\pi^-\pi^+\pi^-$

11 The tag channels are summarized in Tab. 3. To estimate the signal efficiency and model

1 the signal line shape, signal MC samples are generated with 2×10^5 events for each tag channel.
 2 And the signal MC is generated including the quantum correlation effect with the amplitude
 3 model from the partial wave analysis of BAM-00439. [7] For the $K_S^0/K_L^0\pi^+\pi^-$ tag channel, the
 4 decay model is the Dalitz model. [18] To include the quantum correlation effect, the generation
 5 procedure for different tag channel is different. For flavor tagged, CP even and CP odd tagged,
 6 it's quite simple, just using the amplitude of D^0/\bar{D}^0 decays or $D(CPeven)$ and $D(CPodd)$ decays
 7 to describe the $4\pi^\pm$ side. For $K_S^0/K_L^0\pi^+\pi^-$ tagged, the MC generation is a little bit complicated.
 8 At first, huge MC events of $\psi(3770) \rightarrow DD, DD \rightarrow K_S^0/K_L^0\pi^+\pi^-, 4\pi^\pm$ are generated, where the
 9 model of $\psi(3770) \rightarrow DD$ is still VSS model, the models of $D \rightarrow K_S^0/K_L^0\pi^+\pi^-$ and $D \rightarrow 4\pi^\pm$ are
 10 both PHSP model. Then using the amplitude model of $D^0/\bar{D}^0 \rightarrow 4\pi^\pm$ and $D^0/\bar{D}^0 \rightarrow K_S^0/K_L^0\pi^+\pi^-$,
 11 the amplitude of $\psi(3770) \rightarrow DD, DD \rightarrow K_S^0/K_L^0\pi^+\pi^-, 4\pi^\pm$ for each event is calculated including
 12 the quantum correlation effect appropriately. According to the amplitude of each event, the
 13 events from the initial vary large MC are accepted or rejected. The surviving events then are
 14 the appropriate MC for $K_S^0/K_L^0\pi^+\pi^-$ tagged case. (App. B shown a self-check on the signal MC,
 15 which confirm the signal MC is reliable especially for the interests in this analysis.)

16 All the MC samples are generated based on software package GEANT4 [19], in which the
 17 description of geometric and material of BESIII detector, the detector response and digitization
 18 models, as well as the detector running conditions and performance are included. The production
 19 of $\psi(3770)$ in the electron-positron collision is simulated with generator KKMC [20]. The decay
 20 modes of $\psi(3770)$ and D mesons are generated with generator EVTGEN [21].

21 5.2 Binning schemes of $4\pi^\pm$

22 As mentioned before, in the strong-phase difference measurement, the whole phase space of
 23 $4\pi^\pm$ needs to be separated to several local phase spaces (bins). Although an imperfect binning
 24 scheme will not bring any bias in the result of γ , but may influence the sensitivity of γ .

25 For $D \rightarrow 4\pi^\pm$, 5 variables are needed to describe the phase space. In this work, same as
 26 previous CLEO-c's work [8], the variables $\{m_+, m_-, \cos\theta_+, \cos\theta_-, \phi\}$ are chosen, where $m_+(m_-)$ is
 27 the invariant mass of $\pi^+\pi^+(\pi^-\pi^-)$, $\theta_+(\theta_-)$ is the helicity angle of the $\pi^+\pi^+(\pi^-\pi^-)$ pair, and ϕ is the
 28 angle between the $\pi^+\pi^+$ and $\pi^-\pi^-$ decay planes. (A detail defnition of these five variables can be
 29 found in App. A) Then the binning schemes are accessed by the corresponding five-dimensional
 30 hyperbins, which are technically supported by the HyperPlot package, same as CLEO-c's work.

31 3

³<http://samharnew.github.io/HyperPlot/index.html>

For the binning schemes, both the CLEO-c's binning schemes in Ref. [8] and the BESIII's binning schemes are used. All of them separate the phase space of $D \rightarrow 4\pi^\pm$ into 10 phase spaces (5 pairs), labels from -5 to 5. For the CLEO-c's binning schemes, there are five: Equal $\Delta\delta_p^{4\pi}$ Binning, Variable $\Delta\delta_p^{4\pi}$ Binning, Alternative Binning, Optimal Binning, Optimal Alternative Binning. For the binning schemes determined by the BESIII's amplitude model, total four schemes are determined and used in this work: BESIII's Equal $\Delta\delta_p^{4\pi}$ Binning, BESIII's Alternative Binning, BESIII's Optimal Binning, BESIII's Optimal Alternative Binning. The details of these four BESIII's schemes are shown below.

5.2.1 BESIII's Equal $\Delta\delta_p^{4\pi}$ binning scheme

The first scheme is “Equal $\Delta\delta_p^{4\pi}$ binning scheme”, which’s purpose is dividing the phase space according to the strong-phase difference:

$$\begin{aligned} +i &:= \forall p : (i-1)\pi/\mathcal{N} < \Delta\delta_D < i\pi/\mathcal{N}, \\ -i &:= \forall p : -(i-1)\pi/\mathcal{N} > \Delta\delta_D > -i\pi/\mathcal{N}, \end{aligned} \quad (29)$$

where $\Delta\delta_D$ is calculated from the amplitude model [7], \mathcal{N} is 5. Since $\Delta\delta_p^{4\pi} \equiv -\Delta\delta_{\bar{p}}^{4\pi}$, this binning scheme shall automatically fulfil the requirement that bin $+i$ maps to bin $-i$ under CP .

As mentioned before, this scheme is accessed by the five-dimensional hyperbins. Because it’s more convenient to determine the hyper-binning boundaries for rectangle phase space, the $\{m_+, m_-\}$ is transformed to $\{m'_+, m'_-\}$ by:

$$m'_\pm = m_\pm + \delta, \text{ where } \delta = \min\{m_+, m_-\} - m_{\min}, \quad (30)$$

where m_{\min} is the minimum value of m_\pm , i.e. $2m_\pi$. Then the five-dimensional phase space $\{m'_+, m'_-, \cos\theta_+, \cos\theta_-, \phi\}$ is rectangle. The total kinematically allowed region is a hypervolume defined by the corners $\{m_{\min}, m_{\min}, -1, -1, -\pi\}$ and $\{m_{\max}, m_{\max}, +1, +1, +\pi\}$. By the symmetries of the system, including the CP -conjugation and identical particle interchange:

$$\begin{aligned} CP\{m'_+, m'_-, \cos\theta_+, \cos\theta_-, \phi\} &\rightarrow \{m'_-, m'_+, \cos\theta_-, \cos\theta_+, -\phi\}, \\ [\pi_1^+ \leftrightarrow \pi_2^+] \{m'_+, m'_-, \cos\theta_+, \cos\theta_-, \phi\} &\rightarrow \{m'_+, m'_-, -\cos\theta_+, \cos\theta_-, \phi - \pi\}, \\ [\pi_1^- \leftrightarrow \pi_2^-] \{m'_+, m'_-, \cos\theta_+, \cos\theta_-, \phi\} &\rightarrow \{m'_+, m'_-, \cos\theta_+, -\cos\theta_-, \phi - \pi\}, \end{aligned} \quad (31)$$

the entire phase space can be folded to a small one: from $\{m_{\min}, m_{\min}, 0, 0, 0\}$ to $\{m_{\max}, m_{\max}, +1, +1, +\pi\}$.

The algorithm to set the bin boundaries is same with CLEO-c’s work, implemented by the HyperPlot package. Begin with the entire one hypervolume (from $\{m_{\min}, m_{\min}, 0, 0, 0\}$ to $\{m_{\max}, m_{\max}, +1, +1, +\pi\}$), at each iteration of the algorithm, the hypervolumes from the previous

iteration are splits in two, choosing to split in the dimension that has the fastest varying $\Delta\delta_D$, and picking a split point that is as close as possible to one of the bin boundaries defined in Eq. 29. When either: splitting a hypervolume will always result in two hypervolumes with the same bin number; splitting a hypervolume will always result in a hypervolume that has an edge length shorter than the minimum allowed. The minimum edge lengths (bin widths) are {39 MeV, 39 MeV, 0.06, 0.06, 0.19 rad}, which is same as CLEO-c's work. With the current algorithm and the amplitude model of $D \rightarrow 4\pi^\pm$, the total number of hypervolumes are $\sim 280,000$.

5.2.2 BESIII's Alternative binning scheme

Besides the Equal $\Delta\delta_D$ binning scheme, the Alternative binning scheme is also one target scheme. The purpose is to enhance the interference by enlarging the K_i/K_{-i} . This could be achieved by the following bin number definition:

$$\begin{aligned} +i &:= \forall p : \left[-\pi + \frac{2\pi}{N}(i-1) < +\Delta\delta_D < -\pi + \frac{2\pi}{N}i \right] \& [r_p^{4\pi} > 1], \\ -i &:= \forall p : \left[-\pi + \frac{2\pi}{N}(i-1) < -\Delta\delta_D < -\pi + \frac{2\pi}{N}i \right] \& [r_p^{4\pi} < 1], \end{aligned} \quad (32)$$

where $r_p^{4\pi}$ is $|A_p^{4\pi}/\bar{A}_p^{4\pi}|$. The BESIII Equal $\Delta\delta_D$ binning scheme's hypervolumes are used here. With the $D \rightarrow 4\pi^\pm$ amplitude model, the bin number of each hypervolume is re-assigned according to the Eq. 32.

5.2.3 BESIII's Optimal binning and Optimal AlterBin binning

The above Equal $\Delta\delta_D$ binning and Alternative binning schemes could be optimized, by the Q_\pm values defined [22]:

$$Q_\pm^2 = \frac{\sum_i \left(\frac{1}{\sqrt{N_{B^\pm}^i}} \frac{dN_{B^\pm}^i}{dx_\pm} \right)^2 + \left(\frac{1}{\sqrt{N_{B^\pm}^i}} \frac{dN_{B^\pm}^i}{dy_\pm} \right)^2}{\int_D \left[\left(\frac{1}{\sqrt{\Gamma_{B^\pm}(\mathbf{p})}} \frac{d\Gamma_{B^\pm}(\mathbf{p})}{dx_\pm} \right)^2 + \left(\frac{1}{\sqrt{\Gamma_{B^\pm}(\mathbf{p})}} \frac{d\Gamma_{B^\pm}(\mathbf{p})}{dy_\pm} \right)^2 \right] d\mathbf{p}} \quad (33)$$

where $N_{B^\pm}^i$ is the expected yields of $B^\pm \rightarrow K^\pm(4\pi^\pm)_D$ in bin i in Eq. 10, $\Gamma_{B^\pm}(\mathbf{p})$ is the differential decay rate in Eq. 8. The Q_\pm describe the B decay statistical sensitivity on the parameters x_\pm and y_\pm of a certain binning scheme, devided by the statistical sensitivity of an ideal binning scheme with infinite bins. In the Q_\pm calculation, the B decay parameters and γ values are cited from the recent LHCb's measurement [23]: $r_B = 0.0986, \gamma = 67^\circ, \delta_B = 128^\circ$. The average Q value ($Q^2 = \frac{1}{2}(Q_+^2 + Q_-^2)$), is used to compare the sensitivities of different binning schemes. By scanning the bin # of all hypervolumes, the bin scheme with max Q value is determined as the Optimal binning scheme.

Ideally, there will be only one Optimal binning scheme, with the maximum Q value for all bin # possibilities. But since there are $\sim 280,000$ hypervolumes, and each hypervolume has 10 bin # possibilities, the total number of binning schemes are $\sim 10^{280,000}$. Then it's not possible to scan all possibilities. An adaptive optimise procedure is used: the hypervolumes' bin # are optimised one by one; then repeat many rounds of cycling all hypervolumes, until the Q didn't increase any more. With the current procedure and the $\sim 280,000$ hypervolumes, it's unavoidable that the optimal result will be a local maximum result and then sensitive to the initial bin #. The previous two binning schemes (BESIII's Equal $\Delta\delta_D$ and BESIII's Alternative schemes) are used as the initial bin #, corresponding to two Optimal binning schemes: Optimal (Equal) binning and Optimal Alternative binning. (This is also the reason why there are two Optimal binning schemes in CLEO-c's work.) Besides these two initial binning schemes, 1000 random bin # are used as initial bin # to seek binning schemes with larger Q value.

For the optimal binning schemes, it was found that the model predicted $K_i + \bar{K}_i$ are small for one or more bin pairs. To deal with this case, a small modification is applied on the Q value:

$$Q'^2 = Q^2 - \frac{1}{10} \sum_{i=1}^N \begin{cases} K_i + \bar{K}_i < t : & \left[\frac{K_i + \bar{K}_i - t}{t} \right]^2 \\ K_i + \bar{K}_i > t : & 0 \end{cases}, \quad (34)$$

where $t = \frac{2}{3N} \sum_{i=1}^N (K_i + \bar{K}_i)$ is the threshold. The effect of this modification of the Optimal Equal binning scheme is shown in Tab.4.

The Q value for the four BESIII's binning schemes are shown in Tab.5. In the 1000 Optimal random binning schemes, the max Q value is 0.8423, which is not larger than the Q value of Optimal Alternative scheme. So the Optimal random binning schemes are not considered any more.

Table 4: The $K_i + \bar{K}_i$ of the Optimal Equal binning scheme for the original Q and the modified Q .

bin #	1	2	3	4	5
original Q	0.40	0.24	0.11	0.19	0.06
modified Q	0.38	0.15	0.22	0.13	0.12

Table 5: The Q values of the BESIII's four binning schemes.

binning scheme	Equal $\Delta\delta_D$	Alternative	Optimal	Optimal Alternative
Q value	0.7975	0.8341	0.8405	0.8464

¹ 5.2.4 Prediction of BESIII's binning schemes

² For the four BESIII's binning schemes, the model predicted c_i , and s_i are calculated, shown as
³ Figs.2. The CLEO-c's model prediction with CLEO-c's binning schemes are also shown. It's
⁴ interesting to find that they are similar, due to same algorithm for the binning schemes, although
⁵ they are from two different amplitude models.

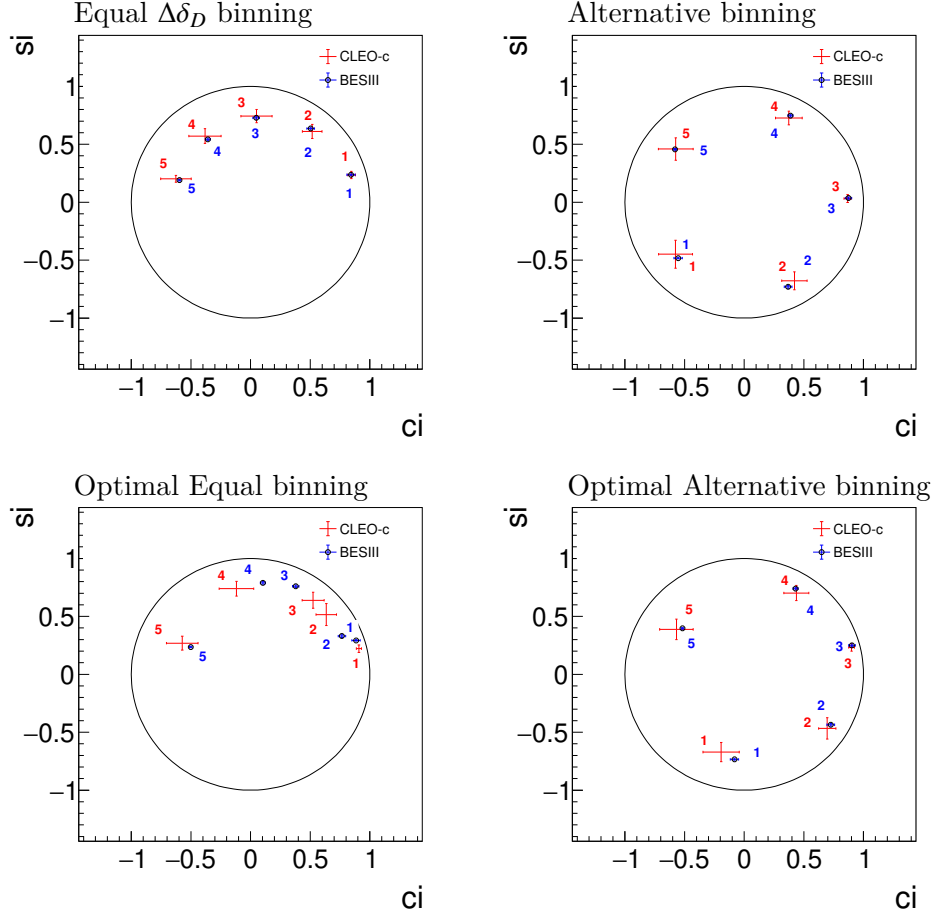
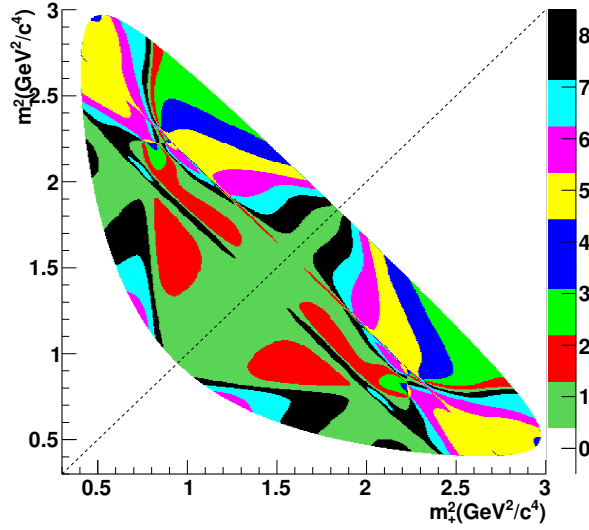


Figure 2: Model predicted c_i and s_i of four binning schemes for BESIII's model (blue dots) and CLEO-c's model (red dots with error bar).

⁶ 5.3 Inputs from $K_S^0/K_L^0\pi^+\pi^-$

⁷ In both measurements of CP-even fraction and strong-phase difference, additional information of
⁸ $K_S^0/K_L^0\pi^+\pi^-$ decay, including the strong-phase parameters (c_i, s_i) and flavor tagged yields K_i, K_{-i} ,
⁹ are needed. These values are taken from previous well measured BESIII's work [11, 12], with
¹⁰ the “Equal $\Delta\delta_D$ BABAR 2008” binning scheme, shown as Tabs. 6,7 and Fig. 3.

Figure 3: “Equal $\Delta\delta_D$ BABAR 2008” binning scheme of $K_S^0/K_L^0\pi^+\pi^-$ with $N = 8$.Table 6: strong-phase parameters of $K_S^0/K_L^0\pi^+\pi^-$ cited from Ref. [11, 12].

Bin i	$c_i(K_S^0\pi^+\pi^-)$	$s_i(K_S^0\pi^+\pi^-)$	$c_i(K_L^0\pi^+\pi^-)$	$s_i(K_L^0\pi^+\pi^-)$
1	$0.708 \pm 0.020 \pm 0.009$	$0.128 \pm 0.076 \pm 0.017$	$0.801 \pm 0.020 \pm 0.013$	$0.137 \pm 0.078 \pm 0.017$
2	$0.671 \pm 0.035 \pm 0.016$	$0.341 \pm 0.134 \pm 0.015$	$0.848 \pm 0.036 \pm 0.016$	$0.279 \pm 0.137 \pm 0.016$
3	$0.001 \pm 0.047 \pm 0.019$	$0.893 \pm 0.112 \pm 0.020$	$0.174 \pm 0.047 \pm 0.016$	$0.840 \pm 0.118 \pm 0.021$
4	$-0.602 \pm 0.053 \pm 0.017$	$0.723 \pm 0.143 \pm 0.022$	$-0.504 \pm 0.055 \pm 0.019$	$0.784 \pm 0.147 \pm 0.022$
5	$-0.965 \pm 0.019 \pm 0.013$	$0.020 \pm 0.081 \pm 0.009$	$-0.972 \pm 0.021 \pm 0.017$	$-0.008 \pm 0.089 \pm 0.009$
6	$-0.554 \pm 0.062 \pm 0.024$	$-0.589 \pm 0.147 \pm 0.031$	$-0.387 \pm 0.069 \pm 0.025$	$-0.642 \pm 0.152 \pm 0.034$
7	$0.046 \pm 0.057 \pm 0.023$	$-0.686 \pm 0.143 \pm 0.028$	$0.462 \pm 0.056 \pm 0.019$	$-0.550 \pm 0.159 \pm 0.030$
8	$0.403 \pm 0.036 \pm 0.017$	$-0.474 \pm 0.091 \pm 0.027$	$0.640 \pm 0.036 \pm 0.015$	$-0.399 \pm 0.099 \pm 0.026$

Table 7: strong-phase parameters of $K_S^0/K_L^0\pi^+\pi^-$ cited from Ref. [11, 12].

Bin i	$K_i(K_S^0\pi^+\pi^-)$	$K_{-i}(K_S^0\pi^+\pi^-)$	$K_i(K_L^0\pi^+\pi^-)$	$K_{-i}(K_L^0\pi^+\pi^-)$
1	10287.4 ± 185.9	4850.2 ± 119.1	14891.9 ± 246	7574.9 ± 165.9
2	5122.9 ± 130.6	1122.0 ± 58.6	6411.3 ± 166	1850.8 ± 89.8
3	3953.6 ± 109	1202.4 ± 58.4	5153.7 ± 143.7	1671.7 ± 83.6
4	1399 ± 67.9	911.9 ± 54.8	1893.2 ± 87.4	1043.1 ± 68.4
5	4982.5 ± 128.3	3131.7 ± 102.8	5893.2 ± 144.5	3104.0 ± 108.4
6	3377.8 ± 111.5	717.8 ± 54.1	5030.1 ± 140.7	842.9 ± 63.2
7	7354.6 ± 160.3	692.6 ± 50.3	10206.1 ± 200.5	1329.1 ± 79.6
8	7839.7 ± 169.2	1669.5 ± 734	10798 ± 222.1	3023.5 ± 109.1

¹ 5.4 Other external inputs

² In this work, there are several external input parameters besides c_i, s_i of $K_S^0/K_L^0\pi^+\pi^-$. They are
³ summaried in Tab. 8.

Table 8: The summary of external input parameters.

y(%)	$0.630^{+0.033}_{-0.030}$ [24]		
$F_+^{\pi\pi\pi^0}$	0.973 ± 0.017 [9]		
r_B	0.0986 [23]		
γ	67° [23]		
δ_B	128° [23]		
tag channel	$r(\%)$	R	$\delta(^{\circ})$
$K\pi$	5.86 ± 0.02 [25]	1	$192.1^{+8.6}_{-10.2}$ [25]
$K\pi\pi^0$	4.41 ± 0.11 [26]	0.79 ± 0.04 [26]	196 ± 11 [26]
$K\pi\pi\pi$	5.50 ± 0.07 [26]	$0.44^{+0.10}_{-0.09}$ [26]	161^{+28}_{-18} [26]

1 6 Event Selection

2 6.1 Tag modes

3 As mentioned in Sec.3, different types of tag modes could provide sensitivity to different pa-
 4 rameters in interests. The decay modes used in this work can be categorized into four types,
 5 shown as Tab. 9. For the channels without ν and K_L^0 , all the final states can be reconstructed,
 6 then these channels are called as fully reconstructed channels. For the channels with ν or K_L^0 ,
 7 due to the missed information of ν and K_L^0 , these channels are called as partially reconstructed
 channels.

Table 9: Summary of tag modes.

type	tag channel
Flavoured	$K^\pm\pi^\mp$, $K^\pm\pi^\mp\pi^0$, $K^\pm\pi^\mp\pi^\pm\pi^\mp$, $K^\pm e^\mp\nu$
CP even	K^+K^- , $\pi^+\pi^-$, $K_S^0\pi^0\pi^0$, $K_L^0\pi^0$, $K_L^0\omega$, $\pi^+\pi^-\pi^0$
CP odd	$K_S^0\pi^0$, $K_S^0\eta_{\gamma\gamma}$, $K_S^0\eta_{\pi^+\pi^-\pi^0}$, $K_S^0\eta'_{\rho\gamma}$, $K_S^0\eta'_{\pi^+\pi^-\eta(\gamma\gamma)}$, $K_S^0\omega$, $K_L^0\pi^0\pi^0$
Self-conjugate	$K_S^0\pi^+\pi^-$, $K_L^0\pi^+\pi^-$, $\pi^+\pi^-\pi^+\pi^-$

8

9 6.2 General event selection

10 The general selection criteria for good charged tracks, good photons and the intermedia reso-
 11 nance are described below.

12 The charged tracks ($\pi^{+/-}, K^{+/-}, e^{+/-}$) are reconstructed with the hits in the MDC, and re-
 13 quired :

- 14 • Helix fit: pass Kalman filter fit successfully;
- 15 • Vertex cut: $R_{xy} \leq 1.0$ cm and $|R_z| \leq 10.0$ cm, where R_{xy} and R_z are distances between the
 16 closest approach point and the run-by-run-determined interaction point (IP) in the plane
 17 perpendicular to and along the beam direction, respectively;
- 18 • Polar angle cut: $|\cos\theta| \leq 0.93$, where θ is the angle between the direction of tracks and
 19 the axis of the main drift chamber.
- 20 • Particle Identification (PID): Using the dE/dx information from MDC and time infor-
 21 mation from TOF, the probability of each particle hypothesis is calculated with the
 22 SimplePIDSvc package. For the charged particle candidates, the probabilities are required:
 23 – $\pi^{+/-}$: $\text{Prob}(\pi) > 0$, $\text{Prob}(\pi) > \text{Prob}(K)$;
 24 – $K^{+/-}$: $\text{Prob}(K) > 0$, $\text{Prob}(K) > \text{Prob}(\pi)$;

1 – $e^{+/-}$: Prob(e) > 0, Prob(e) > Prob(π), Prob(e) > Prob(K);

2 The photon candidates are reconstructed with the energy showers in the EMC, and required

3 :

- 4 • Energy threshold: $E_\gamma > 25$ MeV for the barrel region ($|\cos\theta| < 0.80$) or $E_\gamma > 50$ MeV for
 5 the endcap of EMC ($0.86 < |\cos\theta| < 0.92$).

- 6 • TDC window: the EMC time must be coincident with the collision events ($0 \leq t \leq 14$, in
 7 unit of 50 ns), to suppress electronics noise and energy deposits unrelated to the event.

8 The intermedia resonance, including $\pi^0(\gamma\gamma)$, $\eta(\gamma\gamma$ or $\pi^+\pi^-\pi^0$), $\omega(\pi^+\pi^-\pi^0)$, and $\eta'(\pi^+\pi^-\eta(\gamma\gamma)$ or $\gamma\rho$),

9 are reconstructed using the above charged tracks and photon candidates, and required:

- 10 • π^0 : $0.115 \text{ GeV}/c^2 < m(\gamma\gamma) < 0.150 \text{ GeV}/c^2$; pass the 1-C kinematic fit with invariant mass
 11 constraint to $m(\pi^0)$ in PDG [17], $\chi^2 < 20$; the momentum from the 1-C kinematic fit is
 12 used later.

- 13 • $\eta(\gamma\gamma)$: $0.480 \text{ GeV}/c^2 < m(\gamma\gamma) < 0.580 \text{ GeV}/c^2$; pass the 1-C kinematic fit with invariant
 14 mass constraint to $m(\eta)$ in PDG [17], $\chi^2 < 20$; the momentum from the 1-C kinematic fit
 15 is used later.

- 16 • $\eta(\pi^+\pi^-\pi^0)$: $0.530 \text{ GeV}/c^2 < m(\pi^+\pi^-\pi^0) < 0.565 \text{ GeV}/c^2$.

- 17 • $\omega(\pi^+\pi^-\pi^0)$: $0.750 \text{ GeV}/c^2 < m(\pi^+\pi^-\pi^0) < 0.820 \text{ GeV}/c^2$.

- 18 • $\eta'(\pi^+\pi^-\eta(\gamma\gamma))$: $0.940 \text{ GeV}/c^2 < m(\pi^+\pi^-\eta) < 0.976 \text{ GeV}/c^2$.

- 19 • $\eta'(\gamma\rho)$: $0.940 \text{ GeV}/c^2 < m(\gamma\pi^+\pi^-) < 0.970 \text{ GeV}/c^2$, $0.626 \text{ GeV}/c^2 < m(\pi^+\pi^-) < 0.924 \text{ GeV}/c^2$.

20 The K_S^0 candidates are reconstructed by two oppositely charged tracks, which are satisfied

21 with $R_z < 20.0$ cm and $|\cos\theta| < 0.93$ requirements. A secondary vertex fit is performed and the
 22 flight significance, the ratio of decay length to the decay length error ($L/\sigma(L)$), is required to
 23 be larger than 2.0. The updated momentum from the secondary vertex fit is used later. The
 24 invariant mass of $\pi^+\pi^-$ is required to be satisfied with $0.485 \text{ GeV}/c^2 < m(\pi^+\pi^-) < 0.51 \text{ GeV}/c^2$.

25 6.3 Singly tagged \bar{D}^0 selection

26 To reconstruct D^0 and \bar{D}^0 , two variables are defined: $\Delta E = E_D - E_{\text{beam}}$, $m_{\text{BC}} = \sqrt{E_{\text{beam}}^2 - |\mathbf{P}_D|^2}$,
 27 where E_D and \mathbf{P}_D are the energy and momentum of the reconstructed D, and E_{beam} is the energy
 28 of the beam which is read from data base run by run.

1 For each of the fully reconstructed channels, there may be several combinations in one event.
 2 The singly tagged D combination is selected with minimum $|\Delta E|$ from all combinations with
 3 m_{BC} larger than $1.83 \text{ GeV}/c^2$. Further more, to veto bhabha, dimu and cosmic ray events, the
 4 following selection criteria are applied for two body decay channels if there are only two good
 5 charged tracks:

- 6 • time difference of these two charged tracks should be less than 5 units.
 7 • these two charged tracks should not be identified as e^+e^- pair or $\mu^+\mu^-$ pair.
 8 • there should be at least one good shower.

9 After the above selections, there are significant backgrounds with $K_S^0 \rightarrow \pi^+\pi^-$ in $D \rightarrow$
 10 $K^\mp\pi^\pm\pi^+\pi^-$, $D \rightarrow \pi^+\pi^-\pi^0$ and $D \rightarrow \pi^+\pi^+\pi^-\pi^-$. Especially for the signal process $D \rightarrow 4\pi^\pm$, the
 11 background process $D \rightarrow K_S^0\pi^+\pi^-$'s \mathcal{B} is ~ 3.7 times to $\mathcal{B}(D \rightarrow 4\pi^\pm)$, because one is Cabibbo-
 12 Suppressed and one is Cabibbo-favored. Then it's really necessary to suppress the background
 13 from $D \rightarrow K_S^0\pi^+\pi^-$. This removal can be replicated at the B factories when they use our numbers
 14 as input. This eases the problem of background contamination for them too, just as has been
 15 done in the recently published binned $K3\pi$ analysis.[27] To study such backgrounds, an unbinned
 16 fit is performed on the $D \rightarrow K_S^0\pi\pi$ MC events, where the peak is described by two Gaussian func-
 17 tions, shown as Fig. 4. To suppress these background, K_S^0 -veto is applied: for $D \rightarrow K^\mp\pi^\pm\pi^+\pi^-$
 18 and $D \rightarrow \pi^+\pi^-\pi^+\pi^-$, any $\pi^+\pi^-$ pair satisfied with 5σ region, i.e. $0.481 < m(\pi^+\pi^-) < 0.514 \text{ GeV}/c^2$,
 19 is rejected;⁴ for $D \rightarrow \pi^+\pi^-\pi^0$, to keep an entire phase space and use the well-measured $\pi^+\pi^-\pi^0$'s
 20 F_+ , the flight significance of the $\pi^+\pi^-$ pair satisfied with $0.481 < m(\pi^+\pi^-) < 0.514 \text{ GeV}/c^2$ is
 21 required to be less than 2. According to study through MC simulation, the signal efficiency of
 22 this K_S^0 -veto is $\sim 87\%$, while the background remaining efficiency is $\sim 2.8\%$.

23 To improve the signal purity, ΔE is required to be in the three σ region which is from
 24 the binning-fit on data, shown as Tab. 10. In the binning-fit, the signal is described by two
 25 Gaussian functions and the background is described by 2-nd order Chebychev function. (For
 26 $K\pi\pi\pi$ and $\pi\pi\pi\pi$ channel, the shape from background events in inclusive MC is used to describe
 27 possible peak background.) The total mean value(μ) and standard deviation(σ) are calculated
 28 by: $\mu = f\mu_1 + (1-f)\mu_2$ and $\sigma^2 = f\sigma_1^2 + (1-f)\sigma_2^2 + f(1-f)(\mu_1 - \mu_2)^2$, where $\mu_{1,2}, \sigma_{1,2}$ are the mean
 29 value and standard deviation of the first/second Gaussian function and f is the fraction of the
 30 first Gaussian. The fitting results are shown as Figs. 5.

⁴Here one concern related to $K^\mp\pi^\pm\pi^+\pi^-$ is, after the K_S^0 -veto, the phase space is not entire. But the external strong phase parameters are corresponding to the total phase space. We checked the expected difference due to removal of this phase space region and conclude that the impact on the systematic uncertainties is negligible.

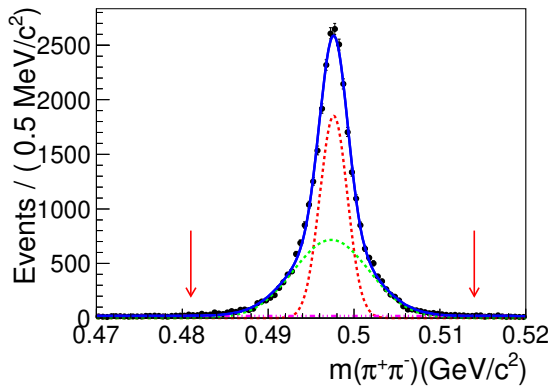


Figure 4: Fit of $m(\pi^+\pi^-)$. Dots with error bar are from $D \rightarrow K_S^0\pi\pi, \bar{D} \rightarrow K\pi$ MC. Blue solid line is total fit result, where red and green dashed lines are the two Gaussian functions and the pink dashed line is the Chebychev function.

Table 10: Summary of ΔE cut

ST channel	Mean(MeV)	Resolution(MeV)	ΔE cuts(GeV)
$K\pi$	0.89	8.71	[-0.025, 0.027]
$K\pi\pi^0$	6.28	15.54	[-0.040, 0.053]
$K\pi\pi\pi$	1.58	7.33	[-0.020, 0.024]
KK	0.67	6.83	[-0.020, 0.021]
$\pi\pi$	0.73	11.92	[-0.035, 0.036]
$K_S^0\pi^0\pi^0$	9.39	20.82	[-0.053, 0.072]
$\pi\pi\pi\pi$	1.05	8.16	[-0.023, 0.026]
$\pi\pi\pi^0$	5.38	18.76	[-0.051, 0.062]
$K_S^0\pi^0$	9.66	20.33	[-0.051, 0.071]
$K_S^0\eta_{\gamma\gamma}$	1.06	12.23	[-0.036, 0.038]
$K_S^0\eta_{\pi\pi\pi}$	3.65	10.45	[-0.028, 0.035]
$K_S^0\omega$	4.49	12.43	[-0.033, 0.042]
$K_S^0\eta'_{\pi\pi\eta}$	1.75	11.03	[-0.031, 0.035]
$K_S^0\eta'_{\gamma\pi\pi}$	3.10	9.32	[-0.025, 0.031]
$K_S^0\pi\pi$	0.92	8.08	[-0.023, 0.025]

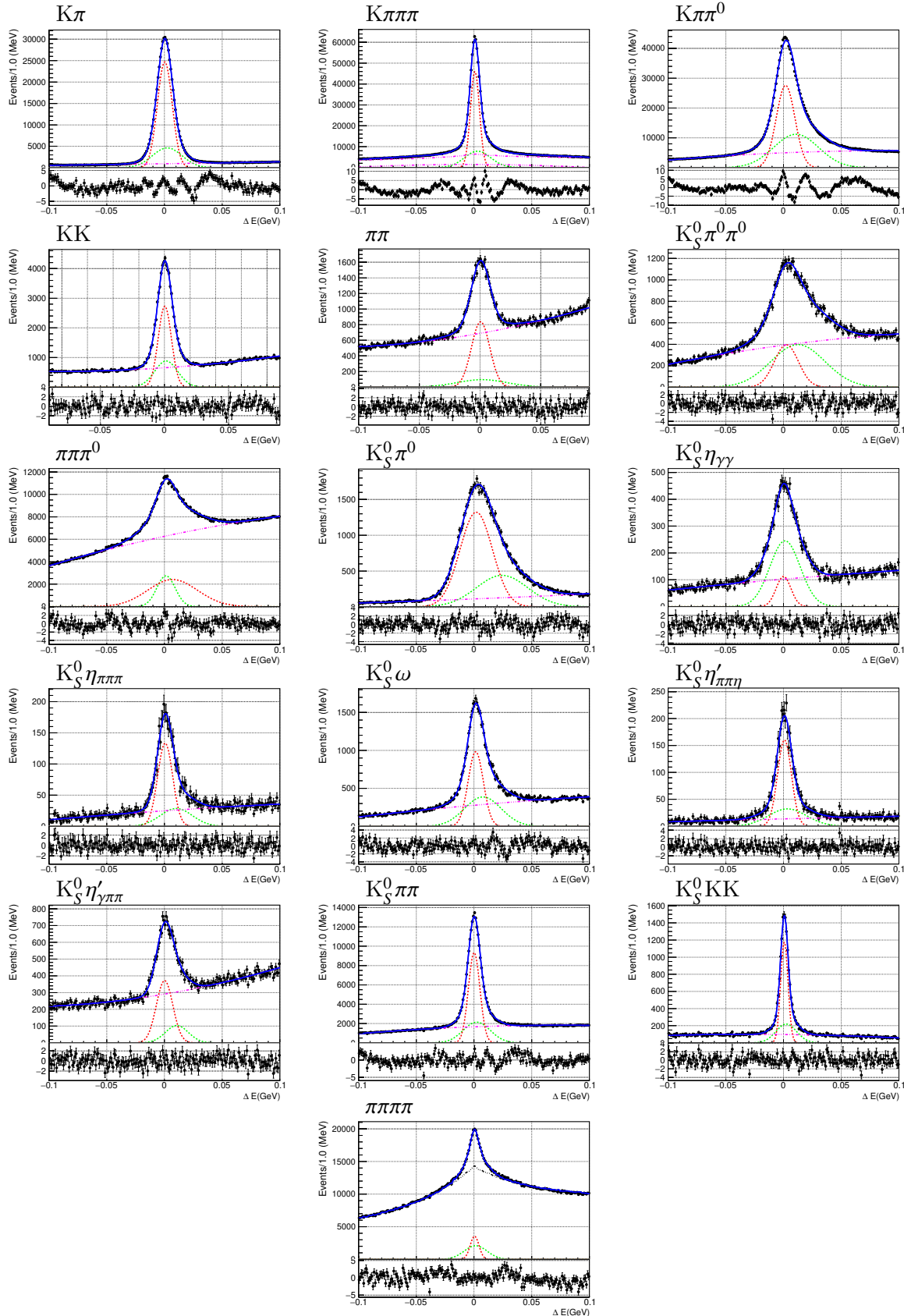


Figure 5: Fit results of ΔE of tagged D. In each plot, the black dots with error bar are data; the total result is shown as the blue solid line; the two Gaussian functions are represented as the red dashed line and green dashed line; the background is shown as the pink dashed line. (For the $K\pi\pi$ and $\pi\pi\pi$ channel, the peak background is shown as the extra pink dashed line and blackdashed line, respectively.)

To get the yields for each channel, binning fits are performed on m_{BC} , shown as Figs. 6. In these fits, the signal is described by the signal shape obtained from signal MC convoluted with a Gaussian function, where the background is described by an Argus function. To get the signal efficiency and peak background yields, same fitting procedures are performed for inclusive MC sample without peak background processes and without signal process, respectively.

The yields from the fit are listed in Tab. 11. A self-check was done, shown as App. C, and the results show there was no obvious bias.

Table 11: Yields of ST.

ST channel	Yields	Peak BKG(21.8x)	Pure Yields	ST efficiency
$K\pi$	548903 ± 775	48567 ± 248	546675 ± 775	0.672 ± 0.001
$K\pi\pi^0$	1051260 ± 1194	61890 ± 961	1048420 ± 1195	0.343 ± 0.001
$K\pi\pi\pi$	658204 ± 926	58219 ± 631	655533 ± 927	0.366 ± 0.001
KK	56668 ± 262	-	56668 ± 262	0.636 ± 0.001
$\pi\pi$	21073 ± 190	-	21073 ± 190	0.691 ± 0.001
$K_S^0\pi^0\pi^0$	24488 ± 258	16284 ± 367	23741 ± 259	0.164 ± 0.001
$\pi\pi\pi\pi$	71776 ± 463	63959 ± 1065	68842 ± 465	0.494 ± 0.001
$\pi\pi\pi^0$	121592 ± 680	131576 ± 1049	115556 ± 682	0.402 ± 0.001
$K_S^0\pi^0$	73408 ± 298	5041 ± 173	73176 ± 299	0.411 ± 0.001
$K_S^0\eta_{\gamma\gamma}$	10071 ± 123	-	10071 ± 123	0.340 ± 0.001
$K_S^0\eta_{\pi\pi\pi}$	3075 ± 64	6551 ± 111	2775 ± 65	0.176 ± 0.001
$K_S^0\omega$	29629 ± 214	74311 ± 372	26220 ± 215	0.166 ± 0.001
$K_S^0\eta'_{\pi\pi\eta}$	3449 ± 67	-	3449 ± 67	0.139 ± 0.001
$K_S^0\eta'_{\gamma\pi\pi}$	9049 ± 125	7818 ± 336	8691 ± 126	0.221 ± 0.001
$K_S^0\pi\pi$	173588 ± 468	42232 ± 358	171651 ± 469	0.392 ± 0.001
K_S^0KK	14061 ± 129	854 ± 64	14022 ± 129	0.183 ± 0.001

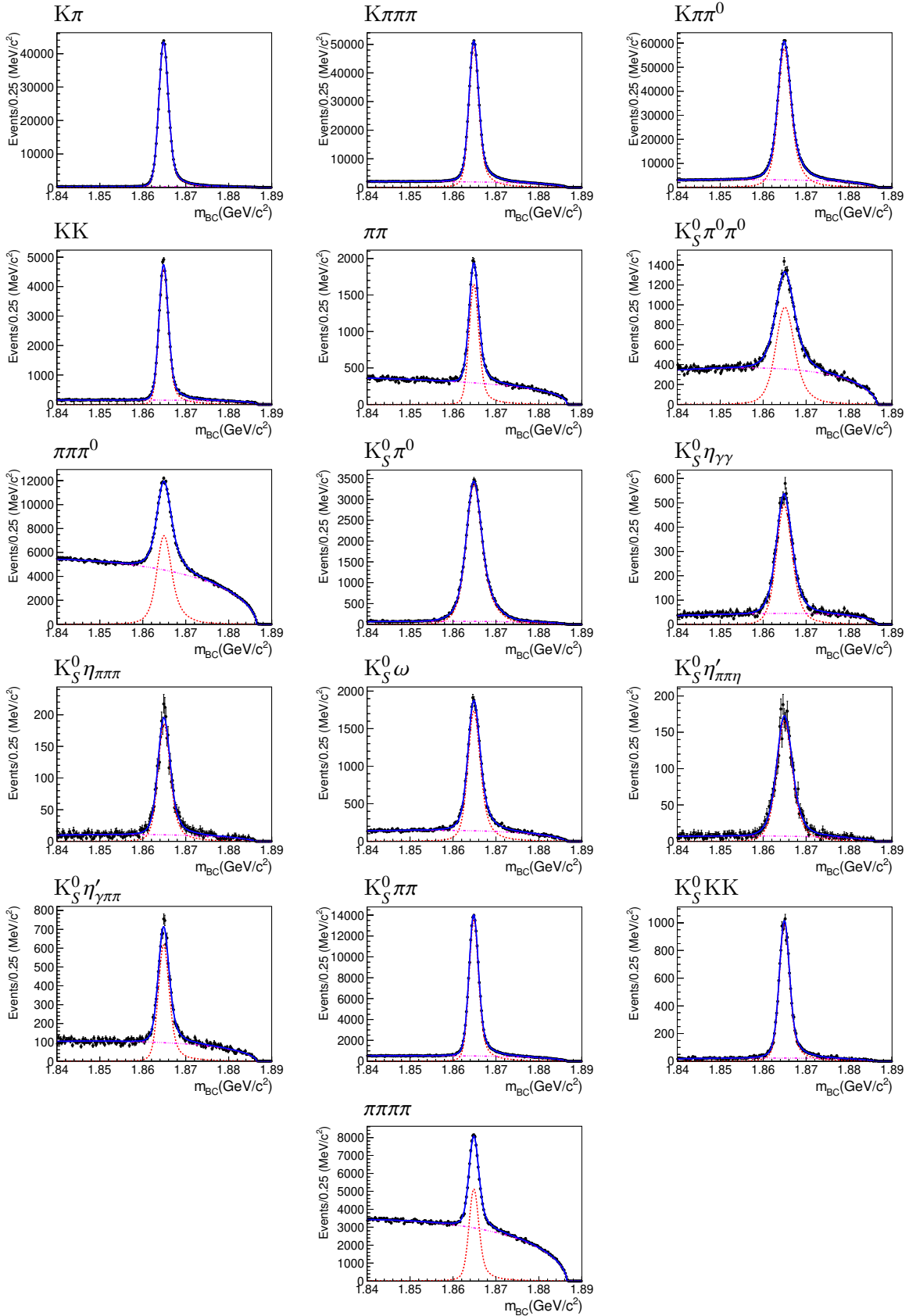


Figure 6: Fit results of m_{BC} of tagged D. In each plot, the black dots with error bar are data; the total result is shown as the blue solid line; the signal shape is represented as the red dashed line; the background is shown as the pink dashed line.

¹ 6.4 Double tagged \bar{D}^0 selection of fully reconstructed channels

² For the double tagged events, the requirements on the tagged side is same as mentioned previ-
³ ously. For the remaining charged tracks, the number of good charged tracks are required to be
⁴ four and the net charge is required to be zero. All of these four charged tracks are required to
⁵ be identified as π . The ΔE of $4\pi^\pm$ signal side are required to be in [-0.023, 0.025] GeV, which is
⁶ same as $4\pi^\pm$ tagged side. Then to suppressed the background from $D \rightarrow K_S^0\pi^+\pi^-$, events with
⁷ any $\pi^+\pi^-$ pair satisfied with $0.481 < m(\pi^+\pi^-) < 0.514$ GeV/ c^2 are rejected.

⁸ In this study because the yields in the local phase spaces are the interests, it's necessary
⁹ to improve the resolution over the lorentz vector of each π in signal side. Then a kinematic fit
¹⁰ constraining the invariant mass of $\pi^+\pi^-\pi^+\pi^-$ to the nominal mass of D^0 is performed on signal
¹¹ side. Furthermore, for the $K_S^0\pi^+\pi^-$ tagged events, the yields will be extracted in local regions of
¹² the Dalitz plane, a kinematic fit constraining the invariant mass of $K_S^0\pi^+\pi^-$ to the nominal mass
¹³ of D^0 is also performed. The χ^2 of the kinematic fit are required to be less than 200. Here the
¹⁴ kinematic fit is only used to calculated the updated lorentz vector of each π . For the ΔE and
¹⁵ m_{BC} , the calculation still used the lorentz vector before the kinematic fit.

¹⁶ After above selections, unbinned fits are performed on m_{BC} of signal side for each channels,
¹⁷ shown as Figs. 7. In these fits, the signal is described by the signal shape obtained from signal MC
¹⁸ convoluted with a Gaussian function, where the background is described by an Argus fucntion.
¹⁹ For most tag channels, the main peak background are from the $D \rightarrow K_S^0\pi^+\pi^-$ in the signal side.
²⁰ For the $\pi^+\pi^-\pi^0$ and $K_S^0\omega$ tag channels, there are still peak background events from $D \rightarrow K_S^0\pi^0$
²¹ and $D \rightarrow K_S^0\pi^+\pi^-\pi^0$, respectively. The background yields from $D \rightarrow K_S^0\pi^+\pi^-$ is estimated by a
²² data-driven method: fit to the mass of $\pi^+\pi^-$ before veto the K_S^0 region, then use the fit result to
²³ estimate the remaining events. In these fits, the K_S^0 shape is taken from $K_S^0\pi^+\pi^-$ MC events, and
²⁴ another peak (green line) represents for the possible K_S^0 components from non-DD process are
²⁵ estimated by the data in the m_{BC} 's sideband region, shown as Figs. 8. The other peak background
²⁶ events are estimated by fit to the inclusive MC events after removing signal and $K_S^0\pi^+\pi^-$ process
²⁷ by truth information. (Here the signal process means two D meson are reconstructed correctly,
²⁸ by the truth match algorithm. Thus the "wrong tag side v.s. right signal side" background is
²⁹ included in this background estimation.) The main background processes' events are corrected
³⁰ for the quantum correlation effect. The numerical fit results are listed in Tab. 12. From both
³¹ plots and numbers, it's obvious that for $\pi^+\pi^-\pi^+\pi^-$ v.s. $\pi^+\pi^-$ and $\pi^+\pi^-\pi^+\pi^-$ v.s. $\pi^+\pi^-\pi^+\pi^-$ the signal
³² is not significant, due to huge background from multi- π s background. So these two tag modes
³³ will not be used in this analysis. The multi-self conjugated channel $K_S^0\text{KK}$ tag mode will also

- ¹ be abandoned, because the DT yields are too small to be divided into many bins (20/30/40,
² depending on the bin pairs of the K_S^0 KK's scheme).

Table 12: Summary of fit results of DT events.

tag channel	DT yields	$K_S \pi^+ \pi^-$	BKG	total peak BKG	pure DT yields
$K\pi$	1975.5 ± 46.3	71.82 ± 1.40	83.39 ± 1.79	1892.11 ± 46.31	
$K\pi\pi^0$	3451.3 ± 63.0	133.49 ± 1.95	162.44 ± 2.83	3288.86 ± 63.04	
$K\pi\pi\pi$	1990.3 ± 49.5	76.54 ± 1.51	95.04 ± 2.53	1895.25 ± 49.58	
KK	128.3 ± 14.3	6.39 ± 0.13	12.89 ± 0.86	115.40 ± 14.35	
$\pi\pi$	30.3 ± 15.2	3.14 ± 0.45	6.38 ± 1.03	23.95 ± 15.19	
$K_S^0 \pi^0 \pi^0$	40.9 ± 10.3	3.39 ± 0.34	4.57 ± 0.56	36.35 ± 10.30	
$\pi\pi\pi\pi$	79.2 ± 40.3	3.57 ± 0.56	3.57 ± 0.56	75.68 ± 40.31	
$\pi\pi\pi^0$	244.6 ± 24.5	14.33 ± 0.73	53.87 ± 1.66	190.68 ± 24.55	
$K_S^0 \pi^0$	337.5 ± 19.1	10.94 ± 0.55	11.49 ± 0.58	326.02 ± 19.12	
$K_S^0 \eta_{\gamma\gamma}$	59.1 ± 7.7	1.41 ± 0.19	1.41 ± 0.19	57.69 ± 7.70	
$K_S^0 \eta_{\pi\pi\pi}$	17.0 ± 4.2	0.54 ± 0.12	0.54 ± 0.12	16.47 ± 4.18	
$K_S^0 \omega$	142.5 ± 13.8	3.95 ± 0.34	13.76 ± 0.90	128.69 ± 13.79	
$K_S^0 \eta'_{\pi\pi\eta}$	12.0 ± 3.5	0.42 ± 0.11	0.42 ± 0.11	11.58 ± 3.47	
$K_S^0 \eta'_{\gamma\pi\pi}$	42.4 ± 7.4	1.26 ± 0.19	1.26 ± 0.19	41.14 ± 7.44	
$K_S^0 \pi\pi$	552.8 ± 26.0	11.03 ± 0.61	13.14 ± 0.85	539.68 ± 25.99	
$K_S^0 KK$	42.8 ± 7.4	1.26 ± 0.20	1.26 ± 0.20	41.55 ± 7.37	

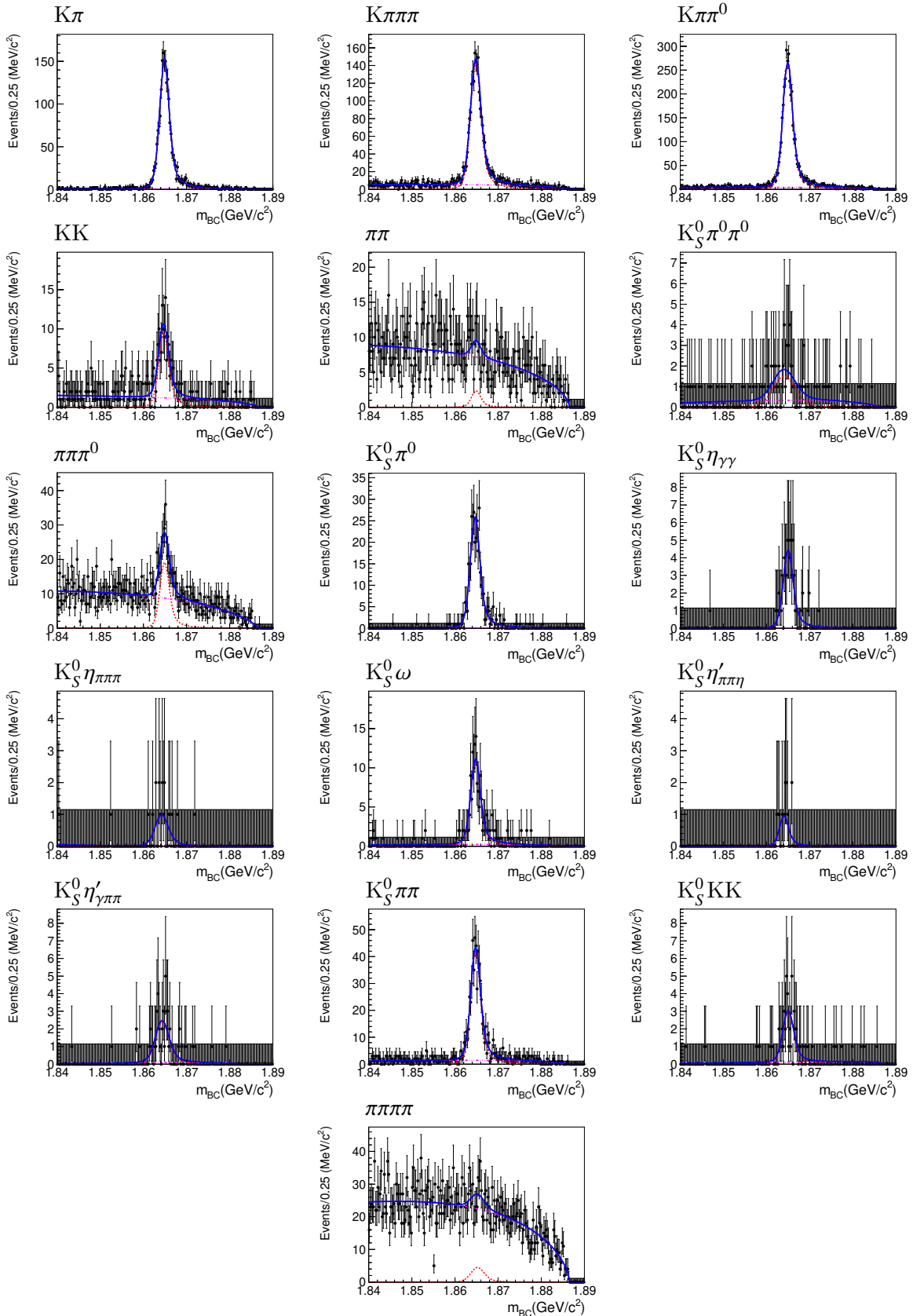


Figure 7: Fit results of m_{BC} of signal side. In each plot, the black dots with error bar are data; the total result is shown as the blue solid line; the signal shape is represented as the red dashed line; the background is shown as the pink dashed line.

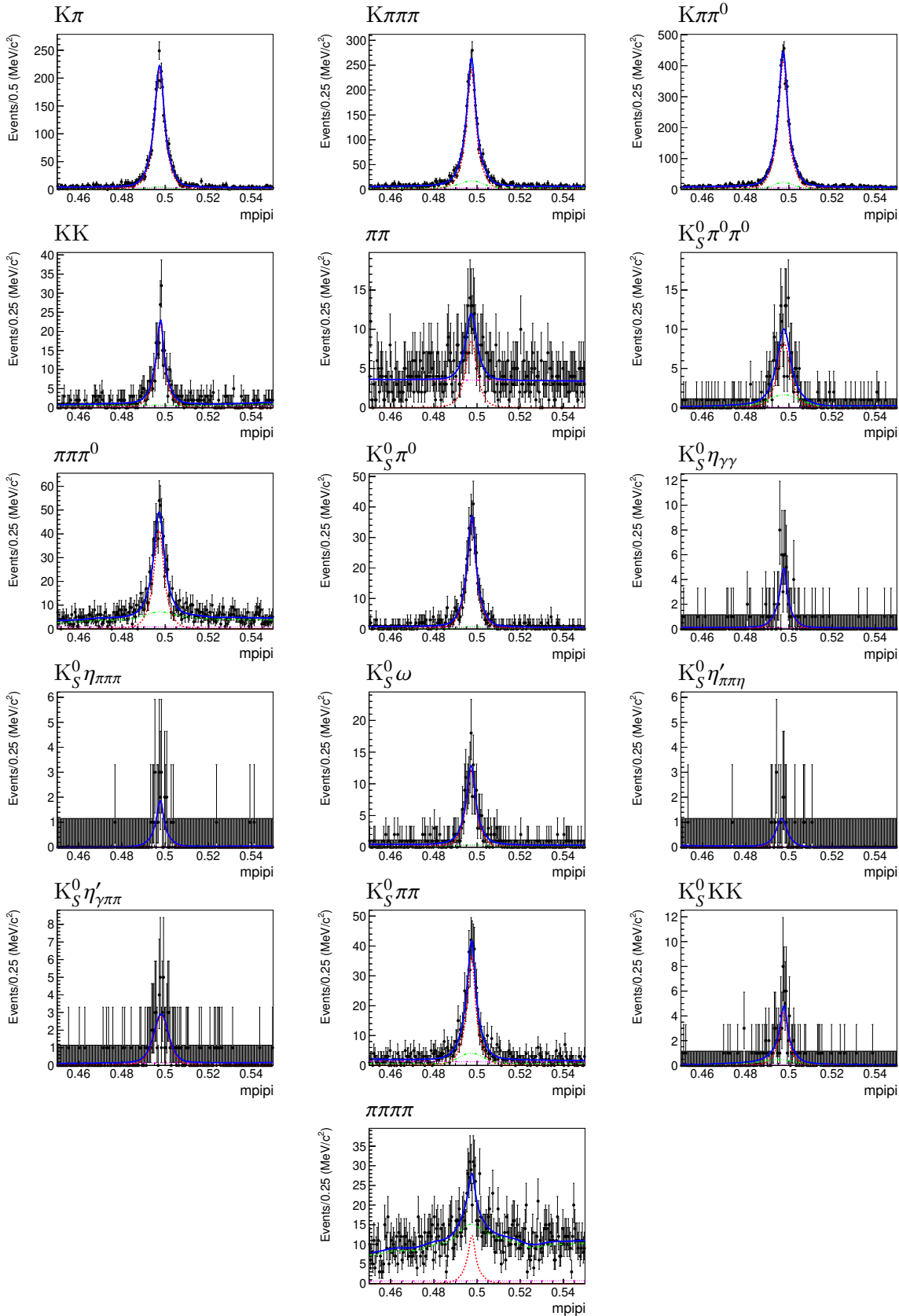


Figure 8: Fit results of $m(\pi^+\pi^-)$ of signal D. In each plot, the black dots with error bar are data; the total result is shown as the blue solid line; the signal shape is represented as the red dashed line; the flat background is shown as the pink dashed line; the peak background is shown as the green dashed line.

1 6.5 Double tagged \bar{D}^0 selection of partially reconstructed channels

2 For the tag modes involving a K_L^0 meson or a ν , named partially reconstructed channels, different
 3 reconstruction method is used due to the incomplete or totally missing information of K_L^0 and
 4 ν in detector. With all other tracks and the total four momentum of the e^+e^- system, missing
 5 particle's four momentum could be calculated and used to identify the signal. So the selections
 6 of partially reconstructed channels would be: First, the $D \rightarrow \pi^+\pi^-\pi^+\pi^-$ process is reconstructed
 7 with same criteria mentioned above. Additionally, the m_{BC} of $\pi^+\pi^-\pi^+\pi^-$ side is required to be
 8 within $(1.86, 1.87) \text{ GeV}/c^2$. The left tracks are reconstructed with the selections in Sec. 6.2.
 9 The events with good $\eta(\gamma\gamma)$ candidates are rejected. Based on the reconstructed tracks and π^0 s,
 10 the events are categorized as five channels:

- 11 • $K_L^0\pi^0$: no good charged tracks ; no extra “bad” charged tracks; only one π^0 .
- 12 • $K_L^0\pi^0\pi^0$: no good charged tracks ; no extra “bad” charged tracks; exactly two π^0 s.
- 13 • $K_L^0\omega$: only two good charged tracks (identified as $\pi^+\pi^-$); no extra “bad” charged tracks;
 14 only one π^0 ; $0.75 < m(\pi^+\pi^-\pi^0) < 0.82 \text{ GeV}/c^2$.
- 15 • $K_L^0\pi^+\pi^-$: only two good charged tracks (identified as $\pi^+\pi^-$); no extra “bad” charged tracks;
 16 no π^0 s.
- 17 • *Kev*: only two good charged tracks (identified as K and e with opposite sign); no π^0 s.

18 Here the “bad” charged tracks are those didn't pass the V_r and V_z requirements.

19 After the above selections, the missing E and missing P are defined:

$$E_{miss} = E_{beam} - E_X \quad (35)$$

$$\vec{p}_{miss} = -\vec{p}_X - \hat{p}_D \sqrt{E_{beam}^2 - m_D^2} \quad (36)$$

20 where X represents the other tracks in the tag side except K_L^0/ν , \hat{p}_D is the unit three vector of
 21 signal D. Then two quantities can be calculated as:

$$M_{miss}^2 = E_{miss}^2 - |\vec{p}_{miss}|^2 \quad (37)$$

$$U_{miss} = E_{miss} - |\vec{p}_{miss}| \quad (38)$$

22 where the first one is used to identify the signal of K_L^0 channels and the second one is used to
 23 identify the *Kev* signal.

24 Similar with $K_S^0\pi^+\pi^-$, for $K_L^0\pi^+\pi^-$ events, a kinematic fit is performed to gain a better reso-
 25 lution of the kinematic variables of $K_L^0\pi^+\pi^-$ side. In the fit, the masses of missing K_L^0 and two

1 D_s are constrained to the nominal mass values, and the total four momentum is constrained to
 2 the initial four momentum of e^+e^- system.

3 To extract the yields, unbinned fits are performed on the M_{miss}^2/U_{miss} . In these fits, the
 4 signal is described by the signal shape obtained from signal MC convoluted with a Gaussian
 5 function, and the background includes possible peak background described by $D^0\bar{D}^0$ inclusive
 6 MC and float background described by a 1-st chebychev function, shown as Figs. 9. The main
 7 peak background, such as $\pi^+\pi^-\pi^+\pi^-v.s.K_L^0\pi^+\pi^-\pi^0$ in $K_L^0\omega$ tag case, is corrected for the QC effect.
 8 The numerical results can be found in Tab. 13.

9 As discussed in Sec. 3, the single tagged yields are also useful. However, for partially recon-
 10 structed channels, the single tagged yields can't be measured experimentally. An adaptive way
 11 is to So the single tagged yields are only estimated by:

$$N(ST) = 2 \times N_{D^0\bar{D}^0} \times \mathcal{B} \times \epsilon \quad (39)$$

12 where $N_{D^0\bar{D}^0}$ is the total $D^0\bar{D}^0$ pair number of this data set $((10597 \pm 28 \pm 98) \times 10^3)$ [29], \mathcal{B} is the
 13 branching ratio of each tag channel [17, 30] and ϵ is the efficiency of tag side. The ϵ is calculated
 14 with two yields of signal MC by number counting, corresponding to signal tag selection and
 15 double tag selection. The numbers are also listed in Tab. 13.

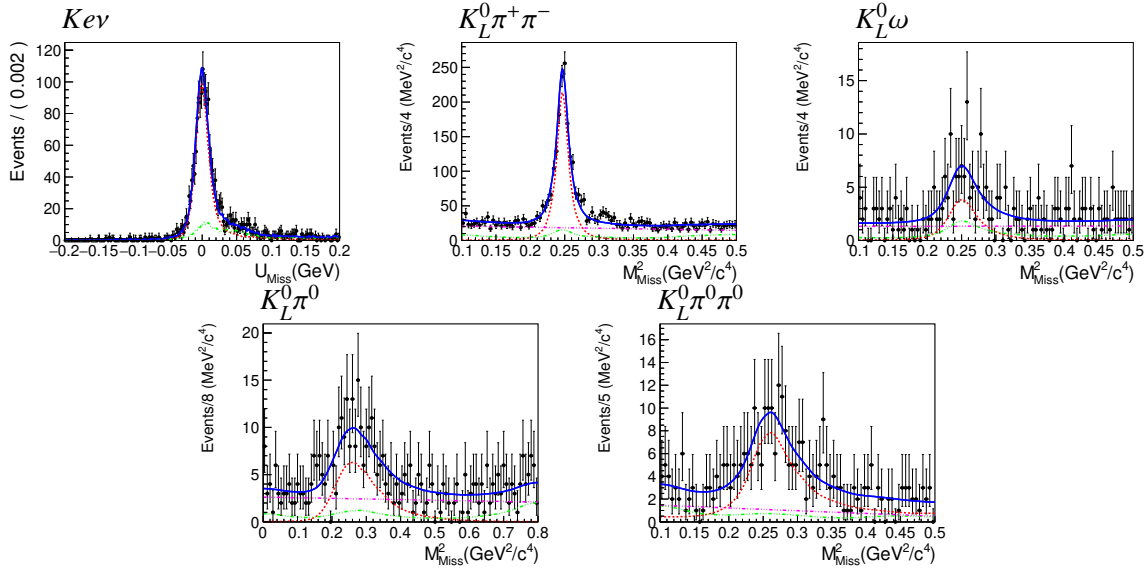


Figure 9: Fit results of partially reconstructed channels. In each plot, the balck dots with error bar are data; the total result is shown as the blue solid line; the signal shape is represented as the red dashed line; the flat background is shown as the pink dashed line; the peak background is shown as the green dashed line.

Table 13: Summary of yields of partially reconstructed channels.

tag channel	DT yields	$\mathcal{B}(\%)$	$\epsilon(\%)$	ST yields
$K\pi$	1559.7 ± 42.6	3.542 ± 0.035	56.5	424141 ± 5850.84
$K_L^0\pi^+\pi^-$	1374.6 ± 50.4	2.85 ± 0.2	57.4	346713 ± 24558.5
$K_L^0\omega$	61.5 ± 13.8	0.804 ± 0.054	17.1	29127.5 ± 1961.97
$K_L^0\pi^0$	130.9 ± 18.8	1.0 ± 0.07	37.6	79689.4 ± 5630.75
$K_L^0\pi^0\pi^0$	178.5 ± 23.9	0.95 ± 0.08	12.8	25771.9 ± 2184.4

1 7 CP Even Fraction Measurement

2 With the above selected events and the Formalism in Sec. 3.3, the CP-even fraction (F_+) in
 3 $D \rightarrow \pi^+\pi^-\pi^+\pi^-$ is measured in this section.

4 7.1 With pure CP tag channels

5 Firstly, the F_+ is measured using pure CP tag channels. For each pure CP tag channel, the N^\pm
 6 is calculated using the Eq. 19:

$$N^\pm \equiv N(4\pi, g)[1 - \eta_{CP}^g y]/N(g).$$

7 The numerical results for each tag channel are listed in Tab. 14 and Fig. 10. For CP even tag or CP
 8 odd tag, the individual channels gave consistent results. Then N^+ and N^- are calculated with
 9 the minimal χ^2 method separately, listed in the Tab. 14 and shown as the yellow bands in the
 10 Fig. 10. The measured N^+ is obviously larger than N^- , which indicated that in $D \rightarrow \pi^+\pi^-\pi^+\pi^-$
 11 the CP-even process is dominated.

Table 14: The summaries of measured N^\pm .

	N^+
$K_S^0\pi^0$	0.004483 ± 0.000261
$K_S^0\eta(\gamma\gamma)$	0.005764 ± 0.000763
$K_S^0\eta(\pi^+\pi^-\pi^0)$	0.005974 ± 0.001502
$K_S^0\omega$	0.004939 ± 0.000525
$K_S^0\eta'(\pi^+\pi^-\eta)$	0.003379 ± 0.001004
$K_S^0\eta'(\rho\gamma)$	0.004763 ± 0.000854
$K_L^0\pi^0\pi^0$	0.006969 ± 0.001092
total	0.004732 ± 0.000205
	N^-
K^+K^-	0.002024 ± 0.000253
$K_S^0\pi^0\pi^0$	0.001522 ± 0.000434
$K_L^0\pi^0$	0.001632 ± 0.000263
$K_L^0\omega$	0.002098 ± 0.000494
total	0.001820 ± 0.000159

12 Then according to the Eq. 20:

$$F_+ = \frac{N^+}{N^+ + N^-},$$

13 the F_+ is calculated as 0.722 ± 0.020 . Here the efficiencies of CP-even process and CP odd process
 14 of $D \rightarrow \pi^+\pi^-\pi^+\pi^-$ are assumed to be same and then cancelled. Then later there is no systematic
 15 uncertainty from the efficiency of signal side. By the signal MC generated including the quantum

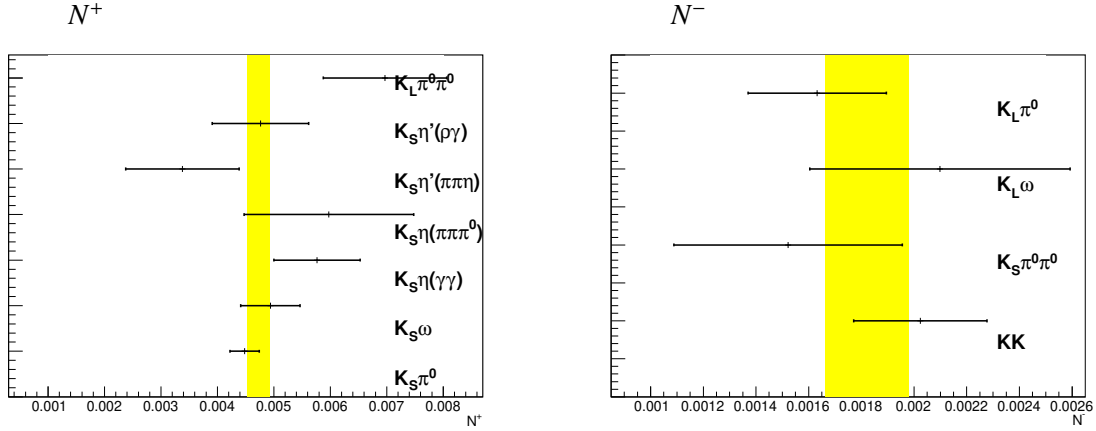


Figure 10: Measured N^+ (left) and N^- (right) of each pure CP tag channels. The yellow bands show the combined value of N^+ and N^- .

1 correlation effect with the amplitude model, this is confirmed well. (The signal efficiencies with
 2 KK tagged and $K_S^0\pi^0$ are 44.4% and 44.7%, respectively.)

3 7.2 With $\pi^+\pi^-\pi^0$ tag channel

4 The F_+ measurement with $\pi^+\pi^-\pi^0$ tag channel is similar with pure CP tag channels. The $N^{\pi^+\pi^-\pi^0}$
 5 is calculated as 0.001641 ± 0.000212 , using the Eq. 24:

$$N^{\pi^+\pi^-\pi^0} \equiv N(4\pi, \pi^+\pi^-\pi^0)[1 - (2F_+^{\pi^+\pi^-\pi^0} - 1)y]/N(\pi^+\pi^-\pi^0)$$

6 where the value of $F_+^{\pi^+\pi^-\pi^0}$ is 0.973 ± 0.017 [9]. Then using the Eq. 26:

$$F_+ = \frac{N^+ F_+^{\pi^+\pi^-\pi^0}}{N^{\pi^+\pi^-\pi^0} - N^+ + 2N^+ F_+^{\pi^+\pi^-\pi^0}},$$

7 the F_+ is calculated as 0.753 ± 0.028 . Here, again, the efficiencies with CP even tag and $\pi^+\pi^-\pi^0$
 8 tag are cancelled. Same as previous, there is no systematic uncertainty from the efficiency of
 9 signal side.

10 7.3 With $K_S^0/K_L^0\pi^+\pi^-$ tag channels

11 The F_+ measurement with $K_S^0/K_L^0\pi^+\pi^-$ tag channels is quite different than with pure CP tag
 12 channels and $\pi^+\pi^-\pi^0$ tag channel.

13 The well measured binning strong phase difference of $K_S^0/K_L^0\pi^+\pi^-$ will help a lot in this
 14 measurement. Here the phase spaces of $K_S^0/K_L^0\pi^+\pi^-$ are divided according to the “Equal $\Delta\delta_D$
 15 BABAR 2008” binning scheme. Due to the no-ideal detector resolution, the bin migration

1 effect should be considered. The possible peak background also should be included. Then the
 2 Eqs. 22,23 should be modified as:

$$N(|i|) = \sum_{j=1}^{Nbin} \epsilon_{ij} h [K_j + K_{-j} - 2\sqrt{K_j K_{-j}} c_j (2F_+^{4\pi} - 1)] + N_{bkg,|i|} \quad (40)$$

$$N'(|i|) = \sum_{j=1}^{Nbin} \epsilon'_{ij} h' [K'_j + K'_{-j} + 2\sqrt{K'_j K'_{-j}} c'_j (2F_+^{4\pi} - 1)] + N'_{bkg,|i|} \quad (41)$$

3 where the ϵ'_{ij} is the efficiency of the reconstruction in $|i|$ -th bin for the events generated in
 4 $|j|$ -th bin, $N_{bkg,|i|}$ is the estimated peak events in $|i|$ -th bin, and K_i, c_i are decay information of
 5 $K_S^0/K_L^0\pi^+\pi^-$ cited from previous BESIII's work BAM-364. [11, 12] The efficiency matrix and
 6 background estimation will be studied in the following.

7 The efficiency matrixes is studied by the exclusive MC of 4π v.s. $K_S^0/K_L^0\pi^+\pi^-$. The numerical results is lists in Tab. 15 and Tab. 16

Table 15: Efficiency matrix ϵ_{ij} for 4π v.s. $K_S^0\pi^+\pi^-$.

Abs.Bin # (Truth) (Rec.)	1	2	3	4	5	6	7	8
1	0.2928	0.0103	0.0014	0.0005	0.0012	0.0009	0.0013	0.0139
2	0.0219	0.2965	0.0121	0.0003	0.0012	0.0006	0.0015	0.0026
3	0.0029	0.0089	0.3424	0.0062	0.0023	0.0010	0.0008	0.0009
4	0.0015	0.0005	0.0110	0.3394	0.0080	0.0015	0.0008	0.0011
5	0.0020	0.0004	0.0011	0.0035	0.3070	0.0074	0.0010	0.0013
6	0.0023	0.0005	0.0013	0.0008	0.0156	0.2810	0.0176	0.0020
7	0.0028	0.0010	0.0009	0.0006	0.0016	0.0134	0.2698	0.0186
8	0.0252	0.0019	0.0010	0.0004	0.0010	0.0012	0.0188	0.2701

8

Table 16: Efficiency matrix ϵ_{ij} for 4π v.s. $K_L^0\pi^+\pi^-$.

Abs.Bin # (Truth) (Rec.)	1	2	3	4	5	6	7	8
1	0.4216	0.0167	0.0010	0.0002	0.0005	0.0008	0.0028	0.0276
2	0.0399	0.4139	0.0150	0.0005	0.0008	0.0012	0.0024	0.0046
3	0.0026	0.0177	0.4366	0.0073	0.0018	0.0009	0.0030	0.0023
4	0.0015	0.0026	0.0196	0.4497	0.0107	0.0026	0.0030	0.0007
5	0.0002	0.0003	0.0009	0.0060	0.4164	0.0150	0.0016	0.0009
6	0.0039	0.0015	0.0011	0.0013	0.0174	0.3653	0.0371	0.0045
7	0.0071	0.0016	0.0006	0.0004	0.0010	0.0164	0.3753	0.0415
8	0.0476	0.0039	0.0006	0.0001	0.0005	0.0013	0.0364	0.3683

9 The peak background number in each bin is estimated by the total peak background and
 10 each bin's fraction, where the total peak background is already studied in previous section.

For $K_S^0\pi^+\pi^-$ case, the peak background includes two parts: $K_S^0\pi^+\pi^-$ v.s. $K_S^0\pi^+\pi^-$ and 4π v.s. others, listed in Tab. 12. For the $K_S^0\pi^+\pi^-$ v.s. $K_S^0\pi^+\pi^-$ process, the fractions of yields in each bin are calculated including the effect of the quantum correlation and non-flat reconstruction efficiency. For the 4π v.s. others, these background events are assumed to be averaged in the total phase space.

For $K_L^0\pi^+\pi^-$ case, the peak background includes two parts: 4π v.s. $K_S^0(\pi^0\pi^0)\pi^+\pi^-$ and $K_S^0\pi^+\pi^-$ v.s. $K_L^0\pi^+\pi^-$.

The yield of the first process is estimated from inclusive MC and the yield of the latter one is also estimated by fitting the $m(\pi^+\pi^-)$ same as fully reconstructed channel. For the fractions of yields in each bin, both quantum correlation effect and non-flat efficiency is included.

The total peak background and the fractions are listed in Tab. 17.

Table 17: Peak background yields and fractions of $K_S^0/K_L^0\pi^+\pi^-$ tag.

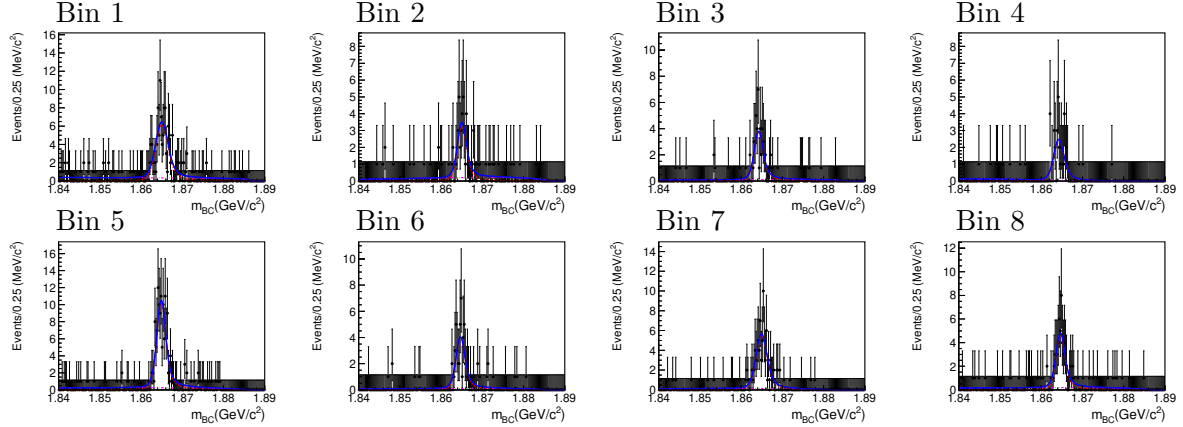
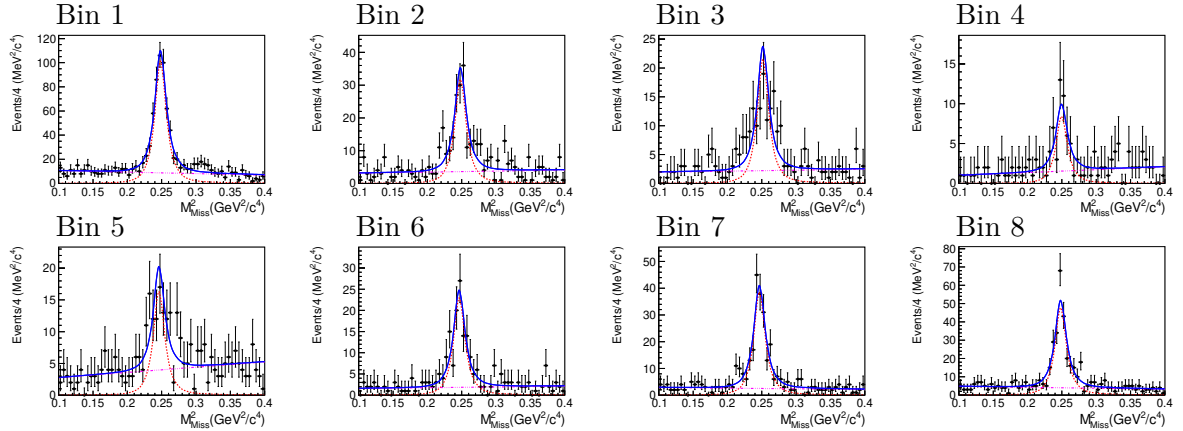
	$K_S^0\pi^+\pi^-$ tag			$K_L^0\pi^+\pi^-$ tag	
	$K_S^0\pi^+\pi^-$ v.s. $K_S^0\pi^+\pi^-$	4π v.s. others	4π v.s. $K_S^0(\pi^0\pi^0)\pi^+\pi^-$	$K_S^0\pi^+\pi^-$ v.s. $K_L^0\pi^+\pi^-$	$K_L^0\pi^+\pi^-$ v.s. $K_L^0\pi^+\pi^-$
total yields	11.03	2.11	68.1	33.4	
f_1	0.234	0.330	0.337	0.283	
f_2	0.087	0.115	0.117	0.086	
f_3	0.102	0.064	0.057	0.121	
f_4	0.049	0.059	0.050	0.032	
f_5	0.175	0.134	0.126	0.108	
f_6	0.095	0.080	0.073	0.057	
f_7	0.126	0.083	0.086	0.135	
f_8	0.124	0.135	0.131	0.146	

The yields in real data are obtained by unbinned fits on m_{BC} and M_{miss}^2 for $K_S^0\pi^+\pi^-$ tag and $K_L^0\pi^+\pi^-$, respectively. For the $K_S^0\pi^+\pi^-$ tag, the signal shape is obtained from signal MC convoluted with a Gaussian function and the background shape is described by an Argus function. For the $K_L^0\pi^+\pi^-$ tag, the signal shape is obtained from signal MC convoluted with a Gaussian function and the background shape is described by a 1-st Chebychev function. To achieve a physical fit result, the width of Gaussian is fixed in each fit. The fit results and numerical results are shown in Figs. 11,12 and Tab. 18.

Using the Eqs. 40, a negative log likelihood is constructed as:

$$\begin{aligned} -2\log\mathcal{L} = & -2 \sum_i \log \text{Gauss}(N_i; \langle N_i \rangle, \sigma_{N_i})_{K_S^0\pi^+\pi^-} \\ & - 2 \sum_i \log \text{Gauss}(N'_i; \langle N'_i \rangle, \sigma_{N'_i})_{K_L^0\pi^+\pi^-}, \end{aligned} \quad (42)$$

where the $\langle N_i \rangle$ is the expected yield in $|i|$ -th bin, the N_i is the observed yield in data. In the fitter all parameters are fixed, except F_+ and h, h' . The uncertainties from external inputs

Figure 11: Fit results on data for $K_S^0 \pi^+ \pi^-$ tag in 8 bins.Figure 12: Fit results on data for $K_L^0 \pi^+ \pi^-$ tag in 8 bins.Table 18: Yields of 8 bins in data for $K_S^0/K_L^0 \pi^+ \pi^-$ tag.

	$K_S^0 \pi^+ \pi^-$ tag	$K_L^0 \pi^+ \pi^-$ tag
Bin 1	103.7 ± 11.5	542.7 ± 27.8
Bin 2	42.06 ± 7.71	170.1 ± 16.5
Bin 3	47.19 ± 7.44	115.2 ± 13.7
Bin 4	34.77 ± 6.38	45.01 ± 8.60
Bin 5	131.3 ± 12.7	87.33 ± 13.15
Bin 6	50.23 ± 7.83	122.9 ± 13.2
Bin 7	83.98 ± 10.27	206.5 ± 16.8
Bin 8	59.08 ± 8.53	255.9 ± 19.0

1 will be included in the systematic uncertainty. Notice that the $K_S^0\pi^+\pi^-$ and $K_L^0\pi^+\pi^-$ could be
 2 used to extract F_+ individually, the fit procedure will be performed for $K_S^0\pi^+\pi^-$, $K_L^0\pi^+\pi^-$, and
 3 $K_S^0/K_L^0\pi^+\pi^-$ separately.

4 Before fitting to real data, it's worth to perform a check on the fit procedure by toy MC. The
 5 toy MC samples are generated 10,000 times by the Poisson function according to the expected
 6 yields with an assumed F_+ and h values. Then with the same fitter, the pull value of F_+ is
 7 calculated and shown in Figs. 13. The fits with a Gaussian function on these pull distributions
 shown that there is no bias on the fitter procedure.

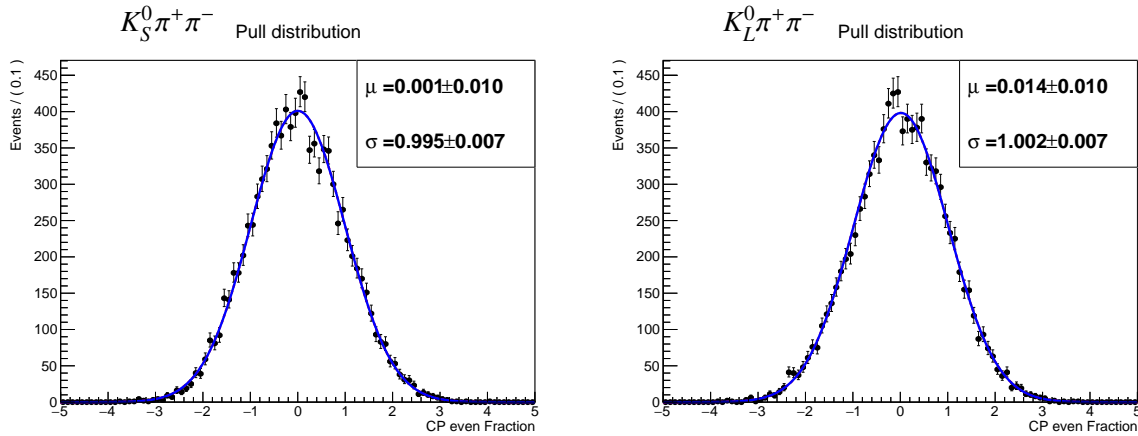


Figure 13: Pull distributions of F_+ for $K_S^0\pi^+\pi^-$ tag with 0.8 input F_+ (left) and $K_L^0\pi^+\pi^-$ tag with 0.6 input F_+ (right).

8
 9 Then the fitter is performed for data with $K_S^0\pi^+\pi^-$ tag, $K_L^0\pi^+\pi^-$ tag, and $K_L^0/K_S^0\pi^+\pi^-$ tag,
 10 seperately. Results are 0.810 ± 0.045 , 0.710 ± 0.037 , and 0.751 ± 0.031 , respectively. The fit results
 11 for $K_S^0/K_L^0\pi^+\pi^-$ are shown in Figs. 14.

12 7.4 With all channels

13 The results of F_+ with pure CP tag, $\pi^+\pi^-\pi^0$ tag and $K_S^0/K_L^0\pi^+\pi^-$ tag are consistent with each
 14 other, summarised in Tab. 19. By a minimal χ^2 fit, which includes the correlation from same
 15 N^+ in CP tag and $\pi^+\pi^-\pi^0$ tag, these results are combined: 0.736 ± 0.015 . Tab. 19 also shows the
 16 result from CLEO-c's, CLEO-c's model prediction and BESIII's model prediction. All results
 17 are consistent with each other.

18 7.5 Systematic uncertainty

19 The systematic uncertainties of CP-even fraction are discussed below.

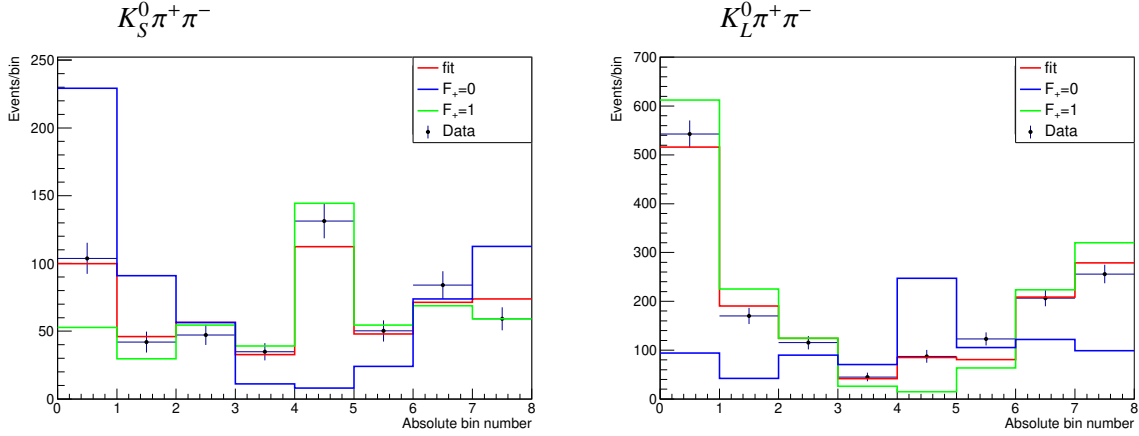


Figure 14: Fit results of $K_S^0 \pi^+ \pi^-$ (left) and $K_L^0 \pi^+ \pi^-$ (right). The black dots with error bar show data. The red lines represent the fit results. And the blue lines and green lines represent the expected yields with 0 and 1 F_+ values, respectively.

Table 19: Summary of fitted F_+ results.

tag channel	F_+
CP eigenstates	0.722 ± 0.020
$\pi^+ \pi^- \pi^0$	0.753 ± 0.028
$K_S^0 \pi^+ \pi^-$	0.810 ± 0.045
$K_L^0 \pi^+ \pi^-$	0.710 ± 0.037
$K_{S,L}^0 \pi^+ \pi^-$	0.751 ± 0.031
total	0.736 ± 0.015
CLEO-c's	0.737 ± 0.028
CLEO-c's model	$0.729 \pm 0.009 \pm 0.015 \pm 0.010$
BESIII's model	$0.732 \pm 0.009 \pm 0.007 \pm 0.012$

1 7.5.1 ST yields

2 According to Eq. 19 and Eq.24, the calculation of N^\pm and $N^{\pi^+\pi^-\pi^0}$ involves the ST yields of the
 3 corresponding channels.

4 For fully reconstructed channels, different sources of possible systematic uncertainties are
 5 considered:

- 6 • For the fits of m_{BC} , the fit range and bin width are changed to confirm there is no bias
 7 in the fits. In the fits, the endpoint of Argus function is fixed at 1.8865 GeV/ c^2 . To
 8 estimate the systematic uncertainty from this assumption, the fits are repeated by floating
 9 the endpoint in ± 0.5 MeV range. The difference of central values between the nominal fits
 10 and the alternative fits are taken as the systematic uncertainty.
- 11 • For the peak background yields, which are estimated from the inclusive MC, the uncertain-
 12 ties are mainly from the uncertainties of branching ratios of the main peak background.
 13 (The statistical uncertainties of the peak background yields are included before.)

14 The fully reconstructed channels' ST yields are summarised in Tab. 20.

15 For the ST yields of partially reconstructed channels, which are from calculation of Eq. 39,
 16 the uncertainties of total $D^0\bar{D}^0$ pairs number and branching ratios of each tag channels are
 17 already included in previous numbers. For the efficiencies, which are estimated from the signal
 18 MC, the uncertainties includes:

- 19 • tracking: each charged track contributes 1.0%.
- 20 • PID: each charged track contributes 1.0%.
- 21 • π^0 reconstruction: each π^0 contributes 2%.
- 22 • no extra π^0 and η : this is studied by the $K\pi\pi^0$ v.s. $4\pi^\pm$ sample. The difference between
 23 the efficiencies of data and MC is assigned as the systematic uncertainty of “no extra π^0
 24 and η ”: 3%.
- 25 • no extra charged tracks: this is also studied by the $K\pi\pi^0$ v.s. $4\pi^\pm$ sample. The difference
 26 between the efficiencies of data and MC is assigned as the systematic uncertainty of “no
 27 extra charged tracks”: 1%.

28 The the partially reconstructed channels' ST yields are also summarised in Tab. 20.

¹ 7.5.2 DT yields

² Same with ST yields, systematic uncertainties related to the DT yields are estimated similarly.

³ For fully reconstructed channels, the uncertainties from the fits are estimated by floating the
⁴ endpoint in ± 0.5 MeV range. The difference of central values between the nominal fits and the
⁵ alternative fits are taken as the systematic uncertainty, which is found to be negligible for most
⁶ channels. The uncertainties from the peak background is already considered before. The fully
⁷ reconstructed channels' DT yields are summarised in Tab. 21.

⁸ In fits of partially reconstructed channels, the fixed peak background, which is estimated
⁹ by $D^0\bar{D}^0$ MC, is floated within the uncertainties of main processes' branching ratio in PDG.
¹⁰ Then the difference between this alternative fits and the nominal fits are taken as the systematic
¹¹ uncertainties of the partially reconstructed DT yields, also shown in Tab. 21.

¹² 7.5.3 Input from $K_S^0/K_L^0\pi^+\pi^-$

¹³ For the $K_S^0\pi^+\pi^-$ tag and $K_L^0\pi^+\pi^-$ tag cases, the $K_S^0/K_L^0\pi^+\pi^-$'s kinematic informations (K_i, c_i)
¹⁴ are cited from external analysis.[11, 12] To estimate the uncertainties from these parameters,
¹⁵ the K_i, c_i are sampled according to their total uncertainties and their correlations. Then with
¹⁶ each new values, the fit on $K_S^0/K_L^0\pi^+\pi^-$ tagged events is repeated. With thousands times, a
¹⁷ new distribution of F_+ is built up. The standard deviation of the distribution is taken as the
¹⁸ systematic uncertainty.

¹⁹ Since in Ref. [11, 12] the $K_S^0\pi^+\pi^-$'s K_i , $K_L^0\pi^+\pi^-$'s K_i , and $K_S^0/K_L^0\pi^+\pi^-$'s c_i/c'_i are measured
²⁰ separately, here the systematic uncertainties of them are also estimated separately. The distri-

Table 20: Yields of ST, the first uncertainty is statistical, the second uncertainty is systematic.

ST channel	Pure Yields
KK	$56668 \pm 262 \pm 56$
$K_S^0\pi^0\pi^0$	$23741 \pm 259 \pm 227$
$\pi\pi\pi^0$	$115556 \pm 682 \pm 360$
$K_S^0\pi^0$	$73176 \pm 299 \pm 709$
$K_S^0\eta_{\gamma\gamma}$	$10071 \pm 123 \pm 16$
$K_S^0\eta_{\pi\pi\pi}$	$2775 \pm 65 \pm 45$
$K_S^0\omega$	$26220 \pm 214 \pm 522$
$K_S^0\eta'_{\pi\pi\eta}$	$3449 \pm 67 \pm 29$
$K_S^0\eta'_{\gamma\pi\pi}$	$8691 \pm 126 \pm 135$
$K_L^0\omega$	$29127.5 \pm 1961.97 \pm 1366$
$K_L^0\pi^0$	$79689.4 \pm 5630.75 \pm 2982$
$K_L^0\pi^0\pi^0$	$25771.9 \pm 2184.4 \pm 1314$

butions of F_+ are shown in Figs. 15. The total systematic uncertainty from $K_S^0/K_L^0\pi^+\pi^-$'s K_i and c_i/c'_i is estimated as 0.006.

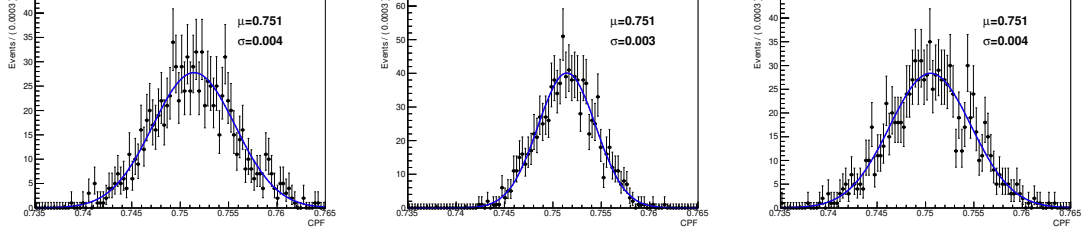


Figure 15: F_+ with $K_S^0/K_L^0\pi^+\pi^-$ tagged distributions corresponding to $K_S^0\pi^+\pi^-$'s K_i (left), $K_L^0\pi^+\pi^-$'s K_i (middle), and $K_S^0/K_L^0\pi^+\pi^-$'s c_i/c'_i (right).

7.5.4 Migration matrix

For the $K_S^0\pi^+\pi^-$ tag and $K_L^0\pi^+\pi^-$ tag cases, the efficiency matrixes are estimated by the MC. Even huge MC sample is generated, there is a non negligible uncertainty from the finite MC size. To evaluate this systematic uncertainty, the efficiency matrixes are smeared within the statistical uncertainty. Then with similar procedure, the F_+ distribution is built up, shown as Fig. 16. And the systematic uncertainty due to limited statistics is estimated to be 0.003.

7.5.5 Peak background estimation with $K_S^0/K_L^0\pi^+\pi^-$ tagged

For the $K_S^0\pi^+\pi^-$ tag and $K_L^0\pi^+\pi^-$ tag cases, the expected yield in each bin includes the peak background, listed in Tab. 17. Then the systematic uncertainty of this background estimation

Table 21: Yields of DT, the first uncertainty is statistical, the second uncertainty is systematic.

DT channel	Pure Yields
KK	$115.40 \pm 14.35 \pm 0.67$
$K_S^0\pi^0\pi^0$	$36.35 \pm 10.30 \pm 13.44$
$\pi\pi\pi^0$	$190.69 \pm 24.55 \pm 14.49$
$K_S^0\pi^0$	$326.02 \pm 19.12 \pm 4.10$
$K_S^0\eta_{\gamma\gamma}$	$57.69 \pm 7.70 \pm 8.02$
$K_S^0\eta_{\pi\pi\pi}$	$16.47 \pm 4.18 \pm 0.93$
$K_S^0\omega$	$128.69 \pm 13.79 \pm 5.10$
$K_S^0\eta'_{\pi\pi\eta}$	$11.58 \pm 3.47 \pm 1.48$
$K_S^0\eta'_{\gamma\pi\pi}$	$41.14 \pm 7.44 \pm 3.67$
$K_L^0\omega$	$61.5 \pm 13.8 \pm 4.7$
$K_L^0\pi^0$	$130.9 \pm 18.8 \pm 0.7$
$K_L^0\pi^0\pi^0$	$178.5 \pm 23.9 \pm 0.7$

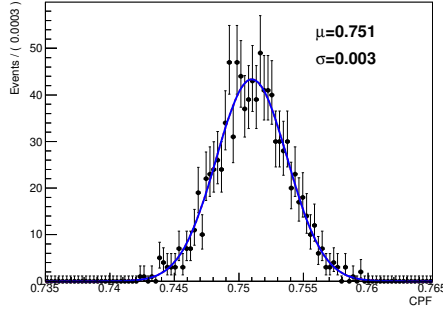


Figure 16: F_+ with $K_S^0/K_L^0\pi^+\pi^-$ tagged distributions corresponding to statistics limit of migration matrix.

- 1 is evaluated by varying each background fraction in each bin within its statistical uncertainty.
- 2 Then fitting to the distribution of the F_+ (Fig. 17), the standard deviation of this distribution
- 3 is taken as the systematic uncertainty, 0.003.

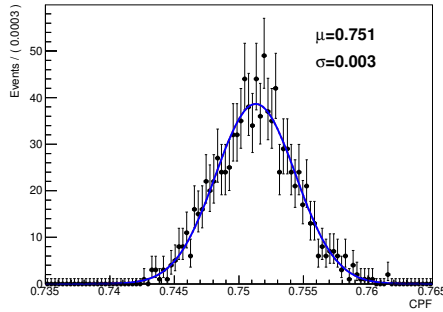


Figure 17: F_+ with $K_S^0/K_L^0\pi^+\pi^-$ tagged distributions corresponding to statistics limit of peak background estimation.

4 7.5.6 External inputs

- 5 In the CP-even fraction measurement, there are two more external inputs: y and $F_+^{\pi^+\pi^-\pi^0}$. They
- 6 are used in the calculation of N^\pm and $N^{\pi^+\pi^-\pi^0}$. By mathematical calculation, the uncertainties
- 7 of y in N^+ , N^- , and $N^{\pi^+\pi^-\pi^0}$ are determined as 0.000003, 0.000001, and 0.000001, respectively.
- 8 Comparing to statistical uncertainties of N^\pm and $N^{\pi^+\pi^-\pi^0}$, uncertainties from y are negligible and
- 9 won't be counted in further study.

10 The uncertainty of $F_+^{\pi^+\pi^-\pi^0}$ in $F_+(\pi^+\pi^-\pi^0)$ is calculated as 0.007.

1 7.5.7 Broken phase space due to K_S^0 veto

2 In this analysis, the F_+ is for the entire phase space. But the measured F_+ is for a broken phase
 3 space due to K_S^0 veto. With huge PHSP MC events and the necessary information (A, \bar{A}, δ)
 4 calculated by the model, according to the Eq. 16, the CP-even fraction for the entire phase space
 5 and the broken phase space are calculated as 0.7273 and 0.7300, respectively. The difference,
 6 0.0027 is taken as a systematic uncertainty corresponding to the non-entire phase space.

7 7.5.8 Results with all systematic uncertainty

8 For the impacts in $K_S^0/K_L^0\pi^+\pi^-$ tagged cases, by combining the systematic uncertainties from
 9 inputs of $K_S^0/K_L^0\pi^+\pi^-$'s K_i, c_i , migration matrix, peak background estimation, the total systematic
 10 uncertainty of $F_+(K_S^0/K_L^0\pi^+\pi^-)$ is calculated as 0.008.

11 For the impacts in CP eigenstates tagged and $\pi^+\pi^-\pi^0$ tagged cases, firstly the N^+, N^- and
 12 $N^{\pi^+\pi^-\pi^0}$ are re-determined within systematic uncertainties of ST tag yields and DT tag yields:
 13 0.004694 ± 0.000219 , 0.001849 ± 0.000169 and 0.001641 ± 0.000214 , respectively. Then the F_+
 14 with CP eigenstates and $\pi^+\pi^-\pi^0$ are re-calculated, shown in Tab. 22. (For the latter one, the
 15 uncertainty from $F_+^{\pi^+\pi^-\pi^0}$ is included.) Within the correlation between them, the F_+ with all
 16 channels are estimated as 0.732 ± 0.0163 . Comparing this result with the result in Tab. 19, the
 17 statistical uncertainty is dominated in the CP-even fraction result. And the systematic uncer-
 18 tainty's impact on the mean value is not large. Then by subtracting the statistical uncertainty
 19 in quadrature, the systematic uncertainty is estimated as 0.007, shown in Tab. 22.

Table 22: Summary of fitted F_+ results.

tag channel	F_+
CP eigenstates	0.716 ± 0.021
$\pi^+\pi^-\pi^0$	0.751 ± 0.028
$K_{S,L}^0\pi^+\pi^-$	0.751 ± 0.032
total	$0.732 \pm 0.015 \pm 0.007$
CLEO-c's	0.737 ± 0.028
CLEO-c's model	$0.729 \pm 0.009 \pm 0.015 \pm 0.010$
BESIII's model	$0.732 \pm 0.009 \pm 0.007 \pm 0.012$

20 With the nominal result, further study is performed to study the systematic contribution
 21 from each source. For each source, the procedure is repeated with zero uncertainty from the
 22 source; then with the new temporary F_+ , the contribution can be estimated by calculating the
 23 difference between the nominal F_+ 's uncertainty and the new temporary F_+ 's:

$$Syst.\text{err.} = \sqrt{err_{nominal}^2 - err_{temporary}^2} \quad (43)$$

- 1 The summary of the contribution from each source is listed in Tab. 23. For the last source,
 2 “others”, which is related to ST yields and DT yeilds, is dominated systematic uncertainty.
 3 Since the sub sources of ST yields and DT yields will mix together into $N^+, N^-, N^{\pi^+\pi^-\pi^0}$, these
 4 sub sources are not divided.

Table 23: Summary of systematic contribution.

source	systematic uncertainty
Broken phase space	0.0027
K_i, c_i from $K_S^0\pi^+\pi^-, K_L^0\pi^+\pi^-$	0.002
Efficiency Matrix	0.001
peak background in $K_S^0\pi^+\pi^-, K_L^0\pi^+\pi^-$	0.001
$F_+^{\pi^+\pi^-\pi^0}$	0.002
others(related to N(ST) and N(DT))	0.005
total	0.007

1 8 Strong phase difference measurement

2 With the above selected events and the Formalism in Sec. 3, the strong phase difference ($\Delta\delta_D$)
 3 between $D^0 \rightarrow \pi^+\pi^-\pi^+\pi^-$ and $\bar{D}^0 \rightarrow \pi^+\pi^-\pi^+\pi^-$ is measured in the section.

4 In this section, results with five CLEO-c's binning schemes and four BESIII's binning schemes
 5 are shown. (Some plots or efficiency matrixes are shown in the App. D.)

6 8.1 K_i measurement

7 First, the flavor channels ($K^-e^+\nu$, $K^-\pi^+$, $K^-\pi^+\pi^0$, $K^-\pi^+\pi^+\pi^-$) are used to measure the K_i , the
 8 flavor tagged yields in each bin. Assuming there is no CP violation in $D \rightarrow \pi^+\pi^-\pi^+\pi^-$, the
 9 $K_i = \bar{K}_{-i}$ relation could use to combine i -th bin of $D^0 \rightarrow 4\pi$ decay and $-i$ -th bin of $\bar{D}^0 \rightarrow 4\pi$
 10 decay.

11 The observed yields are obtained by unbinned fitting on m_{BC} for $K^-\pi^+$, $K^-\pi^+\pi^0$, $K^-\pi^+\pi^+\pi^-$
 12 tag channels and U_{miss} for $K^-e^+\nu$ tag channel. The signal and background functions are same
 13 as the global fit in Sec. 6.4 and Sec. 6.5. The fit plots of BESIII's Equal $\Delta\delta_D$ binning are shown
 14 as Figs. 18 19 20 21. (The plots of other binning schemes are shown in App. D.1.) And the
 15 numerical results are listed in Tab. 24.

16 Due to the finite detector performance, the resolution may cause the events migration accross
 17 bins. The reconstructed events of signal MC in each bin can be written as:

$$N_{Observed}^i = \sum_{j=1}^{Nbin} \epsilon_{ij}^{DT} N_{Generated}^j + N_{bkg} \times f_j, \quad (44)$$

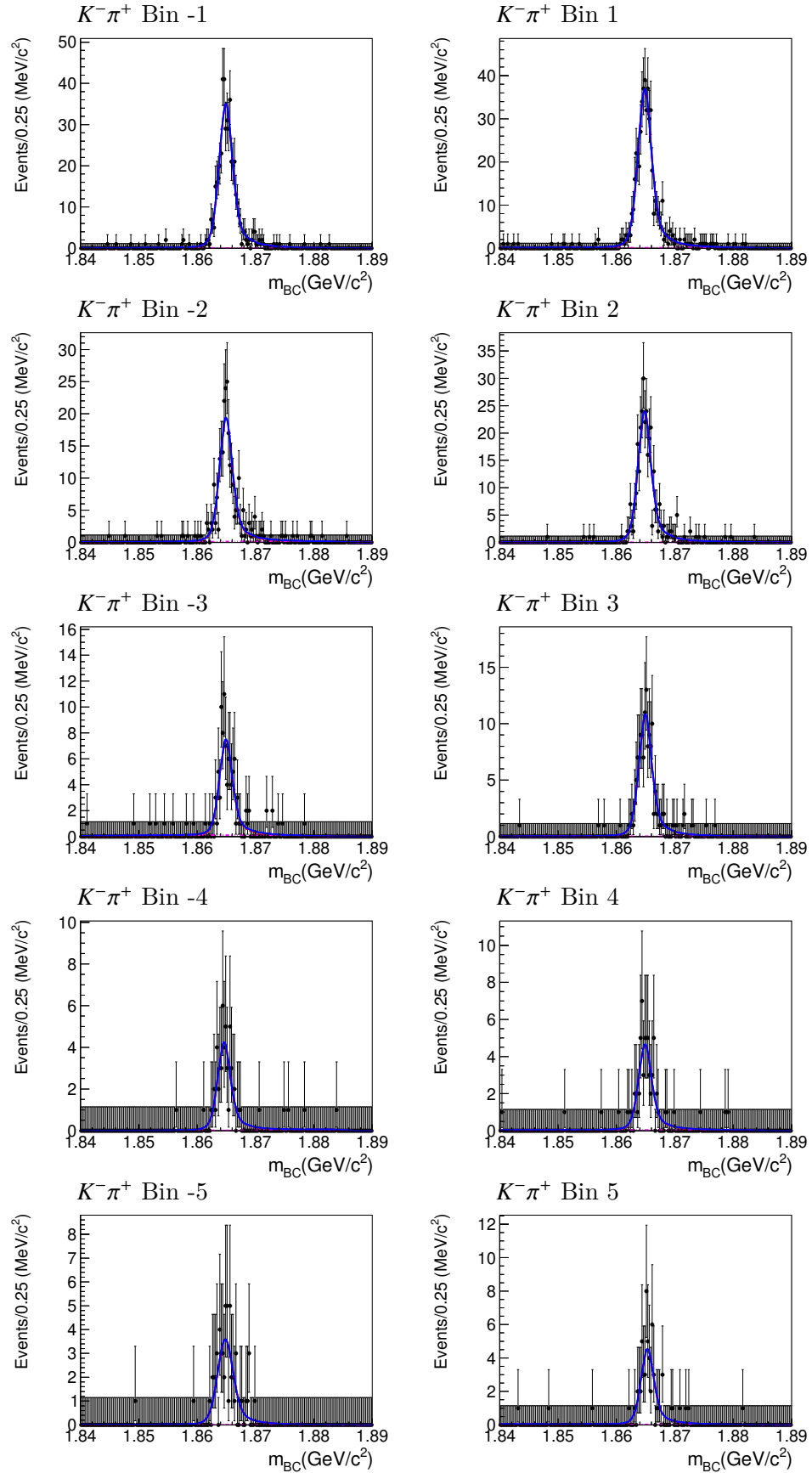
18 where the ϵ_{ij}^{DT} (efficiency matrix) describes the reconstruction efficiency and bin migration effect,
 19 N_{bkg} is the background in the total phase space, and f_j is the fraction of the background in each
 20 bin. Then the yields in generator level, i.e. K_i , can be presented as:

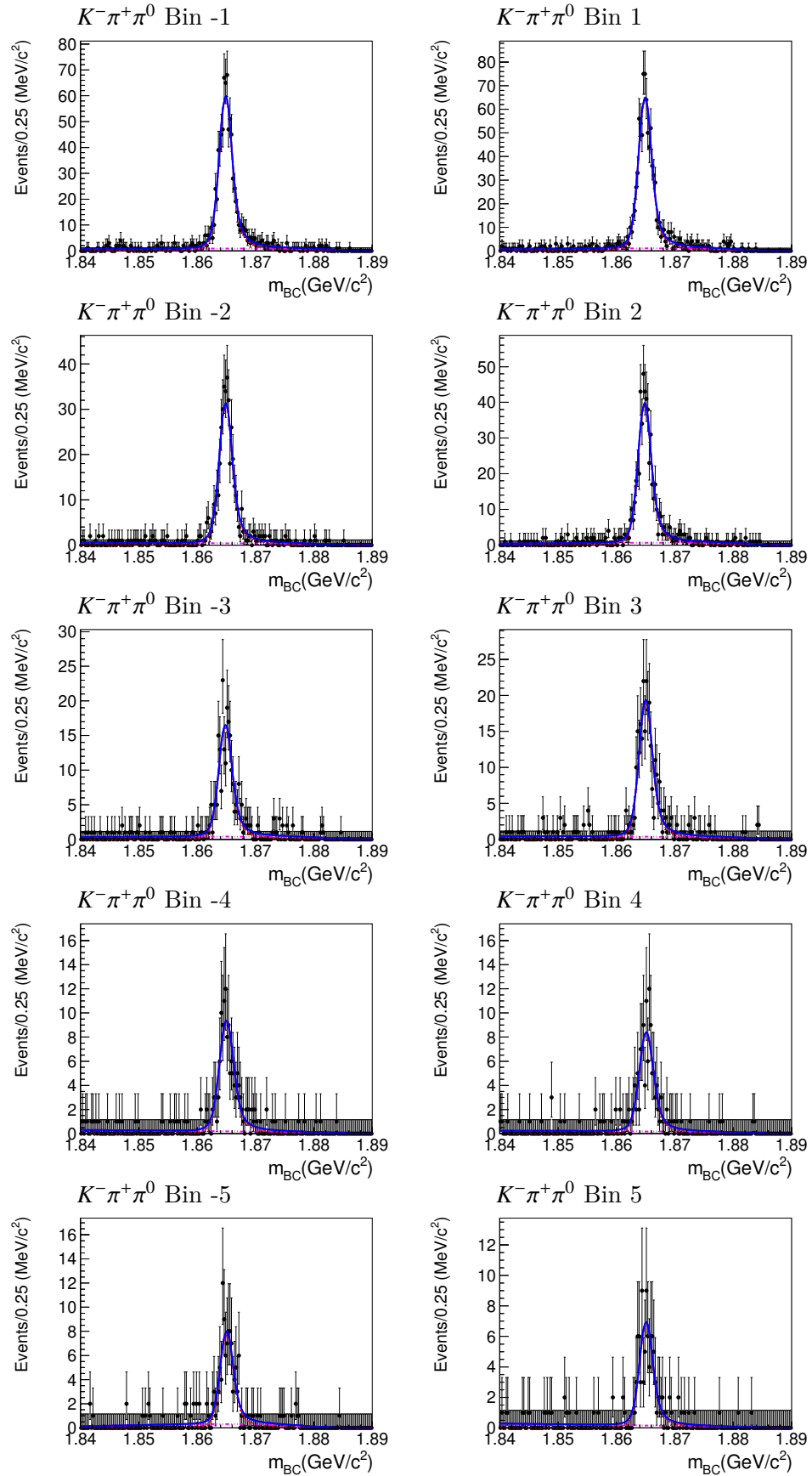
$$K^i \equiv N_{Generated}^i \times \epsilon_{ST} = \sum_{j=1}^{Nbin} (\epsilon^{-1})_{ij} (N_{Observed}^j - N_{bkg} \times f_j), \quad (45)$$

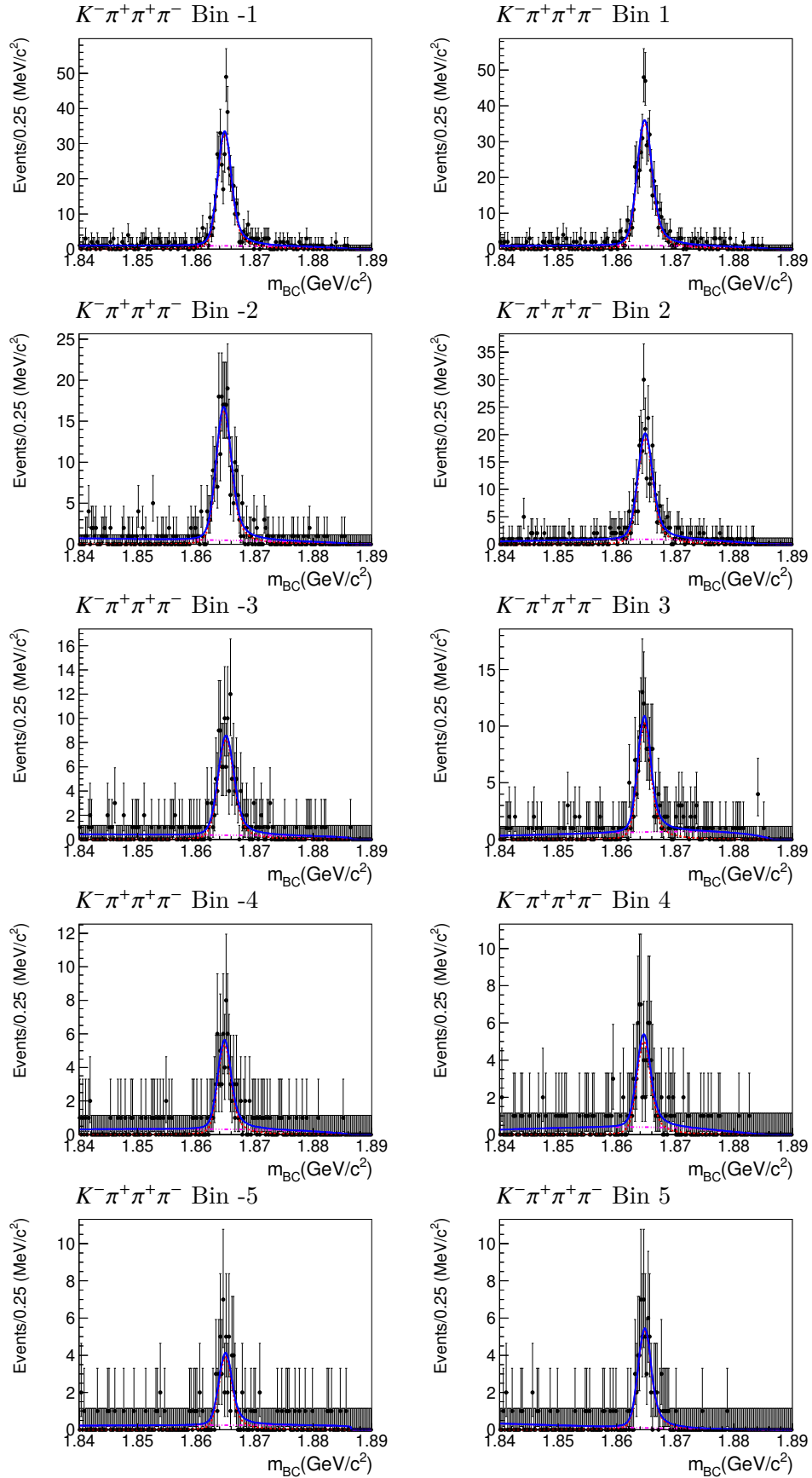
21 In the calculation, N_{bkg} is already shown in Tab. 12, the f_j is obtained from $K_S^0\pi^+\pi^-$ MC events
 22 shown as Tab. 25. and the unfold matrix $(\epsilon^{-1})_{ij}$ is the inversed efficiency matrix $(\epsilon_{ij}^{DT}/\epsilon_{ST})$. The
 23 efficiency matrixes of BESIII's Equal $\Delta\delta_D$ binning scheme, obtained from signal MC, are shown
 24 in Tabs. 26. (The matrixes of other binning schemes are shown in App. D.1.)

25 For the three quasi-flavor tag channels, one more correction factor is needed for the doubly
 26 Cabibbo suppressed decays. The correction factor is presented as:

$$f_i = \frac{\int_i |A_f|^2 d\Phi_f}{\int_i (|A_f|^2 + (r_D^F)^2 |\bar{A}_f|^2 - 2r_D^F R_F \mathcal{R}[e^{i\delta_D^F} A_f \bar{A}_f]) d\Phi_f}, \quad (46)$$

Figure 18: Fit results of $K^- \pi^+$ for different K_i .

Figure 19: Fit results of $K^- \pi^+ \pi^0$ for different K_i .

Figure 20: Fit results of $K^- \pi^+ \pi^+ \pi^-$ for different K_i .

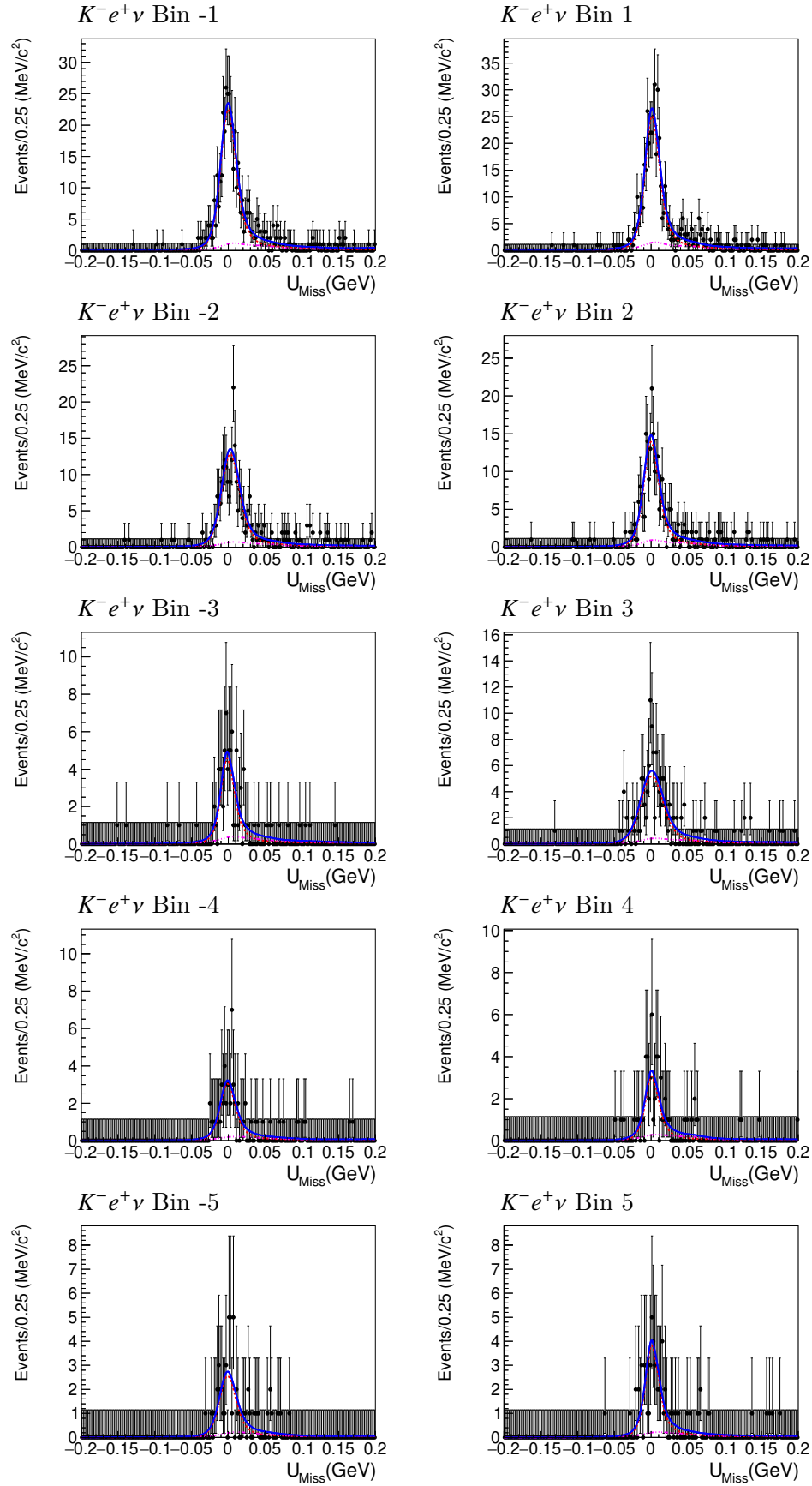
Figure 21: Fit results of $K^- e^+ \nu$ for different K_i .

Table 24: The summaries of fitted yields for flavor tag channels.

Tag Channel	Bin -5	Bin -4	Bin -3	Bin -2	Bin -1	Bin 1	Bin 2	Bin 3	Bin 4	Bin 5
Cleo-c's Equal $\Delta\delta_D$ binning										
$K\pi$	71.40±8.51	93.90±10.04	140.39±12.45	250.86±17.63	445.21±21.31	456.92±22.72	262.35±16.44	121.11±12.09	69.96±9.93	58.26±7.88
$K\pi\pi^0$	151.32±13.40	170.41±13.72	234.58±16.71	433.62±23.37	742.71±29.72	845.66±32.30	420.01±20.38	197.37±15.14	135.89±12.98	119.72±12.27
$K3\pi$	83.99±9.98	98.89±11.09	125.39±13.33	254.14±17.31	434.17±23.44	474.17±24.71	251.61±18.37	116.46±12.46	71.90±9.70	75.95±10.33
K_{ev}	65.65±8.74	68.91±8.88	108.77±11.27	222.24±15.84	351.77±20.17	360.73±20.45	196.32±15.19	73.90±9.59	44.69±7.60	72.42±9.09
Cleo-c's Variable $\Delta\delta_D$ binning										
$K\pi$	194.96±14.69	297.17±18.11	158.75±13.20	224.10±15.28	135.96±12.17	133.37±11.77	227.10±16.03	166.25±13.00	282.88±17.31	149.92±12.55
$K\pi\pi^0$	373.85±20.76	496.58±24.69	271.54±17.94	370.40±21.44	229.35±17.14	253.14±17.82	425.27±21.97	293.79±18.71	438.34±22.70	305.59±19.38
$K3\pi$	212.01±16.49	284.44±19.03	166.53±14.03	214.56±15.86	127.31±12.72	141.20±13.35	245.31±17.03	140.49±14.39	269.36±18.79	184.02±15.41
K_{ev}	167.14±13.85	267.03±17.47	113.63±11.46	191.23±14.69	90.79±10.39	97.08±10.61	185.87±14.73	127.55±12.16	193.59±15.23	131.61±12.66
Cleo-c's Alternative binning										
$K\pi$	41.31±6.94	152.82±13.27	346.02±19.65	117.71±11.60	37.99±6.50	122.95±11.09	241.94±16.35	557.82±25.65	267.03±9.84	90.62±9.72
$K\pi\pi^0$	87.80±10.63	231.60±16.43	694.20±27.85	171.16±0.33	61.49±8.83	231.46±15.84	439.68±23.22	890.29±32.98	446.98±22.93	194.42±15.53
$K3\pi$	60.55±8.64	115.52±12.54	350.35±20.35	112.34±12.57	30.47±6.87	123.66±12.04	269.16±17.84	557.12±27.01	256.44±17.80	115.69±11.93
K_{ev}	37.96±6.81	108.73±11.33	282.77±18.29	78.77±9.99	29.47±6.21	97.05±10.45	222.52±15.79	430.21±22.15	191.93±14.94	88.16±10.06
Cleo-c's Optimal Equal binning										
$K\pi$	73.26±9.09	170.20±13.76	139.39±12.53	243.77±16.21	354.28±19.09	362.24±20.76	76.46±9.12	316.43±18.11	127.86±11.74	107.98±10.61
$K\pi\pi^0$	168.05±13.81	308.05±18.36	225.36±16.51	399.55±21.88	599.54±26.37	661.36±37.95	162.15±14.02	504.27±24.34	195.15±15.19	226.32±16.51
$K3\pi$	88.59±10.65	180.00±14.62	141.55±12.94	239.91±17.11	328.82±20.44	392.76±22.58	86.19±11.29	286.83±19.12	101.56±11.81	132.56±13.23
K_{ev}	67.82±8.98	133.03±12.35	109.69±11.55	231.44±16.03	272.16±17.65	292.87±18.39	64.42±8.99	230.29±16.30	58.06±8.76	108.68±11.23
Cleo-c's Optimal Alternative binning										
$K\pi$	64.43±8.63	148.48±13.09	333.90±18.52	80.37±9.48	75.20±8.92	195.95±14.03	240.78±16.19	391.95±20.52	308.17±17.80	135.67±12.00
$K\pi\pi^0$	131.41±12.49	246.43±17.28	592.81±26.28	172.29±14.49	105.85±11.75	350.87±19.64	395.46±21.84	711.90±29.21	485.05±23.60	256.07±17.14
$K3\pi$	74.78±10.10	150.35±13.86	320.20±20.06	88.70±11.26	59.80±9.64	215.74±15.76	232.38±17.30	414.44±23.51	278.54±18.30	149.40±13.95
K_{ev}	58.85±8.40	131.28±12.52	261.63±17.32	71.13±9.50	37.83±7.28	144.98±12.85	225.98±15.86	292.95±18.42	225.95±16.17	116.76±11.59
BESIII's Equal $\Delta\delta_D$ binning										
$K\pi$	54.65±7.50	54.19±7.63	94.83±10.41	247.11±16.52	464.13±21.93	493.25±23.52	307.59±18.00	138.52±12.82	60.09±8.13	57.86±8.00
$K\pi\pi^0$	101.55±11.29	129.71±12.57	216.30±16.07	408.16±21.79	777.03±29.82	844.47±32.16	516.65±24.28	254.44±17.42	115.51±11.52	90.24±10.27
$K3\pi$	50.91±8.03	70.42±9.81	125.48±12.37	239.44±16.67	438.75±23.32	507.79±24.63	279.16±19.85	134.07±13.17	68.20±10.11	70.01±9.07
K_{ev}	43.77±7.27	48.69±7.58	68.11±9.08	229.02±16.21	362.66±20.32	384.17±21.08	216.33±15.96	115.07±11.60	44.76±7.42	54.15±7.99
BESIII's Alternative binning										
$K\pi$	24.35±5.38	127.77±12.58	356.67±20.20	95.66±10.03	28.45±5.68	83.99±9.18	213.34±15.20	600.03±24.61	348.03±18.78	96.64±10.16
$K\pi\pi^0$	40.68±8.31	248.40±17.59	626.95±27.21	165.23±14.21	42.72±7.66	191.83±14.96	364.39±20.15	992.93±34.76	594.55±26.44	177.11±14.41
$K3\pi$	58.63±7.81	145.73±13.21	330.53±19.97	99.10±12.49	38.88±6.91	89.32±10.23	228.26±16.22	605.50±26.79	320.02±20.48	105.71±12.00
K_{ev}	10.38±4.03	114.01±11.91	277.47±18.06	67.54±9.30	23.05±5.55	80.48±9.52	186.76±14.43	473.58±23.11	255.56±17.17	79.00±9.48
BESIII's Optimal Equal binning										
$K\pi$	107.19±10.51	138.26±12.58	95.04±10.80	248.77±16.23	378.24±19.88	461.29±22.05	66.57±8.58	313.45±18.11	79.68±9.39	89.00±10.21
$K\pi\pi^0$	216.83±16.84	323.81±19.18	176.41±14.95	384.72±21.53	633.14±27.01	747.15±30.15	135.69±13.32	548.47±24.98	132.40±12.39	148.10±13.33
$K3\pi$	97.02±11.50	171.65±14.58	111.88±11.67	249.20±16.78	341.70±20.23	426.73±23.11	75.96±10.08	321.34±20.58	81.40±12.10	112.76±11.95
K_{ev}	90.53±10.36	126.17±11.94	82.47±10.30	206.63±15.15	286.73±18.04	358.85±20.27	49.21±8.31	242.13±16.65	52.65±8.28	68.82±9.16
BESIII's Optimal Alternative binning										
$K\pi$	40.18±6.71	122.53±12.18	323.75±18.37	102.11±10.48	53.71±8.21	153.48±13.17	272.11±16.69	434.17±21.02	332.82±18.56	145.53±12.58
$K\pi\pi^0$	79.18±10.57	206.64±15.95	556.92±25.12	200.88±16.08	102.08±11.21	342.89±19.56	442.93±22.98	689.76±29.06	552.51±25.61	271.78±17.54
$K3\pi$	43.67±8.13	131.76±12.48	300.43±19.73	116.87±12.58	52.60±11.84	181.76±14.76	265.95±17.59	409.99±21.82	329.51±21.00	151.97±14.12
K_{ev}	31.18±6.46	100.13±11.27	242.53±16.63	78.83±10.04	40.65±7.44	129.70±12.01	251.13±16.68	325.75±19.28	246.22±16.83	122.79±11.84

- 1 Using the PWA result in BAM-439 [7], the correction factors are calculated, shown in Tab. 27.
 2 Then the K_i are summarised in Tab. 28. To make a comparision among different channels,
 3 the normalized quantities T_i are calculated in the following way:

$$T_i = K_i / \sum_i K_i, \quad (47)$$

- 4 The results as well as CLEO-c's results are shown in Figs. 22, in which they are consistent with
 5 each other within uncertainties. The comparision between two models' predictions are shown in
 6 Figs. 23.

Table 25: The summaries of background fraction for flavor tag channels.

Binning scheme	Bin -5	Bin -4	Bin -3	Bin -2	Bin -1	Bin 1	Bin 2	Bin 3	Bin 4	Bin 5
Cleo-c's Equal $\Delta\delta_D$ binning	0.031	0.056	0.075	0.112	0.225	0.227	0.114	0.075	0.055	0.030
Cleo-c's Variable $\Delta\delta_D$ binning	0.104	0.139	0.070	0.106	0.080	0.082	0.104	0.071	0.141	0.104
Cleo-c's Alternative binning	0.041	0.104	0.225	0.083	0.047	0.045	0.083	0.227	0.106	0.038
Cleo-c's Optimal Equal binning	0.049	0.097	0.109	0.063	0.180	0.184	0.061	0.111	0.100	0.046
Cleo-c's Optimal Alternative binning	0.053	0.112	0.186	0.064	0.083	0.080	0.066	0.192	0.114	0.050
BESIII's Equal $\Delta\delta_D$ binning	0.024	0.036	0.072	0.134	0.228	0.229	0.137	0.073	0.039	0.027
BESIII's Alternative binning	0.032	0.134	0.227	0.070	0.035	0.032	0.070	0.232	0.136	0.032
BESIII's Optimal Equal binning	0.052	0.066	0.123	0.057	0.199	0.206	0.056	0.122	0.066	0.052
BESIII's Optimal Alternative binning	0.052	0.128	0.185	0.069	0.065	0.063	0.070	0.190	0.129	0.050

Table 26: The efficiency matrix ϵ_{ij} with BESIII’s Equal $\Delta\delta_D$ binning for flavor tag channels.

Bin # (Truth) (Rec.)	-5	-4	-3	-2	-1	1	2	3	4	5
$K^- \pi^+$										
-5	0.3957	0.0258	0.0065	0.0019	0.0007	0.0005	0.0000	0.0014	0.0053	0.0261
-4	0.0187	0.3633	0.0290	0.0033	0.0021	0.0006	0.0002	0.0002	0.0025	0.0068
-3	0.0019	0.0127	0.3942	0.0257	0.0008	0.0003	0.0000	0.0004	0.0004	0.0012
-2	0.0003	0.0012	0.0120	0.3962	0.0180	0.0011	0.0003	0.0003	0.0001	0.0001
-1	0.0003	0.0002	0.0006	0.0108	0.4297	0.0143	0.0008	0.0002	0.0001	0.0002
1	0.0001	0.0001	0.0003	0.0009	0.0154	0.4306	0.0128	0.0009	0.0002	0.0001
2	0.0004	0.0002	0.0001	0.0004	0.0011	0.0230	0.4044	0.0133	0.0012	0.0004
3	0.0008	0.0004	0.0011	0.0004	0.0009	0.0028	0.0237	0.3867	0.0171	0.0027
4	0.0044	0.0004	0.0008	0.0008	0.0004	0.0017	0.0044	0.0338	0.3772	0.0184
5	0.0222	0.0056	0.0019	0.0014	0.0009	0.0007	0.0023	0.0035	0.0236	0.3835
$K^- \pi^+ \pi^0$										
-5	0.3778	0.0211	0.0053	0.0010	0.0014	0.0005	0.0005	0.0014	0.0057	0.0259
-4	0.0239	0.3749	0.0319	0.0040	0.0012	0.0000	0.0004	0.0008	0.0020	0.0044
-3	0.0020	0.0117	0.3806	0.0248	0.0024	0.0013	0.0004	0.0000	0.0002	0.0000
-2	0.0003	0.0014	0.0117	0.3903	0.0173	0.0006	0.0005	0.0003	0.0004	0.0001
-1	0.0002	0.0001	0.0008	0.0104	0.4141	0.0148	0.0011	0.0001	0.0004	0.0003
1	0.0001	0.0001	0.0001	0.0012	0.0150	0.4168	0.0106	0.0013	0.0003	0.0001
2	0.0001	0.0002	0.0005	0.0001	0.0020	0.0179	0.4025	0.0131	0.0012	0.0009
3	0.0005	0.0005	0.0002	0.0002	0.0009	0.0020	0.0223	0.3794	0.0151	0.0009
4	0.0050	0.0015	0.0008	0.0004	0.0004	0.0030	0.0050	0.0252	0.3603	0.0149
5	0.0203	0.0064	0.0014	0.0000	0.0009	0.0009	0.0005	0.0028	0.0239	0.3666
$K^- 3\pi^+$										
-5	0.3441	0.0227	0.0027	0.0022	0.0009	0.0000	0.0004	0.0018	0.0027	0.0218
-4	0.0163	0.3179	0.0205	0.0038	0.0015	0.0008	0.0004	0.0000	0.0019	0.0042
-3	0.0019	0.0112	0.3459	0.0224	0.0007	0.0002	0.0000	0.0005	0.0005	0.0014
-2	0.0003	0.0011	0.0115	0.3471	0.0166	0.0010	0.0004	0.0007	0.0002	0.0003
-1	0.0001	0.0002	0.0008	0.0116	0.3799	0.0126	0.0007	0.0002	0.0002	0.0002
1	0.0002	0.0000	0.0002	0.0011	0.0141	0.3797	0.0102	0.0009	0.0002	0.0003
2	0.0000	0.0001	0.0001	0.0003	0.0023	0.0204	0.3656	0.0125	0.0009	0.0001
3	0.0009	0.0002	0.0009	0.0013	0.0009	0.0034	0.0174	0.3450	0.0098	0.0028
4	0.0032	0.0014	0.0007	0.0000	0.0004	0.0018	0.0025	0.0245	0.3245	0.0202
5	0.0196	0.0034	0.0021	0.0000	0.0013	0.0026	0.0000	0.0043	0.0188	0.3173
$K^- e^+ \nu$										
-5	0.4027	0.0219	0.0033	0.0018	0.0015	0.0003	0.0012	0.0021	0.0068	0.0166
-4	0.0213	0.4046	0.0280	0.0035	0.0013	0.0005	0.0005	0.0005	0.0013	0.0043
-3	0.0022	0.0132	0.4152	0.0269	0.0021	0.0001	0.0000	0.0003	0.0003	0.0001
-2	0.0004	0.0013	0.0142	0.4226	0.0217	0.0012	0.0005	0.0004	0.0002	0.0001
-1	0.0000	0.0001	0.0007	0.0118	0.4500	0.0134	0.0009	0.0004	0.0002	0.0001
1	0.0001	0.0000	0.0002	0.0008	0.0153	0.4587	0.0121	0.0006	0.0002	0.0001
2	0.0002	0.0002	0.0001	0.0004	0.0010	0.0225	0.4308	0.0137	0.0012	0.0003
3	0.0004	0.0001	0.0003	0.0010	0.0007	0.0027	0.0248	0.4038	0.0180	0.0016
4	0.0056	0.0002	0.0007	0.0005	0.0012	0.0009	0.0045	0.0272	0.3855	0.0185
5	0.0204	0.0051	0.0014	0.0011	0.0014	0.0014	0.0023	0.0034	0.0249	0.4295

Table 27: The correction factor for quasi-flavor tag channels.

Tag channel	-5	-4	-3	-2	-1	1	2	3	4	5
Cleo-c's Equal $\Delta\delta_D$ binning										
$K^-\pi^+$	1.0320	1.0016	0.9803	0.9849	1.0107	1.0100	0.9839	0.9755	1.0018	1.0363
$K^-\pi^+\pi^0$	1.0191	1.0012	0.9885	0.9918	1.0062	1.0058	0.9913	0.9857	1.0014	1.0216
$K^-3\pi^+$	1.0081	0.9984	0.9904	0.9891	1.0026	1.0027	0.9883	0.9873	0.9973	1.0092
Cleo-c's Variable $\Delta\delta_D$ binning										
$K^-\pi^+$	1.0114	0.9813	0.9948	1.0092	1.0212	1.0203	1.0087	0.9954	0.9785	1.0139
$K^-\pi^+\pi^0$	1.0070	0.9894	0.9976	1.0054	1.0120	1.0115	1.0051	0.9979	0.9879	1.0085
$K^-3\pi^+$	1.0016	0.9890	0.9929	1.0021	1.0082	1.0081	1.0022	0.9937	0.9870	1.0016
Cleo-c's Alternative binning										
$K^-\pi^+$	1.0399	0.9770	1.0119	0.9635	1.0185	1.0073	0.9865	1.0093	0.9891	1.0193
$K^-\pi^+\pi^0$	1.0236	0.9869	1.0070	0.9796	1.0120	1.0046	0.9925	1.0054	0.9939	1.0114
$K^-3\pi^+$	1.0090	0.9858	1.0025	0.9754	0.9960	1.0009	0.9915	1.0028	0.9936	1.0059
Cleo-c's Optimal Equal binning										
$K^-\pi^+$	1.0340	0.9856	0.9868	0.9868	1.0167	1.0156	0.9576	0.9957	0.9746	1.0232
$K^-\pi^+\pi^0$	1.0202	0.9917	0.9928	0.9927	1.0097	1.0091	0.9761	0.9977	0.9854	1.0138
$K^-3\pi^+$	1.0081	0.9923	0.9889	0.9920	1.0050	1.0050	0.9719	0.9964	0.9854	1.0065
Cleo-c's Optimal Alternative binning										
$K^-\pi^+$	1.0352	0.9783	1.0183	0.9614	0.9805	0.9959	0.9864	1.0157	0.9897	1.0183
$K^-\pi^+\pi^0$	1.0208	0.9877	1.0106	0.9783	0.9895	0.9979	0.9925	1.0091	0.9942	1.0108
$K^-3\pi^+$	1.0081	0.9860	1.0056	0.9744	0.9827	0.9965	0.9916	1.0054	0.9936	1.0055
BESIII's Equal $\Delta\delta_D$ binning										
$K^-\pi^+$	1.0116	1.0009	0.9974	0.9875	1.0062	1.0062	0.9918	0.9984	1.0015	1.0124
$K^-\pi^+\pi^0$	1.0076	1.0012	0.9990	0.9932	1.0036	1.0036	0.9956	0.9995	1.0017	1.0080
$K^-3\pi^+$	0.9988	0.9954	0.9945	0.9904	1.0012	1.0014	0.9935	0.9959	0.9950	0.9992
BESIII's Alternative binning										
$K^-\pi^+$	1.0244	1.0013	1.0079	0.9604	0.9932	0.9998	0.9854	1.0055	1.0030	1.0090
$K^-\pi^+\pi^0$	1.0157	1.0017	1.0046	0.9774	0.9979	1.0004	0.9918	1.0032	1.0020	1.0056
$K^-3\pi^+$	0.9964	0.9919	1.0007	0.9755	0.9828	0.9969	0.9917	1.0017	0.9991	1.0012
BESIII's Optimal Equal binning										
$K^-\pi^+$	1.0055	0.9890	1.0092	0.9845	1.0140	1.0122	0.9372	1.0052	0.9721	1.0074
$K^-\pi^+\pi^0$	1.0038	0.9939	1.0064	0.9910	1.0082	1.0071	0.9630	1.0033	0.9843	1.0051
$K^-3\pi^+$	0.9984	0.9932	0.9937	0.9927	1.0036	1.0035	0.9660	1.0004	0.9812	0.9970
BESIII's Optimal Alternative binning										
$K^-\pi^+$	1.0180	1.0020	1.0201	0.9459	0.9674	0.9918	0.9818	1.0159	1.0032	1.0085
$K^-\pi^+\pi^0$	1.0116	1.0020	1.0116	0.9684	0.9819	0.9955	0.9895	1.0092	1.0022	1.0053
$K^-3\pi^+$	0.9973	0.9923	1.0062	0.9703	0.9762	0.9946	0.9910	1.0054	0.9995	1.0010

Table 28: The summary of K_i for flavor tag channels.

Tag channel	-5	-4	-3	-2	-1	1	2	3	4	5
Cleo-c's Equal $\Delta\delta_D$ binning										
$K^-\pi^+$	166.08±22.56	209.13±26.64	301.11±31.64	532.44±43.50	939.67±50.47	970.77±53.65	543.38±39.33	259.56±31.41	155.45±26.96	939.67±50.47
$K^-\pi^+\pi^0$	350.71±35.17	384.89±37.22	532.15±45.63	927.45±58.11	1573.89±72.58	1873.87±79.41	888.90±50.04	434.05±40.42	317.09±36.92	1573.89±72.58
$K^-3\pi^+$	211.06±29.24	255.79±34.39	309.47±40.05	604.43±48.26	1015.17±62.91	1141.48±66.75	570.58±49.03	288.55±37.79	178.01±31.02	1015.17±62.91
$K^-e^+\nu$	140.38±20.89	149.42±22.14	234.45±27.26	466.59±36.50	734.72±45.63	751.33±45.72	406.10±34.14	161.77±24.19	100.52±19.98	734.72±45.63
All	868.22±55.11	999.24±61.38	1377.18±73.69	2530.91±94.51	4263.45±117.71	4737.45±125.42	2408.95±87.30	1143.94±68.07	751.08±58.74	4263.45±117.71
Cleo-c's Variable $\Delta\delta_D$ binning										
$K^-\pi^+$	438.55±36.30	634.76±44.15	335.91±34.69	468.91±38.50	294.11±33.11	283.24±31.79	479.95±40.41	351.12±33.27	591.18±41.53	294.11±33.11
$K^-\pi^+\pi^0$	857.63±52.33	1086.59±61.59	577.67±47.19	781.65±55.69	493.03±47.83	572.77±50.48	928.94±57.96	638.68±48.99	927.63±56.10	493.03±47.83
$K^-3\pi^+$	543.43±46.81	681.83±52.52	394.62±40.85	481.86±44.86	315.42±41.15	342.46±41.92	599.03±48.94	311.96±40.74	634.77±51.11	315.42±41.15
$K^-e^+\nu$	363.17±31.90	575.34±39.84	228.21±27.87	401.77±35.08	187.49±27.52	202.06±27.34	383.99±34.93	264.86±28.85	406.52±34.78	187.49±27.52
All	2202.78±85.24	2978.52±100.44	1536.40±76.66	2134.18±88.47	1290.05±76.39	1400.53±77.87	2391.91±92.77	1566.62±77.45	2560.11±93.24	1290.05±76.39
Cleo-c's Alternative binning										
$K^-\pi^+$	75.03±17.76	297.18±32.02	698.63±46.45	220.79±28.24	65.64±17.06	298.09±28.85	549.51±40.90	1202.34±59.66	578.11±23.35	65.64±17.06
$K^-\pi^+\pi^0$	173.99±26.70	442.89±40.91	1473.25±67.79	312.17±2.53	99.93±23.58	604.98±44.78	1021.27±59.23	1957.98±80.43	997.46±55.86	99.93±23.58
$K^-3\pi^+$	143.84±25.11	229.33±34.51	783.11±54.70	232.85±34.13	48.65±20.65	328.90±34.64	707.48±51.15	1354.94±71.89	640.01±49.20	48.65±20.65
$K^-e^+\nu$	73.39±15.96	207.24±25.64	565.02±41.05	155.08±22.91	55.05±15.09	223.85±25.49	498.10±36.84	917.10±49.89	415.21±33.89	55.05±15.09
All	466.25±43.74	1176.65±67.43	3520.01±106.92	920.89±49.94	269.27±38.75	1455.81±68.47	2776.36±95.68	5432.36±132.99	2630.78±85.05	269.27±38.75
Cleo-c's Optimal Equal binning										
$K^-\pi^+$	152.91±23.17	383.96±35.14	257.15±30.81	576.40±41.24	742.91±45.07	754.36±48.48	124.90±21.90	712.93±43.89	262.83±30.29	742.91±45.07
$K^-\pi^+\pi^0$	383.58±36.79	694.46±46.83	411.48±40.34	1018.60±59.75	1271.24±65.23	1422.43±92.08	298.94±33.91	1150.54±59.96	400.78±40.94	1271.24±65.23
$K^-3\pi^+$	206.87±30.22	465.81±42.65	291.91±34.93	658.44±50.45	748.45±54.91	935.58±60.99	164.42±30.29	720.05±52.36	218.31±35.42	748.45±54.91
$K^-e^+\nu$	134.95±20.93	297.99±30.05	205.55±26.47	551.07±39.30	551.63±39.69	599.00±40.76	119.18±20.27	499.29±36.71	116.01±22.01	551.63±39.69
All	878.31±56.94	1842.22±78.42	1166.08±67.06	2804.52±96.75	3314.23±104.29	3711.37±127.32	707.44±54.39	3082.81±98.04	997.93±65.83	3314.23±104.29
Cleo-c's Optimal Alternative binning										
$K^-\pi^+$	131.25±21.78	279.65±31.92	692.57±43.72	134.45±22.96	136.96±22.94	455.17±35.33	564.45±41.26	823.80±47.46	680.81±42.76	136.96±22.94
$K^-\pi^+\pi^0$	267.78±32.03	460.07±42.47	1250.00±64.60	318.24±35.19	181.03±31.31	871.93±52.39	983.14±59.10	1545.86±70.75	1103.29±58.75	181.03±31.31
$K^-3\pi^+$	165.27±28.71	320.50±37.88	717.72±53.58	172.77±30.17	109.03±28.60	577.02±45.64	633.37±51.73	991.50±62.69	697.24±50.22	109.03±28.60
$K^-e^+\nu$	113.58±19.33	261.70±28.83	522.04±38.71	129.81±21.26	67.75±18.37	333.70±31.38	535.13±38.95	605.11±40.79	484.76±36.38	67.75±18.37
All	677.89±51.94	1321.92±71.34	3182.33±102.24	755.27±55.93	494.76±51.60	2237.82±84.03	2716.09±96.89	3966.26±113.36	2966.10±95.52	494.76±51.60
BESIII's Equal $\Delta\delta_D$ binning										
$K^-\pi^+$	116.70±19.15	120.53±21.20	193.09±26.61	544.00±41.88	978.03±51.22	1034.44±54.87	672.11±44.75	302.79±33.45	123.67±21.81	978.03±51.22
$K^-\pi^+\pi^0$	221.95±30.21	293.25±33.80	474.45±42.55	899.11±56.09	1677.33±72.29	1826.90±77.44	1133.66±60.60	572.78±46.21	252.85±32.26	1677.33±72.29
$K^-3\pi^+$	116.25±23.61	184.85±31.11	304.05±36.00	585.23±48.30	1021.33±61.65	1204.40±65.15	670.60±54.52	322.27±38.44	171.39±31.40	1021.33±61.65
$K^-e^+\nu$	93.96±18.20	107.21±18.87	136.19±22.04	508.04±38.54	751.29±45.32	789.36±46.12	460.95±37.23	259.02±28.94	91.93±19.45	751.29±45.32
All	548.86±46.56	705.84±54.00	1107.79±65.57	2536.38±93.38	4427.98±117.06	4855.10±124.01	2937.33±100.17	1456.86±74.63	639.84±53.67	4427.98±117.06
BESIII's Alternative binning										
$K^-\pi^+$	35.41±14.00	245.80±31.39	721.95±47.33	166.18±24.84	46.19±14.65	191.32±22.87	479.75±37.22	1279.40±56.31	797.73±46.21	46.19±14.65
$K^-\pi^+\pi^0$	55.12±20.57	483.29±44.61	1304.30±66.08	296.14±35.46	52.26±20.37	486.44±40.99	851.01±51.49	2177.87±82.41	1436.33±68.18	52.26±20.37
$K^-3\pi^+$	138.84±22.73	317.04±37.45	713.38±52.19	189.69±34.57	74.91±20.60	235.41±30.32	593.46±46.05	1479.08±70.46	831.09±57.89	74.91±20.60
$K^-e^+\nu$	10.95±9.66	229.72±27.57	554.88±40.23	120.37±21.82	38.97±13.40	183.54±22.78	422.92±34.09	984.55±49.99	578.49±40.33	38.97±13.40
All	240.32±35.06	1275.84±71.68	3294.51±104.64	772.38±59.54	212.32±35.12	1096.71±60.34	2347.14±85.55	5920.90±132.01	3643.64±108.45	212.32±35.12
BESIII's Optimal Equal binning										
$K^-\pi^+$	234.71±25.64	305.73±31.53	171.98±27.18	573.68±40.17	777.76±45.76	973.07±50.77	109.69±20.58	730.81±44.52	143.79±23.89	777.76±45.76
$K^-\pi^+\pi^0$	524.94±44.85	755.82±48.97	307.82±37.97	956.75±57.48	1327.93±64.29	1558.96±70.35	244.73±33.10	1379.88±66.29	238.22±32.06	1327.93±64.29
$K^-3\pi^+$	235.81±32.36	452.25±42.80	234.01±33.39	637.68±45.57	773.78±52.59	1004.84±61.22	146.76±26.45	847.82±57.60	158.49±34.40	773.78±52.59
$K^-e^+\nu$	196.95±24.31	282.77±28.64	160.91±23.96	456.76±34.71	580.03±39.49	730.61±43.70	86.22±18.89	553.89±38.97	100.18±20.39	580.03±39.49
All	1192.40±65.63	1796.57±77.75	874.73±62.21	2624.87±90.55	3459.50±102.73	4267.48±114.83	587.41±50.75	3512.39±105.89	640.67±56.55	3459.50±102.73
BESIII's Optimal Alternative binning										
$K^-\pi^+$	62.60±16.64	237.95±30.65	662.51±42.29	180.88±25.12	77.02±20.49	348.73±32.97	614.93±40.81	923.53±48.43	768.93±45.63	77.02±20.49
$K^-\pi^+\pi^0$	129.66±25.87	386.20±40.52	1177.88±60.45	383.55±39.62	158.32±29.26	847.44±51.66	1020.65±57.86	1461.73±68.26	1342.12±66.04	158.32±29.26
$K^-3\pi^+$	76.80±22.84	288.07±35.90	674.05±51.62	231.04±32.82	87.62±33.89	495.07±43.35	689.29±49.02	987.00±57.89	850.83±58.07	87.62±33.89
$K^-e^+\nu$	51.12±14.70	202.12±26.40	480.80±36.49	146.11±22.70	71.24±18.14	292.44±28.47	567.09±38.87	667.45±41.85	549.44±38.81	71.24±18.14
All	320.18±41.03	1114.33±67.58	2995.24±97.15	941.59±61.58	394.21±52.47	1983.68±80.28	2892.55±94.48	4039.72±110.03	3511.33±106.40	394.21±52.47

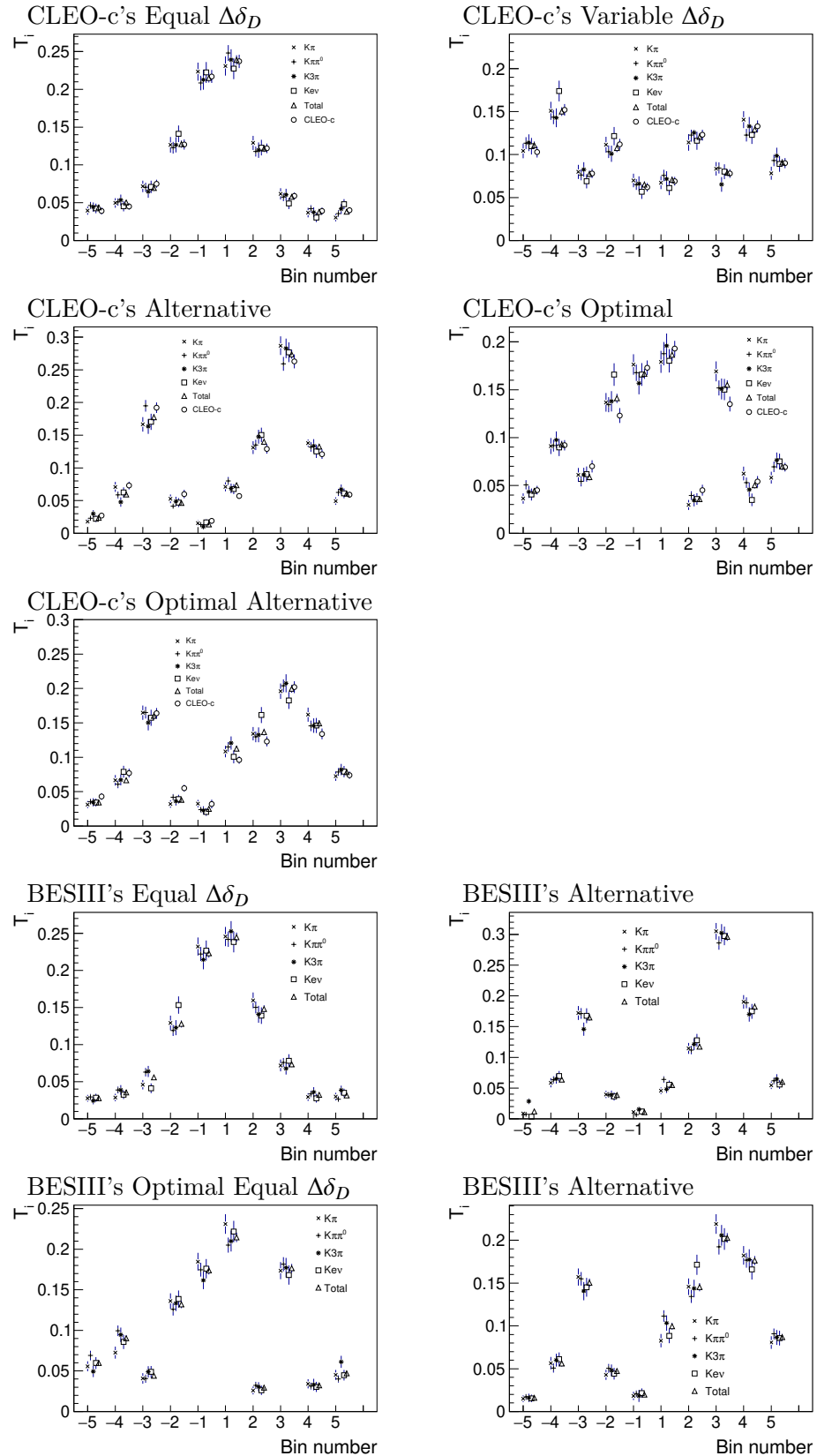


Figure 22: Comparisons of T_i between four flavor tag channels, BESIII's, and CLEO-c's, for different binning schemes. Here for BESIII's results, the uncertainties are only for statistical uncertainties.

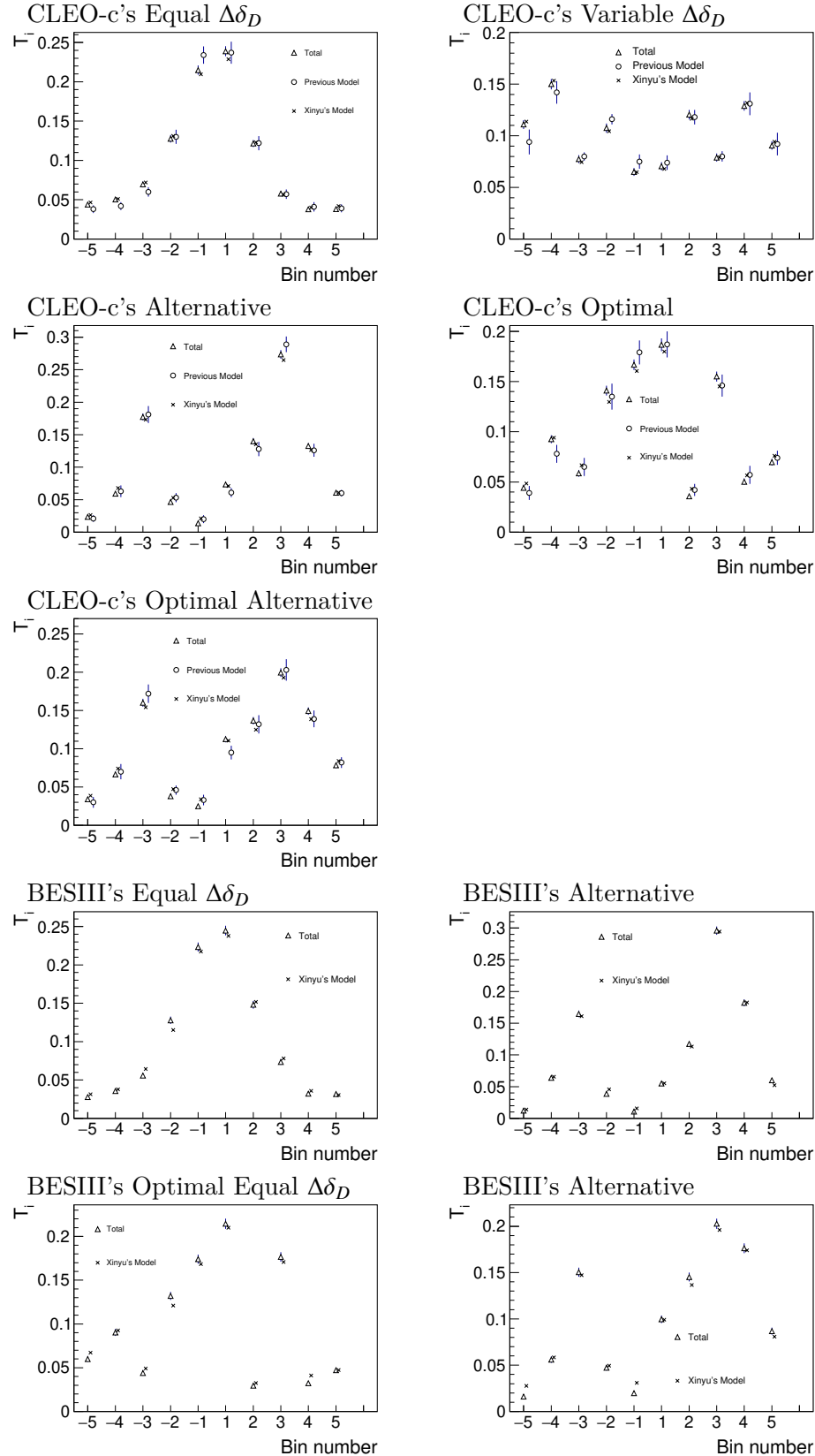


Figure 23: Comparisons of T_i between BESIII's, BESIII's model prediction and CLEO-c's model prediction, for different binning schemes. Here for BESIII's results, the uncertainties are only for statistical uncertainties. For BESIII's model prediction, the uncertainties are meaningless.

1 8.2 c_i & s_i measurement

2 Then the CP tag, $\pi^+\pi^-\pi^0$ tag and $K_S^0/K_L^0\pi^+\pi^-$ tag are used to extracted c_i & s_i .

3 In the Eqs. 27 28, the efficiency of flavor tag side are canceled in the numerator K_i and
4 denominator $N_{flavor,ST}$ terms. (This is also the reason that the K_i is only corrected for signal
5 side's efficiency in previous section.) In Eq. 27, the CP tag efficiency are also canceled in the
6 $N(cp,i)$ and $N_{cp,ST}$ terms. Then for CP tag and $\pi^+\pi^-\pi^0$ tag, after including efficiency and peak
7 background, the expected yield in i -th bin is:

$$< N(cp,i) > = \sum_{j=1}^{Nbin} \epsilon_{ij} \left[\frac{N_{cp,ST}}{2N_{flavour,ST}(1 - \eta_{cp}y)} (K_j + K_{-j} - 2\sqrt{K_j K_{-j}} c_j \eta_{CP}) \right] + N(i)_{bkg}, \quad (48)$$

8 where ϵ_{ij} describes the reconstruction efficiency of the signal side and bin migration effect across
9 the bins of 4π side. For $K_S^0/K_L^0\pi^+\pi^-$ tag, after including efficiency and peak background, the
10 expected yield in bin (i,j) is:

$$< N(i,j) > = \sum_{k,l} \epsilon(i,j,k,l) \left[\frac{N_{D\bar{D}}}{2N_{flavour,ST} N'_{flavour,ST}} * (K_k K_{-l} + K_{-k} K_l \mp 2\sqrt{K_k K_{-l} K_{-k} K_l} (c_k c_l + s_k s_l)) \right] + N(i,j)_{bkg}, \quad (49)$$

11 where the $\epsilon(i,j,k,l)$ describes the reconstruction efficiency of double side and bin migration effect
12 across the bins of $(4\pi, K_S^0/K_L^0\pi^+\pi^-)$. As mentioned in Sec. 8, some bins can be combined: for
13 each CP tag and $\pi^+\pi^-\pi^0$ tag, there are 5 local phase spaces because the i -th and $-i$ -th bins
14 are combined; for $K_S^0/K_L^0\pi^+\pi^-$ tag case, there are 80 local phase spaces because the (i,j) -th and
15 $(-i,-j)$ -th bins are combined.

16 The efficiency matrixes are obtained from signal MC. The peak background in each local
17 phase space is estimated by the product of total background and the background fraction, where
18 the fraction is estimated by $K_S^0\pi^+\pi^-$ MC. For $\pi^+\pi^-\pi^0$ tag channel, the $K_S^0\pi^0$ background's fraction
19 is estimated by $K_S^0\pi^0$ v.s. $4\pi^\pm$ MC.

20 The observed yields in each local bin for each tag modes are obtained by the unbinned fits,
21 summarized in Tab. 29 30. (For $K_S^0\pi^+\pi^-$ and $K_L^0\pi^+\pi^-$ tag channels, the yields for other 8 binning
22 schemes are shown in App. D.2.) Then with the expected yields and observed yields, the c_i and
23 s_i can be extracted by minimizing the negative log likelihood as:

$$\begin{aligned} -2\log\mathcal{L} = & -2 \sum_{CPtag} \sum_i \log P(N_i; < N_i >)_{CP} \\ & - 2 \sum_i \log P(N_i; < N_i >)_{\pi^+\pi^-\pi^0}, \\ & - 2 \sum_i \sum_j \log P(N_{ij}; < N_{ij} >)_{K_S^0\pi^+\pi^-}, \\ & - 2 \sum_i \sum_j \log P(N_{ij}; < N_{ij} >)_{K_L^0\pi^+\pi^-}, \end{aligned} \quad (50)$$

1 where the $P(N, < N >)$ is the Poisson probability. Before fitting to data, a check by toy MC is
 2 performed. In the toy MC, the yield in each bin is generated according to the Poisson distribution
 3 with a set of hypothesis c_i and s_i . The pull value shows there is no bias in the fit procedure,
 4 shown in Figs 24.

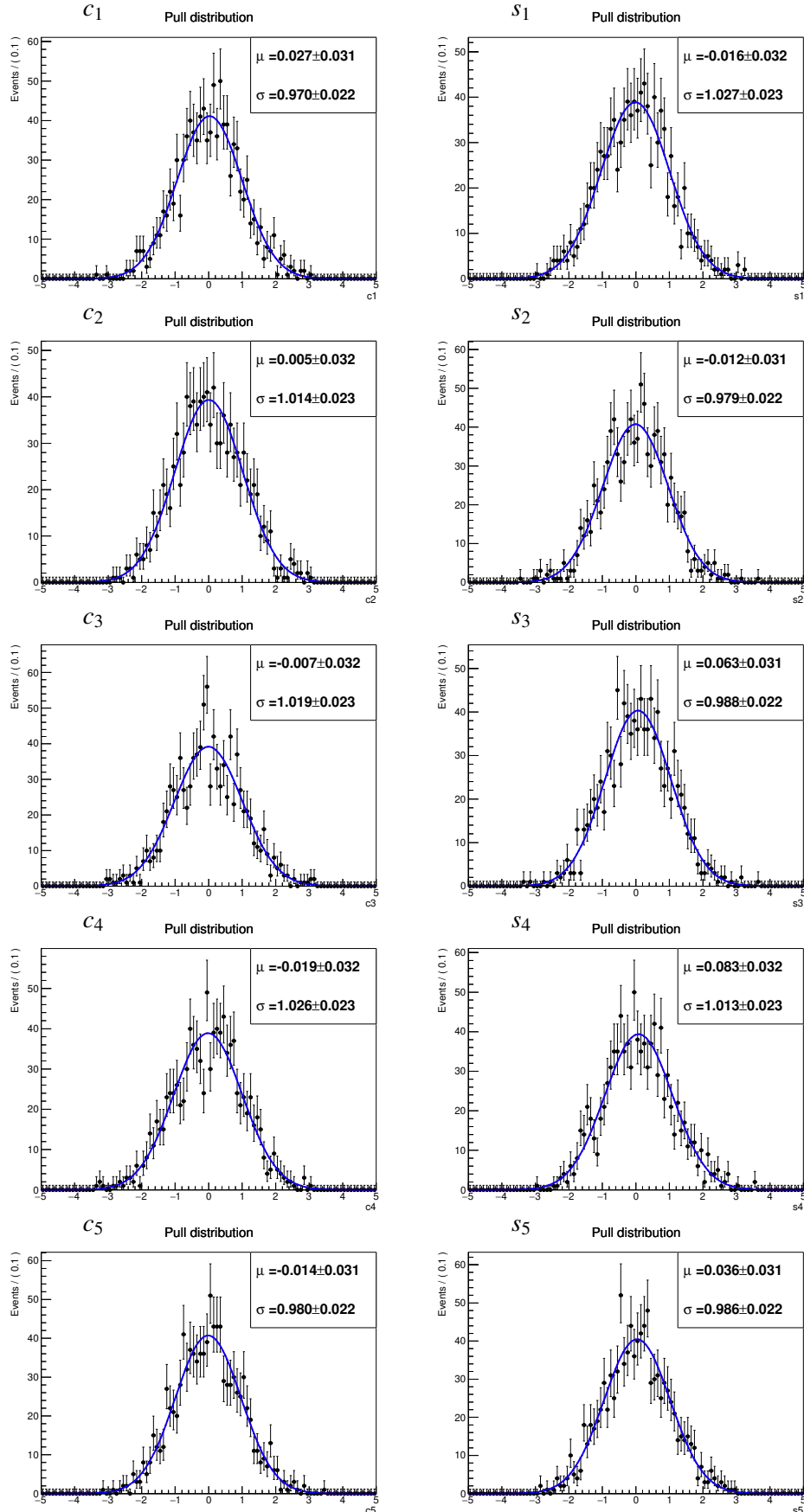
5 The fit results of data are shown in Tab. 31 and Figs. 25–26. With CLEO-c’s binning schemes,
 6 predictions from BESIII’s model (blue circles) and CLEO-c’s model (black circles with err bar)
 7 are significant different. For measured results, BESIII’s are more precise than CLEO-c’s, but
 8 also more close to each other, which is not good for γ measurement. Then the results from
 9 BESIII’s binning schemes are more important in this work.

Table 29: The summaries of fitted yields for cp tag and $\pi^+\pi^-\pi^0$ tag channels.

Bin	$\pi^+\pi^-\pi^0$	$K_S^0\pi^0$	$K_S^0\omega$	$K_S^0\eta(3\pi)$	$K_S^0\eta(\rho\gamma)$	$K_S^0\eta(2\gamma)$	$K_S^0\eta(\pi^+\pi^-\eta)$	K^+K^-	$K_S^0\pi^0\pi^0$	$K_I^0\pi^0\pi^0$	$K_I^0\pi^0$	$K_I^0\omega$
Cleo-c’s Equal $\Delta\delta_D$ binning												
1	71.48±13.53	174.45±13.44	91.12±10.61	7.98±2.82	15.71±4.90	36.05±6.01	7.00±2.65	27.74±7.76	9.43±4.05	69.23±14.59	22.47±10.41	0.00±18.18
2	52.89±11.36	97.92±10.53	24.10±5.46	6.00±2.45	7.51±3.03	15.01±3.87	3.00±1.73	26.35±6.02	5.08±3.14	42.68±11.83	24.47±10.44	19.59±7.27
3	43.37±9.68	35.02±6.12	14.74±4.80	1.52±1.55	6.08±2.67	3.00±1.73	0.00±0.50	25.88±5.77	5.52±2.83	31.42±7.72	25.26±10.05	12.60±5.39
4	36.11±8.66	10.00±3.16	4.85±2.27	0.00±0.50	4.47±2.29	1.00±0.85	0.00±0.50	12.84±4.41	3.12±2.06	13.59±6.38	26.30±8.70	4.00±4.41
5	35.39±7.89	17.01±4.13	6.69±3.01	1.00±0.85	4.66±2.41	4.00±2.00	2.00±1.41	27.29±6.06	4.40±2.76	5.48±4.79	23.39±7.54	11.30±4.97
Cleo-c’s Variable $\Delta\delta_D$ binning												
1	23.25±7.12	39.02±5.84	39.40±6.52	3.01±1.74	3.69±2.94	11.99±3.46	1.00±1.00	9.24±4.40	3.69±2.41	27.46±7.54	7.20±5.79	0.00±1.94
2	36.28±9.49	104.56±10.40	37.17±6.54	1.10±1.25	8.41±3.46	15.00±2.34	4.00±2.00	10.99±4.76	4.74±2.99	31.69±9.67	7.61±7.66	5.34±4.46
3	28.74±8.58	54.55±7.81	23.05±5.20	5.00±2.24	4.88±2.54	11.01±3.32	4.00±1.64	21.48±5.35	3.66±2.42	10.79±8.52	13.31±6.78	0.00±5.19
4	76.86±12.89	98.74±10.46	26.75±11.86	6.00±2.09	9.97±3.46	13.00±2.03	1.00±1.00	36.10±7.44	9.35±3.76	64.31±1.18	49.94±12.92	31.84±8.76
5	77.88±12.56	37.04±6.09	14.51±4.40	0.95±1.02	12.25±3.87	8.00±2.83	2.00±1.41	44.36±7.60	6.53±3.38	23.56±9.46	44.92±11.91	15.58±6.77
Cleo-c’s Alternative binning												
1	28.41±7.99	11.00±3.32	5.83±2.56	0.00±0.50	5.00±1.53	2.00±1.41	0.00±0.50	24.53±5.61	2.32±2.20	3.84±4.70	19.47±8.17	7.82±4.51
2	58.63±11.03	63.23±8.61	23.78±5.30	0.97±1.84	7.86±3.25	10.00±3.16	1.00±1.00	30.06±6.35	3.96±2.66	37.94±10.40	22.46±10.81	18.03±6.42
3	75.39±13.69	174.45±13.44	91.12±10.61	7.98±2.82	16.64±5.03	36.05±6.01	7.00±2.65	27.74±7.76	9.43±4.05	69.23±14.59	22.57±10.40	0.00±18.66
4	38.19±9.78	69.00±5.85	15.13±4.64	6.00±2.45	5.00±2.24	8.03±2.84	2.00±1.41	21.87±5.44	6.46±3.20	36.98±9.99	28.00±9.90	13.69±6.34
5	42.29±8.68	15.97±4.00	6.25±2.95	1.00±0.85	3.04±2.25	3.00±1.73	2.00±1.41	16.54±4.74	5.70±2.73	14.40±6.22	29.61±7.78	7.57±4.94
Cleo-c’s Optimal Equal binning												
1	52.74±11.31	141.13±12.15	74.33±9.11	7.98±2.82	13.99±4.59	28.03±5.30	6.00±2.45	22.40±6.70	4.73±2.99	59.55±13.13	14.24±8.96	0.00±4.13
2	46.25±9.80	56.03±7.49	21.38±5.07	2.00±1.41	8.12±3.23	9.00±3.00	1.00±1.00	27.29±6.01	1.58±2.13	30.13±9.98	15.71±9.50	16.49±6.18
3	42.05±9.86	81.69±9.64	26.07±5.78	2.24±1.94	5.69±2.69	12.00±3.46	2.00±1.41	15.78±4.97	9.94±3.72	23.33±9.72	30.53±9.63	7.38±5.82
4	48.55±10.15	34.42±6.20	7.35±3.68	0.00±2.82	5.96±2.51	5.00±2.24	0.00±0.50	16.99±5.12	4.42±2.79	34.14±9.99	30.16±10.23	8.40±5.26
5	52.64±10.24	20.00±4.47	10.32±3.58	3.00±1.73	6.17±2.88	5.00±2.24	3.00±1.73	41.75±7.21	6.49±3.43	16.04±6.41	34.17±9.30	18.46±6.25
Cleo-c’s Optimal Alternative binning												
1	46.41±10.07	30.00±5.48	5.59±2.99	0.00±2.82	6.99±2.70	5.00±2.24	0.00±0.50	19.68±5.59	3.14±2.39	23.94±8.87	21.09±10.02	11.51±5.63
2	35.91±8.94	56.06±7.49	24.29±5.40	2.00±1.41	8.18±3.23	9.00±3.00	1.00±1.00	25.71±6.03	1.98±2.16	23.85±9.73	15.44±9.11	14.50±6.11
3	51.41±11.72	143.86±12.28	77.60±9.19	7.98±2.82	13.47±4.65	31.04±5.58	7.00±2.65	23.09±6.42	5.82±3.26	57.25±12.93	12.76±9.07	0.00±5.22
4	53.20±11.05	78.48±9.39	23.09±5.53	2.24±1.94	5.39±2.60	9.00±3.00	1.00±0.71	18.58±5.29	10.22±3.77	31.70±8.70	36.42±10.23	10.40±6.08
5	56.05±10.31	24.00±3.10	11.60±3.63	3.00±1.73	4.91±2.66	5.00±2.24	3.00±1.73	35.80±6.65	6.44±3.16	23.19±2.31	37.23±8.87	13.71±5.76
BESIII’s Equal $\Delta\delta_D$ binning												
1	67.75±13.67	192.57±5.12	89.50±10.56	8.00±0.76	27.25±5.62	37.05±6.10	5.98±2.44	27.60±6.80	12.25±7.03	68.49±14.99	28.16±11.20	0.00±5.02
2	74.74±13.78	96.57±10.17	33.99±6.50	5.80±2.51	7.33±3.19	11.98±3.46	3.99±2.01	32.18±6.82	11.38±4.94	51.46±11.93	28.79±10.54	25.56±7.27
3	39.39±10.35	33.85±5.93	9.45±3.50	3.00±1.73	6.36±2.96	7.00±2.65	1.00±0.61	28.11±5.93	7.66±3.13	24.12±7.81	23.40±9.04	15.39±6.20
4	29.01±7.55	9.00±3.00	4.56±2.33	0.00±0.50	4.00±2.00	1.99±1.41	0.00±0.50	16.84±5.01	7.52±3.06	10.65±5.19	15.93±8.15	5.86±4.55
5	37.92±9.12	5.00±2.24	0.00±0.50	1.95±1.43	1.00±1.00	1.00±0.83	22.43±5.63	5.00±2.24	4.00±5.48	28.14±7.43	1.50±3.58	
BESIII’s Alternative binning												
1	36.02±8.14	9.00±3.00	3.99±2.05	0.00±0.50	2.93±1.76	4.00±2.00	1.00±0.83	17.56±4.82	6.13±2.79	16.37±6.93	17.87±8.51	1.97±3.73
2	43.81±10.46	45.81±7.03	16.60±4.56	2.00±1.41	7.00±2.65	3.99±2.00	0.00±0.50	25.91±6.12	9.15±4.72	35.76±10.35	12.40±9.58	6.07±5.23
3	68.82±13.49	200.92±14.45	91.20±10.61	8.00±2.83	27.11±5.67	36.05±6.01	5.98±2.16	75.55±11.22	8.46±4.38	68.47±14.92	24.25±10.98	0.00±11.18
4	68.13±14.06	74.68±8.98	25.16±5.73	8.00±2.83	6.99±3.06	15.00±3.87	3.99±2.00	75.07±18.43	9.60±3.76	42.77±10.75	43.70±10.38	34.02±7.93
5	119.00±27.94	6.00±2.45	0.00±0.50	2.00±1.41	0.00±0.50	1.00±1.00	19.64±5.41	8.82±3.07	1.13±3.44	25.99±7.63	4.61±4.27	
BESIII’s Optimal Equal binning												
1	59.11±12.11	168.46±13.36	73.95±9.36	6.00±2.45	19.00±4.36	33.00±5.74	5.98±2.16	58.65±12.21	12.22±8.46	67.25±14.38	14.91±8.98	0.00±2.23
2	33.58±12.71	63.02±7.99	26.61±6.07	1.00±0.16	10.00±3.16	9.01±3.01	0.00±0.50	17.94±4.87	7.17±3.60	17.17±8.46	17.25±8.51	7.73±5.01
3	69.00±14.91	66.00±8.33	22.55±5.44	9.00±3.00	8.93±3.38	11.00±3.32	3.99±2.00	57.18±12.36	12.07±4.33	32.10±9.87	44.01±9.08	33.99±7.91
4	37.15±9.32	27.18±5.45	11.96±3.97	2.00±1.41	6.00±2.45	2.99±1.73	0.00±0.50	26.42±7.03	4.25±2.63	28.20±5.82	0.00±19.82	6.31±5.21
5	53.54±10.37	10.00±3.16	7.44±3.09	0.00±0.50	3.94±2.03	3.00±1.73	2.00±1.42	31.82±6.65	9.20±8.46	11.85±7.25	49.43±10.93	3.89±5.01
BESIII’s Optimal Alternative binning												
1	101.03±35.55	22.48±4.96	7.43±2.95	1.00±1.00	6.00±2.45	3.99±2.00	1.00±0.83	25.40±5.96	10.69±3.51	24.69±15.37	14.46±9.77	4.66±5.38
2	43.85±11.03	80.07±9.01	34.04±5.84	2.00±1.10	9.00±3.00	9.01±3.01	1.00±0.81	40.08±10.43	6.60±6.56	31.39±9.95	18.65±9.51	10.56±5.46
3	50.59±11.30	147.83±12.40	68.11±9.00	6.00±2.45	20.00±4.47	32.00±5.66	5.00±2.24	52.23±11.32	12.88±5.45	58.82±13.10	15.18±8.37	0.00±1.65
4	62.53±13.44	69.85±8.79	28.23±5.91	8.00±2.83	5.63±2.55	9.00±3.00	3.99±2.00	33.26±6.94	10.15±3.85	36.79±10.91	39.52±9.37	32.08±7.70
5	59.30±14.66	14.98±3.87	9.00±3.00	1.00±1.00	7.67±2.93	5.00±2.24	1.00±1.00	28.27±6.19	10.98±3.95	9.26±6.41	37.43±9.78	5.91±5.07

Table 30: The summaries of fitted yields for $K_S^0\pi^+\pi^-$ and $K_L^0\pi^+\pi^-$ tag channels for BESIII's Equal $\Delta\delta_D$ binning scheme.

		$K_S^0\pi^+\pi^-$ tag							
		1	2	3	4	5	6	7	8
i \ j		-1	-2	-3	-4	-5	-6	-7	-8
1	13.35±4.41	5.81±2.94	12.30±3.83	11.99±3.48	44.95±6.83	15.00±3.87	12.08±3.62	13.97±3.84	
2	18.88±4.37	3.90±2.36	2.00±1.41	1.91±1.44	20.02±4.48	4.93±2.29	17.65±4.56	19.02±4.36	
3	10.89±3.59	3.93±2.42	1.99±1.44	2.00±1.47	5.98±2.46	1.00±1.00	5.00±2.24	6.01±2.45	
4	3.79±2.27	1.64±1.56	1.00±1.00	1.00±1.00	1.61±1.57	0.00±0.59	7.37±2.93	4.00±2.00	
5	8.04±3.12	3.00±1.73	2.00±1.41	1.73±1.48	2.00±1.42	4.09±2.46	3.35±2.16	1.67±1.49	
1	17.31±4.53	6.87±2.99	10.55±24.68	6.96±2.72	31.86±6.16	14.07±3.99	21.99±4.74	6.58±2.94	
2	21.26±5.27	9.00±3.00	4.91±2.35	4.45±2.37	19.33±4.68	5.66±2.53	10.42±3.45	2.60±1.81	
3	6.48±2.82	5.21±2.63	8.00±2.83	1.99±1.41	4.11±2.60	3.13±2.38	2.01±1.53	5.70±2.67	
4	1.04±0.47	1.91±1.48	2.96±1.75	0.99±1.00	4.86±2.29	0.97±1.04	3.00±1.73	2.94±1.83	
5	3.73±2.46	1.00±1.00	2.57±1.85	1.00±1.00	1.86±1.48	1.00±1.00	2.97±1.74	4.00±2.00	
		$K_L^0\pi^+\pi^-$ tag							
i \ j		1	2	3	4	5	6	7	8
1	134.32±13.59	51.95±8.45	26.49±6.16	7.18±3.42	20.17±5.74	30.14±6.60	50.82±7.99	68.88±9.32	
2	84.41±10.59	20.92±5.58	24.60±6.41	4.67±2.70	8.37±4.19	7.84±3.39	19.95±5.43	24.67±5.98	
3	33.20±7.16	9.41±3.95	12.04±4.39	8.44±3.62	11.05±4.95	7.66±3.17	12.33±4.27	15.87±4.92	
4	12.08±4.44	3.69±2.61	1.84±2.86	4.16±2.46	7.93±4.08	2.78±2.03	5.91±3.06	6.08±3.12	
5	6.43±3.94	8.26±3.73	0.01±0.50	2.14±2.07	11.14±3.93	5.78±2.81	2.49±2.17	2.22±2.32	
1	146.07±14.02	40.93±8.36	27.07±6.62	15.85±4.72	9.15±4.89	27.93±6.30	51.74±8.23	76.95±10.06	
2	79.52±10.49	19.67±5.78	8.36±3.86	1.72±2.59	6.94±3.59	21.94±5.59	36.51±7.18	34.93±7.28	
3	31.43±6.96	16.29±4.73	10.13±3.88	0.39±1.34	8.30±4.09	8.89±3.79	19.04±5.02	16.71±4.98	
4	10.84±4.44	4.15±2.87	4.60±2.47	0.92±1.34	5.43±3.30	7.39±3.01	4.42±2.42	7.42±3.49	
5	7.12±3.74	0.83±2.02	3.97±3.13	2.38±1.97	3.24±2.70	4.44±2.43	5.14±3.31	2.87±2.33	

Figure 24: Pull distributions of c_i (left) and s_i (right) for CLEO-c's binning schemes.

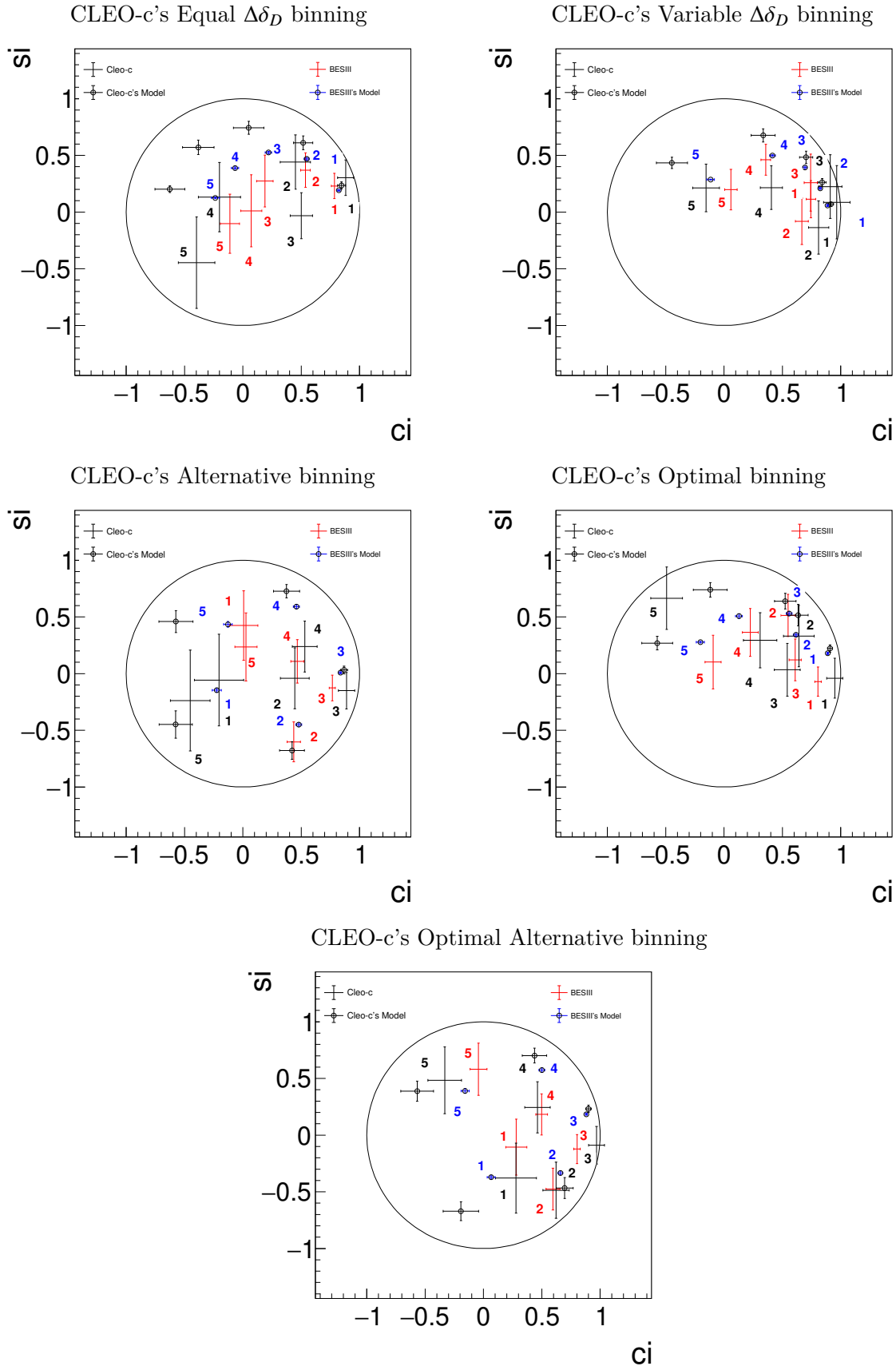


Figure 25: Results of c_i and s_i for CLEO-c's binning schemes. The red cross are our results, the black cross are CLEO-c's results, the black hollow circles with error bar are CLEO-c's model predictions, the blue hollow circles are BESIII's model predictions.

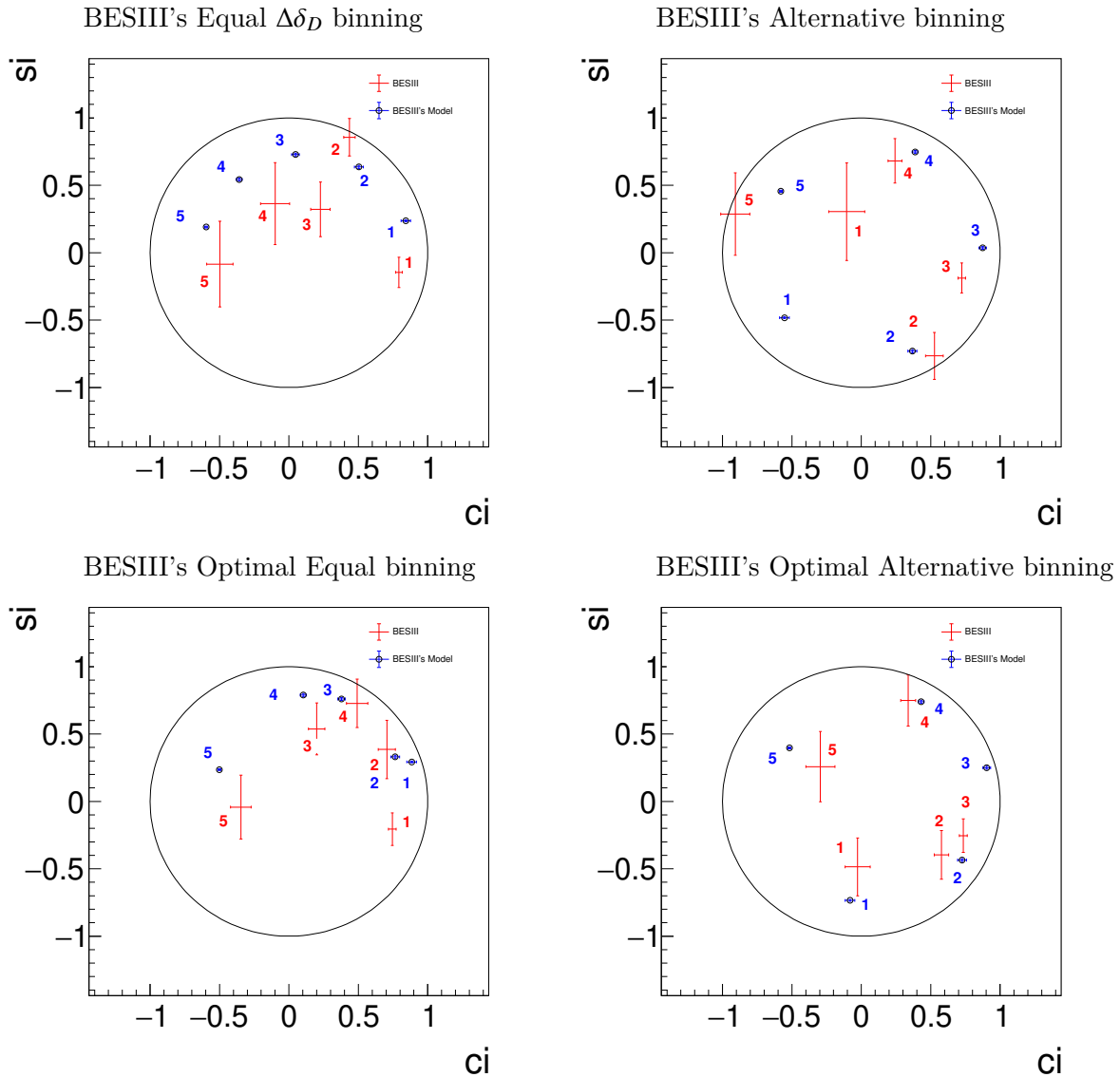


Figure 26: Results of c_i and s_i for BESIII's binning schemes. The red cross are our results, the blue hollow circles are BESIII's model predictions.

Table 31: The summaries of c_i , s_i results. Only statistical uncertainties are shown. The BESIII's model's uncertainties are meaningless.

	c_1	c_2	c_3	c_4	c_5	s_1	s_2	s_3	s_4	s_5
Cleo-c's Equal $\Delta\delta_D$ binning										
BESIII's	0.78±0.03	0.54±0.04	0.19±0.07	0.07±0.09	-0.11±0.08	0.23±0.11	0.37±0.15	0.27±0.23	0.01±0.32	-0.10±0.26
CLEO-c's	0.88±0.07	0.50±0.10	0.45±0.13	-0.20±0.18	-0.40±0.16	0.30±0.16	-0.03±0.20	0.44±0.24	0.13±0.31	-0.45±0.40
BESIII model's	-0.28±0.01	-0.13±0.01	0.17±0.01	0.50±0.01	0.81±0.01	0.12±0.01	0.39±0.01	0.54±0.01	0.51±0.01	0.22±0.01
CLEO-c model's	0.84±0.03	0.52±0.08	0.05±0.13	-0.38±0.14	-0.63±0.13	0.23±0.03	0.61±0.06	0.74±0.06	0.57±0.06	0.20±0.03
Cleo-c's Variable $\Delta\delta_D$ binning										
BESIII's	0.74±0.06	0.74±0.04	0.67±0.06	0.36±0.04	0.06±0.05	0.26±0.25	0.11±0.16	-0.08±0.20	0.46±0.14	0.20±0.18
CLEO-c's	0.97±0.11	0.81±0.09	0.91±0.10	0.41±0.09	-0.15±0.12	0.09±0.32	-0.14±0.23	0.23±0.28	0.21±0.19	0.21±0.21
BESIII model's	-0.17±0.01	0.36±0.01	0.66±0.01	0.81±0.01	0.88±0.01	0.28±0.01	0.53±0.01	0.44±0.01	0.24±0.01	0.06±0.01
CLEO-c model's	0.92±0.02	0.84±0.03	0.70±0.06	0.34±0.10	-0.45±0.13	0.07±0.01	0.26±0.03	0.48±0.06	0.68±0.06	0.43±0.05
Cleo-c's Alternative binning										
BESIII's	0.01±0.12	0.44±0.06	0.77±0.03	0.47±0.05	0.03±0.09	0.42±0.31	-0.60±0.18	-0.13±0.11	0.11±0.19	0.24±0.30
CLEO-c's	-0.20±0.21	0.45±0.12	0.89±0.07	0.53±0.11	-0.45±0.17	-0.06±0.40	-0.04±0.27	-0.15±0.16	0.24±0.23	-0.24±0.44
BESIII model's	-0.15±0.01	0.43±0.01	0.82±0.01	0.41±0.01	-0.31±0.01	0.44±0.01	0.60±0.01	0.00±0.01	-0.51±0.01	-0.13±0.01
CLEO-c model's	-0.58±0.14	0.42±0.11	0.87±0.03	0.37±0.11	-0.57±0.15	-0.45±0.12	-0.68±0.08	0.03±0.03	0.73±0.06	0.46±0.10
Cleo-c's Optimal Equal binning										
BESIII's	0.81±0.03	0.55±0.06	0.61±0.05	0.22±0.07	-0.09±0.07	-0.07±0.13	0.51±0.19	0.12±0.18	0.36±0.21	0.10±0.24
CLEO-c's	0.95±0.07	0.64±0.13	0.54±0.11	0.31±0.14	-0.49±0.14	-0.04±0.18	0.33±0.27	0.03±0.23	0.29±0.24	0.67±0.27
BESIII model's	-0.24±0.01	0.06±0.01	0.52±0.01	0.56±0.01	0.88±0.01	0.26±0.01	0.52±0.01	0.55±0.01	0.41±0.01	0.20±0.01
CLEO-c model's	0.91±0.02	0.64±0.09	0.52±0.09	-0.12±0.14	-0.57±0.13	0.22±0.03	0.52±0.10	0.64±0.07	0.74±0.06	0.27±0.06
Cleo-c's Optimal Alternative binning										
BESIII's	0.28±0.09	0.60±0.06	0.80±0.03	0.50±0.05	-0.04±0.07	-0.11±0.25	-0.48±0.18	-0.12±0.13	0.18±0.18	0.58±0.23
CLEO-c's	0.28±0.18	0.62±0.11	0.97±0.07	0.46±0.11	-0.33±0.14	-0.38±0.31	-0.49±0.25	-0.09±0.17	0.24±0.23	0.48±0.29
BESIII model's	-0.19±0.01	0.47±0.01	0.87±0.01	0.61±0.01	-0.03±0.01	0.38±0.01	0.59±0.01	0.20±0.01	-0.40±0.01	-0.38±0.01
CLEO-c model's	-0.19±0.15	0.70±0.07	0.90±0.02	0.44±0.10	-0.57±0.14	-0.67±0.08	-0.47±0.09	0.23±0.03	0.70±0.07	0.39±0.09
BESIII's Equal $\Delta\delta_D$ binning										
BESIII's	0.79±0.02	0.44±0.04	0.23±0.07	-0.10±0.10	-0.50±0.09	-0.15±0.11	0.86±0.14	0.32±0.20	0.36±0.30	-0.09±0.32
BESIII model's	0.84±0.01	0.50±0.01	0.05±0.01	-0.36±0.01	-0.60±0.01	0.24±0.01	0.64±0.01	0.73±0.01	0.54±0.01	0.19±0.01
BESIII's Alternative binning										
BESIII's	-0.10±0.13	0.53±0.06	0.72±0.03	0.24±0.05	-0.91±0.11	0.30±0.36	-0.77±0.17	-0.19±0.11	0.68±0.16	0.29±0.31
BESIII model's	-0.55±0.01	0.37±0.01	0.87±0.01	0.39±0.01	-0.58±0.01	-0.48±0.01	-0.73±0.01	0.04±0.01	0.75±0.01	0.46±0.01
BESIII's Optimal Equal binning										
BESIII's	0.74±0.03	0.72±0.06	0.20±0.06	0.49±0.08	-0.34±0.07	-0.20±0.12	0.39±0.22	0.54±0.19	0.73±0.18	-0.04±0.24
BESIII model's	0.88±0.01	0.77±0.01	0.38±0.01	0.10±0.01	-0.50±0.01	0.29±0.01	0.33±0.01	0.76±0.01	0.79±0.01	0.24±0.01
BESIII's Optimal Alternative binning										
BESIII's	-0.02±0.09	0.58±0.05	0.74±0.03	0.34±0.05	-0.29±0.10	-0.49±0.21	-0.40±0.18	-0.25±0.12	0.75±0.19	0.26±0.26
BESIII model's	-0.08±0.01	0.73±0.01	0.90±0.01	0.43±0.01	-0.52±0.01	-0.73±0.01	-0.44±0.01	0.25±0.01	0.74±0.01	0.40±0.01

1 8.3 Comparison between two models

2 Given by the experiment results with several binning schemes from two Amplitude models,
 3 quantitative comparison between two models are done by $\chi^2 = \sum_i \frac{(c_i^{mea.} - c_i^{pre.})^2}{\sigma(c_i)^2} + \frac{(s_i^{mea.} - s_i^{pre.})^2}{\sigma(s_i)^2}$, shown as
 4 Tab. 32. Only c_i, s_i of CLEO-c's binning schemes are shown. From the χ^2 values, both BESIII's
 5 data and CLEO-c's data are more in favor of BESIII's model prediction rather than CLEO-c's.
 6 So for this c_i, s_i measurement, the BESIII's model is more reliable than CLEO-c's model. In the
 7 eventual publication, only results with BESIII's binning schemes will be shown.

Table 32: χ^2 between experimental results and model prediction results for five CLEO-c's binning schemes.

CLEO-c's scheme	Equal $\Delta\delta_D$	Variable $\Delta\delta_D$	Alternative	Optimal	Optimal Alternative
CLEO-c's v.s. CLEO-c's model	29.4	22.3	20.8	24.5	20.3
CLEO-c's v.s. BESIII's model	16.8	13.1	14.1	17.6	11.7
BESIII's v.s. BESIII's model	14.9	34.1	27.5	32.1	36.3
BESIII's v.s. CLEO-c's model	85.7	116.8	102	108	118

1 8.4 Systematic uncertainty

2 In this memo version, about the strong phase difference's systematic uncertainty, only the
 3 method will only be discussed. In the further study, once we get solid mature amplitude model
 4 from BAM-484, and the final series of binning schemes are determined, we will measure the
 5 strong phase difference again and estimate the systematic uncertainties.

6 The basic method is smearing the items within their uncertainties, and re-fit for thousands
 7 times to get c_i/s_i distributions. By fits on the distributions, the systematic uncertainties are
 8 extracted as well as the covariance matrixes.

9 Related to the c_i/s_i , these systematic uncertainty's sources will be discussed: K_i , ST yields,
 10 DT yields, efficiency matrix (MC statistics), correction factor for psudo-flavor channels, external
 11 inputs.

12 8.5 Cross check on CP even fraction

13 With the above measured T_i and c_i, s_i results, the CP even fraction could be calculated again
 14 by:

$$\widetilde{F}_+ = \frac{1}{2} + \sum_i c_i \sqrt{T_i \bar{T}_i}. \quad (51)$$

15 The results are shown in the Tab. 33, which are consistent with F_+ results $0.731 \pm 0.015 \pm 0.007$
 16 (Tab. 22) within 3σ . For the smaller \widetilde{F}_+ of last three binning schemes, it may be due to dramatic
 17 c_i results: some c_i are significant smaller than model prediction. To examine this assumption,
 18 another set of “Pseudo” \widetilde{F}_+ is calculated by taking model prediction's c_i as mean value, which
 19 is more “normal”, shown as the third column of Tab. 33.

Table 33: The summaries of \widetilde{F}_+ . Only statistical uncertainties are shown.

binning scheme	\widetilde{F}_+	Pseudo \widetilde{F}_+
CLEO-c's Equal $\Delta\delta_D$	0.755 ± 0.010	0.737 ± 0.010
CLEO-c's Variable	0.743 ± 0.011	0.735 ± 0.011
CLEO-c's Alternative	0.746 ± 0.010	0.735 ± 0.010
CLEO-c's Optimal	0.749 ± 0.010	0.734 ± 0.010
CLEO-c's Optimal Alternative	0.749 ± 0.010	0.734 ± 0.010
BESIII's Equal $\Delta\delta_D$	0.742 ± 0.010	0.739 ± 0.010
BESIII's Alternative	0.695 ± 0.010	0.731 ± 0.010
BESIII's Optimal Equal	0.715 ± 0.010	0.730 ± 0.010
BESIII's Optimal Alternative	0.698 ± 0.010	0.737 ± 0.011

1 8.6 Impact on γ measurement

2 As mentioned before, the c_i and s_i results measured in this analysis can play an important role
 3 in the γ measurement. To estimate the γ 's uncertainty due to the c_i and s_i 's uncertainties, a toy
 4 MC study are performed.

5 The toy MC set of $B^\pm \rightarrow K^\pm D(\pi^+ \pi^- \pi^+ \pi^-)$ are generated. The expected yields for each bin
 6 can be written as:

$$\begin{aligned} N_i^+ &= h_B \left[K_{-i} + r_B^2 K_{+i} + 2r_B \sqrt{K_i K_{-i}} (\cos(\delta_B + \gamma) c_{+i} - \sin(\delta_B + \gamma) s_{+i}) \right], \\ N_{-i}^+ &= h_B \left[K_{+i} + r_B^2 K_{-i} + 2r_B \sqrt{K_i K_{-i}} (\cos(\delta_B + \gamma) c_{+i} + \sin(\delta_B + \gamma) s_{+i}) \right], \\ N_i^- &= h_B \left[K_{+i} + r_B^2 K_{-i} + 2r_B \sqrt{K_i K_{-i}} (\cos(\delta_B - \gamma) c_{+i} + \sin(\delta_B - \gamma) s_{+i}) \right], \\ N_{-i}^- &= h_B \left[K_{-i} + r_B^2 K_{+i} + 2r_B \sqrt{K_i K_{-i}} (\cos(\delta_B - \gamma) c_{+i} - \sin(\delta_B - \gamma) s_{+i}) \right], \end{aligned} \quad (52)$$

7 where the $r_B = 0.0986$, $\gamma = 67^\circ$, $\delta_B = 128^\circ$ [23], the K_i and c_i, s_i are the central values in this
 8 analysis, the h_B is large enough so the statistical uncertainty of this toy MC can be neglected.
 9 Then by the Poisson distribution, the toy MC yields are obtained. The expected yields are
 10 calculated with Eq. 52 using smeared c_i and s_i . When smearing the c_i and s_i , the correlations
 11 are included. By re-sampling c_i, s_i and re-fit to the toy MC sample many times, the γ distribution
 12 is obtained. The γ 's uncertainty from c_i, s_i is estimated by the RMS (root mean square) of the
 13 γ distribution. The results for different binning schemes are shown in Figs. 27. Based on the
 14 results, impact from this work is estimated to be $1.5 \sim 2.5^\circ$.

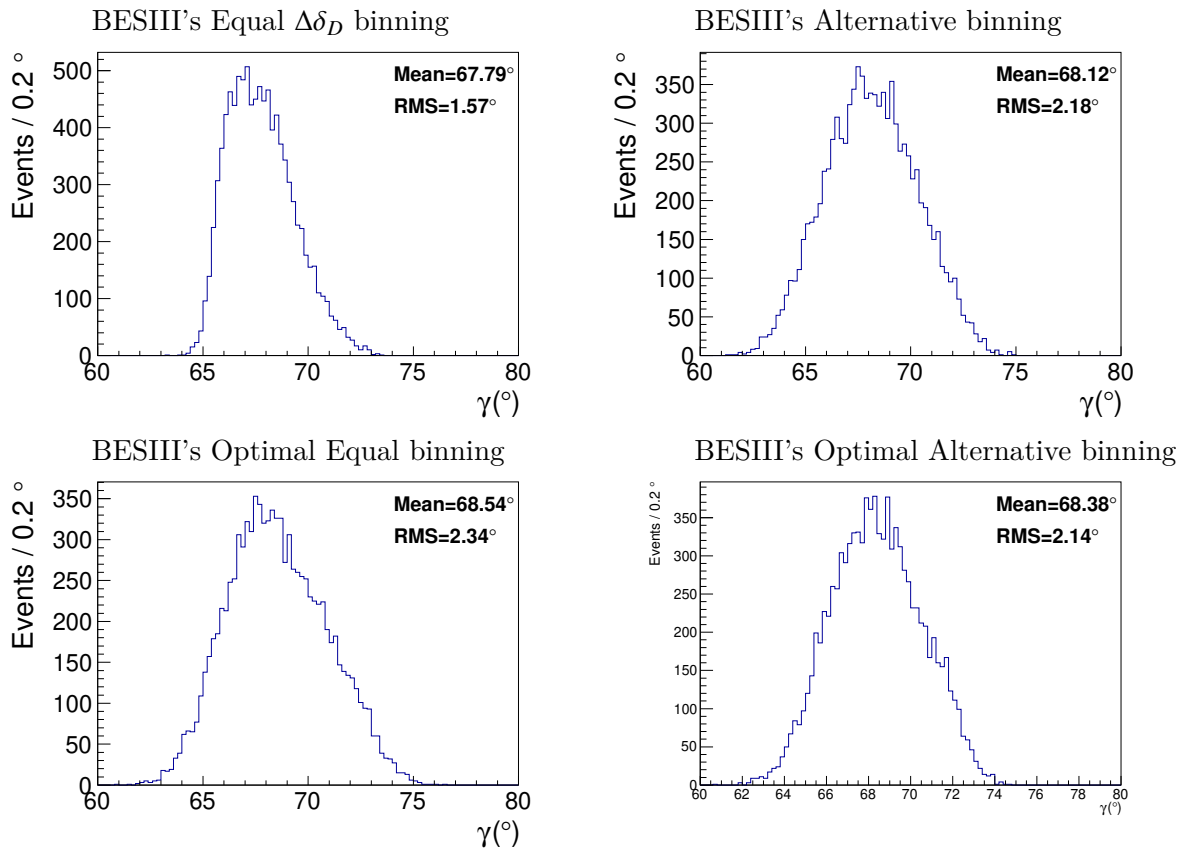


Figure 27: γ distribution from toy MC study for four BESIII's binning schemes.

1 9 Summary and Discussion

2 Using the 2.93 fb^{-1} data set collected at $\sqrt{s} = 3.773 \text{ GeV}$, we measured the CP even fraction
3 and strong-phase difference in $D^0/\bar{D}^0 \rightarrow \pi^+\pi^-\pi^+\pi^-$. These results will play an important role as
4 model-independent inputs for γ measurement by GLW or GGSZ methods.

5 The CP even fraction is measured as $0.732 \pm 0.015 \pm 0.007$, where the first uncertainty is
6 statistical and second is systematic, which is consistent with previous CLEO-c's measured results
7 and CLEO-c's model prediction and BESIII's model prediction.

8 The strong-phase difference is measured with five CLEO-c's binning schemes and four BESIII's
9 binning schemes, where the BESIII's binning schemes are determined in this analysis by using
10 the amplitude model from the partial wave analysis of $D \rightarrow \pi^+\pi^-\pi^+\pi^-$ (BAM-00439). The γ
11 uncertainties from this strong-phase difference results with BESIII's binning schemes are esti-
12 mated to be $1.5 \sim 2.5^\circ$. For the future publication, only strong-phase difference results with
13 BESIII's binning schemes will be shown.

¹ References

- ² [1] M. Gronau and D. London, Phys. Lett. B 253, 483-488 (1991)
- ³ [2] M. Gronau and D. Wyler, Phys. Lett. B 265, 172-176 (1991)
- ⁴ [3] D. Atwood, I. Dunietz and A. Soni, Phys. Rev. Lett. 78, 3257-3260 (1997)
- ⁵ [4] A. Giri, Y. Grossman, A. Soffer and J. Zupan, Phys. Rev. D 68, 054018 (2003)
- ⁶ [5] J. Rademacker and G. Wilkinson, Phys. Lett. B 647, 400-404 (2007)
- ⁷ [6] P. d'Argent, N. Skidmore, J. Benton, J. Dalseno, E. Gersabeck, S. Harnew, P. Naik,
⁸ C. Prouve and J. Rademacker, JHEP 05, 143 (2017)
- ⁹ [7] Xinyu Shan et al, Amplitude analysis of the decay $D^0 \rightarrow 2(\pi^+\pi^-)$, BAM-439.
¹⁰ <https://hnbes3.ihep.ac.cn/HyperNews/get/paper439.html>
- ¹¹ [8] S. Harnew, P. Naik, C. Prouve, J. Rademacker and D. Asner, JHEP 01, 144 (2018)
- ¹² [9] S. Malde, C. Thomas, G. Wilkinson, P. Naik, C. Prouve, J. Rademacker, J. Libby, M. Nayak,
¹³ T. Gershon and R. A. Briere,
- ¹⁴ [10] R. Aaij et al. [LHCb], Phys. Lett. B 760 (2016), 117-131 doi:10.1016/j.physletb.2016.06.022
¹⁵ [arXiv:1603.08993 [hep-ex]].
- ¹⁶ [11] M. Ablikim et al. [BESIII], Phys. Rev. Lett. 124 (2020) no.24, 241802
- ¹⁷ [12] M. Ablikim et al. [BESIII], Phys. Rev. D 101 (2020) no.11, 112002
- ¹⁸ [13] M. Ablikim et al. [BESIII], Phys. Rev. D 102 (2020) no.5, 052008
¹⁹ doi:10.1103/PhysRevD.102.052008 [arXiv:2007.07959 [hep-ex]].
- ²⁰ [14] C. Zhang for BEPC & BEPCII Teams, Performance of the BEPC and the progress of the
²¹ BEPCII, in:Proceeding of APAC,2004,pp. 15-19, Gyeongju, Korea.
- ²² [15] M. Ablikim et al. [BESIII Collaboration], Nucl. Instrum. Meth. A 614, 345 (2010)
- ²³ [16] M. Ablikim [BESIII Collaboration], Chin. Phys. C 37, 123001 (2013)
- ²⁴ [17] M. Tanabashi et al. (Particle Data Group), Phys. Rev. D 98, 030001 (2018).

- 1 [18] P. del Amo Sanchez et al. [BaBar], “Measurement of D0-antiD0 mixing parameters using
2 $D0 \rightarrow K(S)0 \pi^+ \pi^-$ and $D0 \rightarrow K(S)0 K^+ K^-$ decays,” Phys. Rev. Lett. 105 (2010),
3 081803
- 4 [19] S. Agostinelli et al. [GEANT4 Collaboration], Nucl. Instrum. Meth. A 506, 250 (2003)
- 5 [20] S. Jadach, B. F. L. Ward, and Z. Was, Phys. Rev. D 63, 113009 (2001).
- 6 [21] R. G. Ping, Chin. Phys. C 38 083001 (2014).
- 7 [22] A. Bondar and A. Poluektov, Eur. Phys. J. C 55 (2008), 51-56
- 8 [23] [LHCb], “Updated LHCb combination of the CKM angle γ ,” LHCb-CONF-2020-003.
- 9 [24] https://indico.desy.de/event/28202/contributions/105895/attachments/67297/83621/mwhitehe_eps_202
- 10 [25] Y. S. Amhis et al. [HFLAV], Eur. Phys. J. C 81 (2021) no.3, 226
- 11 [26] M. Ablikim et al. [BESIII], JHEP 05 (2021), 164
- 12 [27] [LHCb], “Simultaneous determination of CKM angle γ and charm mixing parameters,”
13 LHCb-CONF-2021-001.
- 14 [28] T. Evans, S. Harnew, J. Libby, S. Malde, J. Rademacker and G. Wilkinson, Phys. Lett. B
15 757 (2016), 520-527 [erratum: Phys. Lett. B 765 (2017), 402-403]
- 16 [29] M. Ablikim et al. [BESIII], Chin. Phys. C 42 (2018) no.8, 083001
- 17 [30] D. M. Asner et al. [CLEO], Phys. Rev. D 86 (2012), 112001

₁ Appendices

¹ A Details about the bin schemes of $D \rightarrow 4\pi^\pm$

² In the strong phase difference measurement, the variables $\{m_+, m_-, \cos\theta_+, \cos\theta_-, \phi\}$ are used to
³ parameterise the phase space of $D \rightarrow 4\pi^\pm$. In this appendix, the definition of these five variables
⁴ are given.

⁵ The invariant masses m_+, m_- are defined as:

$$m_+^2 = (p_{\pi_1^+} + p_{\pi_2^+})^2,$$

$$m_-^2 = (p_{\pi_1^-} + p_{\pi_2^-})^2,$$

⁶ where the $p_{\pi_1^+}$, $p_{\pi_2^+}$ and $p_{\pi_1^-}$, $p_{\pi_2^-}$ are the Lorentz vectors of the positively charged pions and
⁷ negatively charged pions.

⁸ The cosine of the two helicity angles, $\cos\theta_+$, $\cos\theta_-$ are defined as:

$$\cos\theta_+ = \frac{\vec{p}_{\pi_1^+} \cdot \vec{p}_D}{|\vec{p}_{\pi_1^+}| |\vec{p}_D|}, \text{ in the rest frame of } \pi_1^+, \pi_2^+,$$

$$\cos\theta_- = \frac{\vec{p}_{\pi_1^-} \cdot \vec{p}_D}{|\vec{p}_{\pi_1^-}| |\vec{p}_D|}, \text{ in the rest frame of } \pi_1^-, \pi_2^-,$$

⁹ where \vec{p}_π is the three-vector of each π .

¹⁰ The angle between $\pi^+\pi^+$ and $\pi^-\pi^-$ planes ϕ , is defined as:

$$\sin\phi = \left[\frac{\vec{p}_{\pi_1^+} \times \vec{p}_{\pi_2^+}}{|\vec{p}_{\pi_1^+} \times \vec{p}_{\pi_2^+}|} \times \frac{\vec{p}_{\pi_1^-} \times \vec{p}_{\pi_2^-}}{|\vec{p}_{\pi_1^-} \times \vec{p}_{\pi_2^-}|} \right] \cdot \frac{\vec{p}_{\pi_1^-} + \vec{p}_{\pi_2^-}}{|\vec{p}_{\pi_1^-} + \vec{p}_{\pi_2^-}|}, \text{ in the rest frame of D}$$

$$\cos\phi = \left[\frac{\vec{p}_{\pi_1^+} \times \vec{p}_{\pi_2^+}}{|\vec{p}_{\pi_1^+} \times \vec{p}_{\pi_2^+}|} \cdot \frac{\vec{p}_{\pi_1^-} \times \vec{p}_{\pi_2^-}}{|\vec{p}_{\pi_1^-} \times \vec{p}_{\pi_2^-}|} \right], \text{ in the rest frame of D}$$

¹ B Self-check on signal MC generation

² For the signal MC generated according to the amplitude model of $D \rightarrow 4\pi^\pm$ and Dalitz model of
³ $D \rightarrow K_S^0/K_L^0\pi^+\pi^-$, [7, 18] several checks on c_i, s_i are done, by re-fit the generated yields in local
⁴ phase spaces. Some check results are shown in this appendix.

⁵ For generation of $K_S^0\pi^+\pi^-$, by re-fitting to the MC sample of $5 \times 10^6 K_S^0\pi^+\pi^- v.s. K_S^0\pi^+\pi^-$ events,
⁶ the c_i, s_i of $K_S^0\pi^+\pi^-$ are found to be consistent with the model prediction values, shown as Fig. 28.

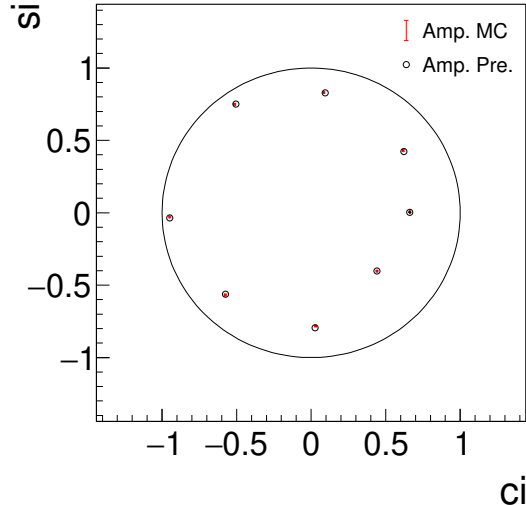


Figure 28: The $K_S^0\pi^+\pi^-$'s c_i, s_i extracted from $K_S^0\pi^+\pi^- v.s. K_S^0\pi^+\pi^-$ MC (red dots) and predicted from Dalitz model (black circle).

⁷ For generation of $\pi^+\pi^-\pi^+\pi^-$, by re-fitting to the MC sample of $1 \times 10^4 K_S^0\pi^+\pi^- v.s. \pi^+\pi^-\pi^+\pi^-$
⁸ events and $K_L^0\pi^+\pi^- v.s. \pi^+\pi^-\pi^+\pi^-$ separately, the c_i, s_i of $\pi^+\pi^-\pi^+\pi^-$ are found to be consistent with
⁹ the model prediction values, shown as Fig. 29.

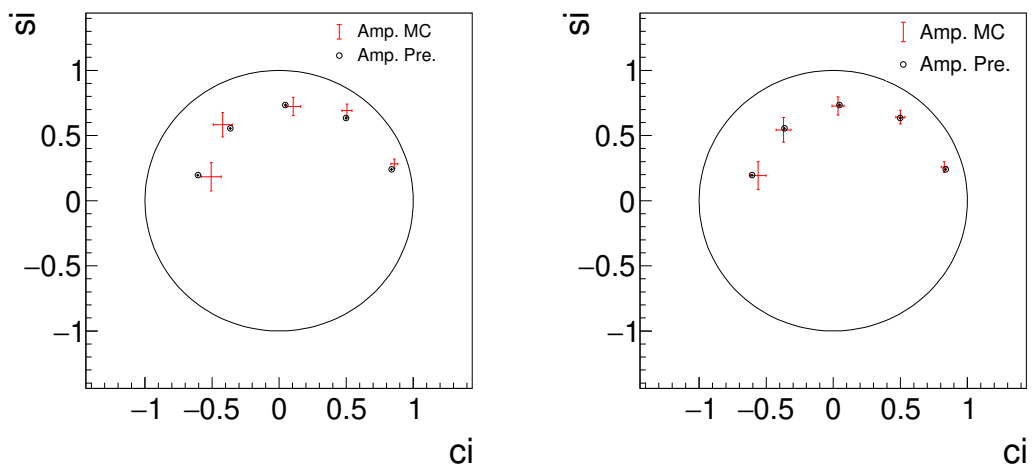


Figure 29: The $\pi^+\pi^-\pi^+\pi^-$'s c_i , s_i extracted from MC (red dots) and predicted from Dalitz model (black circle) for $K_S^0\pi^+\pi^-v.s.\pi^+\pi^-\pi^+\pi^-$ (left) and $K_L^0\pi^+\pi^-v.s.\pi^+\pi^-\pi^+\pi^-$ (right).

¹ C Self-check on ST

² Using the ST yield and efficiency of each channel in Tab.¹¹, the branching fraction is calculated
³ with the $D^0 \rightarrow K^-\pi^+\pi^0$'s branching fraction in PDG. The uncertainty only includes the statistical
⁴ uncertainty and the uncertainty from $Br(D^0 \rightarrow K^-\pi^+\pi^0)$. The self-check results agree with PDF
values in 3σ region.

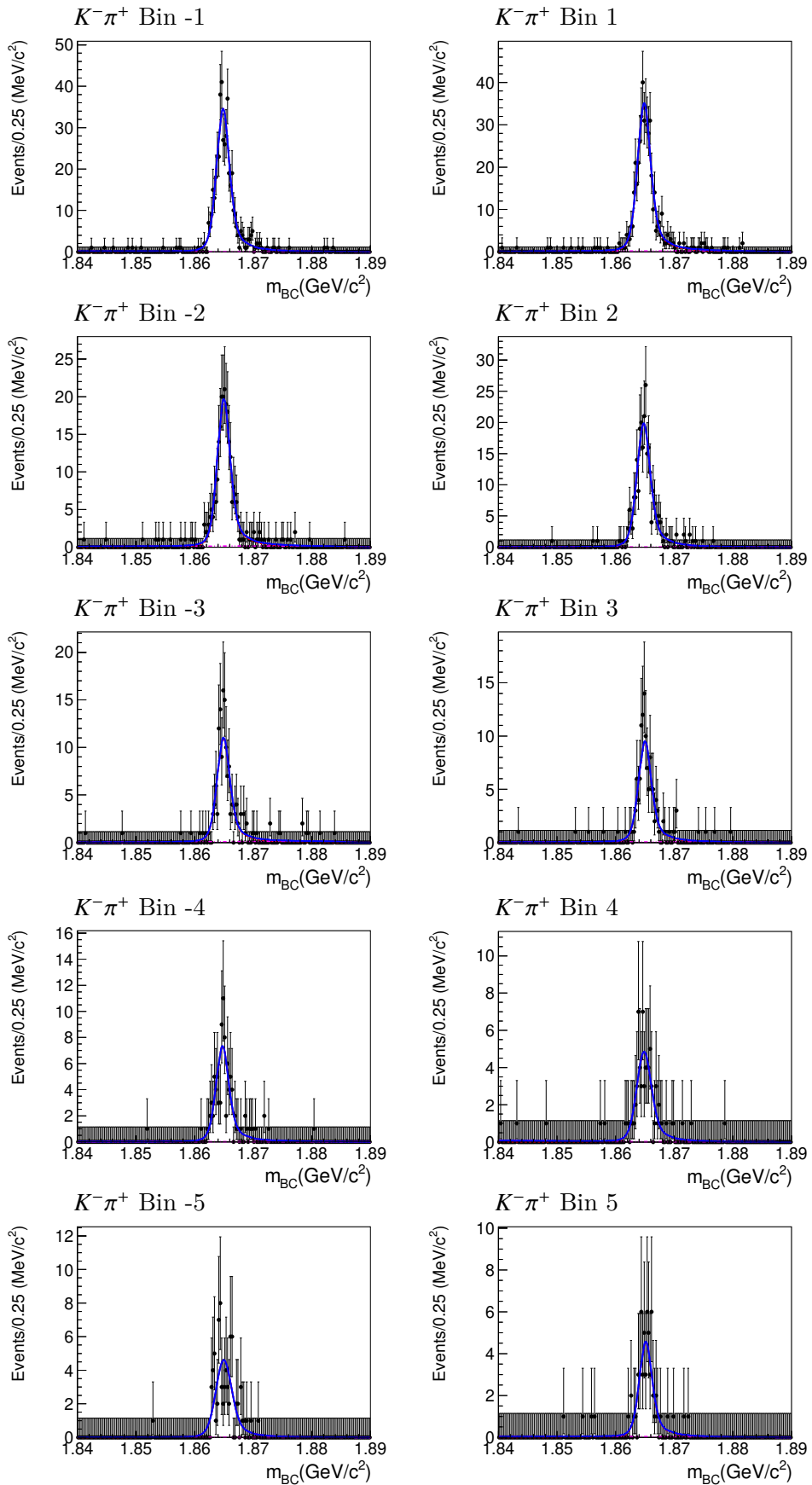
ST channel	BR (%)	PDG(2020) (%)
$K\pi$	3.83 ± 0.134	3.95 ± 0.031
$K\pi\pi^0$	14.4 ± 0.504	14.4 ± 0.5
$K\pi\pi\pi$	8.45 ± 0.296	8.23 ± 0.14
KK	0.42 ± 0.0148	0.408 ± 0.006
$\pi\pi$	0.144 ± 0.0052	0.1455 ± 0.0024
$K_S^0\pi^0\pi^0$	0.983 ± 0.036	0.91 ± 0.11
$\pi\pi\pi\pi$	0.656 ± 0.0234	0.756 ± 0.020
$\pi\pi\pi^0$	1.35 ± 0.048	1.49 ± 0.06
$K_S^0\pi^0$	1.21 ± 0.0427	1.24 ± 0.022
$K_S^0\eta_{\gamma\gamma}$	0.512 ± 0.019	0.509 ± 0.013
$K_S^0\eta_{\pi\pi\pi}$	0.469 ± 0.0199	0.509 ± 0.013
$K_S^0\omega$	1.21 ± 0.0434	1.11 ± 0.06
$K_S^0\eta'_{\pi\pi\eta}$	1.01 ± 0.0406	0.949 ± 0.032
$K_S^0\eta'_{\gamma\pi\pi}$	0.926 ± 0.0352	0.949 ± 0.032
$K_S^0\pi\pi$	2.98 ± 0.105	2.80 ± 0.18
K_S^0KK	0.52 ± 0.0189	0.442 ± 0.032

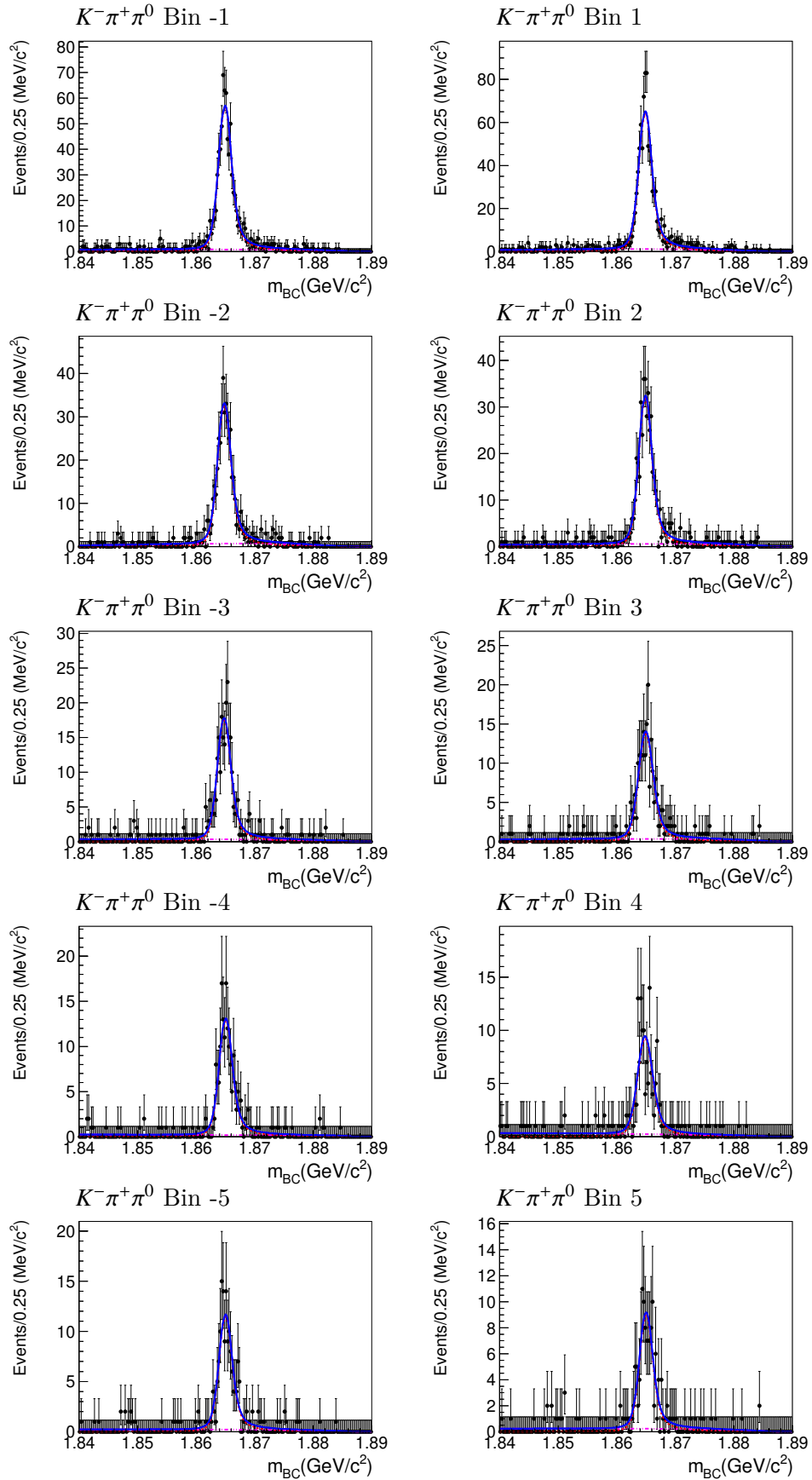
¹ D Additional plots and tables in strong-phase difference measurement

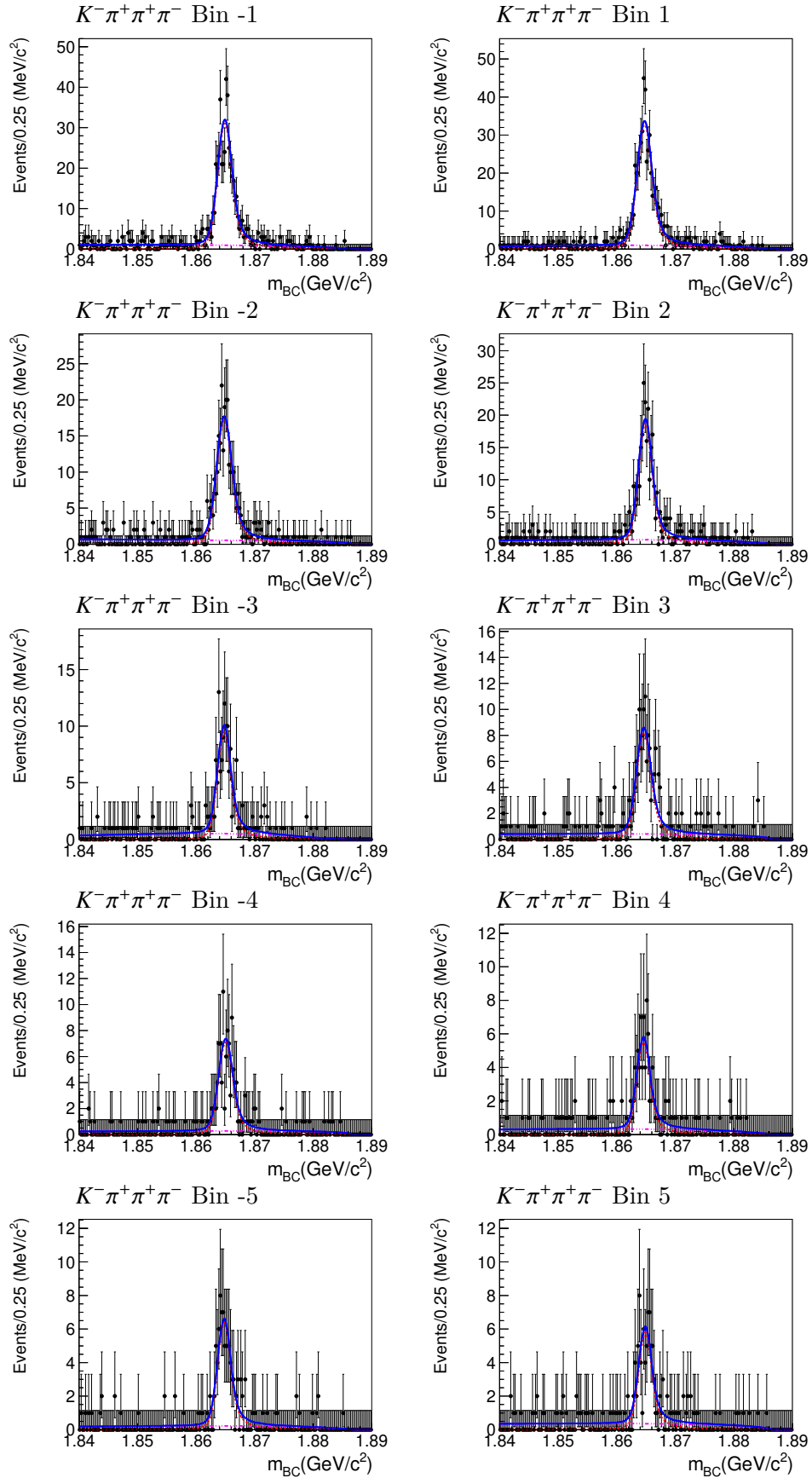
² In this section, many plots and tables are shown.

³ D.1 Additional plots and tables in K_i measurement

⁴ D.2 Additional plots and tables in c_i, s_i measurement

Figure 30: Fit results of $K^- \pi^+$ for different K_i with CLEO-c's Equal $\Delta\delta_D$ binning scheme.

Figure 31: Fit results of $K^- \pi^+ \pi^0$ for different K_i with CLEO-c's Equal $\Delta\delta_D$ binning scheme.

Figure 32: Fit results of $K^- \pi^+ \pi^+ \pi^-$ for different K_i with CLEO-c's Equal $\Delta\delta_D$ binning scheme.

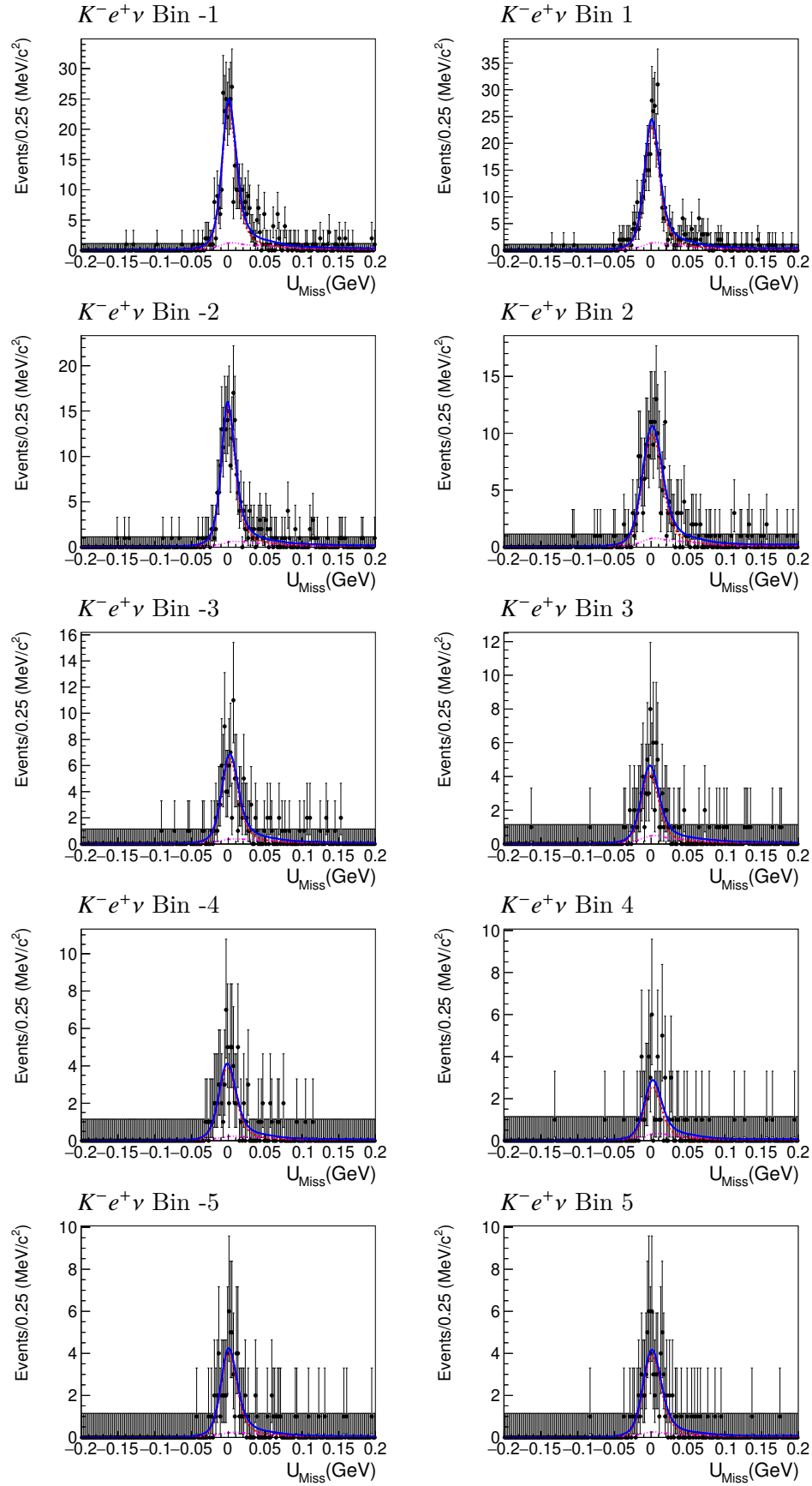
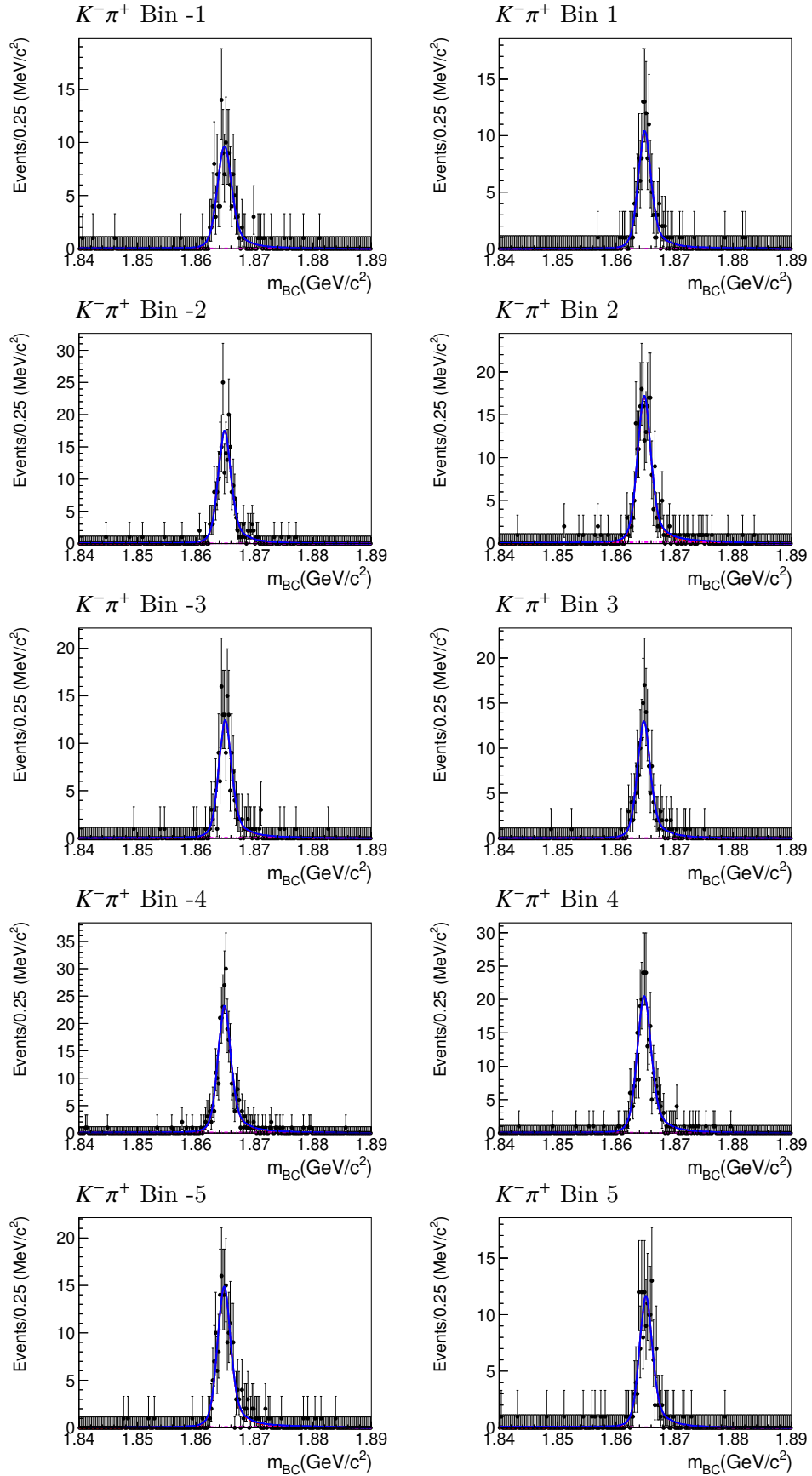


Figure 33: Fit results of $K^- e^+ \nu$ for different K_i with CLEO-c's Equal $\Delta\delta_D$ binning scheme.

Figure 34: Fit results of $K^- \pi^+$ for different K_i with CLEO-c's Variable $\Delta\delta_D$ binning scheme.

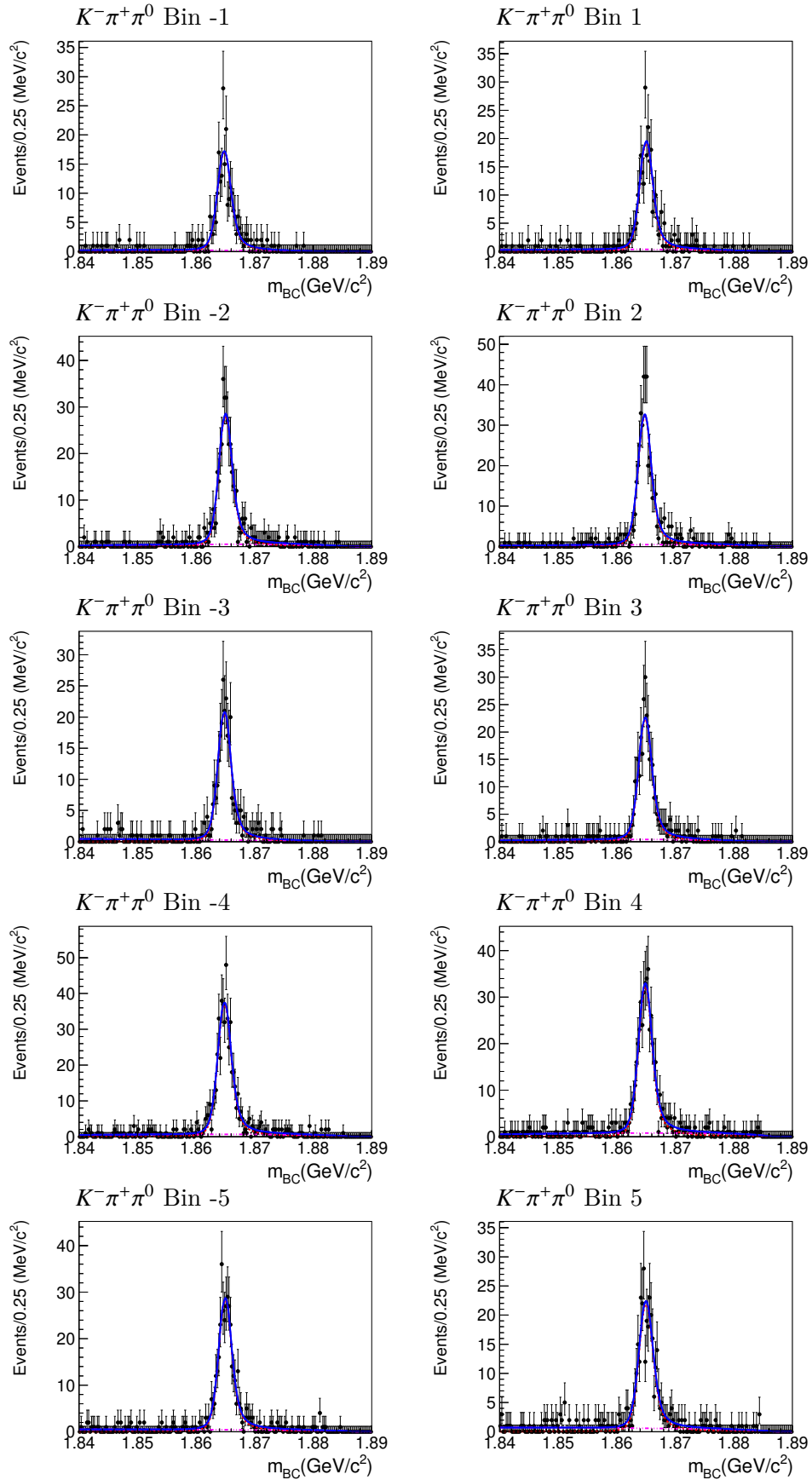
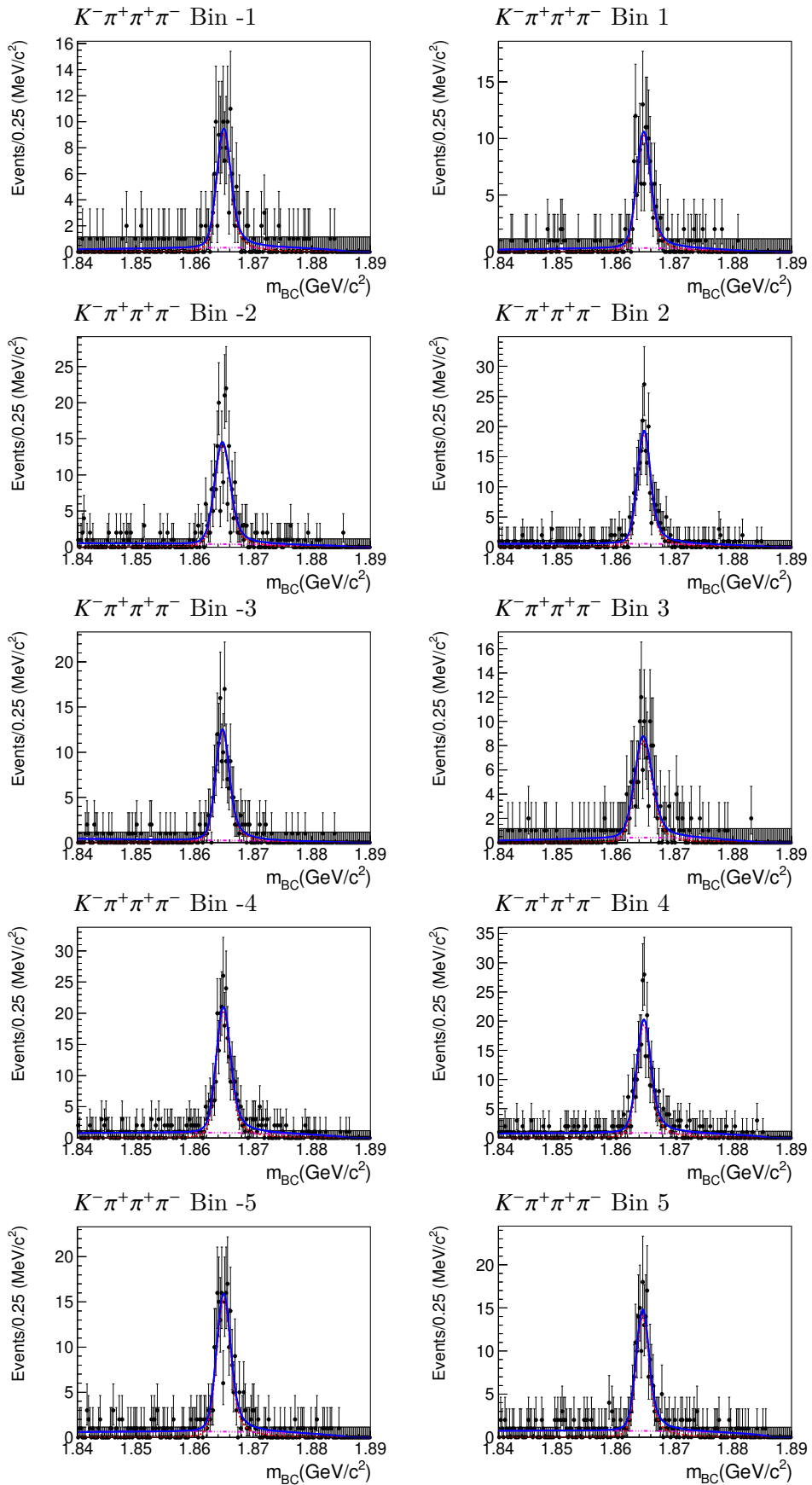


Figure 35: Fit results of $K^- \pi^+ \pi^0$ for different K_i with CLEO-c's Variable $\Delta\delta_D$ binning scheme.

Figure 36: Fit results of $K^- \pi^+ \pi^+ \pi^-$ for different K_i with CLEO-c's Variable $\Delta\delta_D$ binning scheme.

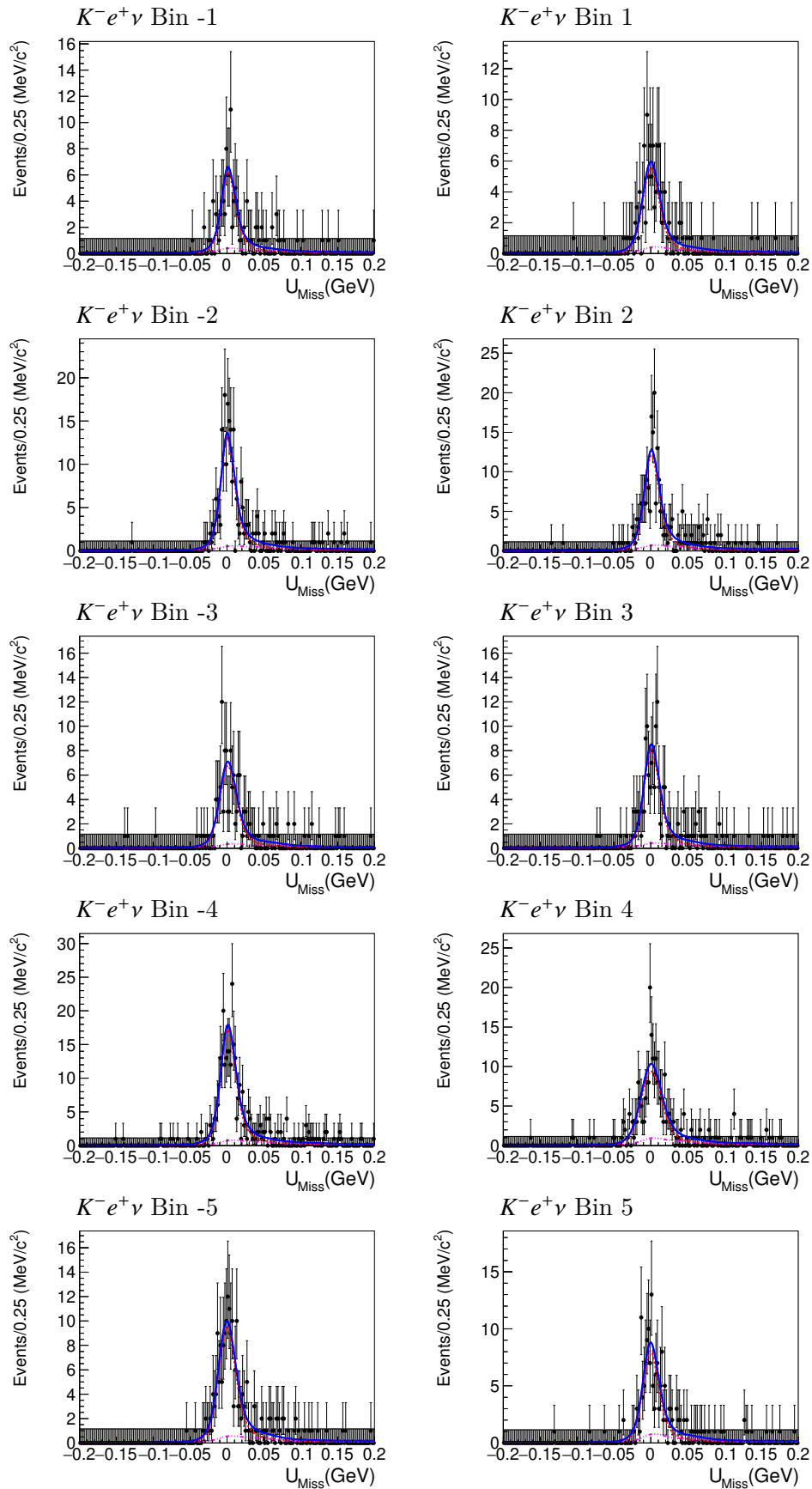
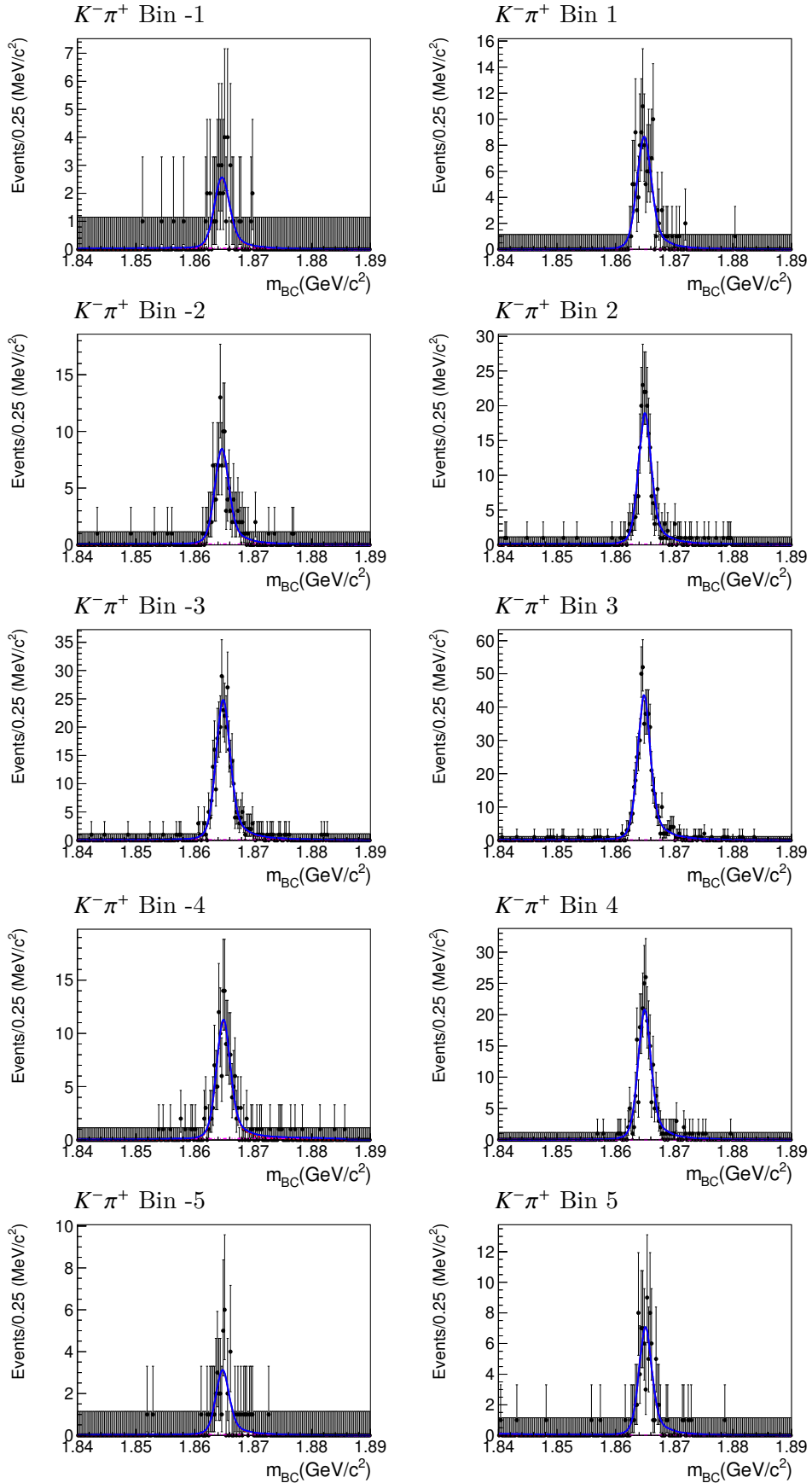


Figure 37: Fit results of $K^- e^+ \nu$ for different K_i with CLEO-c's Variable $\Delta\delta_D$ binning scheme.

Figure 38: Fit results of $K^- \pi^+$ for different K_i with CLEO-c's Alternative binning scheme.

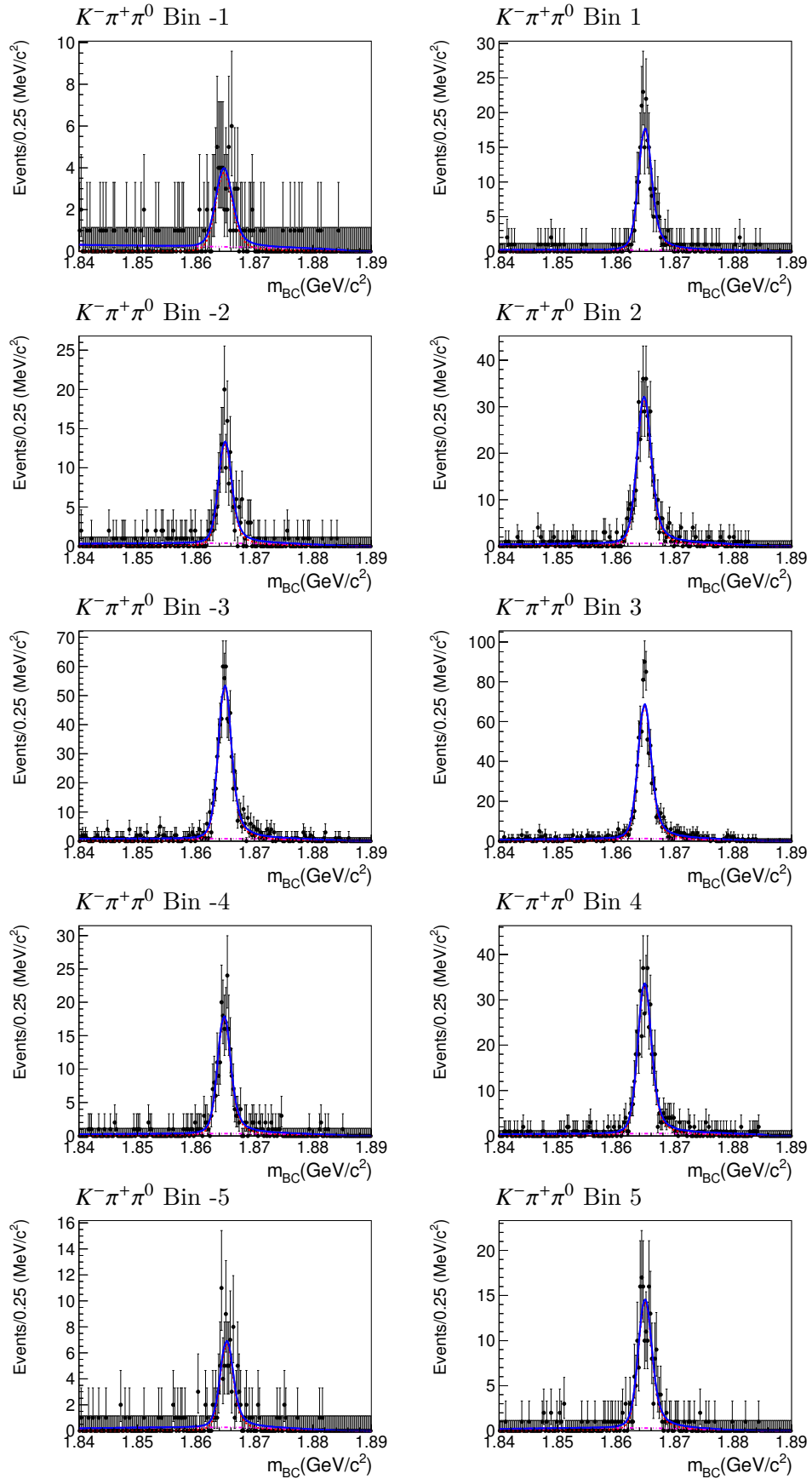
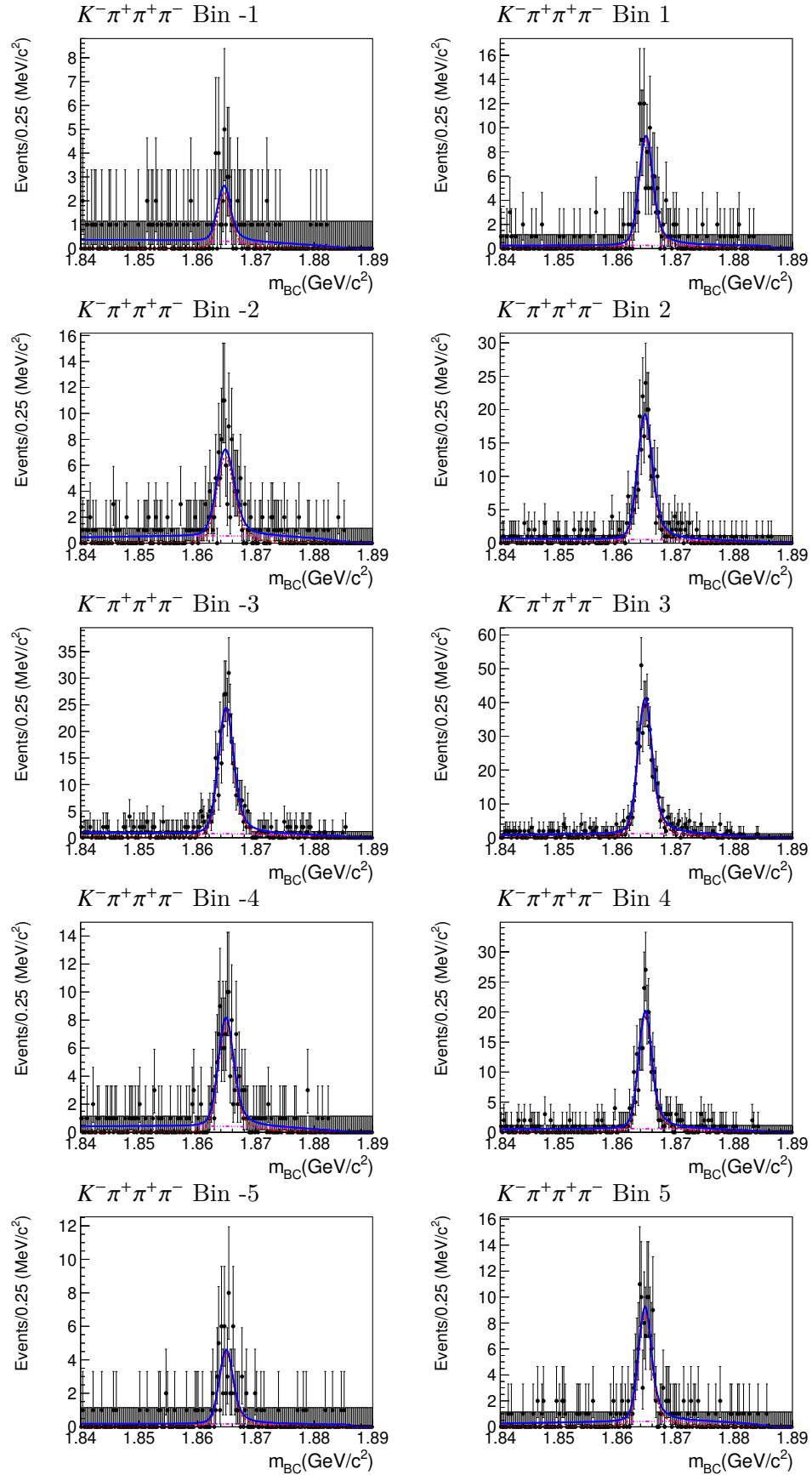
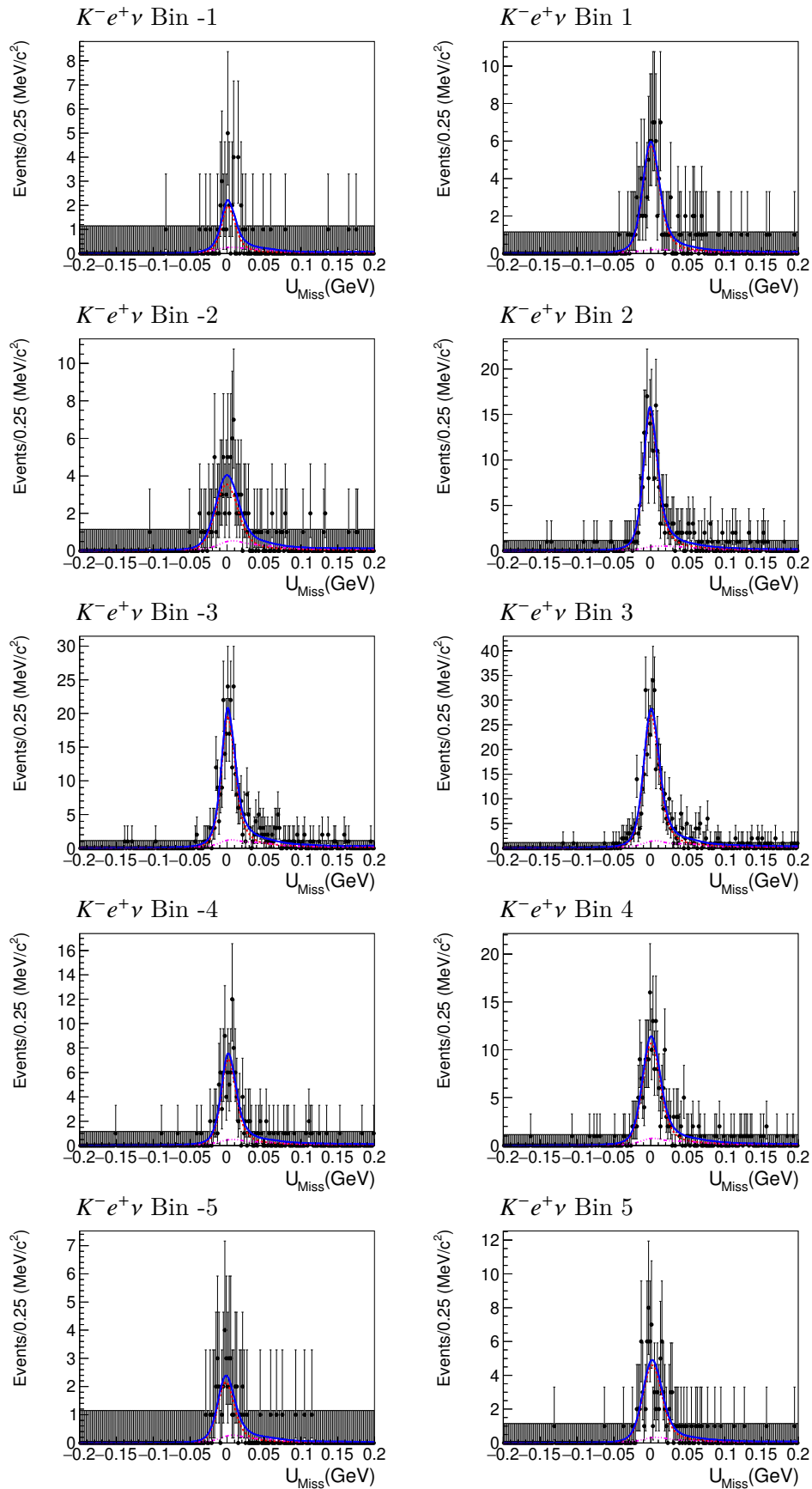
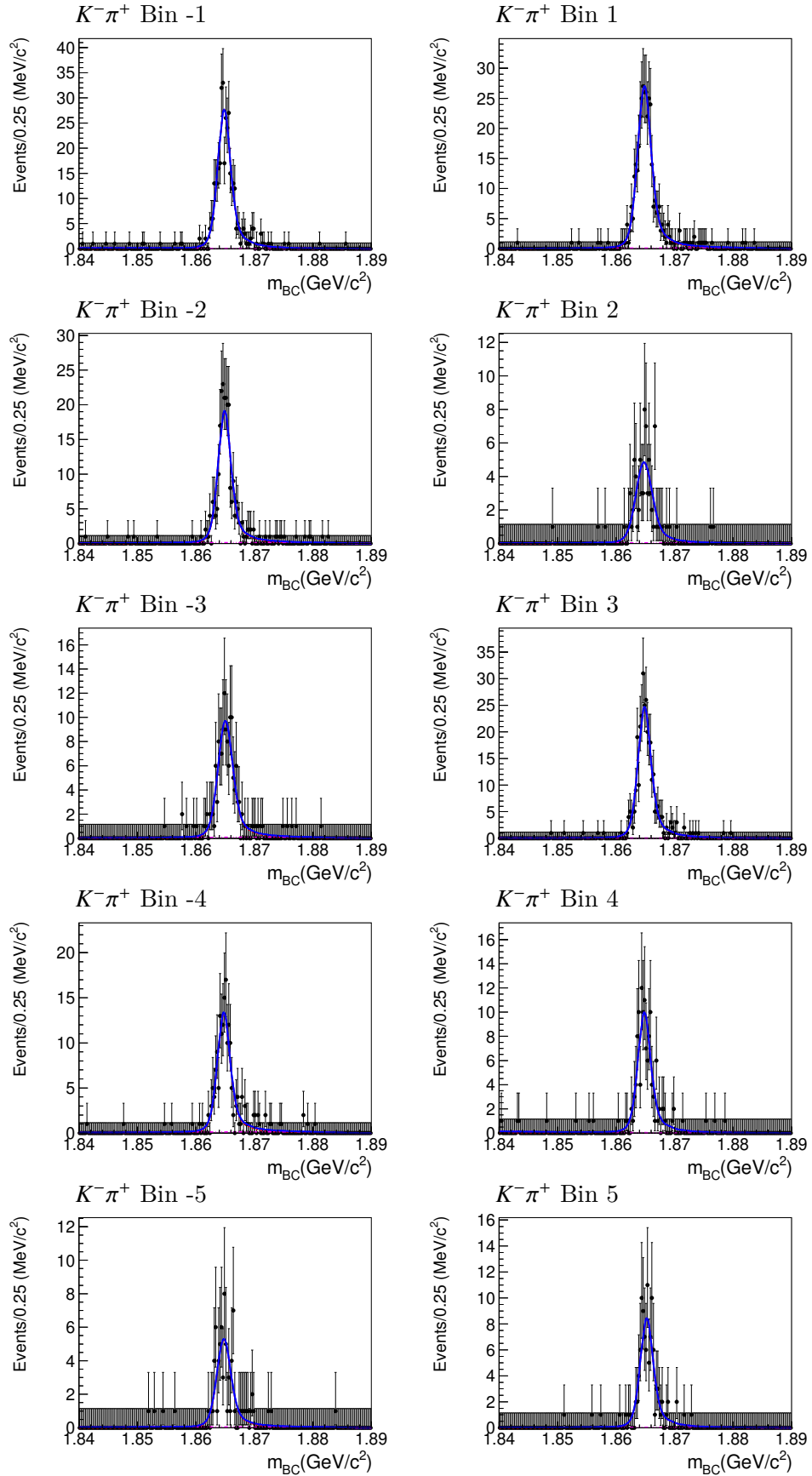


Figure 39: Fit results of $K^- \pi^+ \pi^0$ for different K_i with CLEO-c's Alternative binning scheme.

Figure 40: Fit results of $K^- \pi^+ \pi^+ \pi^-$ for different K_i with CLEO-c's Alternative binning scheme.

Figure 41: Fit results of $K^- e^+ \nu$ for different K_i with CLEO-c's Alternative binning scheme.

Figure 42: Fit results of $K^- \pi^+$ for different K_i with CLEO-c's Optimal binning scheme.

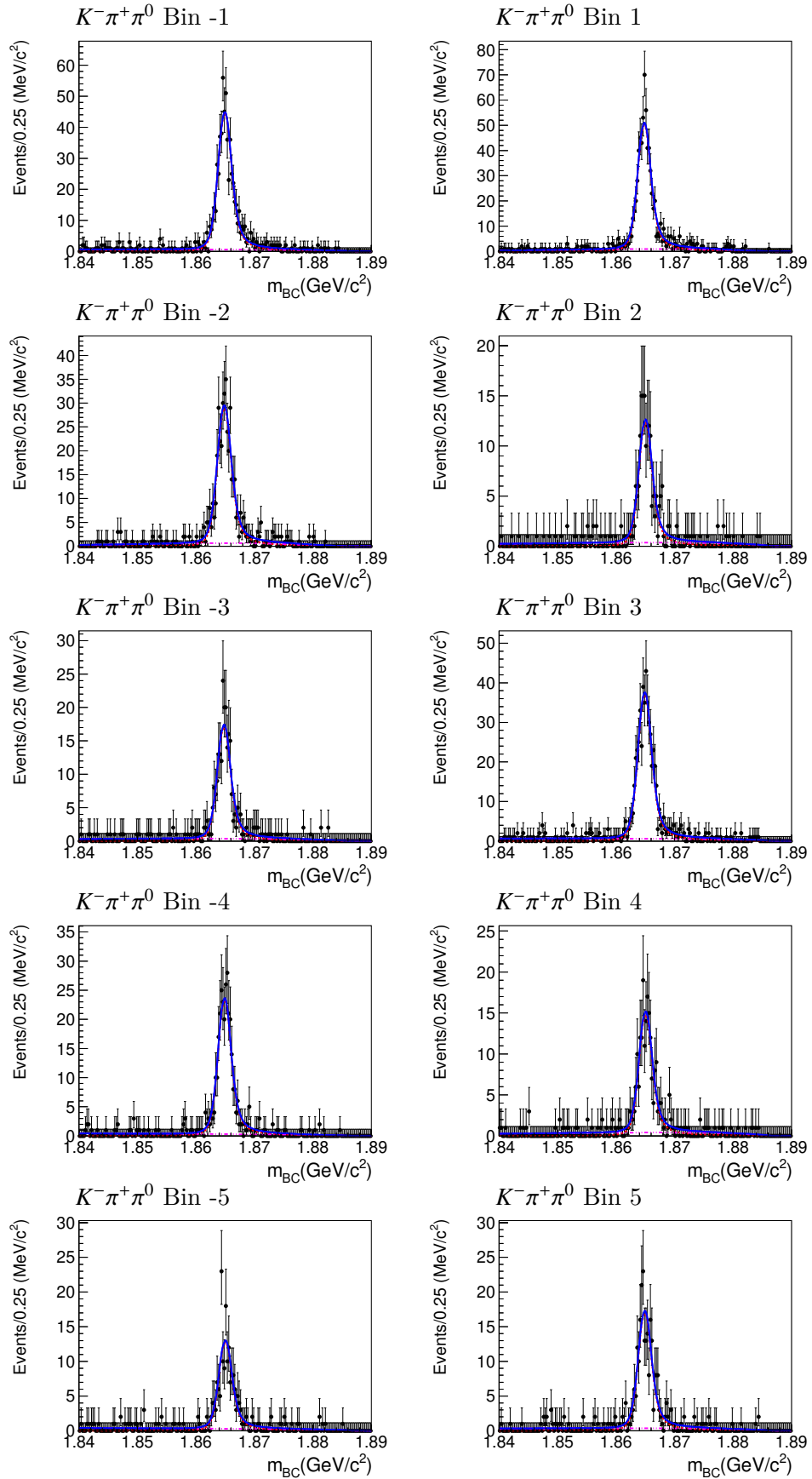
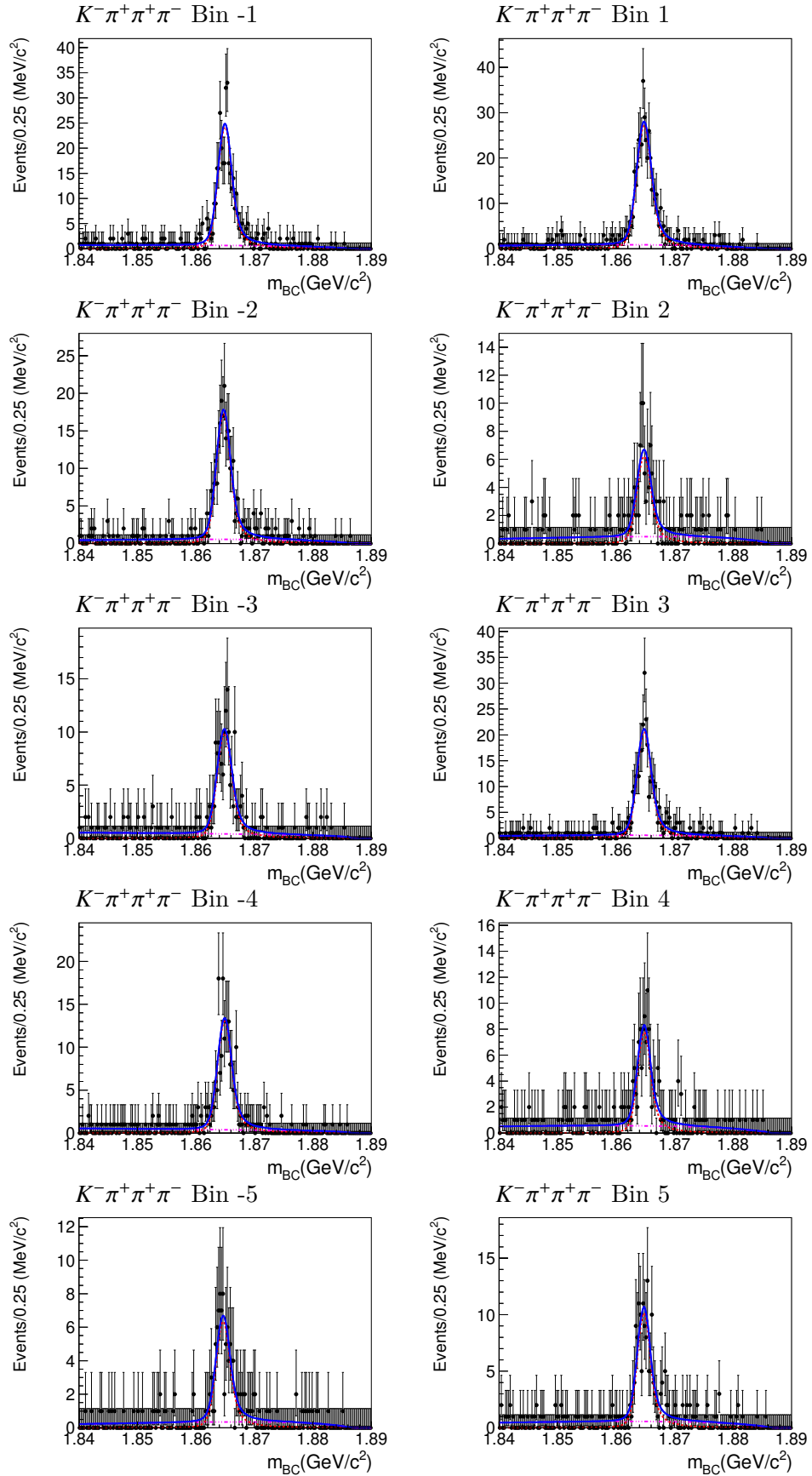
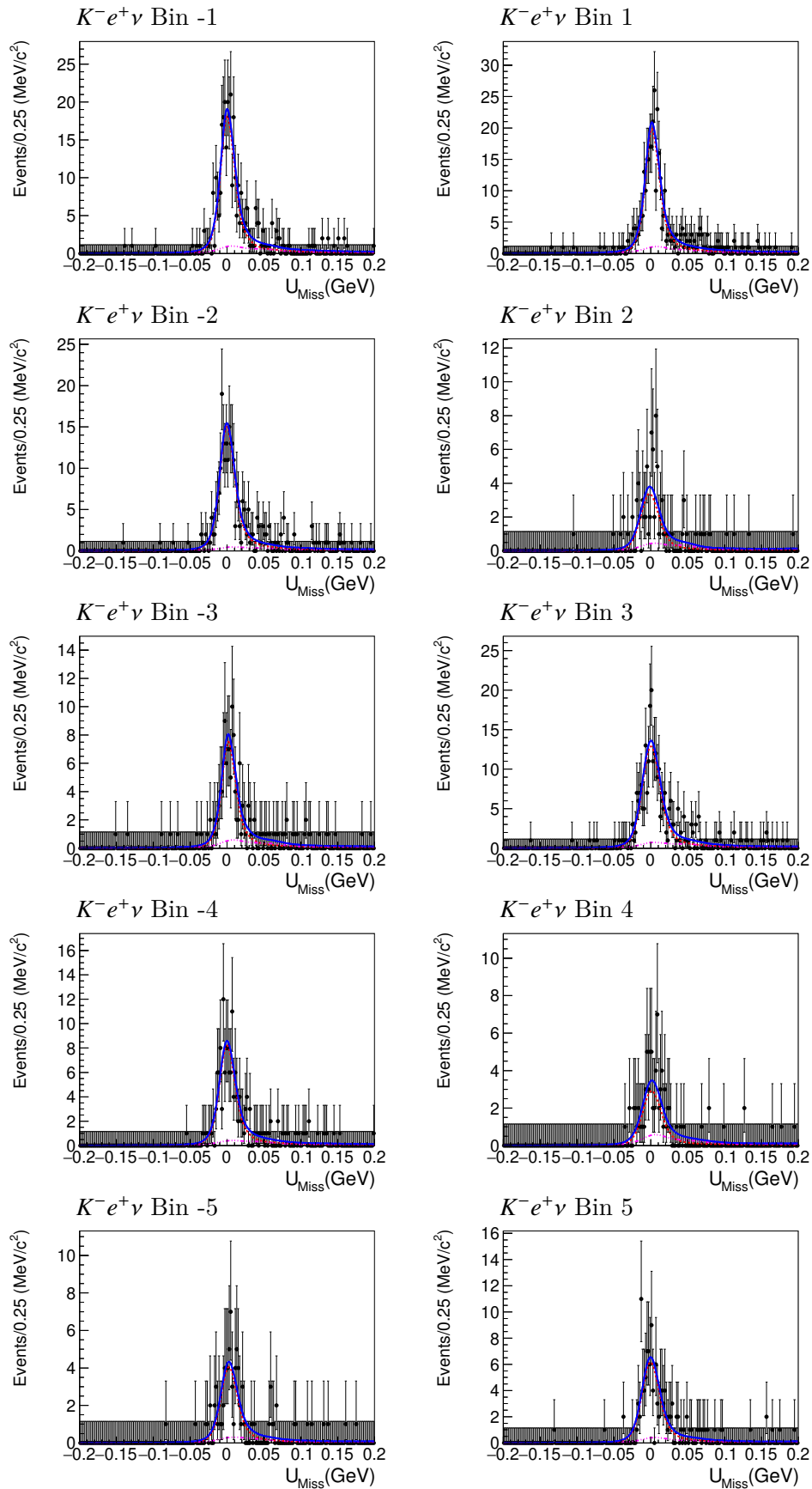


Figure 43: Fit results of $K^- \pi^+ \pi^0$ for different K_i with CLEO-c's Optimal binning scheme.

Figure 44: Fit results of $K^- \pi^+ \pi^+ \pi^-$ for different K_i with CLEO-c's Optimal binning scheme.

Figure 45: Fit results of $K^- e^+ \nu$ for different K_i with CLEO-c's Optimal binning scheme.

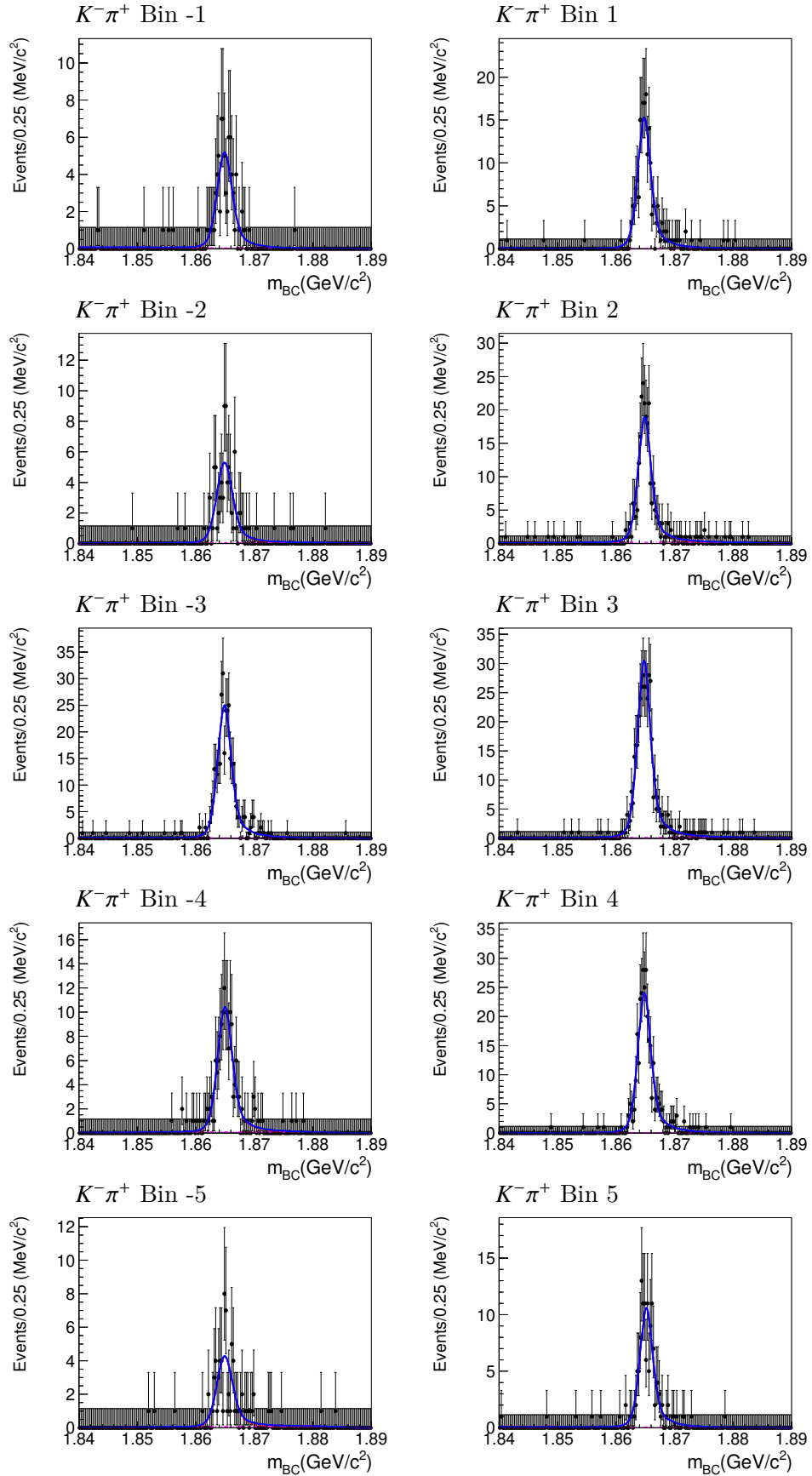


Figure 46: Fit results of $K^- \pi^+$ for different K_i with CLEO-c's Optimal Alternative binning scheme.

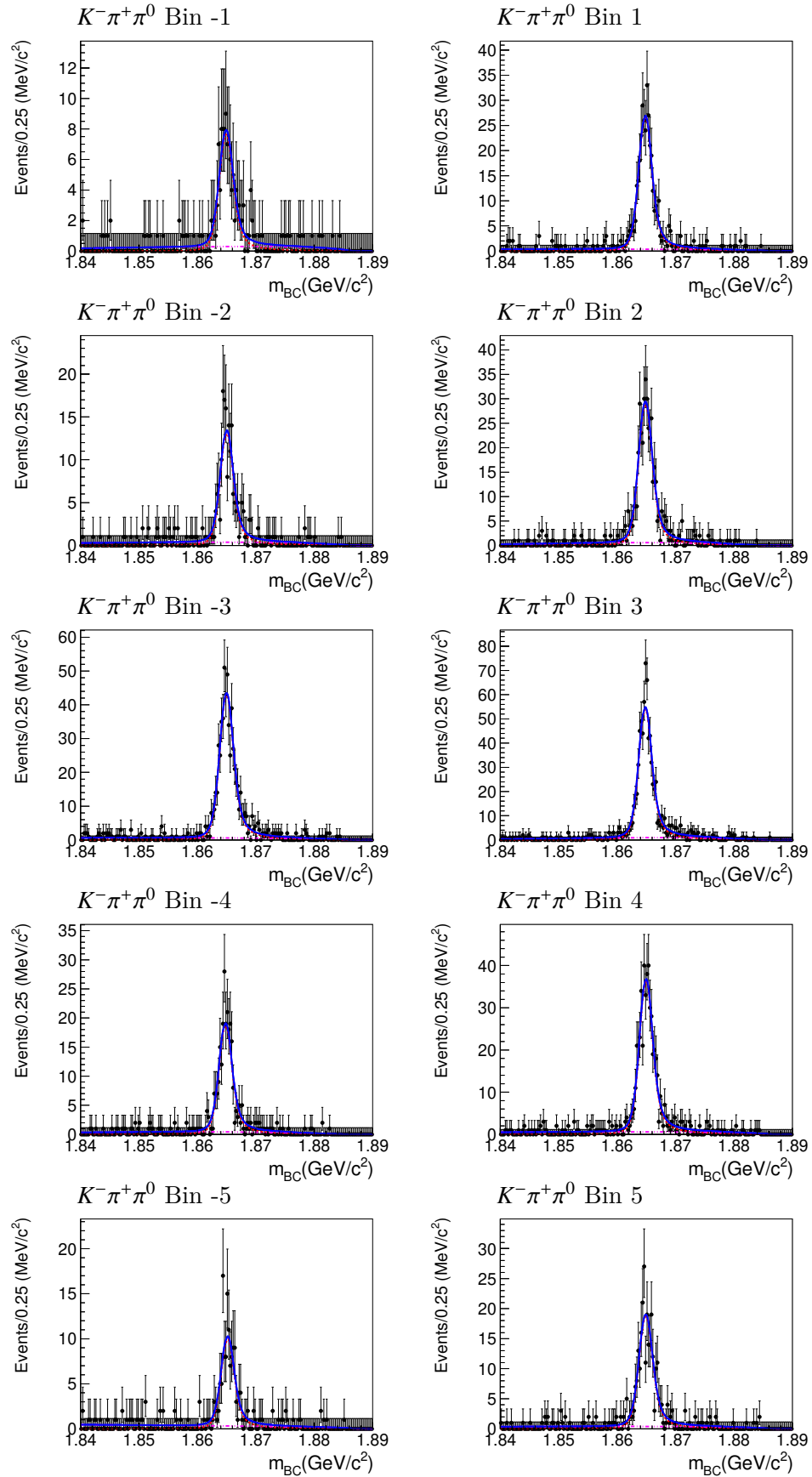


Figure 47: Fit results of $K^- \pi^+ \pi^0$ for different K_i with CLEO-c's Optimal Alternative binning scheme.

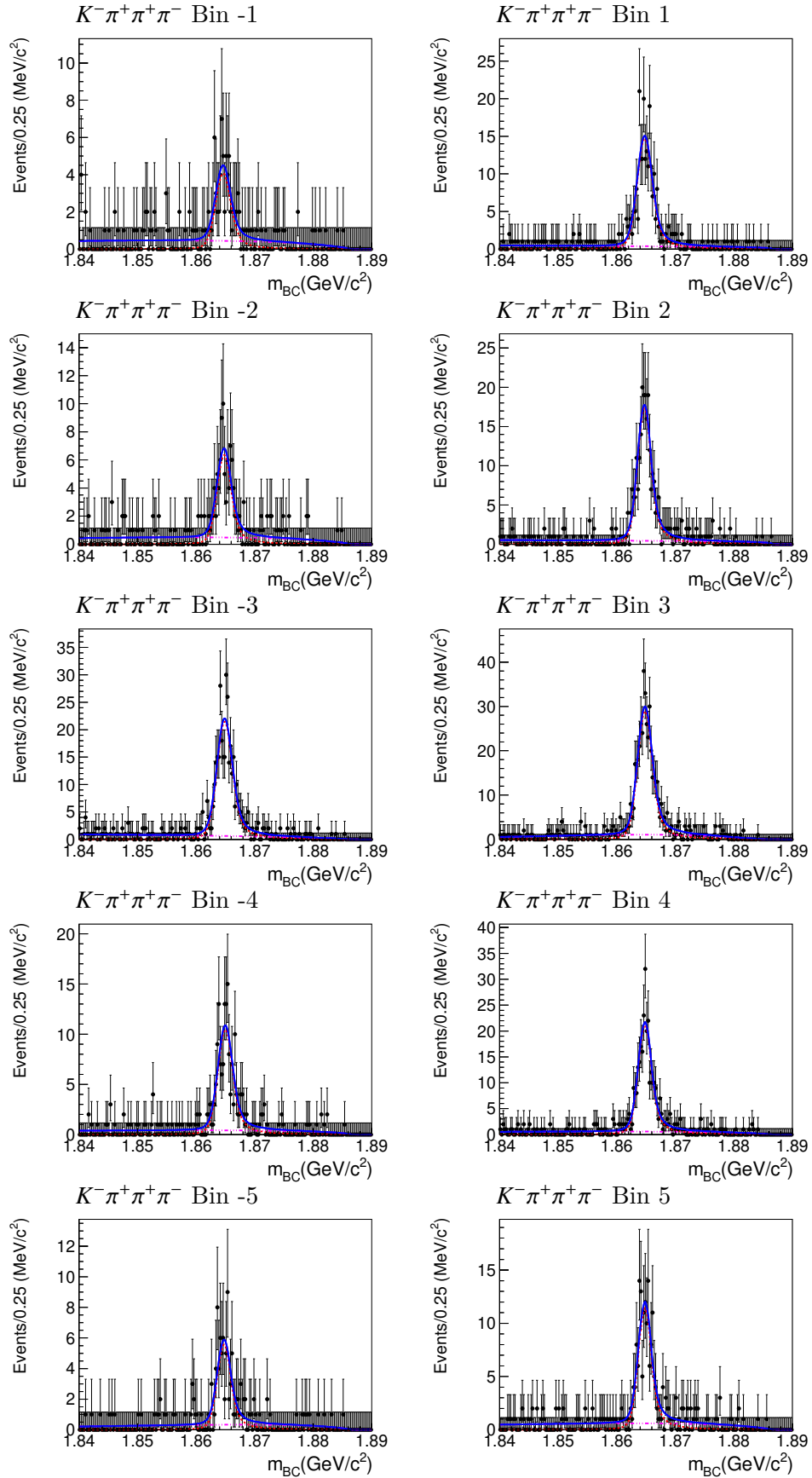


Figure 48: Fit results of $K^- \pi^+ \pi^+ \pi^-$ for different K_i with CLEO-c's Optimal Alternative binning scheme.

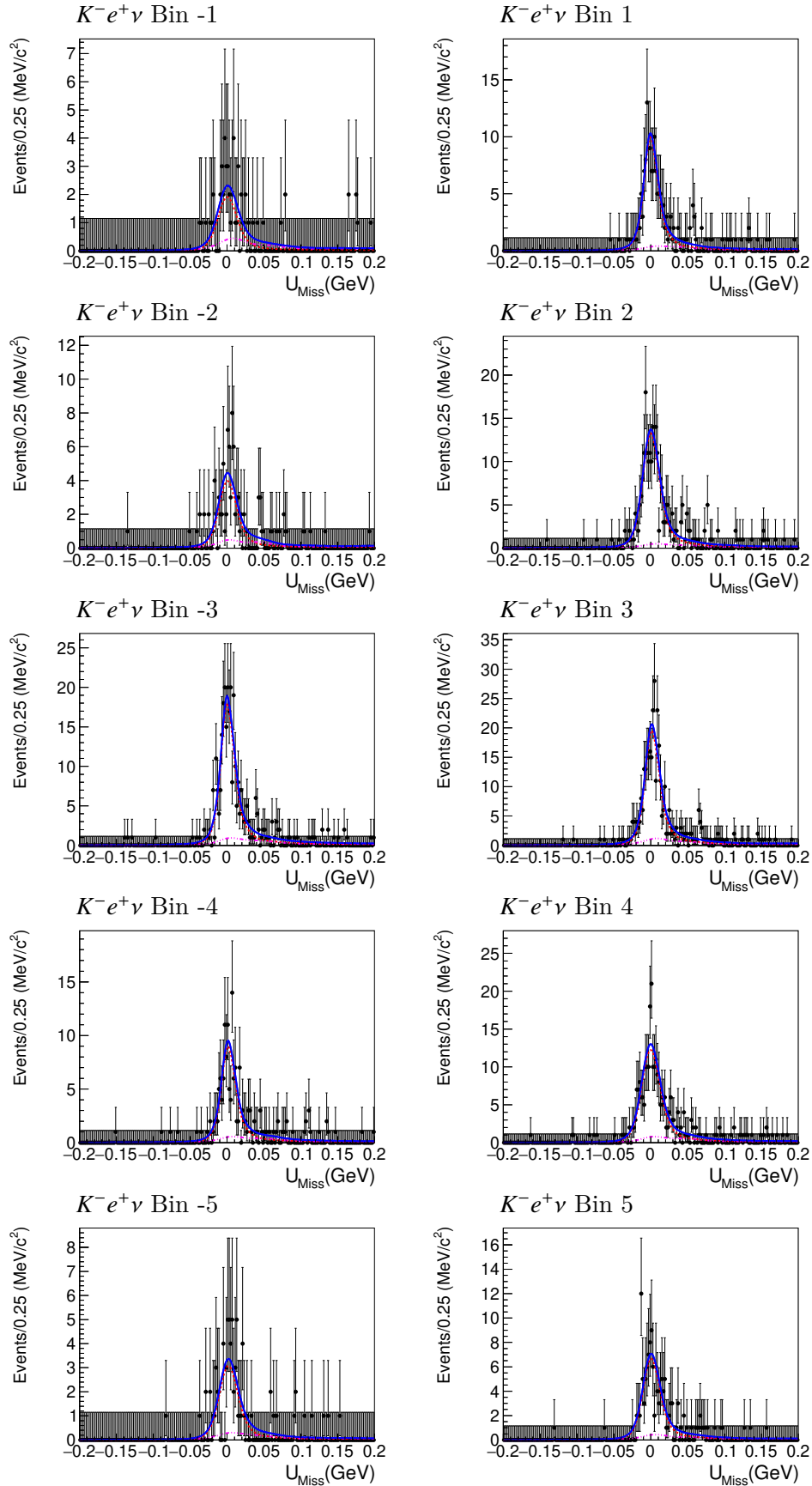


Figure 49: Fit results of $K^- e^+ \nu$ for different K_i with CLEO-c's Optimal Alternative binning scheme.

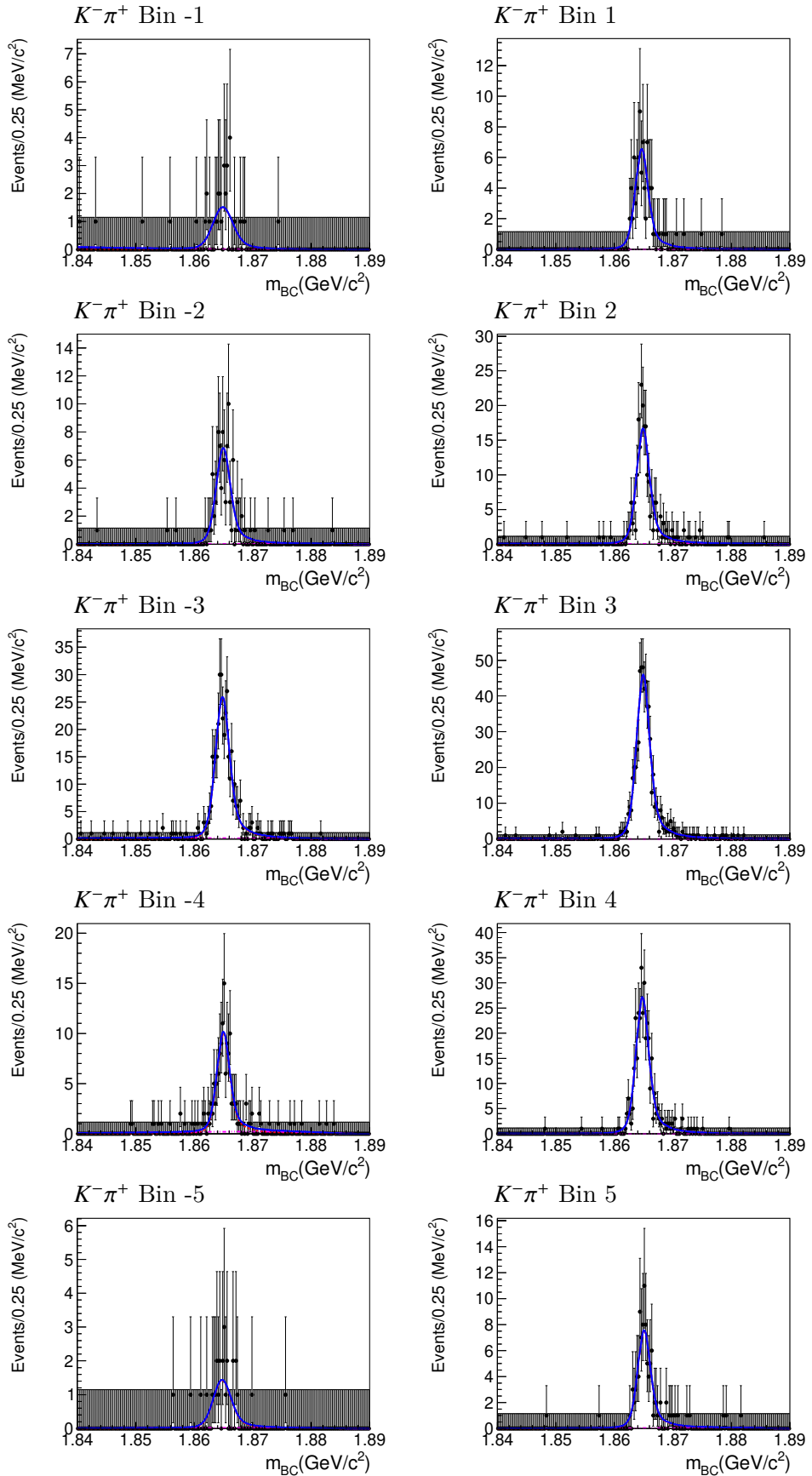


Figure 50: Fit results of $K^- \pi^+$ for different K_i with BESIII's Alternative binning scheme.

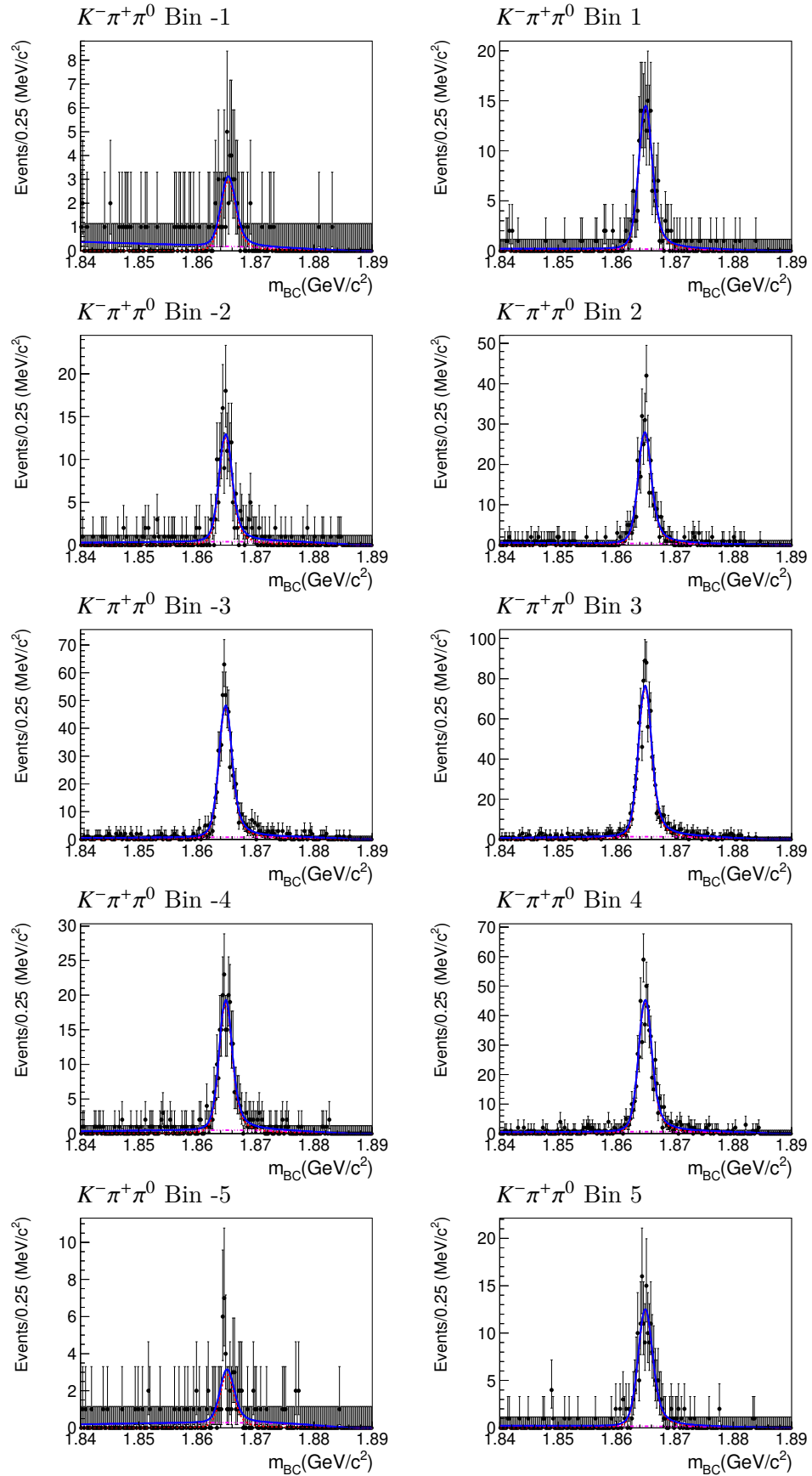


Figure 51: Fit results of $K^- \pi^+ \pi^0$ for different K_i with BESIII's Alternative binning scheme.

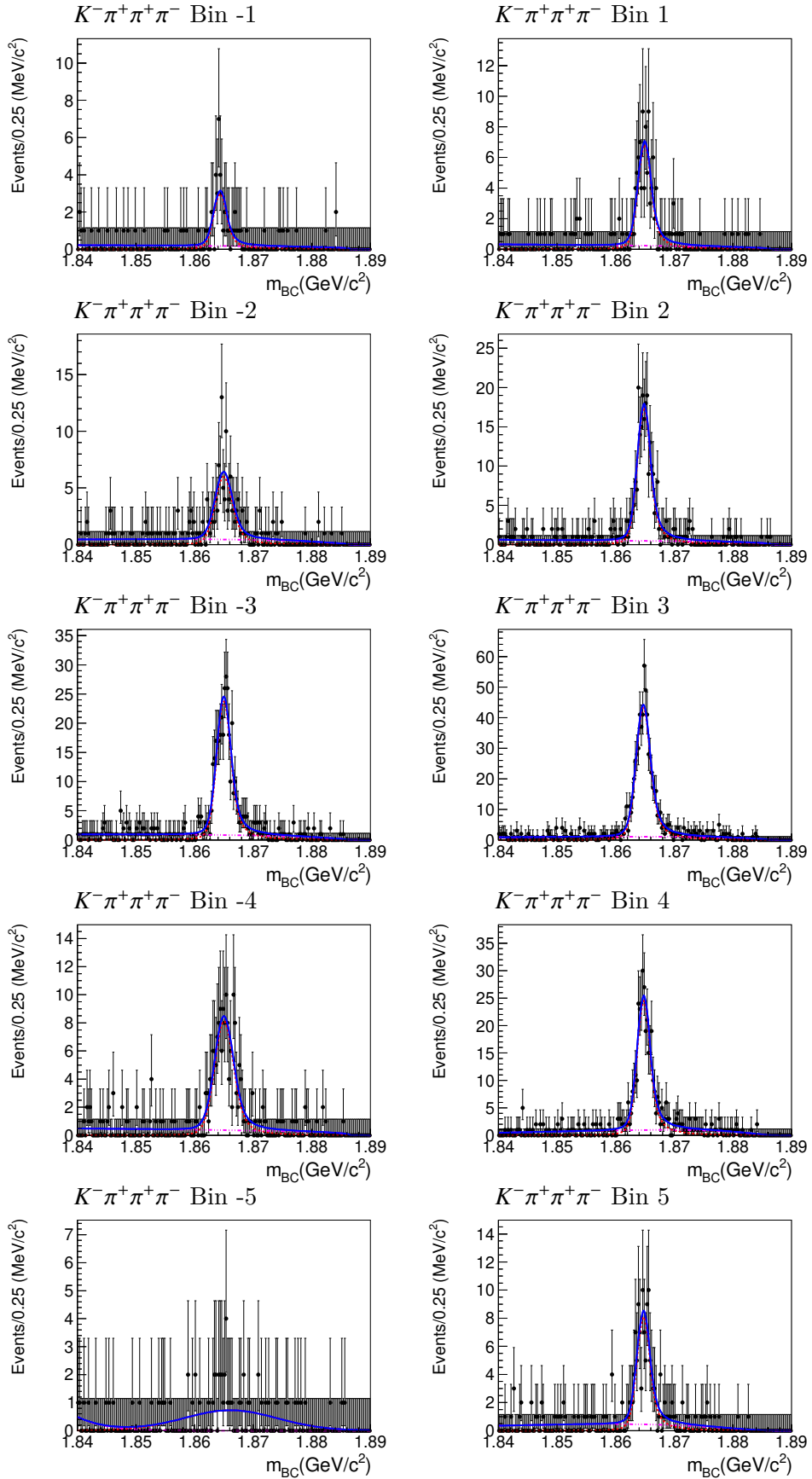


Figure 52: Fit results of $K^- \pi^+ \pi^+ \pi^-$ for different K_i with BESIII's Alternative binning scheme.

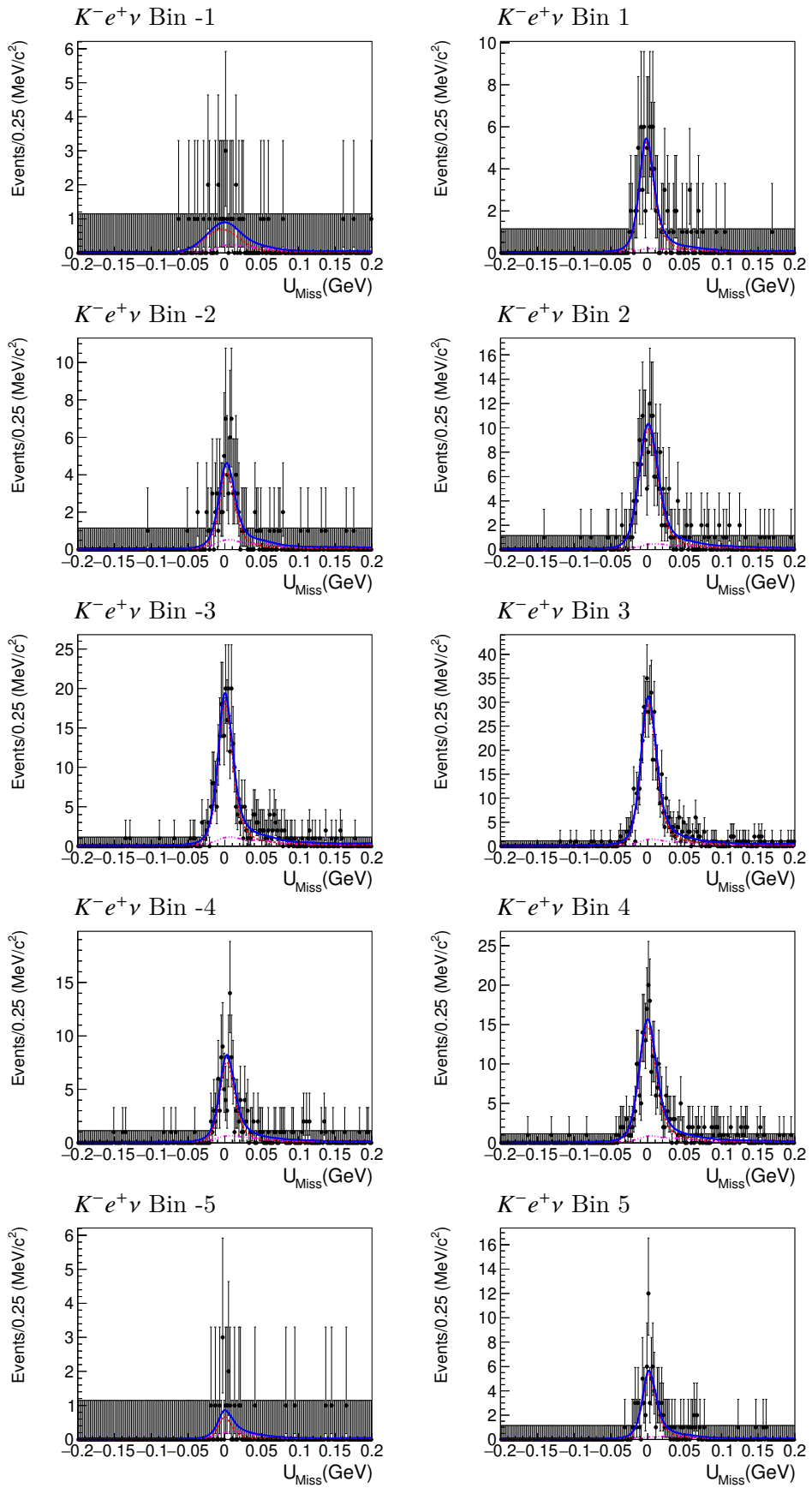


Figure 53: Fit results of $K^- e^+ \nu$ for different K_i with BESIII's Alternative binning scheme.

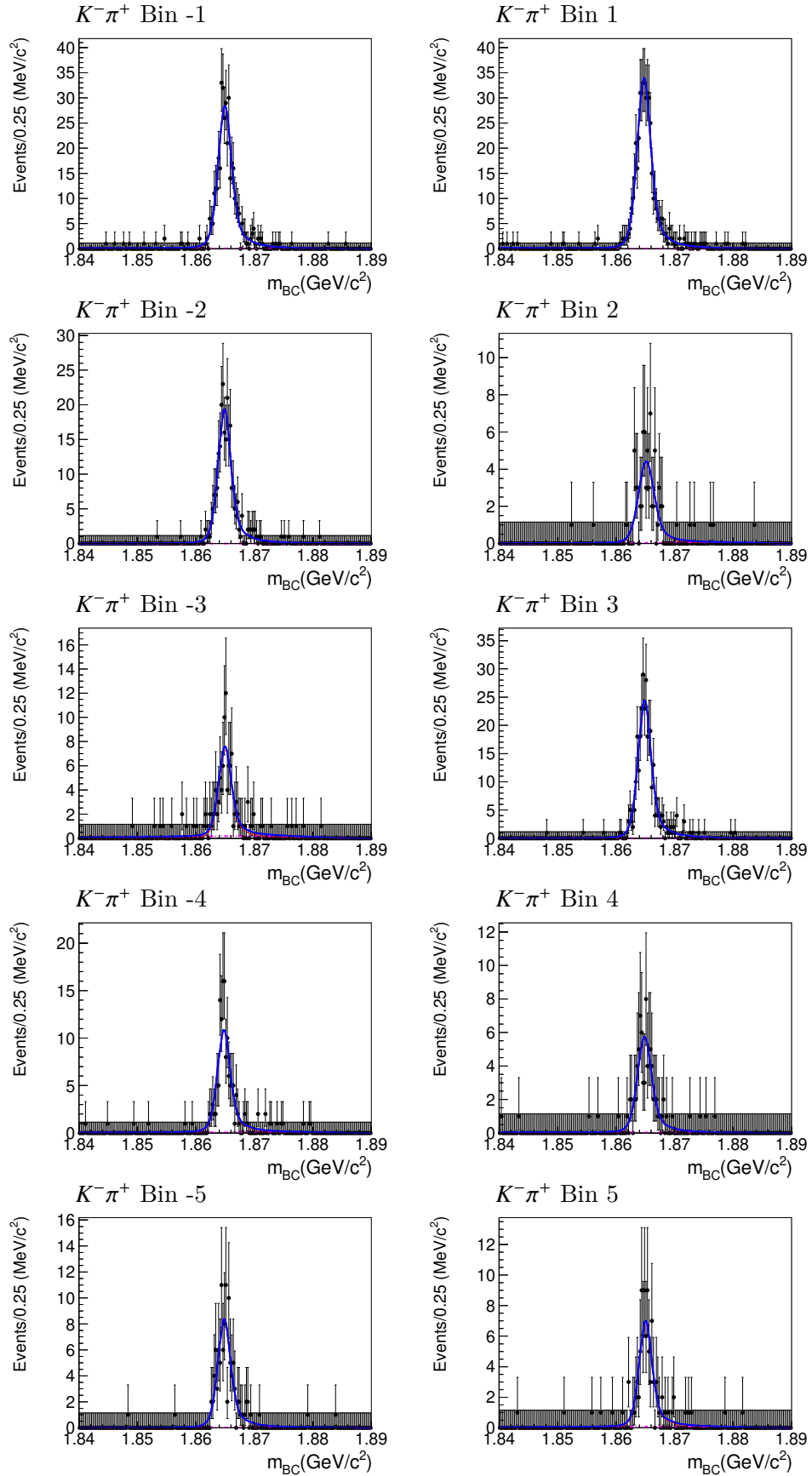


Figure 54: Fit results of $K^- \pi^+$ for different K_i with BESIII's Optimal Equal $\Delta\delta_D$ binning scheme.

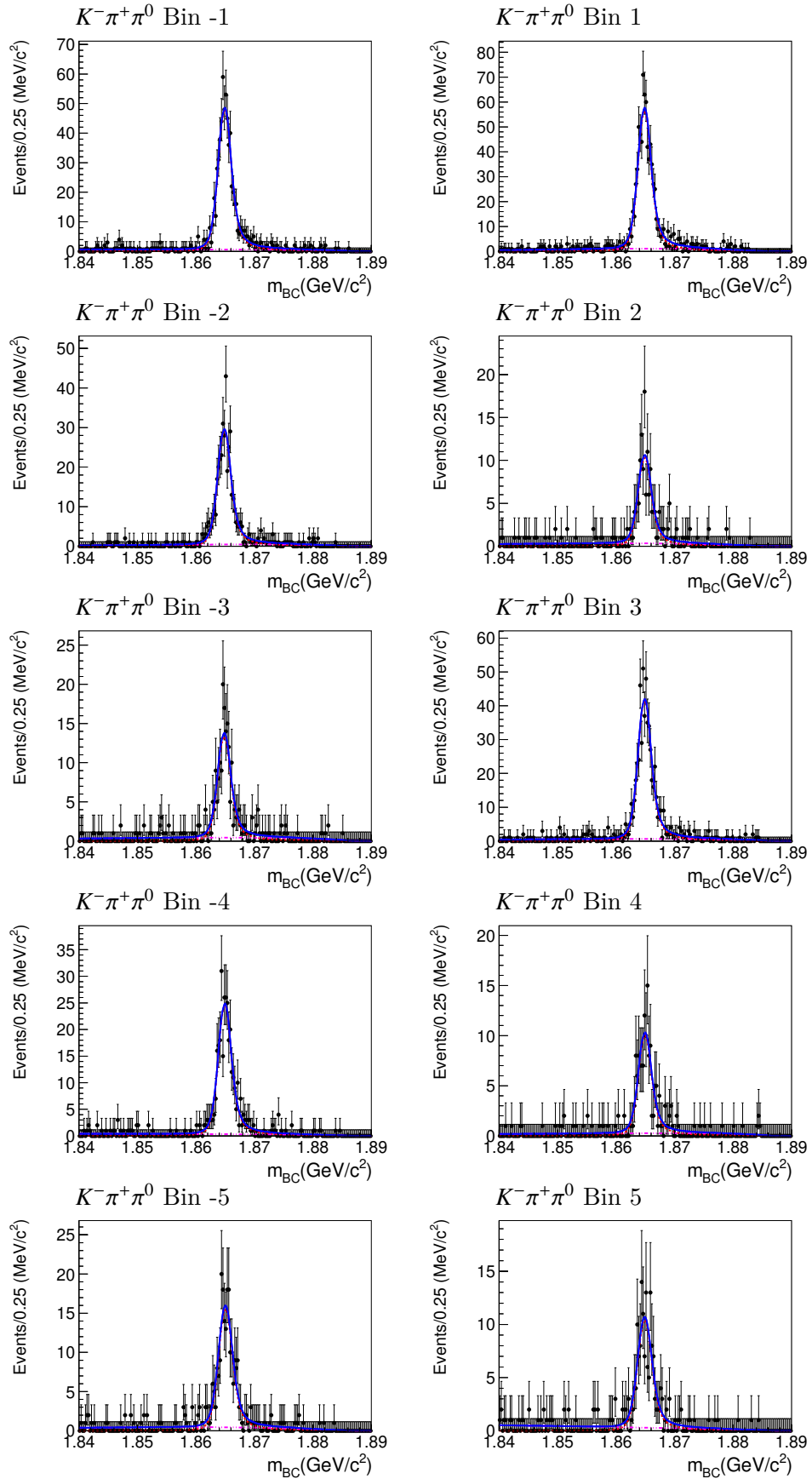


Figure 55: Fit results of $K^- \pi^+ \pi^0$ for different K_i with BESIII's Optimal Equal $\Delta\delta_D$ binning scheme.

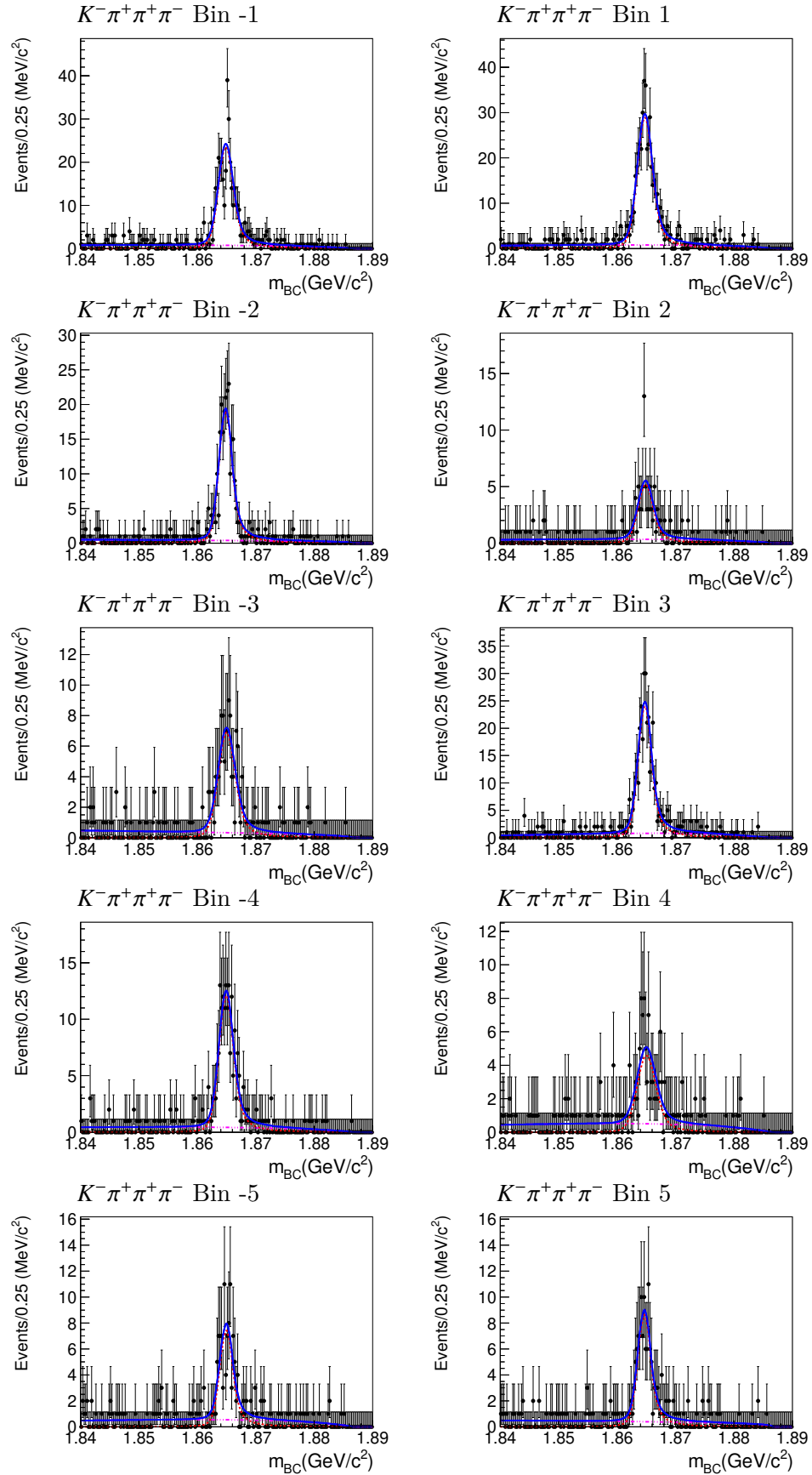
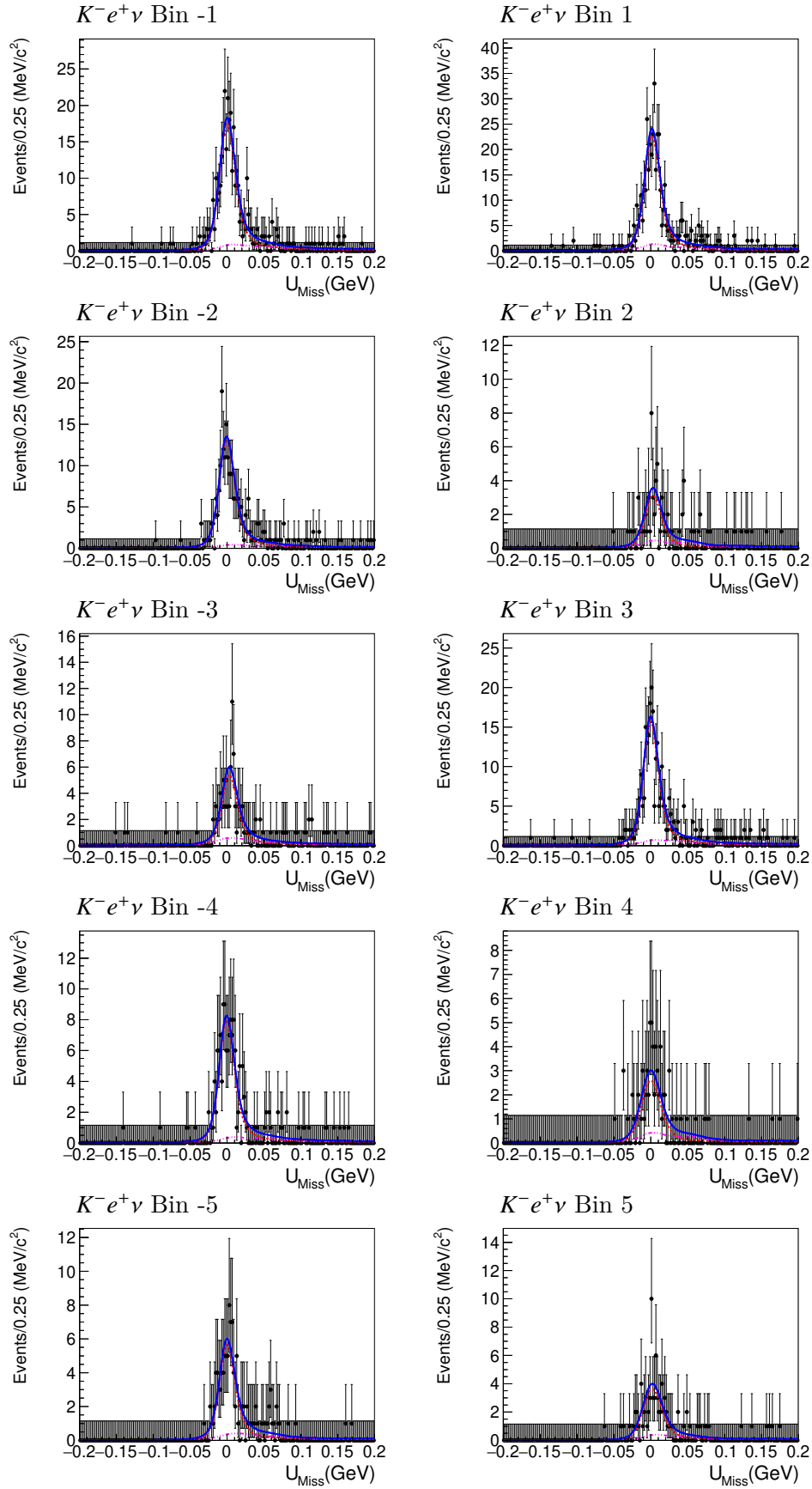
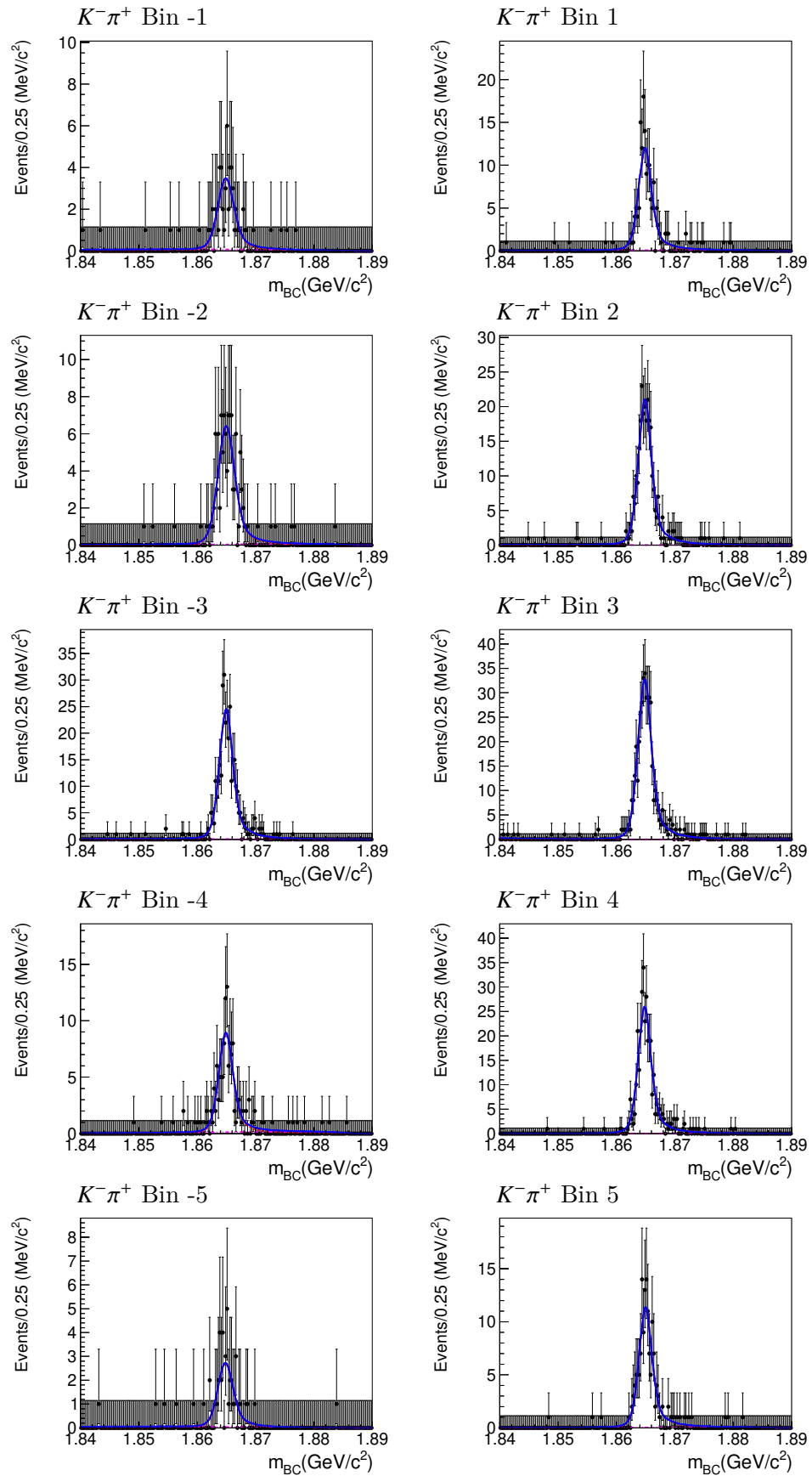


Figure 56: Fit results of $K^- \pi^+ \pi^+ \pi^-$ for different K_i with BESIII's Optimal Equal $\Delta\delta_D$ binning scheme.

Figure 57: Fit results of $K^- e^+ \nu$ for different K_i with BESIII's Optimal Equal $\Delta\delta_D$ binning scheme.

Figure 58: Fit results of $K^- \pi^+$ for different K_i with BESIII's Optimal Alternative binning scheme.

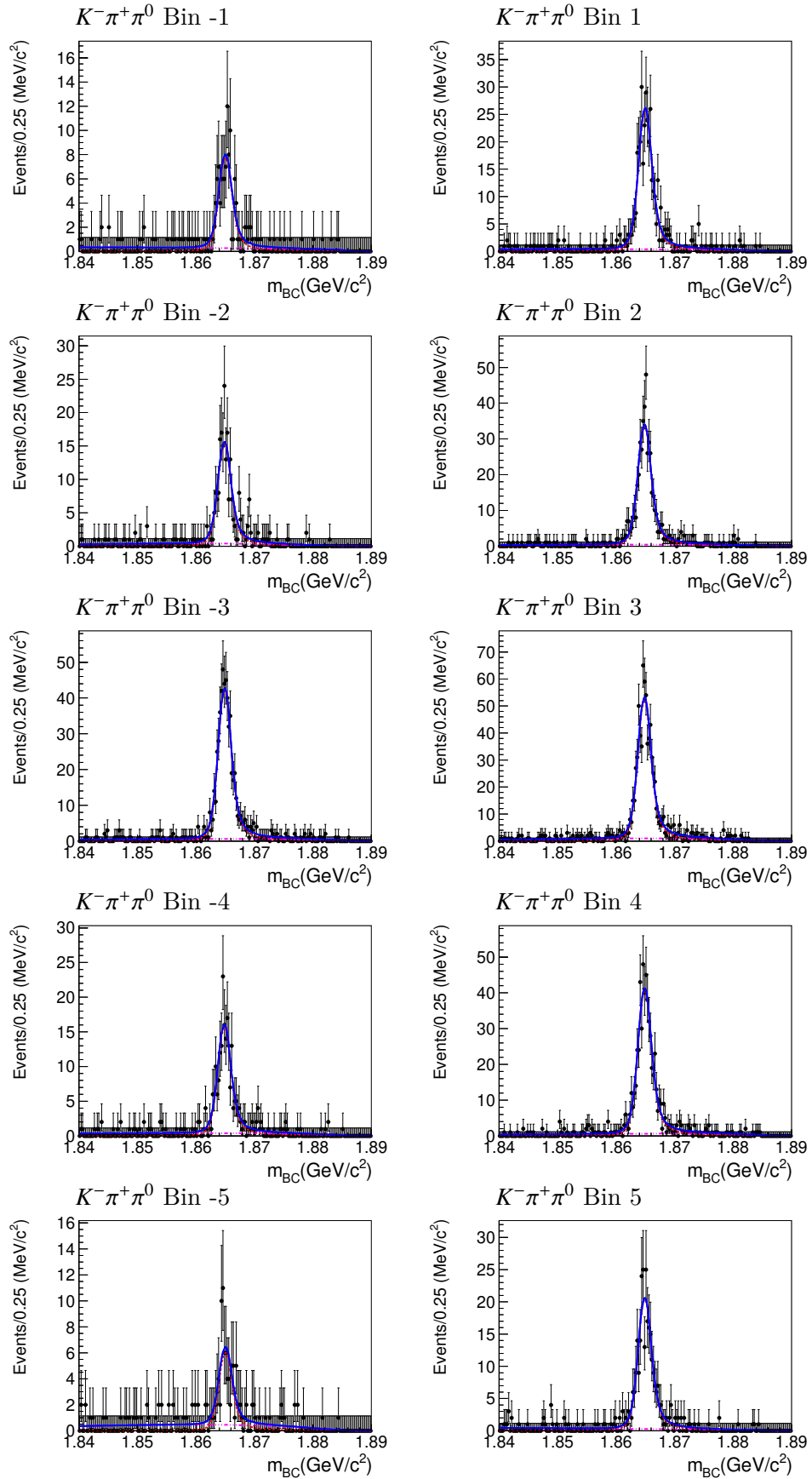


Figure 59: Fit results of $K^-\pi^+\pi^0$ for different K_i with BESIII's Optimal Alternative binning scheme.

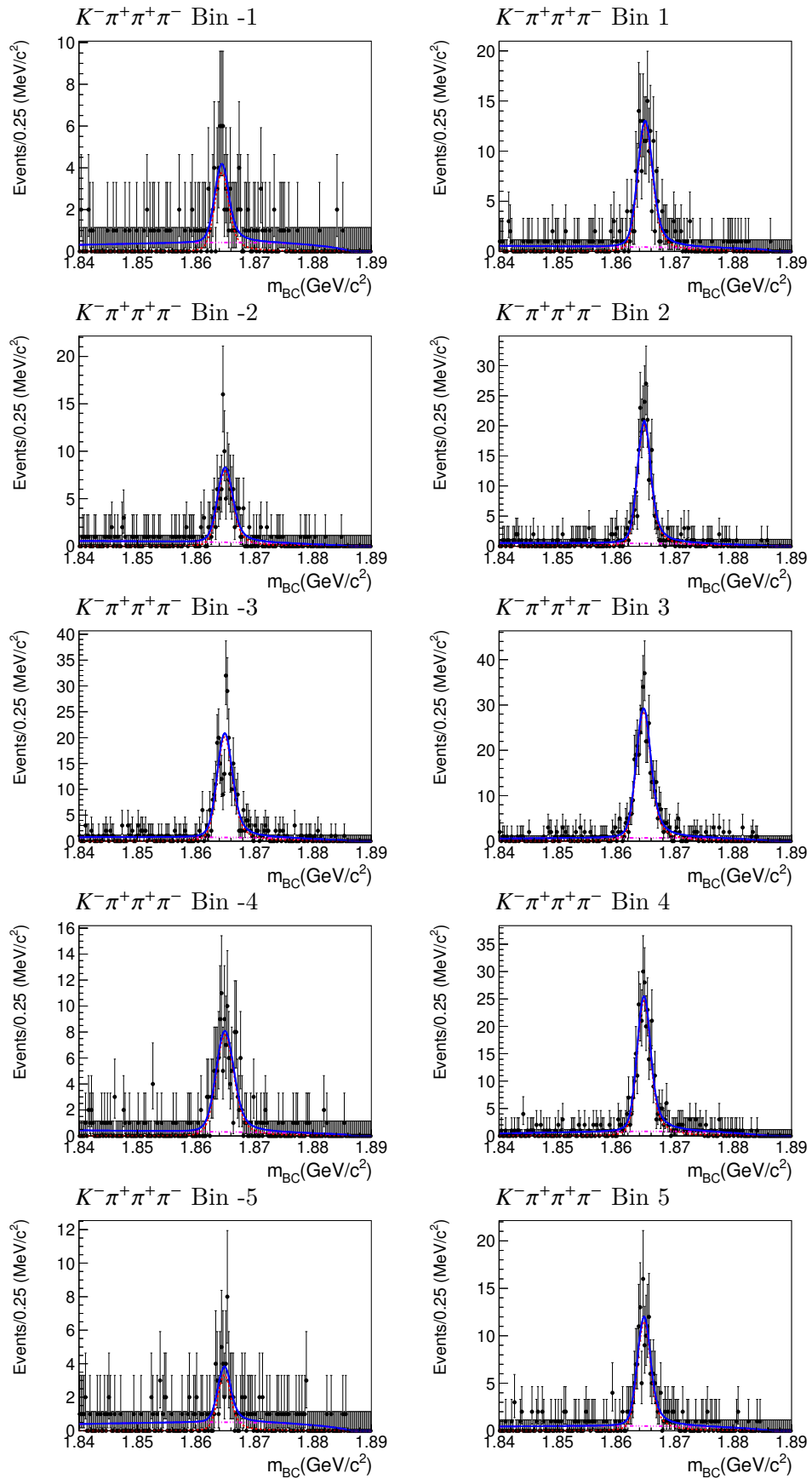


Figure 60: Fit results of $K^- \pi^+ \pi^+ \pi^-$ for different K_i with BESIII's Optimal Alternative binning scheme.

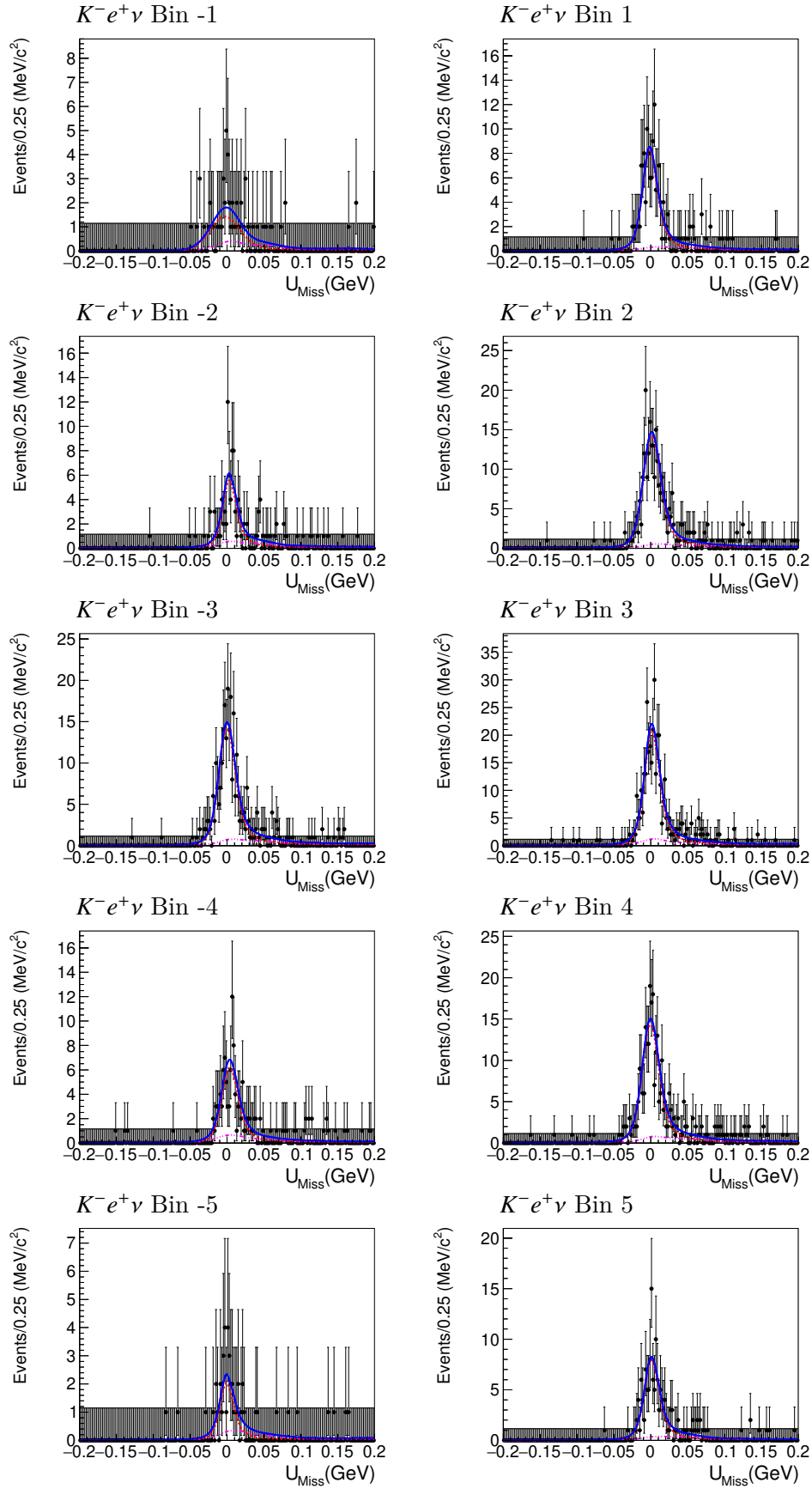


Figure 61: Fit results of $K^- e^+ \nu$ for different K_i with BESIII's Optimal Alternative binning scheme.

Table 34: The efficiency matrix ϵ_{ij} with CLEO-c's Equal $\Delta\delta_D$ binning for flavor tag channels.

Bin # (Truth) (Rec.)	-5	-4	-3	-2	-1	1	2	3	4	5
$K^- \pi^+$										
-5	0.3801	0.0183	0.0033	0.0017	0.0012	0.0002	0.0007	0.0002	0.0024	0.0190
-4	0.0197	0.3797	0.0212	0.0033	0.0002	0.0002	0.0005	0.0004	0.0011	0.0027
-3	0.0018	0.0179	0.3960	0.0275	0.0031	0.0003	0.0004	0.0001	0.0003	0.0004
-2	0.0002	0.0016	0.0122	0.4075	0.0237	0.0013	0.0006	0.0002	0.0000	0.0003
-1	0.0001	0.0001	0.0006	0.0116	0.4245	0.0169	0.0009	0.0002	0.0001	0.0002
1	0.0000	0.0001	0.0001	0.0005	0.0175	0.4254	0.0131	0.0008	0.0001	0.0002
2	0.0001	0.0001	0.0001	0.0006	0.0010	0.0209	0.4201	0.0126	0.0013	0.0002
3	0.0005	0.0003	0.0002	0.0005	0.0005	0.0027	0.0232	0.3871	0.0149	0.0021
4	0.0027	0.0011	0.0003	0.0000	0.0006	0.0013	0.0031	0.0210	0.3708	0.0184
5	0.0177	0.0014	0.0013	0.0005	0.0013	0.0002	0.0009	0.0036	0.0180	0.3899
$K^- \pi^+ \pi^0$										
-5	0.3837	0.0157	0.0024	0.0017	0.0003	0.0007	0.0007	0.0003	0.0017	0.0211
-4	0.0192	0.3717	0.0223	0.0032	0.0018	0.0000	0.0007	0.0004	0.0007	0.0025
-3	0.0018	0.0202	0.3691	0.0282	0.0030	0.0005	0.0003	0.0000	0.0008	0.0008
-2	0.0004	0.0008	0.0133	0.4046	0.0234	0.0012	0.0002	0.0001	0.0000	0.0001
-1	0.0001	0.0002	0.0007	0.0109	0.4118	0.0156	0.0005	0.0001	0.0003	0.0001
1	0.0000	0.0001	0.0003	0.0008	0.0193	0.4086	0.0121	0.0005	0.0003	0.0001
2	0.0002	0.0002	0.0000	0.0010	0.0011	0.0226	0.4094	0.0122	0.0006	0.0003
3	0.0010	0.0002	0.0000	0.0008	0.0014	0.0016	0.0211	0.3768	0.0143	0.0016
4	0.0008	0.0000	0.0003	0.0003	0.0003	0.0008	0.0017	0.0206	0.3540	0.0144
5	0.0170	0.0025	0.0006	0.0006	0.0003	0.0009	0.0015	0.0015	0.0213	0.3796
$K^- 3\pi^+$										
-5	0.3439	0.0159	0.0013	0.0019	0.0003	0.0013	0.0006	0.0003	0.0022	0.0131
-4	0.0175	0.3249	0.0175	0.0037	0.0010	0.0003	0.0007	0.0003	0.0010	0.0020
-3	0.0010	0.0155	0.3351	0.0238	0.0024	0.0007	0.0002	0.0002	0.0005	0.0007
-2	0.0005	0.0016	0.0117	0.3612	0.0208	0.0012	0.0008	0.0003	0.0002	0.0001
-1	0.0001	0.0004	0.0008	0.0127	0.3748	0.0154	0.0008	0.0002	0.0001	0.0001
1	0.0001	0.0001	0.0004	0.0005	0.0166	0.3721	0.0132	0.0008	0.0002	0.0001
2	0.0002	0.0002	0.0003	0.0003	0.0007	0.0197	0.3769	0.0125	0.0016	0.0002
3	0.0006	0.0004	0.0000	0.0006	0.0002	0.0019	0.0204	0.3318	0.0136	0.0011
4	0.0029	0.0003	0.0003	0.0003	0.0008	0.0003	0.0024	0.0173	0.3157	0.0181
5	0.0148	0.0020	0.0009	0.0006	0.0000	0.0003	0.0006	0.0029	0.0205	0.3326
$K^- e^+ \nu$										
-5	0.4210	0.0194	0.0032	0.0011	0.0006	0.0004	0.0011	0.0008	0.0032	0.0188
-4	0.0193	0.4040	0.0219	0.0055	0.0009	0.0000	0.0009	0.0002	0.0000	0.0027
-3	0.0016	0.0186	0.4163	0.0318	0.0019	0.0002	0.0005	0.0002	0.0000	0.0005
-2	0.0001	0.0017	0.0135	0.4366	0.0239	0.0014	0.0003	0.0002	0.0001	0.0001
-1	0.0000	0.0001	0.0007	0.0129	0.4442	0.0169	0.0008	0.0001	0.0000	0.0000
1	0.0002	0.0001	0.0005	0.0005	0.0170	0.4492	0.0130	0.0012	0.0000	0.0001
2	0.0002	0.0004	0.0003	0.0002	0.0015	0.0231	0.4469	0.0135	0.0006	0.0003
3	0.0005	0.0000	0.0003	0.0003	0.0008	0.0027	0.0222	0.3987	0.0133	0.0016
4	0.0023	0.0005	0.0002	0.0005	0.0002	0.0018	0.0021	0.0228	0.3831	0.0205
5	0.0170	0.0019	0.0004	0.0004	0.0004	0.0004	0.0008	0.0023	0.0207	0.4192

Table 35: The efficiency matrix ϵ_{ij} with CLEO-c's Variable $\Delta\delta_D$ binning for flavor tag channels.

Bin # (Truth) (Rec.)	-5	-4	-3	-2	-1	1	2	3	4	5
$K^- \pi^+$										
-5	0.4056	0.0139	0.0007	0.0005	0.0001	0.0001	0.0002	0.0001	0.0008	0.0111
-4	0.0092	0.4124	0.0161	0.0040	0.0007	0.0004	0.0003	0.0003	0.0005	0.0006
-3	0.0013	0.0275	0.3844	0.0299	0.0015	0.0008	0.0011	0.0004	0.0006	0.0004
-2	0.0003	0.0045	0.0222	0.4027	0.0216	0.0057	0.0036	0.0006	0.0008	0.0003
-1	0.0005	0.0016	0.0027	0.0348	0.3731	0.0254	0.0115	0.0012	0.0009	0.0002
1	0.0002	0.0008	0.0018	0.0104	0.0276	0.3757	0.0310	0.0035	0.0012	0.0005
2	0.0003	0.0003	0.0009	0.0037	0.0056	0.0216	0.4018	0.0220	0.0052	0.0008
3	0.0002	0.0002	0.0003	0.0013	0.0010	0.0026	0.0308	0.3945	0.0269	0.0007
4	0.0002	0.0002	0.0003	0.0002	0.0002	0.0007	0.0032	0.0140	0.4189	0.0097
5	0.0103	0.0013	0.0003	0.0001	0.0001	0.0003	0.0007	0.0008	0.0130	0.3976
$K^- \pi^+ \pi^0$										
-5	0.3975	0.0142	0.0009	0.0007	0.0003	0.0001	0.0003	0.0006	0.0009	0.0111
-4	0.0085	0.4027	0.0161	0.0031	0.0009	0.0002	0.0002	0.0001	0.0002	0.0009
-3	0.0009	0.0224	0.3840	0.0301	0.0026	0.0015	0.0009	0.0008	0.0006	0.0004
-2	0.0011	0.0044	0.0212	0.3903	0.0202	0.0062	0.0030	0.0006	0.0008	0.0008
-1	0.0004	0.0019	0.0024	0.0319	0.3636	0.0237	0.0132	0.0013	0.0002	0.0006
1	0.0002	0.0011	0.0007	0.0113	0.0267	0.3578	0.0348	0.0025	0.0018	0.0007
2	0.0001	0.0010	0.0010	0.0054	0.0051	0.0194	0.3847	0.0200	0.0058	0.0010
3	0.0000	0.0002	0.0004	0.0012	0.0010	0.0020	0.0303	0.3854	0.0252	0.0010
4	0.0009	0.0001	0.0001	0.0004	0.0004	0.0003	0.0039	0.0136	0.4066	0.0074
5	0.0092	0.0009	0.0001	0.0004	0.0000	0.0003	0.0005	0.0010	0.0129	0.3838
$K^- 3\pi^+$										
-5	0.3530	0.0105	0.0001	0.0009	0.0003	0.0000	0.0003	0.0000	0.0007	0.0100
-4	0.0077	0.3644	0.0143	0.0038	0.0005	0.0002	0.0004	0.0001	0.0006	0.0005
-3	0.0012	0.0258	0.3473	0.0289	0.0024	0.0009	0.0007	0.0002	0.0003	0.0003
-2	0.0002	0.0045	0.0211	0.3595	0.0164	0.0069	0.0038	0.0006	0.0006	0.0004
-1	0.0000	0.0008	0.0026	0.0335	0.3137	0.0247	0.0088	0.0014	0.0008	0.0004
1	0.0004	0.0008	0.0015	0.0107	0.0234	0.3232	0.0278	0.0023	0.0013	0.0002
2	0.0003	0.0007	0.0004	0.0039	0.0062	0.0177	0.3524	0.0202	0.0045	0.0004
3	0.0000	0.0007	0.0004	0.0007	0.0011	0.0035	0.0252	0.3565	0.0239	0.0007
4	0.0006	0.0004	0.0001	0.0003	0.0004	0.0005	0.0030	0.0121	0.3695	0.0076
5	0.0085	0.0011	0.0001	0.0004	0.0000	0.0002	0.0005	0.0006	0.0132	0.3460
$K^- e^+ \nu$										
-5	0.4350	0.0131	0.0005	0.0005	0.0001	0.0002	0.0004	0.0002	0.0008	0.0113
-4	0.0101	0.4403	0.0158	0.0037	0.0006	0.0002	0.0002	0.0003	0.0003	0.0007
-3	0.0006	0.0265	0.4150	0.0313	0.0026	0.0007	0.0010	0.0007	0.0006	0.0003
-2	0.0004	0.0049	0.0211	0.4242	0.0234	0.0060	0.0041	0.0003	0.0005	0.0005
-1	0.0005	0.0005	0.0025	0.0346	0.3833	0.0260	0.0101	0.0007	0.0007	0.0005
1	0.0003	0.0004	0.0008	0.0147	0.0279	0.3936	0.0338	0.0022	0.0017	0.0003
2	0.0003	0.0006	0.0008	0.0042	0.0057	0.0231	0.4272	0.0204	0.0053	0.0004
3	0.0002	0.0001	0.0002	0.0005	0.0019	0.0028	0.0352	0.4251	0.0280	0.0002
4	0.0007	0.0005	0.0003	0.0002	0.0004	0.0006	0.0037	0.0143	0.4399	0.0077
5	0.0083	0.0010	0.0002	0.0002	0.0002	0.0002	0.0005	0.0007	0.0137	0.4187

Table 36: The efficiency matrix ϵ_{ij} with CLEO-c's Alternative binning for flavor tag channels.

Bin # (Truth) (Rec.)	-5	-4	-3	-2	-1	1	2	3	4	5
$K^- \pi^+$										
-5	0.3929	0.0123	0.0006	0.0010	0.0129	0.0048	0.0013	0.0001	0.0000	0.0002
-4	0.0067	0.4158	0.0158	0.0007	0.0005	0.0013	0.0073	0.0022	0.0001	0.0001
-3	0.0002	0.0064	0.4248	0.0070	0.0003	0.0000	0.0009	0.0128	0.0007	0.0000
-2	0.0004	0.0007	0.0133	0.4117	0.0059	0.0000	0.0001	0.0017	0.0069	0.0010
-1	0.0103	0.0008	0.0016	0.0107	0.3829	0.0012	0.0001	0.0001	0.0030	0.0064
1	0.0173	0.0052	0.0003	0.0007	0.0045	0.3849	0.0117	0.0010	0.0000	0.0076
2	0.0021	0.0158	0.0045	0.0001	0.0000	0.0045	0.4004	0.0140	0.0005	0.0000
3	0.0000	0.0014	0.0179	0.0012	0.0001	0.0000	0.0043	0.4310	0.0050	0.0001
4	0.0000	0.0000	0.0034	0.0137	0.0027	0.0004	0.0006	0.0123	0.4226	0.0046
5	0.0014	0.0008	0.0003	0.0048	0.0184	0.0085	0.0003	0.0011	0.0133	0.4043
$K^- \pi^+ \pi^0$										
-5	0.3992	0.0127	0.0012	0.0005	0.0113	0.0068	0.0012	0.0002	0.0002	0.0007
-4	0.0068	0.4034	0.0140	0.0004	0.0005	0.0016	0.0086	0.0031	0.0001	0.0001
-3	0.0002	0.0062	0.4125	0.0065	0.0003	0.0001	0.0012	0.0143	0.0007	0.0001
-2	0.0005	0.0009	0.0142	0.4000	0.0048	0.0002	0.0003	0.0021	0.0063	0.0008
-1	0.0096	0.0010	0.0008	0.0090	0.3763	0.0006	0.0000	0.0006	0.0032	0.0068
1	0.0093	0.0046	0.0000	0.0000	0.0053	0.3545	0.0120	0.0013	0.0020	0.0113
2	0.0028	0.0163	0.0057	0.0000	0.0000	0.0041	0.3928	0.0137	0.0000	0.0005
3	0.0000	0.0012	0.0177	0.0017	0.0002	0.0000	0.0043	0.4114	0.0035	0.0001
4	0.0000	0.0002	0.0027	0.0147	0.0017	0.0006	0.0002	0.0139	0.4111	0.0059
5	0.0006	0.0000	0.0000	0.0033	0.0156	0.0078	0.0006	0.0006	0.0123	0.3715
$K^- 3\pi^+$										
-5	0.3452	0.0102	0.0016	0.0011	0.0084	0.0040	0.0013	0.0002	0.0002	0.0004
-4	0.0066	0.3649	0.0140	0.0008	0.0009	0.0008	0.0062	0.0015	0.0002	0.0000
-3	0.0003	0.0072	0.3740	0.0069	0.0003	0.0001	0.0010	0.0116	0.0009	0.0001
-2	0.0004	0.0006	0.0120	0.3696	0.0064	0.0002	0.0000	0.0018	0.0076	0.0006
-1	0.0097	0.0010	0.0002	0.0107	0.3345	0.0013	0.0000	0.0004	0.0015	0.0072
1	0.0100	0.0056	0.0006	0.0000	0.0031	0.3478	0.0075	0.0000	0.0000	0.0075
2	0.0019	0.0133	0.0053	0.0002	0.0000	0.0027	0.3494	0.0121	0.0005	0.0000
3	0.0001	0.0016	0.0183	0.0010	0.0000	0.0001	0.0047	0.3769	0.0054	0.0001
4	0.0002	0.0000	0.0027	0.0119	0.0019	0.0004	0.0006	0.0115	0.3624	0.0033
5	0.0005	0.0000	0.0000	0.0026	0.0133	0.0056	0.0010	0.0010	0.0082	0.3336
$K^- e^+ \nu$										
-5	0.4285	0.0126	0.0006	0.0018	0.0119	0.0063	0.0016	0.0001	0.0003	0.0001
-4	0.0073	0.4436	0.0149	0.0007	0.0004	0.0013	0.0076	0.0020	0.0000	0.0000
-3	0.0003	0.0078	0.4475	0.0069	0.0001	0.0000	0.0011	0.0140	0.0010	0.0000
-2	0.0005	0.0006	0.0145	0.4370	0.0045	0.0001	0.0000	0.0019	0.0065	0.0006
-1	0.0089	0.0008	0.0013	0.0126	0.4130	0.0008	0.0000	0.0001	0.0023	0.0054
1	0.0131	0.0082	0.0000	0.0000	0.0057	0.4106	0.0111	0.0016	0.0000	0.0082
2	0.0016	0.0164	0.0062	0.0000	0.0000	0.0040	0.4292	0.0136	0.0002	0.0000
3	0.0001	0.0014	0.0213	0.0014	0.0001	0.0000	0.0040	0.4454	0.0049	0.0000
4	0.0001	0.0001	0.0043	0.0105	0.0017	0.0005	0.0003	0.0139	0.4414	0.0058
5	0.0020	0.0000	0.0003	0.0024	0.0146	0.0106	0.0007	0.0010	0.0116	0.4132

Table 37: The efficiency matrix ϵ_{ij} with CLEO-c's Optimal binning for flavor tag channels.

Bin # (Truth) (Rec.)	-5	-4	-3	-2	-1	1	2	3	4	5
$K^- \pi^+$										
-5	0.3940	0.0082	0.0074	0.0003	0.0001	0.0000	0.0013	0.0004	0.0042	0.0098
-4	0.0122	0.3927	0.0206	0.0060	0.0006	0.0000	0.0004	0.0000	0.0005	0.0027
-3	0.0035	0.0083	0.4090	0.0027	0.0156	0.0004	0.0051	0.0000	0.0003	0.0001
-2	0.0002	0.0077	0.0066	0.3935	0.0177	0.0025	0.0003	0.0023	0.0000	0.0011
-1	0.0001	0.0004	0.0127	0.0053	0.4257	0.0155	0.0019	0.0003	0.0000	0.0000
1	0.0000	0.0000	0.0008	0.0005	0.0173	0.4299	0.0095	0.0087	0.0003	0.0001
2	0.0007	0.0001	0.0056	0.0000	0.0026	0.0107	0.4176	0.0028	0.0082	0.0001
3	0.0001	0.0002	0.0000	0.0017	0.0005	0.0181	0.0056	0.4134	0.0110	0.0012
4	0.0033	0.0003	0.0002	0.0000	0.0001	0.0009	0.0094	0.0086	0.3891	0.0101
5	0.0167	0.0029	0.0003	0.0006	0.0000	0.0003	0.0003	0.0017	0.0189	0.4067
$K^- \pi^+ \pi^0$										
-5	0.3767	0.0107	0.0079	0.0004	0.0004	0.0000	0.0017	0.0004	0.0038	0.0107
-4	0.0109	0.3930	0.0165	0.0062	0.0007	0.0000	0.0002	0.0000	0.0002	0.0025
-3	0.0029	0.0058	0.4109	0.0028	0.0163	0.0008	0.0055	0.0001	0.0006	0.0002
-2	0.0000	0.0084	0.0071	0.3667	0.0225	0.0029	0.0000	0.0013	0.0000	0.0006
-1	0.0000	0.0003	0.0101	0.0041	0.4071	0.0166	0.0018	0.0004	0.0002	0.0000
1	0.0000	0.0001	0.0005	0.0007	0.0185	0.4137	0.0079	0.0071	0.0006	0.0001
2	0.0009	0.0000	0.0049	0.0000	0.0023	0.0092	0.4148	0.0040	0.0067	0.0002
3	0.0000	0.0000	0.0000	0.0011	0.0004	0.0181	0.0043	0.4066	0.0116	0.0022
4	0.0028	0.0002	0.0003	0.0000	0.0002	0.0005	0.0086	0.0074	0.3727	0.0094
5	0.0158	0.0027	0.0009	0.0000	0.0000	0.0003	0.0006	0.0021	0.0173	0.3965
$K^- 3\pi^+$										
-5	0.3535	0.0068	0.0047	0.0004	0.0000	0.0000	0.0014	0.0004	0.0040	0.0084
-4	0.0107	0.3435	0.0176	0.0045	0.0009	0.0000	0.0005	0.0000	0.0000	0.0014
-3	0.0035	0.0061	0.3721	0.0027	0.0132	0.0007	0.0039	0.0001	0.0003	0.0003
-2	0.0000	0.0072	0.0057	0.3396	0.0189	0.0030	0.0003	0.0024	0.0000	0.0003
-1	0.0002	0.0004	0.0091	0.0047	0.3744	0.0147	0.0013	0.0001	0.0004	0.0000
1	0.0000	0.0001	0.0005	0.0007	0.0162	0.3721	0.0086	0.0080	0.0002	0.0000
2	0.0011	0.0002	0.0047	0.0001	0.0032	0.0099	0.3741	0.0029	0.0060	0.0001
3	0.0000	0.0004	0.0000	0.0016	0.0006	0.0191	0.0050	0.3660	0.0121	0.0012
4	0.0028	0.0004	0.0003	0.0000	0.0000	0.0010	0.0120	0.0075	0.3353	0.0077
5	0.0121	0.0020	0.0006	0.0006	0.0000	0.0000	0.0000	0.0011	0.0183	0.3398
$K^- e^+ \nu$										
-5	0.4309	0.0112	0.0055	0.0001	0.0000	0.0001	0.0019	0.0002	0.0043	0.0101
-4	0.0133	0.4122	0.0203	0.0070	0.0008	0.0000	0.0003	0.0002	0.0005	0.0025
-3	0.0035	0.0088	0.4387	0.0021	0.0173	0.0006	0.0042	0.0001	0.0002	0.0002
-2	0.0000	0.0103	0.0087	0.4084	0.0189	0.0018	0.0000	0.0022	0.0002	0.0006
-1	0.0001	0.0004	0.0122	0.0050	0.4469	0.0148	0.0022	0.0002	0.0001	0.0000
1	0.0001	0.0001	0.0005	0.0007	0.0183	0.4531	0.0084	0.0076	0.0003	0.0001
2	0.0013	0.0001	0.0055	0.0001	0.0021	0.0122	0.4444	0.0026	0.0084	0.0001
3	0.0000	0.0007	0.0001	0.0011	0.0004	0.0212	0.0057	0.4447	0.0114	0.0013
4	0.0049	0.0001	0.0004	0.0001	0.0001	0.0011	0.0100	0.0100	0.3998	0.0091
5	0.0166	0.0022	0.0006	0.0004	0.0000	0.0000	0.0000	0.0032	0.0155	0.4181

Table 38: The efficiency matrix ϵ_{ij} with CLEO-c's Optimal Alternative binning for flavor tag channels.

Bin # (Truth) (Rec.)	-5	-4	-3	-2	-1	1	2	3	4	5
$K^- \pi^+$										
-5	0.3971	0.0114	0.0003	0.0010	0.0096	0.0051	0.0001	0.0000	0.0002	0.0035
-4	0.0059	0.4116	0.0167	0.0027	0.0007	0.0047	0.0036	0.0002	0.0000	0.0001
-3	0.0002	0.0116	0.4256	0.0043	0.0000	0.0001	0.0047	0.0127	0.0001	0.0000
-2	0.0005	0.0037	0.0070	0.4140	0.0087	0.0000	0.0000	0.0103	0.0044	0.0000
-1	0.0068	0.0009	0.0003	0.0091	0.3905	0.0001	0.0000	0.0004	0.0062	0.0054
1	0.0108	0.0139	0.0004	0.0000	0.0004	0.3976	0.0081	0.0000	0.0002	0.0054
2	0.0002	0.0080	0.0175	0.0006	0.0000	0.0066	0.3929	0.0057	0.0017	0.0005
3	0.0000	0.0006	0.0156	0.0079	0.0001	0.0000	0.0017	0.4337	0.0079	0.0000
4	0.0000	0.0000	0.0002	0.0076	0.0088	0.0004	0.0013	0.0153	0.4170	0.0036
5	0.0060	0.0002	0.0002	0.0002	0.0159	0.0048	0.0008	0.0008	0.0092	0.4179
$K^- \pi^+ \pi^0$										
-5	0.3914	0.0145	0.0002	0.0007	0.0089	0.0048	0.0003	0.0000	0.0002	0.0046
-4	0.0055	0.4085	0.0173	0.0037	0.0007	0.0040	0.0028	0.0004	0.0001	0.0000
-3	0.0002	0.0094	0.4091	0.0036	0.0003	0.0001	0.0046	0.0160	0.0002	0.0001
-2	0.0007	0.0021	0.0059	0.4127	0.0079	0.0000	0.0001	0.0085	0.0044	0.0001
-1	0.0081	0.0008	0.0001	0.0100	0.3768	0.0003	0.0000	0.0003	0.0063	0.0052
1	0.0132	0.0144	0.0004	0.0000	0.0000	0.3754	0.0084	0.0000	0.0004	0.0060
2	0.0003	0.0083	0.0198	0.0000	0.0000	0.0044	0.3700	0.0071	0.0009	0.0003
3	0.0000	0.0004	0.0170	0.0082	0.0003	0.0001	0.0019	0.4144	0.0074	0.0001
4	0.0000	0.0000	0.0004	0.0062	0.0079	0.0002	0.0008	0.0143	0.4024	0.0044
5	0.0065	0.0004	0.0000	0.0000	0.0145	0.0031	0.0000	0.0004	0.0076	0.3985
$K^- 3\pi^+$										
-5	0.3529	0.0088	0.0003	0.0008	0.0075	0.0037	0.0003	0.0000	0.0003	0.0030
-4	0.0052	0.3673	0.0161	0.0030	0.0004	0.0033	0.0036	0.0004	0.0000	0.0001
-3	0.0002	0.0099	0.3767	0.0030	0.0002	0.0003	0.0049	0.0129	0.0001	0.0001
-2	0.0003	0.0020	0.0073	0.3742	0.0069	0.0000	0.0001	0.0085	0.0041	0.0000
-1	0.0051	0.0014	0.0000	0.0098	0.3384	0.0002	0.0000	0.0005	0.0054	0.0045
1	0.0119	0.0115	0.0004	0.0000	0.0008	0.3458	0.0081	0.0004	0.0004	0.0061
2	0.0000	0.0066	0.0187	0.0000	0.0000	0.0058	0.3349	0.0044	0.0022	0.0003
3	0.0001	0.0004	0.0151	0.0074	0.0000	0.0000	0.0019	0.3764	0.0070	0.0000
4	0.0002	0.0000	0.0000	0.0066	0.0081	0.0007	0.0007	0.0158	0.3651	0.0031
5	0.0060	0.0000	0.0000	0.0000	0.0140	0.0046	0.0011	0.0000	0.0039	0.3528
$K^- e^+ \nu$										
-5	0.4360	0.0109	0.0001	0.0013	0.0082	0.0058	0.0001	0.0001	0.0002	0.0033
-4	0.0066	0.4358	0.0177	0.0028	0.0005	0.0047	0.0032	0.0001	0.0000	0.0001
-3	0.0001	0.0117	0.4496	0.0048	0.0001	0.0003	0.0049	0.0126	0.0001	0.0000
-2	0.0005	0.0035	0.0057	0.4480	0.0085	0.0001	0.0001	0.0103	0.0036	0.0001
-1	0.0083	0.0009	0.0001	0.0098	0.3980	0.0002	0.0001	0.0005	0.0071	0.0057
1	0.0153	0.0120	0.0010	0.0000	0.0000	0.4103	0.0087	0.0000	0.0003	0.0069
2	0.0002	0.0096	0.0189	0.0000	0.0000	0.0078	0.4077	0.0058	0.0016	0.0002
3	0.0001	0.0003	0.0180	0.0089	0.0002	0.0000	0.0018	0.4529	0.0085	0.0000
4	0.0001	0.0001	0.0004	0.0073	0.0105	0.0006	0.0007	0.0161	0.4452	0.0042
5	0.0061	0.0000	0.0000	0.0000	0.0131	0.0058	0.0002	0.0000	0.0115	0.4253

Table 39: The efficiency matrix ϵ_{ij} with BESIII's Alternative binning for flavor tag channels.

Bin # (Truth) (Rec.)	-5	-4	-3	-2	-1	1	2	3	4	5
$K^- \pi^+$										
-5	0.3874	0.0208	0.0029	0.0014	0.0166	0.0066	0.0007	0.0001	0.0000	0.0015
-4	0.0056	0.4025	0.0110	0.0006	0.0008	0.0006	0.0056	0.0012	0.0000	0.0000
-3	0.0005	0.0077	0.4283	0.0065	0.0004	0.0000	0.0008	0.0106	0.0009	0.0000
-2	0.0010	0.0014	0.0173	0.4058	0.0094	0.0001	0.0001	0.0018	0.0084	0.0009
-1	0.0160	0.0021	0.0028	0.0213	0.3906	0.0007	0.0004	0.0000	0.0029	0.0045
1	0.0174	0.0080	0.0000	0.0005	0.0023	0.4022	0.0155	0.0000	0.0009	0.0127
2	0.0013	0.0172	0.0035	0.0002	0.0002	0.0047	0.4090	0.0117	0.0002	0.0003
3	0.0001	0.0010	0.0163	0.0010	0.0000	0.0001	0.0025	0.4380	0.0052	0.0000
4	0.0002	0.0000	0.0032	0.0132	0.0011	0.0000	0.0003	0.0118	0.4072	0.0033
5	0.0063	0.0000	0.0000	0.0078	0.0146	0.0068	0.0000	0.0005	0.0162	0.3902
$K^- \pi^+ \pi^0$										
-5	0.4062	0.0270	0.0011	0.0017	0.0171	0.0047	0.0014	0.0000	0.0003	0.0011
-4	0.0047	0.3961	0.0129	0.0006	0.0006	0.0006	0.0052	0.0014	0.0001	0.0000
-3	0.0006	0.0069	0.4133	0.0069	0.0008	0.0000	0.0006	0.0099	0.0008	0.0000
-2	0.0006	0.0004	0.0159	0.4026	0.0075	0.0000	0.0000	0.0016	0.0093	0.0009
-1	0.0131	0.0005	0.0045	0.0183	0.3790	0.0018	0.0003	0.0003	0.0018	0.0052
1	0.0135	0.0063	0.0000	0.0000	0.0036	0.3656	0.0135	0.0009	0.0000	0.0036
2	0.0019	0.0208	0.0022	0.0000	0.0000	0.0038	0.3920	0.0098	0.0000	0.0003
3	0.0000	0.0014	0.0162	0.0013	0.0003	0.0000	0.0031	0.4225	0.0039	0.0000
4	0.0000	0.0000	0.0035	0.0114	0.0026	0.0002	0.0000	0.0106	0.3883	0.0035
5	0.0030	0.0020	0.0000	0.0050	0.0141	0.0101	0.0000	0.0000	0.0071	0.3511
$K^- 3\pi^+$										
-5	0.3456	0.0164	0.0013	0.0021	0.0135	0.0042	0.0005	0.0003	0.0000	0.0010
-4	0.0050	0.3539	0.0103	0.0008	0.0010	0.0002	0.0044	0.0016	0.0000	0.0001
-3	0.0004	0.0070	0.3843	0.0064	0.0005	0.0000	0.0009	0.0081	0.0007	0.0000
-2	0.0005	0.0016	0.0161	0.3634	0.0065	0.0000	0.0001	0.0026	0.0077	0.0002
-1	0.0162	0.0015	0.0032	0.0172	0.3379	0.0012	0.0002	0.0000	0.0007	0.0049
1	0.0126	0.0075	0.0008	0.0000	0.0025	0.3381	0.0109	0.0000	0.0000	0.0084
2	0.0009	0.0136	0.0041	0.0003	0.0003	0.0047	0.3528	0.0086	0.0000	0.0006
3	0.0001	0.0013	0.0150	0.0008	0.0001	0.0001	0.0038	0.3809	0.0036	0.0000
4	0.0000	0.0000	0.0040	0.0142	0.0010	0.0004	0.0002	0.0109	0.3544	0.0018
5	0.0019	0.0010	0.0000	0.0068	0.0135	0.0077	0.0000	0.0000	0.0155	0.3106
$K^- e^+ \nu$										
-5	0.4195	0.0207	0.0024	0.0022	0.0130	0.0055	0.0009	0.0002	0.0000	0.0014
-4	0.0062	0.4335	0.0129	0.0012	0.0007	0.0007	0.0063	0.0013	0.0001	0.0000
-3	0.0004	0.0076	0.4505	0.0071	0.0005	0.0000	0.0008	0.0089	0.0012	0.0000
-2	0.0006	0.0010	0.0175	0.4284	0.0089	0.0000	0.0000	0.0017	0.0071	0.0006
-1	0.0142	0.0020	0.0036	0.0199	0.4167	0.0015	0.0000	0.0000	0.0013	0.0033
1	0.0136	0.0057	0.0000	0.0000	0.0034	0.4184	0.0090	0.0017	0.0011	0.0085
2	0.0014	0.0181	0.0059	0.0000	0.0000	0.0045	0.4238	0.0136	0.0002	0.0000
3	0.0001	0.0011	0.0182	0.0011	0.0001	0.0001	0.0037	0.4631	0.0050	0.0000
4	0.0000	0.0000	0.0030	0.0157	0.0018	0.0001	0.0000	0.0104	0.4263	0.0037
5	0.0018	0.0000	0.0006	0.0043	0.0184	0.0073	0.0018	0.0006	0.0116	0.4070

Table 40: The efficiency matrix ϵ_{ij} with BESIII’s Optimal Equal binning for flavor tag channels.

Bin # (Truth) (Rec.)	-5	-4	-3	-2	-1	1	2	3	4	5
$K^- \pi^+$										
-5	0.4108	0.0072	0.0133	0.0002	0.0002	0.0000	0.0011	0.0009	0.0039	0.0203
-4	0.0078	0.3997	0.0182	0.0073	0.0060	0.0000	0.0002	0.0000	0.0000	0.0025
-3	0.0033	0.0042	0.3988	0.0002	0.0087	0.0002	0.0031	0.0000	0.0006	0.0032
-2	0.0009	0.0086	0.0007	0.4044	0.0208	0.0091	0.0002	0.0016	0.0000	0.0000
-1	0.0001	0.0014	0.0071	0.0038	0.4357	0.0092	0.0040	0.0000	0.0001	0.0000
1	0.0000	0.0001	0.0000	0.0021	0.0114	0.4353	0.0063	0.0045	0.0025	0.0000
2	0.0006	0.0002	0.0059	0.0001	0.0080	0.0101	0.4184	0.0005	0.0114	0.0012
3	0.0012	0.0003	0.0000	0.0015	0.0000	0.0156	0.0006	0.4073	0.0109	0.0024
4	0.0027	0.0002	0.0010	0.0000	0.0001	0.0044	0.0128	0.0076	0.3951	0.0115
5	0.0107	0.0017	0.0074	0.0000	0.0002	0.0001	0.0029	0.0026	0.0156	0.3972
$K^- \pi^+ \pi^0$										
-5	0.3764	0.0067	0.0149	0.0006	0.0000	0.0003	0.0003	0.0009	0.0055	0.0179
-4	0.0049	0.3923	0.0175	0.0056	0.0084	0.0000	0.0000	0.0000	0.0000	0.0032
-3	0.0036	0.0039	0.3954	0.0002	0.0096	0.0002	0.0036	0.0000	0.0004	0.0022
-2	0.0000	0.0079	0.0018	0.3749	0.0202	0.0110	0.0004	0.0009	0.0000	0.0009
-1	0.0001	0.0010	0.0068	0.0030	0.4213	0.0091	0.0054	0.0000	0.0001	0.0002
1	0.0000	0.0001	0.0001	0.0021	0.0093	0.4296	0.0066	0.0042	0.0020	0.0002
2	0.0004	0.0005	0.0050	0.0002	0.0070	0.0092	0.4038	0.0001	0.0110	0.0019
3	0.0018	0.0000	0.0000	0.0012	0.0006	0.0161	0.0006	0.3772	0.0102	0.0026
4	0.0008	0.0002	0.0005	0.0000	0.0003	0.0052	0.0159	0.0070	0.3885	0.0088
5	0.0124	0.0024	0.0071	0.0000	0.0000	0.0002	0.0013	0.0009	0.0150	0.3941
$K^- 3\pi^+$										
-5	0.3563	0.0057	0.0108	0.0006	0.0000	0.0000	0.0020	0.0006	0.0054	0.0148
-4	0.0053	0.3412	0.0142	0.0043	0.0053	0.0003	0.0003	0.0000	0.0000	0.0020
-3	0.0027	0.0033	0.3507	0.0002	0.0087	0.0003	0.0033	0.0000	0.0007	0.0029
-2	0.0000	0.0099	0.0004	0.3685	0.0148	0.0086	0.0000	0.0021	0.0000	0.0000
-1	0.0002	0.0016	0.0067	0.0028	0.3856	0.0080	0.0031	0.0001	0.0001	0.0002
1	0.0000	0.0000	0.0003	0.0016	0.0103	0.3786	0.0063	0.0037	0.0025	0.0000
2	0.0005	0.0001	0.0048	0.0005	0.0074	0.0097	0.3822	0.0001	0.0092	0.0018
3	0.0011	0.0000	0.0000	0.0013	0.0000	0.0162	0.0003	0.3577	0.0100	0.0022
4	0.0015	0.0001	0.0010	0.0000	0.0004	0.0049	0.0108	0.0061	0.3532	0.0079
5	0.0117	0.0008	0.0067	0.0000	0.0000	0.0004	0.0018	0.0010	0.0141	0.3370
$K^- e^+ \nu$										
-5	0.4273	0.0049	0.0123	0.0004	0.0000	0.0002	0.0009	0.0006	0.0043	0.0161
-4	0.0087	0.4176	0.0170	0.0059	0.0076	0.0000	0.0000	0.0004	0.0000	0.0011
-3	0.0044	0.0046	0.4314	0.0003	0.0088	0.0001	0.0040	0.0000	0.0010	0.0031
-2	0.0000	0.0116	0.0003	0.4370	0.0190	0.0102	0.0008	0.0019	0.0000	0.0000
-1	0.0000	0.0014	0.0074	0.0039	0.4578	0.0086	0.0044	0.0000	0.0001	0.0000
1	0.0000	0.0001	0.0000	0.0022	0.0113	0.4647	0.0065	0.0046	0.0017	0.0000
2	0.0004	0.0001	0.0058	0.0004	0.0074	0.0094	0.4413	0.0004	0.0100	0.0010
3	0.0018	0.0000	0.0000	0.0024	0.0000	0.0152	0.0009	0.4275	0.0117	0.0013
4	0.0027	0.0000	0.0008	0.0000	0.0001	0.0040	0.0167	0.0061	0.4080	0.0097
5	0.0129	0.0013	0.0055	0.0000	0.0003	0.0000	0.0034	0.0016	0.0144	0.4270

Table 41: The efficiency matrix ϵ_{ij} with BESIII’s Optimal Alternative binning for flavor tag channels.

Bin # (Truth) (Rec.)	-5	-4	-3	-2	-1	1	2	3	4	5
$K^- \pi^+$										
-5	0.4053	0.0160	0.0005	0.0018	0.0104	0.0053	0.0002	0.0001	0.0002	0.0042
-4	0.0069	0.3985	0.0082	0.0028	0.0011	0.0032	0.0017	0.0002	0.0000	0.0001
-3	0.0002	0.0080	0.4356	0.0051	0.0001	0.0002	0.0049	0.0095	0.0000	0.0000
-2	0.0010	0.0040	0.0067	0.4183	0.0101	0.0001	0.0002	0.0090	0.0031	0.0002
-1	0.0099	0.0021	0.0001	0.0120	0.4036	0.0002	0.0000	0.0004	0.0056	0.0046
1	0.0089	0.0142	0.0007	0.0000	0.0005	0.3999	0.0084	0.0000	0.0007	0.0038
2	0.0006	0.0078	0.0168	0.0001	0.0000	0.0065	0.4094	0.0080	0.0009	0.0000
3	0.0001	0.0001	0.0125	0.0082	0.0004	0.0002	0.0028	0.4351	0.0055	0.0000
4	0.0002	0.0000	0.0000	0.0045	0.0074	0.0005	0.0010	0.0128	0.4073	0.0037
5	0.0132	0.0005	0.0000	0.0011	0.0210	0.0051	0.0000	0.0000	0.0089	0.4049
$K^- \pi^+ \pi^0$										
-5	0.4101	0.0193	0.0002	0.0016	0.0118	0.0050	0.0002	0.0002	0.0002	0.0034
-4	0.0061	0.3953	0.0091	0.0033	0.0005	0.0028	0.0021	0.0002	0.0000	0.0001
-3	0.0003	0.0073	0.4169	0.0058	0.0002	0.0002	0.0045	0.0097	0.0002	0.0001
-2	0.0012	0.0028	0.0069	0.4071	0.0094	0.0001	0.0002	0.0087	0.0032	0.0007
-1	0.0067	0.0010	0.0000	0.0164	0.3856	0.0003	0.0000	0.0006	0.0049	0.0045
1	0.0079	0.0172	0.0005	0.0000	0.0005	0.3792	0.0102	0.0000	0.0005	0.0028
2	0.0003	0.0057	0.0187	0.0003	0.0003	0.0055	0.3978	0.0075	0.0006	0.0003
3	0.0000	0.0003	0.0102	0.0078	0.0000	0.0000	0.0022	0.4266	0.0040	0.0001
4	0.0002	0.0000	0.0005	0.0042	0.0091	0.0000	0.0022	0.0137	0.3882	0.0034
5	0.0097	0.0005	0.0000	0.0005	0.0158	0.0031	0.0005	0.0000	0.0036	0.3715
$K^- 3\pi^+$										
-5	0.3575	0.0119	0.0002	0.0017	0.0092	0.0032	0.0003	0.0003	0.0000	0.0043
-4	0.0068	0.3489	0.0094	0.0028	0.0015	0.0023	0.0020	0.0005	0.0000	0.0001
-3	0.0004	0.0076	0.3834	0.0042	0.0002	0.0000	0.0046	0.0082	0.0001	0.0000
-2	0.0012	0.0037	0.0078	0.3846	0.0081	0.0001	0.0004	0.0085	0.0026	0.0004
-1	0.0089	0.0019	0.0003	0.0107	0.3507	0.0001	0.0000	0.0006	0.0039	0.0044
1	0.0075	0.0150	0.0000	0.0004	0.0009	0.3408	0.0075	0.0000	0.0000	0.0040
2	0.0000	0.0049	0.0149	0.0000	0.0000	0.0054	0.3592	0.0052	0.0011	0.0000
3	0.0001	0.0002	0.0112	0.0072	0.0006	0.0000	0.0014	0.3778	0.0041	0.0000
4	0.0000	0.0000	0.0000	0.0077	0.0057	0.0005	0.0007	0.0114	0.3620	0.0030
5	0.0098	0.0005	0.0000	0.0005	0.0142	0.0024	0.0000	0.0000	0.0078	0.3422
$K^- e^+ \nu$										
-5	0.4412	0.0148	0.0004	0.0018	0.0095	0.0033	0.0004	0.0001	0.0000	0.0042
-4	0.0079	0.4279	0.0098	0.0027	0.0018	0.0039	0.0021	0.0001	0.0000	0.0001
-3	0.0000	0.0087	0.4571	0.0051	0.0000	0.0001	0.0050	0.0088	0.0001	0.0000
-2	0.0010	0.0032	0.0078	0.4435	0.0093	0.0000	0.0003	0.0086	0.0029	0.0001
-1	0.0087	0.0016	0.0001	0.0155	0.4122	0.0000	0.0000	0.0001	0.0036	0.0045
1	0.0093	0.0128	0.0006	0.0000	0.0000	0.4224	0.0070	0.0000	0.0006	0.0029
2	0.0002	0.0071	0.0197	0.0005	0.0000	0.0065	0.4296	0.0071	0.0007	0.0002
3	0.0000	0.0001	0.0122	0.0087	0.0002	0.0001	0.0028	0.4618	0.0059	0.0000
4	0.0000	0.0000	0.0002	0.0065	0.0079	0.0003	0.0008	0.0145	0.4340	0.0045
5	0.0121	0.0010	0.0000	0.0006	0.0162	0.0044	0.0000	0.0000	0.0089	0.4186

Table 42: The summaries of fitted yields for $K_S^0\pi^+\pi^-$ tag channel for CLEO-c's binning schemes.

		Cleo-c's Equal $\Delta\delta_D$ binning							
		1	2	3	4	5	6	7	8
i \ j		-1	-2	-3	-4	-5	-6	-7	-8
1	23.32±6.75	5.14±2.78	10.17±3.46	5.65±2.54	33.15±6.13	11.01±3.35	16.00±4.54	14.10±4.02	
2	15.39±4.43	5.35±2.53	3.01±1.74	4.99±2.23	19.62±4.54	9.99±2.56	22.00±4.69	8.95±3.03	
3	12.66±3.71	5.00±2.24	0.97±1.02	3.53±2.51	3.98±2.01	3.00±1.47	5.86±3.18	7.92±2.86	
4	5.75±2.75	4.42±2.39	1.93±1.49	0.00±0.88	7.66±3.03	1.97±1.42	8.01±2.83	3.00±1.73	
5	3.93±2.09	2.00±0.93	1.00±1.00	1.97±1.42	2.00±1.41	2.47±1.94	1.00±0.16	4.98±2.23	
1	19.69±5.05	4.46±2.41	18.79±4.59	4.98±2.29	33.47±6.48	12.01±3.65	9.97±3.17	7.86±2.92	
2	12.10±3.73	8.37±3.48	3.45±2.23	5.99±2.45	17.58±1.22	3.82±2.06	11.73±3.63	7.05±4.29	
3	5.00±2.24	7.96±11.21	3.00±1.73	2.91±1.78	5.75±3.13	3.64±2.12	6.00±2.45	5.99±2.79	
4	3.97±2.26	1.95±1.45	1.00±1.00	2.00±1.41	3.96±0.23	2.98±1.74	3.00±1.73	6.01±2.45	
5	9.00±3.00	1.00±1.00	4.17±2.14	2.00±1.42	4.71±2.41	0.98±1.06	5.00±2.24	3.01±1.74	
Cleo-c's Variable $\Delta\delta_D$ binning									
i \ j		1	2	3	4	5	6	7	8
1	3.97±2.40	3.26±2.15	4.52±2.35	0.99±1.00	8.02±0.03	1.23±1.35	3.99±2.01	5.01±2.19	
2	9.53±3.29	7.98±2.84	5.03±2.31	4.42±2.35	21.90±3.12	6.00±2.45	12.02±3.47	8.62±3.04	
3	9.02±3.01	2.00±1.10	2.00±1.42	4.01±1.94	12.68±3.75	4.95±2.29	3.30±2.42	5.79±2.66	
4	17.69±4.68	6.11±3.01	4.00±2.00	5.99±2.45	15.98±4.01	11.00±3.32	21.79±4.82	15.02±3.88	
5	14.95±4.43	9.49±3.27	3.85±2.08	7.01±2.68	10.79±3.49	6.02±6.86	11.55±3.89	6.99±2.65	
1	8.28±3.35	2.79±1.81	5.03±2.42	0.00±0.56	13.79±23.15	1.00±1.00	2.00±1.42	3.03±1.80	
2	13.00±3.84	0.00±4.07	9.02±3.16	2.99±1.80	15.12±6.04	7.30±2.86	6.00±2.45	1.97±1.46	
3	3.27±2.86	2.99±1.74	2.98±0.74	2.00±1.41	9.15±3.23	2.58±1.79	8.09±2.93	5.00±2.24	
4	16.14±4.69	11.34±3.95	6.84±2.94	9.00±3.00	18.03±4.75	7.49±2.94	9.92±3.20	9.21±3.49	
5	11.46±4.37	5.02±0.43	5.16±2.42	3.00±1.73	7.91±3.10	2.79±1.91	9.00±2.64	8.14±3.31	
Cleo-c's Alternative binning									
i \ j		1	2	3	4	5	6	7	8
1	5.89±2.47	0.94±1.03	0.99±1.07	1.00±0.92	3.99±2.04	0.00±4.82	6.00±2.45	2.00±1.41	
2	11.87±0.11	8.01±2.83	4.66±2.46	5.54±0.03	9.43±3.79	4.78±2.30	8.00±2.86	5.23±2.57	
3	24.06±5.40	7.87±31.33	11.96±3.69	5.59±2.58	20.14±5.16	9.82±3.29	5.82±0.03	8.76±3.31	
4	12.65±4.74	3.00±1.73	1.98±1.45	4.00±2.00	12.63±3.74	5.02±1.88	13.00±3.61	3.80±2.05	
5	3.99±2.00	2.87±1.77	2.01±1.42	0.00±0.50	3.00±1.73	2.00±1.42	3.01±1.74	4.00±2.00	
1	5.27±2.61	3.93±2.03	2.00±1.42	1.73±1.51	6.67±2.80	3.57±2.08	5.99±2.45	4.01±2.00	
2	10.97±3.66	5.15±2.58	2.01±1.42	4.75±2.29	11.14±3.39	7.98±0.03	15.52±4.29	13.01±3.63	
3	18.06±4.85	9.99±3.16	17.22±4.46	5.01±2.29	45.71±6.95	13.46±3.10	19.01±4.38	12.93±3.78	
4	4.82±3.13	8.14±0.00	2.00±1.42	3.00±1.03	14.90±0.23	2.81±1.80	10.01±3.33	4.85±2.57	
5	5.33±2.67	1.99±1.41	3.99±2.00	3.00±1.73	4.75±2.38	2.98±1.72	1.06±1.18	7.00±2.64	
Cleo-c's Optimal Equal binning									
i \ j		1	2	3	4	5	6	7	8
1	14.66±4.21	8.98±3.01	9.59±3.29	4.97±2.26	35.20±6.28	8.00±2.85	6.89±2.83	9.11±3.18	
2	9.00±2.39	3.63±1.01	4.02±2.07	4.01±1.19	9.07±3.10	7.99±2.80	20.87±4.76	8.71±0.01	
3	15.89±4.51	3.01±1.74	1.99±1.41	4.00±1.93	17.01±4.13	5.00±2.24	9.02±0.01	8.00±2.83	
4	9.04±5.67	9.00±3.00	2.93±1.78	3.52±2.10	9.91±3.19	5.98±2.47	11.00±2.35	10.00±3.16	
5	6.97±2.67	2.00±1.41	0.97±0.05	0.00±0.23	5.31±2.62	1.01±1.00	5.65±2.56	4.86±2.29	
1	14.41±4.42	4.86±2.48	10.27±3.38	2.98±1.74	21.16±5.28	7.05±2.81	11.00±3.32	4.95±2.31	
2	13.50±3.85	2.98±1.74	5.56±1.16	3.98±2.01	6.33±0.73	5.01±2.32	5.69±2.48	2.71±1.86	
3	10.46±3.56	10.14±3.58	4.10±2.33	3.96±2.03	19.16±4.72	5.22±2.30	8.73±3.21	6.21±2.69	
4	4.97±2.59	5.03±2.48	4.00±2.00	3.99±2.00	5.32±0.37	4.62±2.35	5.99±2.45	6.17±2.92	
5	8.36±3.63	6.01±2.45	4.19±2.15	4.00±2.00	3.01±1.80	2.08±0.15	4.00±2.00	6.31±2.72	
Cleo-c's Optimal Alternative binning									
i \ j		1	2	3	4	5	6	7	8
1	5.35±1.10	2.92±1.93	2.03±1.52	2.01±1.42	1.84±5.08	2.92±1.75	3.98±2.01	3.58±2.19	
2	13.14±3.21	0.00±11.43	8.97±3.14	3.98±2.01	6.02±2.86	5.01±2.32	6.79±2.72	3.43±2.17	
3	13.90±4.10	7.01±2.65	9.85±3.24	5.55±0.32	33.11±6.09	8.00±2.85	5.85±2.98	8.94±3.19	
4	14.36±4.86	4.00±2.00	1.97±1.44	4.00±2.00	17.02±4.13	6.00±2.45	12.07±3.64	4.92±11.61	
5	7.67±3.04	2.87±1.77	0.97±0.05	0.00±0.23	4.96±2.26	3.01±1.74	9.00±2.72	4.86±2.29	
1	7.82±3.30	6.99±2.44	3.00±1.73	3.66±2.10	10.60±3.47	5.39±2.67	7.57±3.23	10.00±3.16	
2	13.01±3.61	5.66±2.67	4.60±2.34	4.00±2.00	9.88±3.28	6.00±0.97	16.02±4.00	9.86±0.00	

Table 43: The summaries of fitted yields for $K_S^0\pi^+\pi^-$ tag channel for other BESIII's 3 binning schemes.

BESIII's Alternative binning								
i \ j	1	2	3	4	5	6	7	8
1	2.46±1.78	2.09±16.25	0.97±1.13	0.00±0.50	3.23±2.10	1.00±1.00	4.00±2.00	1.87±1.78
2	10.94±3.58	6.00±2.45	4.36±2.47	0.94±1.02	6.48±2.95	3.51±2.22	2.99±1.73	0.00±0.55
3	19.30±5.49	3.22±2.16	13.26±3.81	9.86±3.27	34.89±38.03	8.67±19.35	12.59±3.76	9.32±3.26
4	19.96±4.49	3.06±2.22	2.08±1.62	0.98±1.00	14.73±1.17	3.00±1.73	9.94±3.54	7.01±2.65
5	7.29±3.16	0.70±1.14	0.98±1.05	1.00±1.00	1.00±1.00	0.00±0.65	4.00±2.00	2.00±1.46
	-1	-2	-3	-4	-5	-6	-7	-8
1	3.66±2.47	4.00±2.00	1.00±1.00	1.91±1.43	4.00±2.00	3.28±2.08	6.19±2.86	3.60±2.16
2	9.70±3.34	5.47±2.76	2.00±1.41	4.02±2.07	10.00±3.16	4.00±2.00	14.01±3.75	17.02±4.13
3	19.57±4.53	10.84±3.83	8.60±3.55	8.02±2.89	38.79±6.86	18.01±4.25	21.01±4.59	11.84±3.62
4	14.35±4.35	6.88±3.00	8.97±3.02	6.00±2.45	20.98±4.89	8.00±2.84	9.08±3.35	6.99±2.85
5	3.73±2.36	1.96±0.33	5.01±2.24	2.00±1.42	1.97±1.48	1.56±1.71	1.00±1.00	3.99±2.00
BESIII's Optimal Equal binning								
i \ j	1	2	3	4	5	6	7	8
1	11.01±4.10	3.12±2.31	9.84±3.22	6.82±2.87	34.09±5.97	8.01±2.87	8.41±3.39	12.59±3.72
2	10.99±3.32	4.60±2.35	3.57±0.42	5.00±2.24	16.45±4.33	8.99±3.00	12.00±3.46	10.70±20.37
3	17.19±4.42	3.81±2.28	1.00±1.00	0.98±1.00	12.01±3.55	2.00±1.41	9.54±3.46	1.87±0.00
4	6.01±2.81	3.59±2.25	0.97±1.02	2.89±1.81	6.88±0.52	3.43±2.05	9.01±3.00	9.01±3.00
5	9.67±3.55	4.00±2.00	4.00±2.00	1.84±1.44	2.94±2.14	4.52±2.45	8.54±3.33	3.61±2.16
	-1	-2	-3	-4	-5	-6	-7	-8
1	13.77±4.04	7.26±3.01	9.87±3.43	5.97±2.52	28.76±5.62	8.08±3.01	17.01±4.13	5.85±2.57
2	8.98±2.99	0.96±1.01	0.81±1.06	5.00±2.24	6.00±23.96	6.14±2.56	4.96±2.26	2.98±1.94
3	12.28±4.14	7.32±3.12	6.96±2.66	4.00±1.64	15.68±4.26	7.00±2.65	6.74±2.92	5.22±2.44
4	7.07±2.85	4.90±2.51	8.00±2.83	0.00±0.51	5.33±2.70	0.00±3.71	4.00±0.57	0.61±1.11
5	6.22±2.96	3.98±2.05	3.64±2.24	2.00±1.42	2.91±1.91	1.15±1.46	2.99±1.73	9.00±3.00
BESIII's Optimal Alternative binning								
i \ j	1	2	3	4	5	6	7	8
1	4.94±2.63	3.75±2.22	4.81±2.63	1.00±0.54	3.71±2.25	2.01±1.44	3.00±1.73	0.00±0.55
2	10.00±3.16	2.59±1.87	0.68±1.06	4.78±2.33	8.59±3.29	5.66±0.11	8.99±3.03	2.11±1.83
3	8.98±3.69	2.04±1.83	9.85±3.22	5.63±2.64	31.77±5.83	8.01±2.87	6.91±2.80	10.17±3.29
4	17.06±4.36	3.81±2.28	0.00±0.50	0.98±1.00	14.02±3.75	2.00±1.41	8.97±3.35	3.61±2.45
5	7.55±3.32	1.80±1.53	4.10±2.09	1.00±1.00	0.99±1.00	1.63±1.61	9.00±0.09	4.54±3.32
	-1	-2	-3	-4	-5	-6	-7	-8
1	6.69±3.15	5.57±3.02	1.00±1.00	3.62±2.14	4.80±2.46	1.99±0.99	9.34±3.43	10.01±3.17
2	14.00±3.74	5.63±2.49	4.70±2.33	6.00±2.45	21.75±4.69	9.99±3.16	11.75±3.67	13.71±3.94
3	13.76±3.94	7.37±3.16	8.95±3.27	3.95±2.05	27.65±5.61	7.17±2.86	15.01±3.88	4.89±0.57
4	14.06±6.22	8.15±3.04	7.98±2.23	5.00±2.24	19.25±4.64	8.00±2.83	8.04±3.22	4.83±2.30
5	6.11±2.87	4.02±2.12	6.91±2.66	1.96±1.42	3.92±2.30	3.74±2.34	2.00±1.41	9.00±1.31

Table 44: The summaries of fitted yields for $K_L^0\pi^+\pi^-$ tag channel for CLEO-c's binning schemes.

Cleo-c's Equal $\Delta\delta_D$ binning								
i \ j	1	2	3	4	5	6	7	8
1	148.76±14.15	45.65±8.17	31.69±6.91	14.10±4.40	13.70±4.92	26.39±6.24	51.61±8.04	60.59±9.11
2	59.52±9.40	20.49±5.76	21.95±5.67	3.44±2.37	10.61±4.48	8.20±3.41	28.11±5.98	39.06±7.06
3	34.86±6.94	3.10±2.67	8.89±4.06	3.52±2.29	12.48±5.10	11.92±4.03	5.56±3.61	9.20±3.75
4	23.94±6.04	8.36±3.92	2.00±2.72	2.13±2.36	7.64±3.65	5.90±1.16	0.73±1.63	10.05±3.74
5	13.52±4.76	10.14±4.04	2.79±3.26	0.36±3.68	12.53±4.27	4.31±2.58	2.68±2.52	8.35±3.44
	-1	-2	-3	-4	-5	-6	-7	-8
1	127.60±13.21	50.48±8.71	16.44±5.58	12.29±4.18	7.98±4.82	24.77±6.04	54.61±8.48	66.76±9.39
2	72.91±10.05	11.89±4.66	13.28±4.27	3.79±2.74	9.67±4.54	20.57±5.24	33.04±6.61	39.04±7.15
3	29.80±6.74	14.22±4.68	5.08±2.84	0.41±1.44	5.03±2.92	10.55±4.07	14.11±4.24	11.91±4.59
4	20.36±5.52	10.08±3.91	2.47±1.86	0.00±0.74	6.89±3.89	3.78±2.73	5.90±3.08	6.87±3.65
5	16.24±5.20	6.37±3.03	9.95±3.40	4.10±2.31	6.32±3.20	9.09±3.52	9.13±3.76	5.21±3.37
Cleo-c's Variable $\Delta\delta_D$ binning								
i \ j	1	2	3	4	5	6	7	8
1	39.63±7.34	11.52±4.00	9.74±3.71	4.58±2.51	3.16±2.59	7.22±3.29	17.25±4.63	21.20±5.20
2	71.54±9.87	24.91±6.04	15.44±5.11	5.85±2.87	12.50±4.26	15.58±4.52	30.96±6.12	30.77±6.46
3	47.62±8.07	22.60±5.52	6.60±3.47	3.61±2.18	2.96±2.85	7.56±3.50	14.03±4.13	19.69±5.09
4	67.60±9.79	15.69±5.35	26.30±6.33	7.19±3.16	11.58±4.99	16.98±4.90	20.81±5.62	38.74±7.26
5	44.41±8.55	13.03±4.93	14.26±5.51	7.35±3.58	22.34±6.03	15.81±4.44	9.30±4.41	15.19±4.80
	-1	-2	-3	-4	-5	-6	-7	-8
1	42.56±7.41	9.59±3.96	5.04±2.80	2.00±1.20	1.99±2.45	9.43±3.59	12.14±3.98	13.91±4.43
2	67.10±9.64	27.89±6.43	11.64±4.45	5.10±2.78	4.75±3.45	10.31±3.86	28.93±6.30	37.61±7.03
3	51.48±8.45	14.10±4.83	2.88±3.07	9.31±3.53	4.06±2.86	6.71±3.42	21.39±5.12	24.15±5.77
4	71.40±10.02	19.20±5.66	17.67±5.03	1.61±2.15	12.09±4.85	23.08±5.67	33.40±6.65	42.70±7.68
5	43.51±8.33	20.88±5.47	6.05±3.19	0.45±1.66	16.76±5.61	13.32±4.60	15.28±5.10	14.33±5.27
Cleo-c's Alternative binning								
i \ j	1	2	3	4	5	6	7	8
1	19.94±5.45	4.87±2.73	7.07±1.22	3.49±2.28	8.29±3.89	2.04±2.27	4.16±2.68	5.59±3.51
2	48.14±8.30	12.79±4.44	7.76±1.38	0.05±9.57	6.50±3.58	19.25±5.04	15.46±4.75	21.10±5.49
3	122.25±13.06	38.26±7.76	30.47±6.96	9.50±3.80	10.85±4.88	24.05±5.75	52.96±8.15	59.92±9.13
4	39.60±7.63	8.83±4.02	11.41±4.37	2.87±2.02	11.68±4.71	11.27±3.77	14.08±4.81	13.27±4.32
5	17.21±5.15	5.66±3.57	1.73±2.57	0.88±2.39	12.86±4.76	4.52±2.38	0.55±1.42	7.77±3.47
	-1	-2	-3	-4	-5	-6	-7	-8
1	20.11±5.71	11.99±1.21	4.08±4.01	4.14±2.35	5.58±3.06	6.16±1.24	2.95±2.62	11.71±3.86
2	54.53±8.85	14.52±4.91	19.46±5.40	4.11±2.59	11.35±4.74	8.28±3.57	20.08±5.14	34.91±6.78
3	153.83±14.28	58.00±9.11	18.38±5.57	16.77±4.72	11.57±4.86	26.80±6.51	53.51±8.41	67.57±9.38
4	54.89±8.81	12.53±4.98	10.90±4.13	4.04±2.55	8.50±4.05	11.58±4.18	31.83±6.29	28.87±6.51
5	16.54±5.27	11.68±4.14	5.47±2.61	0.00±1.79	4.94±3.09	10.61±3.80	11.16±4.09	5.25±3.33
Cleo-c's Optimal Equal binning								
i \ j	1	2	3	4	5	6	7	8
1	109.85±12.06	33.99±7.30	24.94±6.29	9.63±3.74	12.47±4.59	23.51±5.55	39.51±6.91	46.44±7.73
2	53.62±8.54	17.77±5.15	13.32±4.43	1.86±2.10	9.73±4.27	8.90±3.33	23.28±5.52	33.20±6.53
3	48.75±8.57	13.21±4.69	11.20±4.23	3.31±2.22	3.28±3.12	10.59±3.87	13.77±4.37	23.90±5.72
4	38.08±7.54	0.97±2.21	13.86±5.10	6.43±3.33	20.69±5.77	12.34±4.24	10.24±4.20	15.16±4.78
5	19.19±5.53	11.73±4.15	2.02±2.57	7.05±3.07	11.89±4.44	5.38±2.80	8.23±3.81	12.00±4.15
	-1	-2	-3	-4	-5	-6	-7	-8
1	112.79±12.31	46.22±8.22	15.85±4.98	11.33±3.84	8.15±4.08	16.23±5.01	42.98±7.48	42.01±7.64
2	41.03±7.67	12.47±4.17	5.12±2.69	3.43±2.85	4.93±3.50	15.61±4.44	11.63±4.09	26.57±5.89
3	67.04±9.61	10.71±4.86	15.38±4.83	3.07±2.22	5.80±3.97	12.79±4.50	36.40±6.75	36.36±7.14
4	29.44±6.99	18.33±5.39	2.99±2.77	0.48±1.54	8.05±3.94	7.90±3.92	13.61±4.64	14.54±4.98
5	27.55±6.58	13.03±4.25	12.93±4.20	0.00±0.91	8.59±4.19	11.48±3.92	7.58±3.52	6.84±3.74
Cleo-c's Optimal Alternative binning								
i \ j	1	2	3	4	5	6	7	8
1	23.96±6.48	10.32±4.08	8.20±1.43	0.00±1.20	6.54±3.64	8.65±3.70	4.47±3.01	7.89±4.17
2	39.84±7.70	12.44±4.24	5.07±2.75	2.92±2.61	5.62±3.73	12.81±4.04	12.15±4.14	31.57±6.30
3	111.75±12.20	40.58±7.68	22.76±6.23	9.27±3.72	10.64±4.42	22.82±5.52	39.76±7.01	45.59±7.79
4	51.01±8.62	6.30±3.87	9.73±4.22	3.65±2.34	4.54±3.54	11.00±3.79	16.77±4.71	18.98±5.12
5	17.72±5.42	8.02±3.78	7.83±3.64	5.97±2.83	18.62±5.19	6.03±2.85	3.01±2.72	13.33±4.36
	-1	-2	-3	-4	-5	-6	-7	-8
1	38.75±7.44	6.54±3.49	15.82±5.27	5.66±3.03	13.94±4.84	14.86±4.66	11.58±4.37	16.57±4.94
2	57.14±8.86	18.36±5.21	14.01±4.52	3.19±2.37	9.47±4.32	8.02±1.60	26.23±5.79	33.77±6.45

Table 45: The summaries of fitted yields for $K_L^0\pi^+\pi^-$ tag channel for other BESIII's 3 binning schemes.

		BESIII's Alternative binning							
i \ j		1	2	3	4	5	6	7	8
1		12.98±4.64	0.12±3.75	5.74±2.95	0.71±1.20	7.88±3.52	6.82±2.69	1.52±1.58	0.21±1.94
2		44.50±7.97	13.28±4.45	6.25±3.36	2.65±2.90	6.42±3.29	14.74±4.42	21.07±5.27	20.65±5.28
3		127.84±13.09	45.13±8.29	22.38±5.91	9.96±3.98	14.26±5.37	25.86±5.99	52.64±8.05	70.83±9.65
4		64.99±9.54	17.61±5.19	19.69±5.42	6.95±3.21	14.80±5.24	8.18±3.45	14.76±4.86	13.74±5.09
5		2.00±3.01	5.25±2.53	0.00±0.70	4.50±2.53	8.56±3.45	3.22±2.28	3.41±2.55	2.98±2.62
	-1		-2	-3	-4	-5	-6	-7	-8
1		14.06±4.64	7.81±3.10	0.00±14.34	3.83±2.28	10.35±4.26	4.57±2.66	6.30±3.14	5.94±3.05
2		51.05±8.34	13.92±4.70	18.50±5.65	4.45±2.53	6.25±4.14	6.30±2.95	18.50±5.05	23.81±5.57
3		150.52±14.40	45.60±8.33	29.74±6.73	12.22±4.14	10.77±4.78	34.81±7.11	48.56±8.05	74.41±9.89
4		71.52±10.03	22.08±6.05	10.44±3.93	0.26±1.56	11.08±4.55	13.94±4.84	37.47±6.98	35.83±7.24
5		7.48±3.91	7.67±3.81	2.50±3.07	1.08±1.52	1.20±2.51	5.33±2.60	4.89±3.04	8.96±3.68
BESIII's Optimal Equal binning									
i \ j		1	2	3	4	5	6	7	8
1		117.08±12.49	38.65±7.79	23.67±5.87	5.41±2.79	15.16±5.16	25.59±5.93	44.28±7.36	59.93±8.60
2		52.73±8.47	25.74±5.81	13.00±4.45	2.64±2.08	3.04±2.71	16.98±4.59	22.57±5.47	23.72±5.59
3		48.01±8.31	13.63±4.48	14.03±4.85	5.19±2.69	14.28±5.15	9.82±3.63	14.12±4.70	10.18±4.54
4		33.14±7.04	7.96±3.77	14.82±4.94	5.18±2.79	6.60±4.28	2.98±2.03	7.31±3.43	15.25±4.72
5		11.90±4.95	12.79±4.17	0.00±3.10	7.07±3.10	14.41±4.71	7.17±3.09	9.69±4.00	11.43±4.43
	-1		-2	-3	-4	-5	-6	-7	-8
1		130.49±13.20	31.37±7.27	26.36±6.34	14.32±4.54	6.80±3.83	17.59±5.17	41.31±7.40	61.66±9.14
2		32.51±7.00	17.74±4.99	0.00±3.04	3.15±2.60	2.51±2.93	10.63±3.81	14.62±4.57	21.10±5.43
3		69.63±9.80	18.60±5.54	7.85±3.52	0.39±1.20	12.34±4.77	14.29±4.91	31.49±6.35	32.86±6.87
4		33.18±7.17	8.43±3.80	9.80±3.32	1.57±2.36	6.98±3.48	12.30±4.08	15.43±4.52	14.27±4.54
5		18.45±5.60	2.17±2.92	6.62±3.53	2.09±2.09	10.66±4.34	7.58±3.44	6.32±3.24	5.61±3.16
BESIII's Optimal Alternative binning									
i \ j		1	2	3	4	5	6	7	8
1		29.56±6.78	6.48±3.31	8.57±3.58	1.59±2.12	11.15±4.24	7.79±3.37	12.20±4.00	12.73±4.24
2		39.08±7.62	21.41±5.62	1.26±2.51	4.58±2.85	3.51±2.94	15.69±4.72	19.22±5.25	24.92±6.03
3		102.52±11.78	38.33±7.64	19.38±5.43	5.72±2.97	12.76±4.69	25.17±5.81	44.48±7.32	54.58±8.26
4		61.04±9.07	15.74±4.79	14.99±4.86	4.65±2.61	12.57±4.76	7.54±3.26	12.52±4.34	15.38±5.07
5		12.31±4.87	7.06±3.33	2.46±2.56	4.82±2.66	11.77±4.36	6.95±3.09	5.94±3.27	2.67±2.92
	-1		-2	-3	-4	-5	-6	-7	-8
1		25.64±6.30	9.10±3.89	14.27±4.87	7.21±2.96	12.54±5.17	4.81±2.62	10.14±4.06	19.99±5.29
2		66.97±9.43	24.93±5.93	18.64±5.34	1.89±2.03	4.17±3.06	15.84±4.52	22.48±5.38	21.13±5.41
3		127.64±13.01	26.86±6.67	26.32±6.28	13.45±4.33	6.96±3.96	16.27±4.90	37.94±7.18	59.61±8.83
4		64.10±9.61	16.29±5.43	6.09±3.15	0.71±1.63	9.68±4.27	15.69±5.04	30.87±6.38	32.93±6.93
5		16.53±5.60	11.34±4.27	6.43±3.93	2.20±2.29	7.89±4.24	9.70±3.55	10.92±4.17	12.31±4.30